Reliability Quantification of Printed Circuit Boards Subjected to Thermal and Vibration Loads

by

Zishan Wei

A Dissertation Submitted to the Faculty of the

DEPARTMENT OF AEROSPACE AND MECHANICAL ENGINEERING

In Partial Fulfillment of the Requirements

For the Degree of

DOCTOR OF PHILOSOPHY

WITH A MAJOR IN MECHANICAL ENGINEERING

In the Graduate College

The University of Arizona

2 0 0 4

The University of Arizona ®
Graduate College

As members of the Final Examination Committee, we certify that we have read the

dissertation prepared by Zishan Wei

entitled Reliability Quantification of Printed Circuit Boards Subjected to Thermal and Vibration Loads

and recommend that it be accepted as fulfilling the dissertation requirement for the

Degree of Doctor of Philosophy

Dr. Dimitri B. Kececioglu	11/10/04 Date
Dr. Barry D. Ganapol	11/10/04 Date
Dr. Ferenc Szidarovszky	11/10/04 Date
Dr. Olgierd A. Palusinski	Nov. 10/04 Date
Dr. Kathleen Melde	11/10/04 Date

Final approval and acceptance of this dissertation is contingent upon the candidate's submission of the final copies of the dissertation to the Graduate College.

I hereby certify that I have read this dissertation prepared under my direction and recommend that it be accepted as fulfilling the dissertation requirement.

Dissertation Director: Dr. Dimitri B. Kececioglu	11/10/04 Date

STATEMENT BY AUTHOR

This dissertation has been submitted in partial fulfillment of the requirements for an advanced degree at The University of Arizona and is deposited in the University Library to be made available to borrowers under rules of the Library.

Brief quotations from this dissertation are allowable without special permission, provided that accurate acknowledgement of source is made. Requests for permission for extended quotation from or reproduction of this manuscript in whole or in part may be granted by the head of the major department or the Dean of the Graduate College when in his or her judgment the proposed use of the material is in the interests of scholarship. In all other instances, however, permission must be obtained from the author.

SIGNED: ______________________

ACKNOWLEDGMENTS

First and foremost, I wish to express my deepest gratitude and greatest thanks to Professor Dimitri B. Kececioglu, for his continuous and precious guidance, encouragement and support during my study and research in pursuing my degree here at The University of Arizona. I would also like to express my sincere appreciation to Professor Barry Ganapol, Professor Ferenc Szidarovszky, Professor Olgierd A. Palusinski, and Professor Kathleen Melde for their teachings and advice to my studies, for sharing their ideas, their knowledge and their time with me, for their support as members of my doctoral committee and for their help in completing my degree requirements.

Most of all, I thank my wife, Fang Gu, for her constant encouragement, care, and support throughout my studies, and my son, for his bringing to our family happiness.

TABLE OF CONTENTS

TABLE OF CONTENTS – Continued

TABLE OF CONTENTS – Continued

TABLE OF CONTENTS – Continued

TABLE OF CONTENTS – Continued

TABLE OF CONTENTS – Continued

LIST OF FIGURES

LIST OF FIGURES - Continued

LIST OF TABLES

ABSTRACT

Reliability quantification is one of the most important tasks in Reliability Engineering. During the design, development, and operational phase, this information can be very valuable to the product's designers, and users. The designers can use it to guide their design, find the design's weak points. Users can use it to setup maintenance plans and schedule.

PCBs, as the major building block of electronic equipment, have been widely used in modern complex systems, such as aircraft, automotives, laptop computers, etc. Its reliability plays a vital role in the whole system's reliability. Thus, effective and accurate quantification of PCB's reliability becomes very essential to the whole electronic system's reliability quantification. Random vibration and thermal cycling are two common environments experienced by PCB's. As a result, quantifying the reliability of a PCB under these two environments becomes necessary. Currently, in industry, the commonly used methods to quantify the reliability of a PCB are the MIL-HDBK-217 and Bellcore type methods. However, the lack of accuracy and slow pace of updating the databases have limited the usage of these methods.

In this dissertation, a Modified Stress-Strength Interference (MSSI) method is proposed to quantify the reliability of a PCB. In this method, not only the stress and the strength are assumed to be distributed, but also is the mean value of the strength, so that both the initial designed-in reliability and the reliability at any time can be quantified. Based on this method, a reliability quantification model for the PCB is developed. In this model, a PCB is divided into three parts: i.e., board, interconnects, and parts and modules

mounted on the board. Seven (7) failure modes related to the board and the interconnects, and one (1) failure mode related to the module have been investigated. The dependence between these failure modes is studied and incorporated into the reliability quantification model. A three-step popcorn effect reliability quantification model is also proposed by means of considering the failure mechanism of the popcorn effect. Finally, a comprehensive example is given to demonstrate the usage of the methodology proposed in this dissertation.

CHAPTER 1
INTRODUCTION

1.1 Importance of Reliability Quantification

Reliability Quantification is one of the most important tasks in Reliability Engineering. During the concept feasibility study phase, reliability quantification can provide a baseline for feasibility evaluation, and be used for comparing and evaluating different design concepts; during the design phase, it can help the designers to determine the potential reliability problems and verify if the design concept is acceptable in terms of the reliability requirements so that the expensive late design changes can be avoided; during the usage phase, it can help users to determine the maintenance strategy and logistic support planning, such as determining the number of spares, establishing the correct timing for maintenance if the reliability-centered maintenance concept is adopted. Reliability quantification can also be used as inputs to other reliability tasks, such as Failure Mode, Effect, and Criticality Analysis (FAMECA), and cost analysis.

The most effective way to conduct reliability quantification, in my opinion, is through reliability testing and/or collecting field data. But unfortunately, many factors restrict the usage and effectiveness of this method. First of all, reliability testing is expensive and time-consuming for the majority of current products, especially electronic equipment, including Printed Circuit Boards (PCB), which encounter extremely strong global competition and have a very short time to market. Thus, there is not enough time available to conduct reliability testing. For example, Parry [1, pp. 862-868] reported that the time-to-market for today's electronic systems is only a few months; secondly, as we all know, the accuracy of the test results, and in turn the accuracy of the reliability quantification rely, to a large extent, on the test sample size. Study results [2, p. 725] show that for an exponential distribution case, 270 units are required if the required precision is ±10% at 90% confidence level. Thirdly, there are many cases, especially in the early development phase, where no prototype or product is available for reliability testing. Therefore, using the analytical method to quantify product reliability becomes a very attractive and desired tool, particularly for product designers.

1.2. Statement of the Problem

Printed Circuit Boards are the most important parts in electronic systems. Their reliability will directly affect the reliability of the electronic system. In past years, much research has been conducted and aimed at improving PCB reliability. For example, much research focused on solder joint reliability and its fatigue life quantification [3, pp. 347-353; 4, pp. 266-270; etc.]; some focused on the plastic package popcorn problems [5, pp. 56-65; 6, pp. 301-308; 7, pp. 362-367; etc]. However, to my knowledge, there is no research on reliability quantification of PCBs other than using the MIL-HDBK-217 [8, 250 pp.] types of methods, which we will show have some big shortcomings. One of the closest works was done by Zhang [9, 187 pp.]. He studied the reliability quantification of plates under random vibration, such as ideal white noise excitation, band limited white noise excitation, and temperature loads. However, PCBs are different from plates in many aspects: Firstly, a PCB is a multi-layer laminate board and one of its major failure modes is delamination; secondly, it includes many active parts which will generate heat;

thirdly, there are many solder joints between parts/modules and the board. Therefore, reliability quantification of PCBs is much more complicated than that of a plate. Figures 1 and 2 illustrate a PCB and a part mounted on the board using solder balls (leadless joints).

Before we proceed further, some terminologies used in this dissertation needs to be clarified.

Part: 1. A certain portion of anything; 2. General term for components, and modules mounted on the board.

Component: Discrete part mounted on the board, such as a resistor, or a capacitor.

Module: Part mounted on the board in the form of a package. It is also called a package.

Packaging part: Anything other than the chips in the Module.

Board: The base of the PCB on which parts are mounted.

Figure 1.1 illustrates a PCB, and Figure 1.2 illustrates a part on the board with ball grid array interconnect. We can see from these two figures that a PCB can be roughly divided into three sections: board, interconnects between the board and the parts on the board, and the parts. Therefore, the reliability of the PCB can be found by studying the failure modes of each section.

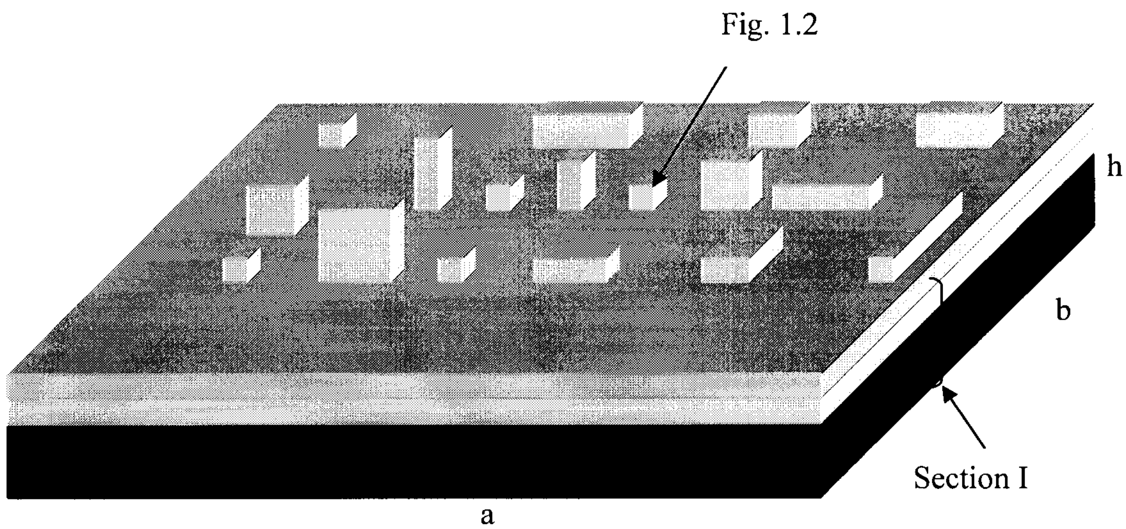

Fig. 1.1 – Illustration of a PCB.

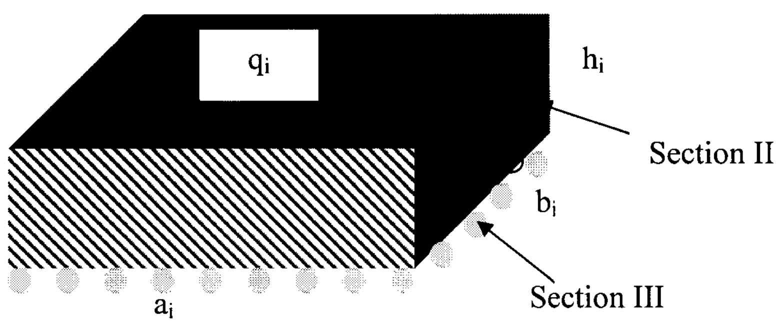

Fig. 1.2 – i^{th} active part illustration.

1.3 Thermal Load and Vibration Profiles

In this dissertation, we will only consider two environment conditions; namely thermal and vibration. This is because almost all the electromechanical failures of electronics is due to these two conditions, about 80% thermal and 20% vibration [10, p. 39; 11, 12 pp.].

Considering that most of the PCBs, especially in the consumer products, will keep working for a long period of time after they are turned on. We will ignore the transient temperature effect and only consider the steady state case in this dissertation, which means we assume that the temperature is constant. Figure 1.3 illustrates an example of this thermal profile.

For vibration environments, we assume that the electronic box is experiencing a random vibration. Figure 1.4 illustrates one of these profiles.

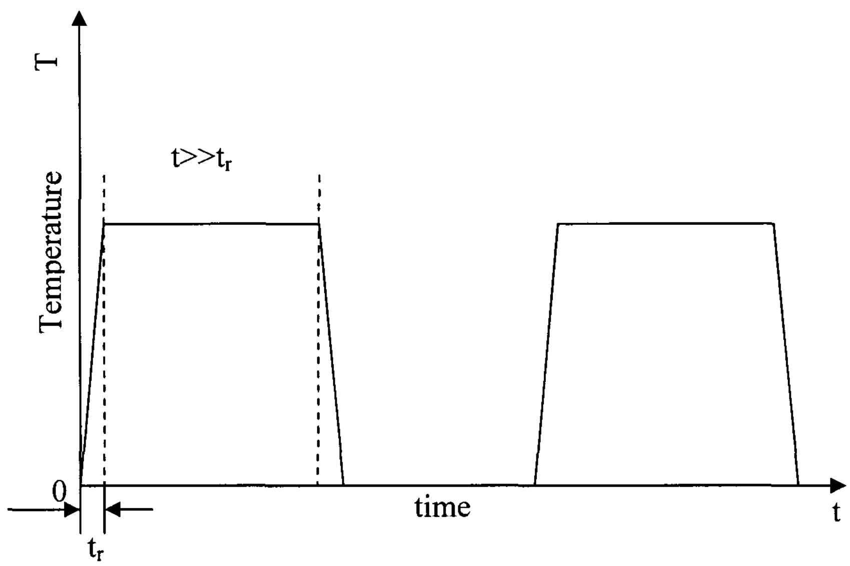

Fig. 1.3 – Illustration of the thermal profile.

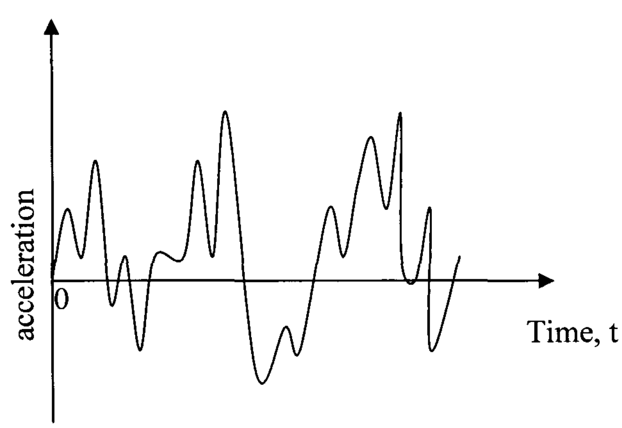

Fig. 1.4 – Illustration of vibration profile.

1.4 Current Commonly Used Analytical Reliability Quantification Methods of PCBs and Their Status

In electronic industries, the reliability quantification of PCBs was mainly done by using the MIL-HDBK-217 type of method, such as Bellcore Reliability Prediction Procedures for Electronic Equipment (Bellcore RPP, now called Telcordia) [12, 138 pp.]; Nippon Telegraph and Telephone Corporation Standard Reliability Table for Semiconductor Devices (NTT Procedure); British Telecom Handbook of Reliability Data for Components Used in Telecommunications Systems (British Telecom HRD-4); French National Center for Telecommunications Studies Recueil De Donnees De Fiabilite Du CNET (CNET Procedures); and Siemens Reliability and Quality Specification Failure Rates of Components (Siemens Procedure). John, B. B [13, pp. 2-12] analyzed and compared these six widely used reliability prediction procedures. These types of methods are all based on the following assumptions:

- The product failures are only due to the failures of parts in the product. Normally it is assumed the mechanical and electrical connections between parts or between parts and the board are perfect. Mechanical parts reliability is normally assumed to be 1.
- The base failure rates of parts are known and are constant.
- The time-to-failure of products follows the Exponential Distribution.
- Environmental, product quality, and other effects can be incorporated by using environment, quality, and other factors.

We take the MIL-HDBK-217 as an example to demonstrate how these methods work.

In MIL-HDBK-217, two methods are provided. One is called the Part Stress Analysis (PSA) method, mainly used at the later design and development phase when more information about the product is available. The other is called the Parts Count Method, which is mainly used in the early design, or concept phase where there is not enough information available.

1.4.1- Failure Rate Models for the Part Stress Method

Based on the product type, there are two models available. For microcircuits, including bipolar, MOS, and microprocessors, the failure rate model is given as [8, 5-3]:

$$\lambda_P = (C_1\pi_T + C_2\pi_E)\pi_Q\pi_L, \tag{1-1}$$

where

λ_P = part failure rate,

C_1 = die complexity failure rate, depending on the number of gates for bipolar, MOS parts, and number of bits for microprocessors, etc,

C_2 = package failure rate, depending on number of function pins,

π_T = temperature factor,

π_E = environment factor, including ground, naval, airborne, space, missile environment, there are also several subcategories within each category,

π_Q = quality factor,

and

π_L = learning factor. This factor considers the effect of production maturity on the part failure rate. A new part might have higher factor than a mature part.

For the rest of the types of parts, such as discrete semiconductors, tubes, lasers, resistors, capacitors, inductive devices, rotating devices, relays, switches, connectors, interconnection assemblies, connections, meters, quartz crystals, lamps, electronic filters, fuses, etc., the following type of a model is used [8, 3-6]:

$$\lambda_P = \lambda_b \pi_T \pi_A \pi_R \pi_S \pi_C \pi_Q \pi_E, \quad (1\text{-}2)$$

where

λ_P, π_T, π_Q, and π_E are as defined previously,

λ_b = base failure rate,

π_A = application factor,

π_R = resistor factor,

π_S = stress factor,

and

π_C = capacitance factor.

1.4.2- Parts Count Method

The Parts Count Method is used when there is insufficient information available. The basic model for this method is given as [8, Appendix A]:

$$\lambda_P = \sum_{i=1}^{n} N_i (\lambda_g \pi_Q)_i, \quad (1\text{-}3)$$

where

λ_P = total product failure rate,

λ_g = failure rate for the i^{th} part,

π_Q = quality factor for the i^{th} part,

N_i = quantity of the i^{th} part in this product,

and

n = number of different parts in the product.

It should be noted that Eq. (1-3) is only applied if the entire product is being used in one environment. If not, this equation should be used for each environment and then, sum the failure rates in each environment together to obtain the product's failure rate.

The advantage of this method is that it is simple and easy to use. However, it has a big drawback; its accuracy is very poor. Therefore, using its result to guide the design may mislead the designers. Pecht, M. [14, pp. 1-7] even suggested abandoning the usage of the MIL-HDBK-217 type of method after reviewing the development history of reliability quantification methods, technology advances, and the drawbacks of these methods. His conclusion may be overstated but he really pointed out some problems embedded in these methods. For example, he found out that through his study: a) the base failure rates of the parts were not updated quickly to reflect the technology advances; b) the exponential distribution can not represent the failure mechanism of some products; c) Arrhenius type formulations of the failure rate in terms of temperature can not represent the failure mechanism related to thermal loading, etc. Regarding the point "c" that Pecht, M. made above, Parr [15, pp. 533-538] also found that using the Arrhenius law to express diffusion-dominated or chemical-related failure mechanism is not proper. He thinks that the reasons for the Arrhenius law being unfavorable are that some failure mechanisms only occur above a certain temperature and some may be suppressed at high temperature. Data had shown that in the temperature range of -55°C to 150 °C, failure mechanisms are mainly not due to high steady-state temperatures, but thermal gradients. I also found in my personal experience that reliability quantification results obtained from the MIL-HDBK-217 or similar methods can be different from the field results by an order of several magnitudes. Leonard [16, pp. 895-902] reported that the MTBF predicted (10,889 hr) using MIL-HDBK-217D for a full authority electronic control was about three times different than its field observed MTBF (30,000 hr). The reasons for the disagreement, in my opinion, are mainly due to the following:

a. The base failure rates of the parts given in the standard did not correctly represent the parts in the product, or not updated as technology advanced.
b. Employing factors to reflect the environment, stress, quality effects may cause a big accuracy problem since several factors cannot cover all kinds of environments, stress condition and quality level.
c. Missing consideration of the effect of mechanical and electrical interconnects and other failure mechanisms on the product failure rate, such as solder joint failures, and board delamination. Not considering these effects was alright in the past because parts used to be very unreliable and parts' failures dominated the failure rate of the product. Now the reliabilities of

parts have improved, and they are much higher than that of solder joints and other mechanical parts, consequently not considering their failure rates is definitely unacceptable. For example, Pecht [17, pp. 1160-1164] reported that for avionics system, 50% of total failures are due to part failures in the 70's, but in the 90's the part failures is almost negligible, the major failures are due to handling, electrical overloading, process related failures, etc. The five-year study issued in 1992 by the Semiconductor Industry Association (SIA) also indicated that the electronic parts reliability had been improved from 200 ppm. defects to 40 ppm. defects. If considering the fact that Pecht's report and the SIA's research were conducted in the early 90's and much improvement on parts reliability has been achieved since then, we can conclude that the parts' failures are no longer dominating the failure rates of the electronic devices, therefore interconnect and other failure mechanisms must be considered.

1.4.3 – The RAC PRISM Method

In response to the shortcomings of the MIL-HDBK-217 type of methods, the Reliability Analysis Center (RAC) developed a new method, PRISM [11, 12 pp.], intended to improve the accuracy of reliability quantification. In this method, two models are introduced: one is the system level reliability quantification model, and the other is the part level reliability quantification model. In both models, more factors are incorporated. For example, in the system level model, besides the environment factor, parts process multiplier, infant mortality factor, design process multiplier, system management process multiplier, reliability growth factor, manufacturing process multiplier, etc. are also included.

In the part level model, a solder joint factor is introduced with other factors. Equations (1-4) and (1-5) depict these two models. Unfortunately, this method still doesn't completely solve the shortcomings which the MIL-HDBK-217 type of methods possesses. For example, the levels of the factors are still unable to cover all of the situations, and many failure modes, such as the popcorn effect of plastic packages, are still not considered. Regarding the data update problem, the frequency of RAC updating its data bank is not clear yet, thus whether the data used in the quantification reflects the current technology or not is still uncertain.

The system level model is given as [11, p. 4]:

$$\lambda_S = \lambda_I\left(\pi_p \pi_{IM} \pi_E + \pi_D \pi_G + \pi_M \pi_{IE} \pi_E \pi_G + \pi_S \pi_G + \pi_I + \pi_N + \pi_W\right) + \lambda_{sw}, \qquad (1\text{-}4)$$

where

λ_S = system failure rate,

λ_I = initial failure rate of the system,

π_p = parts process multiplier,

π_{IM} = infant mortality factor,

π_E = environmental factor,

π_D = design process multiplier,

π_G = reliability growth factor,

π_M = manufacturing process multiplier,

π_S = system management process multiplier,

π_I = induced process multiplier,

π_N = no-defect process multiplier,

π_W = wearout process multiplier,

and

λ_{SW} = software failure rate.

The part level reliability model is given as [11, p. 7]:

$$\lambda_P = \lambda_O \pi_O + \lambda_E \pi_E + \lambda_C \pi_C + \lambda_{sj} \pi_{sj} + \lambda_i , \tag{1-5}$$

where

λ_P = part failure rate,

λ_O = failure rate from operational stresses,

π_O = failure rate multiplier for operational stresses,

λ_E = failure rate from environmental stresses,

π_E = failure rate multipliers for environmental stresses,

λ_C = failure rate from power or temperature cycling stresses,

π_C = failure rate multipliers for cycling stresses,

λ_i = failure rate from induced stresses,

λ_{sj} = failure rate from solder joint,

and

π_{sj} = failure rate multipliers for solder joint stresses.

To my knowledge, there is only one application [18, 14 pp.] for this method so far, and its accuracy is not yet confirmed since it was used in a newly developed product and there are no data available.

In this dissertation, a new reliability quantification method for the PCBs will be developed by considering different kinds of failure modes of PCBs and using the modified stress-strength interference theory.

CHAPTER 2

MODIFIED STRESS-STRENGTH INTERFERENCE THEORY

2.1 Introduction

The stress-strength interference method originates from the mechanical reliability field. It is based on the assumption that both stress and strength are distributed variables and failure will occur when strength is less than stress. This assumption is true since uncertainties exist everywhere in our real life. For example, in engineering, the uncertainties may be due to physical phenomena that are random or the variability of the physical process, such as manufacturing process, or due to the measurement error, or prediction error. The existences of these uncertainties require us to consider all the design variables as randomly distributed instead of a single deterministic value.

One thing needs to be clarified is that even though this method is called the stress-strength interference method; it can be applied to a broader class of problems. The term "stress" should be considered in a broader sense as any load or load-induced response quantity that has the potential to cause failure. The term strength should also be considered in a broader sense as the capacity of the part to withstand the "stress". For example, if the reliability of a PCB is defined as the probability of the deflection of the PCB being less than an allowable value. Then, the "stress" in this case will be the PCB's real deflection, and the strength will be the allowable value of the deflection. In this dissertation, stress and strength terms will still be utilized, but it should be kept in mind that it is in a broader sense. Kececioglu, D.B. [19, 688 pp.] applied this theory to mechanical components and structures and obtained very good results. Kim. J. [20, pp.

286-295] applied this theory to quantify the reliability of high voltage ceramic capacitors, and Suhir, E. [21, pp. 215-223] utilized the coefficient of thermal expansion as stress and strength parameters to quantify the reliability of seal glass.

One shortcoming of the method used by all three authors above is that they only consider that the stress and strength are constant-parameter distributions, meaning that the distribution parameters for stress and strength do not change. This may be true for the stress distribution as long as the product is used at one specified condition, but it is obviously not true for strength distribution. Without considering strength degradation, one can only determine one reliability value; i.e., the designed-in reliability of the product. But the time dependent reliability, which is just what the users, even designers want cannot be determined. The reliability definition also shows the importance of the time dependent reliability, which is stated as "Reliability is the probability that parts, components, products, or systems will perform their designed-for functions without failure in specified environments for desired periods at a given confidence level" [22, p. 2]. MIL-STD-721 [23, P.8] gives a similar definition. This definition tells us that whenever talking about reliability, it must be related to the environment the product is operated in and the length of the operation. Kececioglu, D. B. [19, 688 pp.] considered the fatigue failure case but assumed that the strengths are known.

The modified stress-strength interference (MSSI) method will consider strength change with time so that the time-dependent reliability can be determined.

2.2 Modified Stress-Strength Interference (MSSI) Reliability Quantification

The modified stress-strength interference method is very simple mathematically. If we assume that the stress, s,† and the strength, S,†† of a product follow a distribution with pdf $f_{sS}(s,S)$, then the failure probability (unreliability) of this product is defined as

$$F = P(s > S) = \int_{-\infty}^{\infty} \int_{-\infty}^{S} f_{sS}(s',S')\, ds' dS', \tag{2-1}$$

where

f_{sS} = joint pdf of stress and strength distribution.

The shaded area shown in Fig. 2.1 represents the failure probability or unreliability.

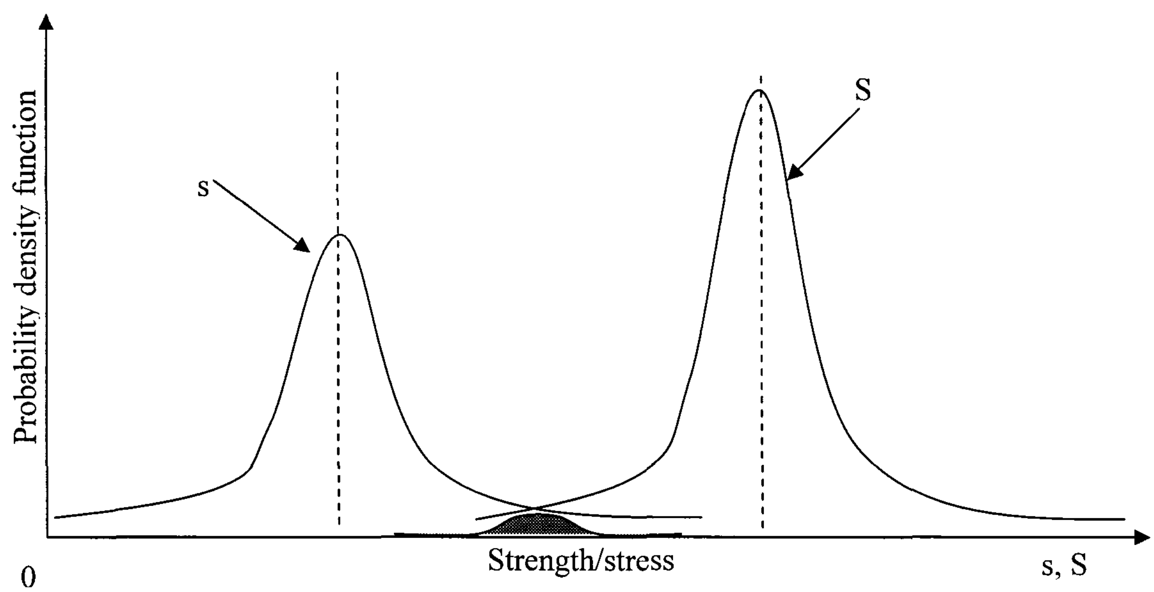

Fig.2.1 Illustration of the stress-strength interference theory.

---

† We will use lower case s denoting stress hereafter.

†† We will use capital letter S representing strength hereafter.

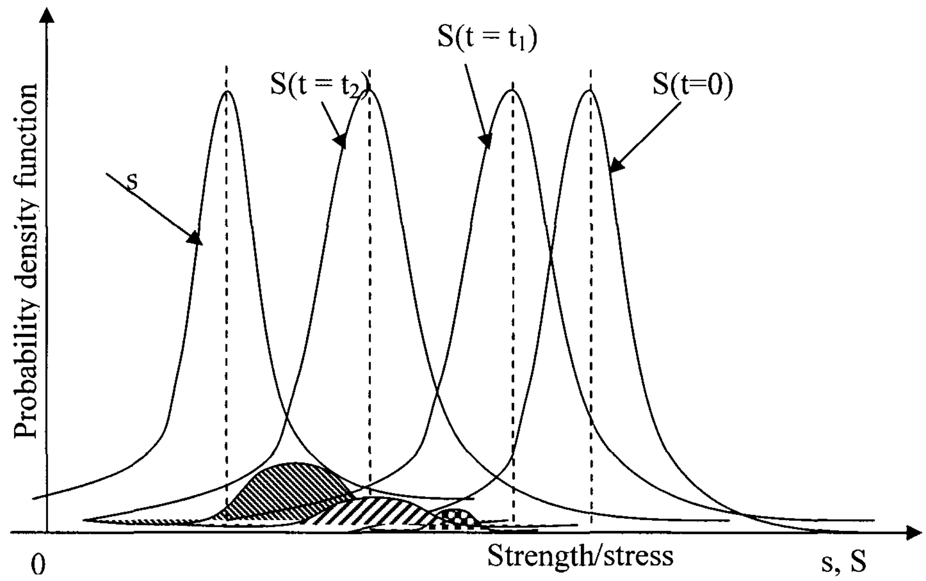

Fig. 2.2 - Unreliability using the stress-strength interference method.

Figure 2.2 illustrates the unreliability change with time at given stress and strength distribution. From this figure, we see that the unreliability (shaded area) is getting larger and larger with time due to the degradation of the strength.

It should be noted that s' and S' in Eq. (2-1) represent two variables not the derivatives. The purpose of doing this is to differentiate them with s and S. In mathematics, these are called dummy variables. Other symbols such as x, y could be used instead, the results are the same. For example, $\int_1^2 xdx = \int_1^2 ydy = \cdots = \int_1^2 zdz = 3/2$.

2.2.1 Reliability Quantification for a Single Failure Mode

If a product in question has only one failure mode, its reliability can be quantified using the following several methods based on the dependence between the stress and the strength distributions, the distribution types of the stress and the strength, and other factors which will be clear as we are moving on.

2.2.1.1 Stress and Strength Distributions Are Known and Independent

In this case, the failure probability is given as:

$$\begin{aligned} P(s > S) &= \int_{-\infty}^{\infty} \int_{S'}^{\infty} f_s(s')\, g_S(S',t)\, ds'\, dS', \\ &= \int_{-\infty}^{\infty} g_S(S',t) \left(\int_{S'}^{\infty} f_s(s')\, ds' \right) dS', \\ &= \int_{-\infty}^{\infty} g_S(S',t)\, R_s(S')\, dS', \end{aligned} \tag{2-2}$$

where

$R_s(S) = \int_S^{\infty} f_s(s')ds'$ is the reliability function,

and

f_s and g_S = pdf of the stress and the strength, respectively.

The reliability is given as

$$\begin{aligned} R = P(S > s) &= \int_{-\infty}^{\infty} \int_{s'}^{\infty} f_s(s')\, g_S(S',t)\, ds'\, dS', \\ &= \int_{-\infty}^{\infty} f_s(s') \left(\int_{s'}^{\infty} g_S(S',t)\, dS' \right) ds', \\ &= \int_{-\infty}^{\infty} f_s(s')\, R_S(s',t)\, ds', \end{aligned} \tag{2-3}$$

or

$$R = P(S > s) = \int_{-\infty}^{\infty} \int_{-\infty}^{S'} f_s(s')\, g_S(S',t)\, ds'\, dS',$$

$$= \int_{-\infty}^{\infty} g_S(S',t) \left(\int_{-\infty}^{S'} f_s(s')\, ds' \right) dS', \tag{2-4}$$

$$= \int_{-\infty}^{\infty} g_S(S',t)\, F_s(S')\, dS'.$$

Then, the reliability can be found by finding the value of this integral.

Example 2-1

Assume both the stress and the strength follow the exponential distribution with mean of 100 and 1,000 kpsi at age zero. Find the product's reliability at the age zero.

Solution to Example 2-1

From Eq. (2-3), the reliability of the component at age zero is given by

$$R(t) = \int_{-\infty}^{\infty} f_s(s)\, R_S(s)\, ds,$$

$$= \int_{0}^{\infty} \frac{1}{\bar{s}} e^{-\frac{x}{\bar{s}}} e^{-\frac{x}{\bar{S}}} dx = \int_{0}^{\infty} \frac{1}{100} e^{-(\frac{1}{100} + \frac{1}{1,000})x} dx,$$

or

$$R(t) = 90.91\%.$$

Example 2-2

Assume that the stress follows the exponential distribution with mean of 100 kpsi, and the strength follows the two-parameter Weibull distribution with the shape parameter, β, of 2 and the scale parameter, η, of 1,000 kpsi at age zero. Find the product's reliability when the product is first put into operation.

Solution to Example 2-2

From Eq. (2-3), the reliability of the product at age zero is given by

$$R(t) = \int_{-\infty}^{\infty} f_S(s)\, R_S(s)\, ds,$$

$$= \int_0^{\infty} \frac{1}{s} e^{-\frac{x}{s}} e^{-\left(\frac{x}{\eta}\right)^{\beta}} dx = \int_0^{\infty} \frac{1}{100} e^{-\frac{x}{100}} e^{-\left(\frac{x}{1,000}\right)^2} dx.$$

Using Mathcad yields

$$R(t) = 98.1\%.$$

It is easy to show that if both stress and strength follow the normal distribution, using Eq. (2-3) or (2-4) will be very difficulty to quantify. In that case, the following method should be utilized.

2.2.1.2 Both Stress and Strength Are Normally Distributed and Independent

In this case, one of the important properties of the normal distribution will be used. As we know if two independent normal variables 's' and 'S' have mean $\bar{s}$ and $\bar{S}$, and variance σ_s^2 and σ_S^2, respectively, then, S-s is also a normal random variable with mean of $\bar{S} - \bar{s}$ and variance of $\sigma_S^2 + \sigma_s^2$.

If we define a performance function or a limit state as Z = S-s, then, Z follows a normal distribution with mean $\mu_z = \bar{S} - \bar{s}$ and variance $\sigma_z^2 = \sigma_S^2 + \sigma_s^2$. Then, Z > 0 means no failure occurs, and Z < 0 means failure occurs.

If now 's' is stress, and 'S' is strength, then the reliability at any time t is computed from

$$R(t) = P(z \geq 0) = \int_0^\infty f(z)dz = 1 - \Phi\left(-\frac{\mu_z}{\sigma_z}\right),$$

$$= 1 - \Phi\left(-\frac{\bar{S} - \bar{s}}{\sqrt{\sigma_s{}^2 + \sigma_S{}^2}}\right), \qquad (2\text{-}5)$$

$$= \Phi\left(\frac{\bar{S} - \bar{s}}{\sqrt{\sigma_s{}^2 + \sigma_S{}^2}}\right),$$

where

$\Phi(z) = \int_{-\infty}^{z} \frac{1}{\sqrt{2\pi}} e^{-t^2/2} dt$, it is the cdf of the standard normal distribution

as illustrated in Figure 2-3.

If we denote

$$m = \frac{\mu_z}{\sigma_z} = \frac{\bar{S} - \bar{s}}{\sqrt{\sigma_S^2 + \sigma_s^2}} \qquad (2\text{-}6)$$

m = reliability index.

Then, Eq.(2-5) becomes

$$R(t) = 1 - \Phi(-m) = \Phi(m). \qquad (2\text{-}7)$$

This is due to $\Phi(-m) = 1 - \Phi(m)$

The derivation of Eq. (2-5) is given in Appendix A.

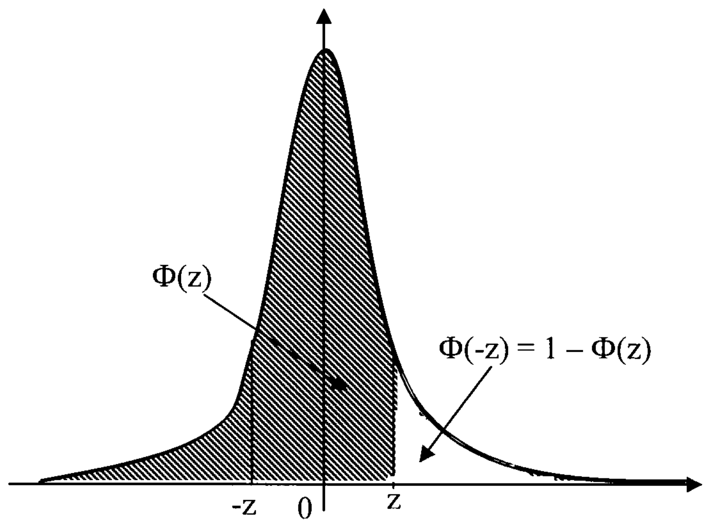

Fig. 2.3 - Illustration of the definition of Φ(z) and Φ(-z).

2.2.1.3 Geometric Explanation of the Reliability Index

The reliability index defined in Eq. (2-6) has been widely used in the stress-strength interference method. Its geometric explanation has been a topic of interest to many researchers, such as Hasofer [24, pp. 111-121], Grigori, [25, pp. 155-165], Lind [26, pp. 447-452], and Dolinski [27, pp. 211-231]. In this section, a brief introduction of the reliability index geometric explanation will be discussed to provide a foundation for later section discussions.

For a performance function

$Z(S,s) = S - s$,

if we make the changes of variables $u = (S - \bar{S})/\sigma_S$ and $v = (s - \bar{s})/\sigma_s$, then

$S = \bar{S} + \sigma_S u$, and $s = \bar{s} + \sigma_s v$,

thus, the performance function can be written as

$$Z(u,v) = \overline{S} - \overline{s} + \sigma_S u - \sigma_s v. \tag{2-8}$$

Plotting z(u,v) in the coordinates of 'u', and 'v' yields the Fig. 2.4. After some basic algebraic operations, we can see the "shortest distance" from the origin to the Z(u,v) = 0 line (or curve when the Z function is non-linear, which will be discussed in detail later) is the reliability index m given by Eq. (2-6). Appendix B provides the proof. The coordinates of the intersection point 'C' of the shortest line OC and Z = 0 line are $\left(-m \cdot \frac{\sigma_S}{\sqrt{\sigma_S^2 + \sigma_s^2}}, m \cdot \frac{\sigma_s}{\sqrt{\sigma_S^2 + \sigma_s^2}} \right)$, as shown in Fig. 2.4,

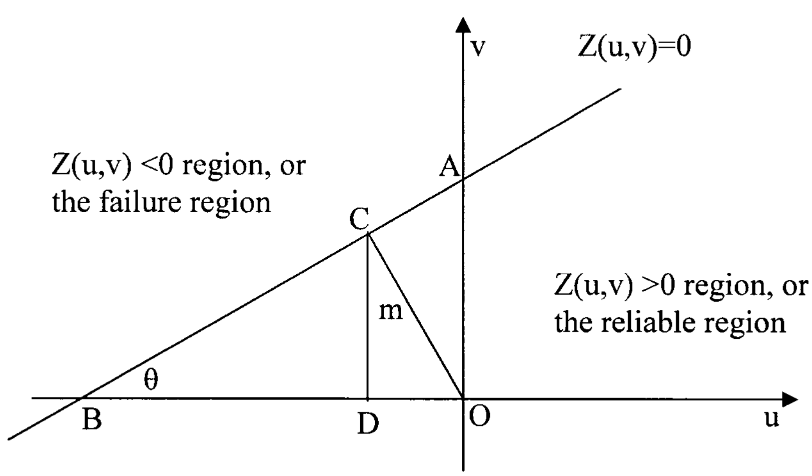

Fig. 2.4 - Illustration of the geometric expression of the reliability index.

In general, if both the stress and the strength are linear functions of many independent normal variables, such as

$$S(X_1, X_2, ..., X_n) = a_0 + a_1 X_1 + a_2 X_2 + \cdots + a_n X_n = a_0 + \sum_{i=1}^{n} a_i X_i, \tag{2-9}$$

and

$$s(Y_1, Y_2, \ldots, Y_m) = b_0 + b_1 Y_1 + b_2 Y_2 + \cdots + b_m X_m = b_0 + \sum_{i=1}^{m} b_i Y_i \,. \tag{2-10}$$

Then, the reliability of the product can be computed using Eqs. (2-6) and (2-7), with

$$\overline{S} = a_0 + \sum_{i=1}^{n} a_i \overline{X}_i, \quad \sigma_S^2 = \sum_{i=1}^{n} a_i^2 \sigma_{X_i}^2 \,,$$

and

$$\overline{s} = b_0 + \sum_{i=1}^{m} b_i \overline{Y}_i, \quad \sigma_s^2 = \sum_{i=1}^{n} b_i^2 \sigma_{Y_i}^2 \,.$$

2.2.1.4 Both the Stress and the Strength Distributions Are Unknown

In reality, we always find we are in the situation where the stress, the strength, and in turn the performance function are nonlinear functions of many independent normal variables. In this case, to find the reliability, an integration of the joint probability density function over the nonlinear region should be performed, that is

$$R = \int\int \cdots \int f_{X_1, X_2, \ldots, X_n}(X_1, X_2, \ldots, X_n) dX_1 \cdots dX_n \,. \tag{2-11}$$

In practice, however, it is almost impossible to know the joint pdf of the performance function due to many reasons, such as insufficient data. Furthermore, even when the pdf is known, the exact evaluation of the multiple integral generally requires numerical integration which may be impractical in engineering. In addition, since the stress and the strength are always a nonlinear function of many variables, it is hard to find the explicit stress and strength distributions. Thus, using Eqs. (2-6), (2-7), or (2-11) to quantify the reliability, is either not possible or not applicable. In this case, the following methods can be used.

2.2.1.4.1 The Taylor Series Expansion Method (TSEM)

In the case of nonlinear functions of the stress and the strength, the performance function can be expressed as

$$Z = S(X_1, X_2, ..., X_n) - s(Y_1, Y_2, ..., Y_m), \tag{2-12}$$

where X_i and Y_j are normal variables, i = 1,…,n and j = 1,…,m.. Using the Taylor series expansion, we have

$$\begin{aligned} Z = S(\overline{X}_1, \overline{X}_2, ..., \overline{X}_n) + \sum_{i=1}^{n} \frac{\partial S}{\partial X_i}\bigg|_{\overline{X}_{1,2,..,n}} (X - X_i) + o(X - X_i)^2 \\ - s(\overline{Y}_1, \overline{Y}_2, ..., \overline{Y}_m) - \sum_{i=1}^{m} \frac{\partial S}{\partial Y_i}\bigg|_{\overline{Y}_{1,2,..,n}} (Y - Y_i) - o(Y - Y_i)^2. \end{aligned} \tag{2-13}$$

where

$o(\bullet)$ = second or higher order terms.

If we believe that the second order and higher order terms can be dropped without causing too much error, then the performance function can be expressed as:

$$\begin{aligned} Z \approx S(\overline{X}_1, \overline{X}_2, ..., \overline{X}_n) + \sum_{i=1}^{n} \frac{\partial S}{\partial X_i}\bigg|_{\overline{X}_{1,2,..,n}} (X - X_i) - \\ s(\overline{Y}_1, \overline{Y}_2, ..., \overline{Y}_m) - \sum_{i=1}^{m} \frac{\partial S}{\partial Y_i}\bigg|_{\overline{Y}_{1,2,..,n}} (Y - Y_i). \end{aligned} \tag{2-14}$$

Since $E(X - X_i) = \overline{X} - \overline{X} = 0$, and $E(Y - Y_i) = \overline{Y} - \overline{Y} = 0$;

then,

$$\overline{Z} \approx S(\overline{X}_1, \overline{X}_2, \ldots, \overline{X}_n) - s(\overline{Y}_1, \overline{Y}_2, \ldots, \overline{Y}_m), \tag{2-15}$$

and

$$\sigma_Z^2 \approx \sum_{i=1}^{n} \left(\frac{\partial S}{\partial X_i} \bigg|_{\overline{X}_{1,2,\ldots n}} \right)^2 \sigma_{X_i}^2 + \sum_{i=1}^{n} \left(\frac{\partial S}{\partial Y_i} \bigg|_{\overline{Y}_{1,2,\ldots m}} \right)^2 \sigma_{Y_i}^2 \ . \tag{2-16}$$

Then, the reliability can be computed using Eqs. (2-6) and (2-7).

2.2.1.4.2 Minimum Distance Method (MDM)

The problem with the Taylor Series Expansion Method used in the nonlinear performance function case is that expanding the series about the mean value of each variable may cause a big error, which can be seen from Eq. (2-13). To solve this problem, a Minimum Distance Method can be used. From the geometric explanation given in Section 2.2.1.3, we see that the shortest distance from the origin to the limit state line (or the so called failure surface) may be more proper to represent the reliability index 'm' in this case. The point on the failure surface with minimum distance to the origin is called the most probable failure point [28, pp. 109] or the design point. The actual meaning of the MDM method is that we use the tangent plane at the most possible failure point to represent the actual failure surface. Therefore, in some sense, this method is the same as the TSEM; the only difference is that the Taylor Series Expansion Method is expanded about the mean values of each variable, while this method is expanded about a set of optimum values. This method has been used by many researchers, such as [24, pp. 111-121], [25, pp. 155-165], [26, pp. 447-452], and [27, pp. 211-231]. Figure 2.5 illustrates a simple nonlinear performance case, and compares the TSEM and the MDM methods. In this figure, the dashed line represents the case when the Taylor Series Expansion Method is used; the short-dashed line is the case when the Minimum Distance Method is used, while the solid curve is the plot of the real limit state curve. We see that the Taylor series Expansion Method might overestimate or underestimate the reliability depending on whether the failure surface is convex or concave. For this example, since it is concave, the Taylor Series Expansion Method underestimates the reliability since the smaller m value.

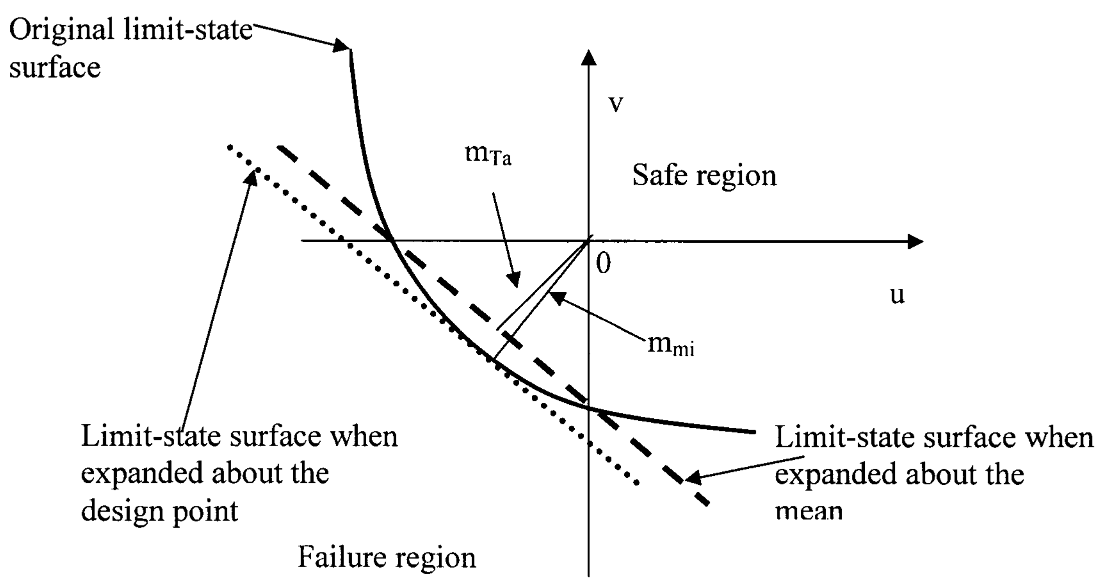

Fig. 2.5 - Comparison of Taylor Series Expansion Method with Minimum Distance Method.

In general, let's denote the performance function as

$$Z(X_1, X_2, ..., X_n) = f(X_1, X_2, ..., X_n)\,. \tag{2-17}$$

It should be noted that now the performance function 'f' is a nonlinear function of normally distributed variables X_i (i = 1,…, n). To use the MDM method, we need to change the original normally distributed variables, into what we call, the standard variables (some researchers call them reduced variables) using the following equation:

$$x_i = \frac{X_i - \overline{X}_i}{\sigma_{X_i}}. \tag{2-18}$$

Then, the performance function given by Eq. (2-17) becomes

$$Z(x_1, x_2, ..., x_n) = f(\overline{X}_1 + \sigma_1 x_1, \overline{X}_2 + \sigma_2 x_2, ..., \overline{X}_n + \sigma_n x_n).$$

Thus, the MDM method becomes an optimization problem, that is to find a $\vec{x}$ on the failure surface $f(\overline{X}_1 + \sigma_1 x_1, \overline{X}_2 + \sigma_2 x_2, ..., \overline{X}_n + \sigma_n x_n) = 0$ such that $\sqrt{\vec{x}^T \vec{x}}$ is minimized, where $\vec{x} = [x_1, x_2, ..., x_n]^T$. In other words, we need to find a point $(x_1^*, x_2^*, ..., x_n^*)$ on the failure surface such that if we expand the performance function about this point, we can obtain a linear performance function and then, the shortest distance of this line from the origin is the reliability index. Figure 2.5 illustrates this idea.

From the above, we see that the major problem for this method is how to find the design point. Many methods can be used to find this point. One of the widely used methods is the one proposed by Rackwitz, R. etc. [29, pp. 484-494].

If we assume that the design point on the failure surface is located at $\vec{X}^* = [X_1^*, X_2^*, ..., X_n^*]^T$, then the following procedures can be followed to find the product's reliability:

1. Set the mean value of each variable as the initial value of iteration.
2. Compute the following two quantities:

$$\frac{\partial f}{\partial x_i} = \sigma_{X_i} \frac{\partial f}{\partial X_i}\bigg|_{X_i^*}, \text{ and } a_i^* = \frac{\left(\frac{\partial f}{\partial X_i}\right)\bigg|_{X_i^*}}{\sqrt{\sum_{i=1}^{n}\left(\frac{\partial f}{\partial X_i}\right)^2\bigg|_{X_i^*}}}. \tag{2-19a}$$

3. Compute new X_i^* using the following equation:

$$X_i^* = \overline{X}_i - a_i^* \sigma_{X_i} m. \tag{2-19b}$$

4. Plug this new X_i^* into the constraint equation and solve for m.
5. Using this m compute

$$x_i^* = -a_i m. \tag{2-19c}$$

6. Repeat Step 2 to 5 until the desired accuracy is met.

It should be noted here that the capital letter represents the original variables, the small letter represents the standard variable. This method works well as long as the limit-state surface has only one minimal distance point and when it is nearly flat in the neighborhood of the design point. If the failure surface is not flat, a higher order approximation should be used. Breitung [30, pp. 357-366], Kiureghian [31, pp. 1208-1225] and other researchers discussed second order approximation method.

Grigoriu [32, pp. 155-165] introduced a control variable method and a linearization method to improve the accuracy of the quantified reliability.

In this dissertation, however, the Matlab software will be used to solve this optimization problem. Appendix C gives a sample Matlab code used for the optimization.

2.2.1.4.3 The Monte Carlo Simulation Method

The Monte Carlo Simulation (MCS) method is a powerful method for solving the nonlinear case problem. In this method, based on the distribution and its parameters of each variable, a random number, which follows that distribution, can be generated. For example, for any normal distribution with the mean μ and the standard deviation σ, the following equation can be used to obtain a random number which is normally distributed with the mean μ and the standard deviation σ.

$$\mu + \sigma \cdot U, \tag{2-20}$$

where

U = standard normally distributed value.

For other distributions, it is also easy to obtain the random number using different software, such as Matlab, Minitab etc. After obtaining the random number for each variable, substitute them into the performance function, and compute the Z value. Repeat this process N times (we suggest $N \geq 10{,}000$), record the number of times at which the Z value is greater than zero, then this number divided by N gives the reliability. Repeat this process M times (we suggest $M \geq 10$). Then, the reliability for the system can be obtained by averaging the M reliabilities. Figure 2.6 illustrates this process.

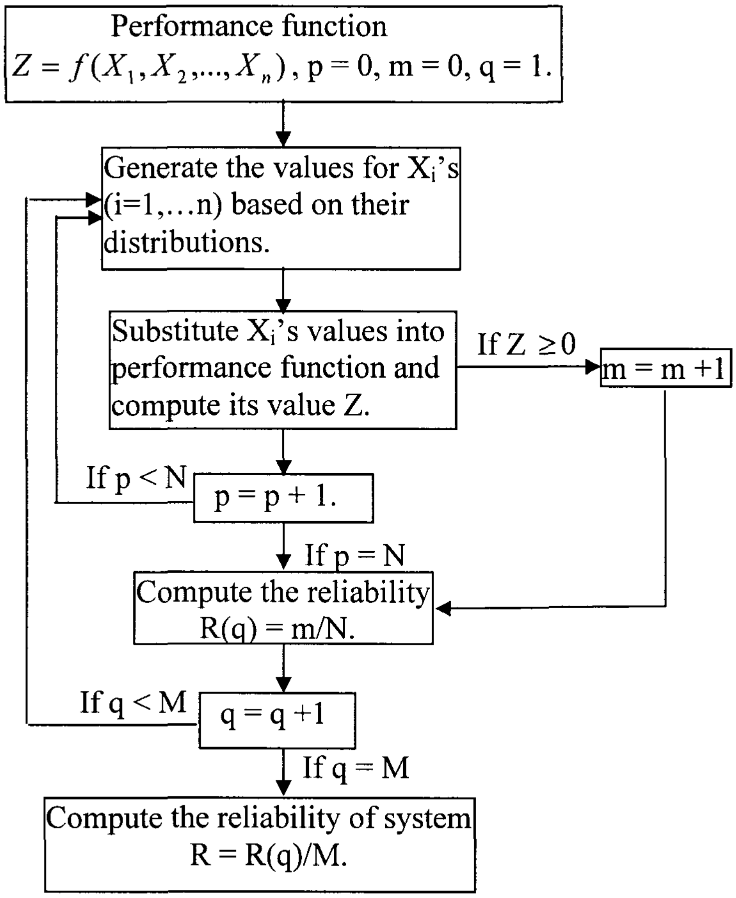

Fig.2.6 - Procedures for Monte Carlo simulation.

Example 2-3

Assume the performance function is given as follows: $Z = a \cdot b - c$ where $a \sim N(5,1)$, $b \sim N(10,1)$, and $c = 20$. Find the reliability of this product using the following methods.

a. Taylor Series Expansion.

b. Minimum Distance Method.

c. Monte Carlo Simulation.

Solution to Example 2-3

a. Taylor Series Expansion Method

Using Eqs. (2-15) and (2-16) yields,

$$\overline{Z} = \overline{a} \cdot \overline{b} - c = 5 \times 10 - 20 = 30,$$

and

$$\begin{aligned} \sigma_Z^2 &= \overline{a}^2 \sigma_a^2 + \overline{b}^2 \sigma_a^2, \\ &= 5^2 \times 1^2 + 10^2 \times 1^2, \end{aligned}$$

or

$$\sigma_Z^2 = 125\,.$$

Then, the reliability index is computed from Eq. (2-6)

$$m_{Ta} = \frac{30}{\sqrt{125}} = 2.683\,.$$

Then, using Eq. (2-7) yields,

$$R = \Phi(2.683) = 0.996352.$$

b. Minimum Distance Method

First let's rewrite the performance function as

$$Z = (\mu_a + \sigma_a\, u)(\mu_b + \sigma_b\, v) - c = \mu_a\, \mu_b - c + u\, \sigma_a\, \mu_b + v\, \sigma_b\, \mu_a + \sigma_a\, \sigma_b\, u\, v\,.$$

Then, the partial derivatives are

$$\frac{\partial Z}{\partial u} = \sigma_a\, b\,,\ \frac{\partial Z}{\partial v} = \sigma_b\, a\,.$$

Here u and v are standard variables of a and b.

For the first iteration, assume $a^* = 5$, and $b^* = 10$. Then,

$$\frac{\partial Z}{\partial u} = \sigma_a \, b^* = 1 \times 10 = 10,$$

and

$$\frac{\partial Z}{\partial v} = \sigma_b \, a^* = 1 \times 5 = 5.$$

Then, from Eq. (2-19a),

$$a_a^* = \frac{10}{\sqrt{10^2 + 5^2}} = 0.894,$$

and

$$b_a^* = \frac{5}{\sqrt{10^2 + 5^2}} = 0.447.$$

Therefore, the new components of design point are computed using Eq. (2-19b), or

$$a^* = \bar{a} - 0.894m = 5 - 0.894m,$$

and

$$b^* = \bar{b} - 0.447m = 10 - 0.447m.$$

Substituting these two values into the performance function equation Z = a b –c yields

$$0.4m^2 - 11.175\,m + 30 = 0.$$

Solving this equation yields

$$\text{m} = 3.0086.$$

Then, the new failure point becomes

$$a^* = \bar{a} - 0.894\,m = 5 - 0.894\,m = 2.310,$$

and

$$b^{*} = \bar{b} - 0.447\, m = 10 - 0.447\, m = 8.655.$$

Repeating this process and the results are given in Table 2.1.

Then, from Eq. (2-7), the reliability is obtained as

$$R = \Phi(2.933) = 0.9983.$$

Next, we use Matlab to compute the reliability index. Using Eq. (2-20) and changing variables yield the following performance function:

$$Z = (\bar{a} + \sigma_a\, u)(\bar{b} + \sigma_b\, v) - c = \bar{a}\,\bar{b} - c + \bar{a}\,\sigma_b\, v + \bar{b}\,\sigma_a\, u + \sigma_a\,\sigma_b\, u\, v,$$

or

$$Z = 30 + 5\, v + 10\, u + u\, v.$$

Now we need to find u and v such that $\sqrt{u^2 + v^2}$ is minimum, and u and v satisfy

$$Z = 30 + 5\, v + 10\, u + u\, v = 0.$$

Using Matlab we find that at u = -0.6549, and v =-2.8598, $\sqrt{u^2 + v^2}$ is minimum and equals to 2.9339. Then, the reliability index is

$$m_{mi} = 2.9339$$

Then, using Eq. (2-7) yields

R = 0.9983.

Appendix C lists the code used for the optimization.

Table 2.1 - Iteration results of Example 2-3.

Iteration no.	Variable	Values	$\frac{\partial Z}{\partial x_i}$	a_a^* a_b^*	New x^*	m
1	a	5	10	0.894	2.310	
	b	10	5	0.447	8.665	3.009
2	a	2.310	8.665	0.966	2.164	
	b	8.665	2.310	0.258	9.243	2.936
3	a	2.164	9.243	0.974	2.142	
	b	9.243	2.164	0.228	9.331	2.933
4	a	2.142	9.331	0.975		
	b	9.331	2.142	0.224		2.933

c. Monte Carlo Simulation

The performance function can be written as follow using Eq. (2-20), or

$$Z = (\bar{a} + \sigma_a\, u)(\bar{b} + \sigma_b\, v) - c,$$

or

$$Z = (5 + u)(10 + v) - 3,$$

where

u and v are standard normal variates. We can use Matlab to solve this problem. Table 2.2 lists the ten times (each run 10,000 times) reliability results and their average value. Appendix C gives the Matlab code used for this computation.

From the above, we see that the reliability obtained using the Taylor Series Expansion Method is 0.996352, the reliability from Minimum Distance Method is 0.9983, and the reliability from the Monte Carlo Simulation is 0.99834. We can conclude that the Taylor Series Expansion Method underestimates the reliability, and the Minimum Distance Method is more accurate than the Taylor Series Expansion Method.

Table 2.2 - Results of the Monte Carlo simulation for Example 2-3.

Number of run	Reliability
1	0.9989
2	0.9983
3	0.9983
4	0.9979
5	0.9984
6	0.9982
7	0.9982
8	0.9993
9	0.9980
10	0.9979
Average reliability	0.99834

It should be noted that one of the implicit assumptions associated with the Taylor Series Expansion Method and the Minimum Distance Method introduced previously is that each variable in the stress and strength equations is uncorrelated and normally distributed. If, in reality, that is not the case, some additional work should be done before using these two methods. In both cases, a transformation should be performed. Rackwitz [29, pp. 484-494] suggested a two-parameter transformation method to transforming the non-normal variables into equivalent normal variables. Chen and Lind [33, pp. 269-276] extended the Rackwitz method and proposed a three-parameter transformation algorithm. Wu and Wirsching [34, pp. 1,339 -1,336] further increased the accuracy of the equivalent normal transformation within the context of the three-parameter normal. Ang and Tang [35, 532 pp.], and Tang and Melchers [36, pp. 81-93] introduced a method to transform the correlated variates into uncorrelated variates through a covariance matrix.

2.2.2 Reliability Quantification for Multiple Failure Modes

In practice, there are many products which have more than one failure mode, and each failure mode might not be independent. In this case, there will be many limit-states or performance functions as shown in Fig. 2.5.

Consider a system with k potential failure modes, with performance functions given as

$$Z_i = f_i(X_1, X_2, \ldots, X_n),\ i = 1,2,\ldots,k.$$

Then, the system's reliability is computed using

$$R = P(\bigcap_{i=1}^{k}(Z_i \geq 0) = \int\int\cdots\int f_{X_1,X_2,\ldots,X_n}(x_1,x_2,\ldots,x_n)dx_1dx_2\cdots dx_n \ . \qquad (2\text{-}21)$$

This equation is very useful when the joint pdf is known or each performance function is independent. In the latter case, the system's reliability is computed from

$$R = \Phi(m_1)\Phi(m_2)\cdots\Phi(m_n)\ , \qquad (2\text{-}22)$$

where

m_i = reliability index for i^{th} failure mode.

However, in reality, rarely has the case arisen where the joint pdf of the performance function is known or each failure mode is independent. Therefore, Eq. (2-21) cannot be used directly.

To solve this problem, much research has been conducted aiming to simplify the computation of Eq. (2-21), such as Tang, L. K. et al [36, pp. 81-93], Hohenbichler, M., [37, pp. 177-188], Dolinski, K., [38, pp. 211-231], and

Ditlevsen,[39, pp. 453-472; 40, 412 pp.]. But so far, no method was developed to compute the exact value of the multiple integral. Meanwhile, finding the approximate value of Eq. (2-21) has obtained some progress. For example, Ditlevsen [39, pp. 453-472] proposed a narrow bound of reliability computation, and has been used to quantify the reliability of composite laminates [41, pp. 523-536]. Johnson [42, 333 pp.] summarizes the methods of calculating the multivariate distribution probability.

The two bounds of the system's reliability for a system with k failure modes are given by [39, pp. 453-472; 40, 412 pp.]

$$R_U = P(Z_1 \geq 0) - \sum_{i=2}^{k} \max\left\{ P(Z_i < 0) - \sum_{j=1}^{i-1} P[(Z_i < 0) \cap (Z_j < 0)],\ 0 \right\}, \tag{2-23}$$

and

$$R_L = 1 - \sum_{i=1}^{k} P(Z_i < 0) + \sum_{i=2}^{k} \max_{j<i} \quad P\left[(Z_i < 0) \cap (Z_j < 0)\right]. \tag{2-24}$$

Then,

$$R = \frac{1}{2}(R_U + R_L). \tag{2-25}$$

In Eqs. (2-23) and (2-24), we see that the only term unknown is $P(F_i \cap F_j)$. Here we use F_i and F_i to represent the two events of $Z_i < 0$ and $Z_i < 0$, respectively.

From previous discussion, we know we always can transform a non-normal distribution to a normal distribution, so here we can assume that the two performance functions are normally distributed. Therefore, $P(F_i \cap F_j)$ becomes a bi-normal failure probability.

The bivariate normal probability density function is given by [43, p. 79]

$$f(Z_i, Z_j) = \frac{1}{2\pi\,\sigma_{Z_i}\,\sigma_{Z_j}\sqrt{1-\rho^2}} \cdot \exp\left(-\frac{Q}{2(1-\rho^2)}\right),$$

where

$$Q = \frac{(Z_i - \overline{Z}_i)^2}{\sigma_{Z_i}^2} + \frac{(Z_j - \overline{Z}_j)^2}{\sigma_{Z_j}^2} - \frac{2\rho(Z_i - \overline{Z}_i)(Z_j - \overline{Z}_j)}{\sigma_{Z_i}\sigma_{Z_j}},$$

and

ρ = correlation coefficient of Z_i and Z_j.

Making the change of variables $u = (Z_i - \overline{Z}_i)/\sigma_{Z_i}$ and $v = (Z_j - \overline{Z}_j)/\sigma_{Z_j}$, then, $dZ_i = \sigma_{Z_i} du$ and $dZ_j = \sigma_{Z_j} dv$. Thus, $P(F_i \cap F_j)$ can be computed as,

$$P(F_i \cap F_j) = \int_{-\infty}^{0}\int_{-\infty}^{0} f(Z_i, Z_j)\,dZ_i\,dZ_j,$$

or

$$P(F_i \cap F_j) = \int_{-\infty}^{-m_1}\int_{-\infty}^{-m_2} \frac{1}{2\pi\sqrt{1-\rho^2}} \exp\left(-\frac{u^2 - 2\,r\,u\,v + v^2}{2(1-\rho^2)}\right) du\,dv.$$

It can be proved that [44, p. 102] [45, pp. 1,075-1,090] the above integral is equal to

$$P(F_i \cap F_j) = \frac{1}{2\pi}\int_0^{\rho} \frac{1}{\sqrt{1-r^2}} \exp\left(-\frac{m_1^2 - 2\,r\,m_1\,m_2 + m_2^2}{2\,(1-r^2)}\right) dr + \Phi(-m_1)\cdot\Phi(-m_2), \quad (2\text{-}26)$$

or

$$P(F_i \cap F_j) = \int_0^{\rho} w(-m_1, -m_2, r)\, dr + \Phi(-m_1)\Phi(-m_2), \tag{2-27}$$

where

$$w(u, v, \rho) = \frac{1}{2\pi\sqrt{1-\rho^2}} \exp\left(-\frac{u^2 - 2\rho\, u\, v + v^2}{2(1-\rho^2)}\right) \tag{2-28}$$

Appendix D gives the proof of this equation.

For a bivariate normal distribution, the reliability and the cdf have the following relation [44, p. 102]:

$$\Phi = R + \Phi(m_1) + \Phi(m_2) - 1.$$

Then, considering $\Phi(-m) = 1 - \Phi(m)$, the reliability for the bivariate normal case is

$$R = \int_0^{\rho} w(-m_1, -m_2, r)\, dr + \Phi(m_1) \cdot \Phi(m_2). \tag{2-29}$$

This equation will be used to compute the product's reliability when there are two dependent failure modes in the products.

If ρ is small (< 0.6) or 0.1% error is acceptable, the following approximate equation [44, p. 102] can be used to calculate the reliability:

$$\begin{aligned} R = \frac{\rho}{18} \cdot (5 \cdot w\left(-m_1, -m_2, \left(1-\sqrt{3/5}\right)\rho/2\right) + 8 \cdot w\left(-m_1, -m_2, \rho/2\right) \\ + 5 \cdot w\left(-m_1, -m_2, \left(1+\sqrt{3/5}\right)\rho/2\right) + \Phi(m_1) \cdot \Phi(m_2), \end{aligned} \tag{2-30}$$

where function w is as defined previously.

In this equation, the *m* values can be found through the MDM method. The correlation coefficient can be found as follows [35, 562 pp.]:

$$\rho_{ij} = \frac{\sum_{i=1}^{n}\left(\frac{\partial f_i}{\partial x_i}\right)_*\left(\frac{\partial f_j}{\partial x_i}\right)_*}{\sqrt{\sum_{i=1}^{n}\left(\frac{\partial f_i}{\partial x_i}\right)_*^2}\sqrt{\sum_{i=1}^{n}\left(\frac{\partial f_j}{\partial x_i}\right)_*^2}}, \tag{2-31}$$

where * represent using the values of the design point.

Considering $\frac{\partial f}{\partial x} = \frac{\partial f}{\partial X}\frac{\partial X}{\partial x} = \sigma\frac{\partial f}{\partial X}$, where X represents the basic variable and x represents the standard variable, Eq. (2-31) becomes

$$\rho_{ij} = \frac{\sum_{i=1}^{n}\left(\frac{\partial f_i}{\partial X_i}\right)_*\left(\frac{\partial f_j}{\partial X_i}\right)_*\sigma_{X_i}^2}{\sqrt{\sum_{i=1}^{n}\left(\frac{\partial f_i}{\partial X_i}\right)_*^2\sigma_{X_i}^2}\sqrt{\sum_{i=1}^{n}\left(\frac{\partial f_j}{\partial X_i}\right)_*^2\sigma_{X_i}^2}}. \tag{2-32}$$

2.3 Residual Strength Determination

Residual strength is the remaining strength of a material, or a structure, after a time of usage. In the MSSI method, we assume that the strength distribution type and its standard deviation do not change with time, but its mean strength value does decrease with time as shown in Fig. 2.7. It should be pointed out that in this figure, the mean strength decreases linearly, but in reality it can change following any distribution. The method proposed in this dissertation can apply to any distribution.

The following model is proposed in this dissertation to compute the mean residual strength:

$$\overline{S} = S_I(1-D), \tag{2-33}$$

where

$\bar{S}$ = mean residual strength,

S_I = initial mean strength,

and

D = total strength damage caused by all stresses after a certain period of usage. It is in decimals and can be calculated using Eq. (2-35).

From Eq. (2-33), we can see that finding the total damage becomes the key to obtain the residual strength.

The current commonly used method for determining the damage is due to Miner's work [46, p. A160], which is expressed as

$$D = \sum_{i=1}^{m} \frac{n_i}{N_i}, \tag{2-34}$$

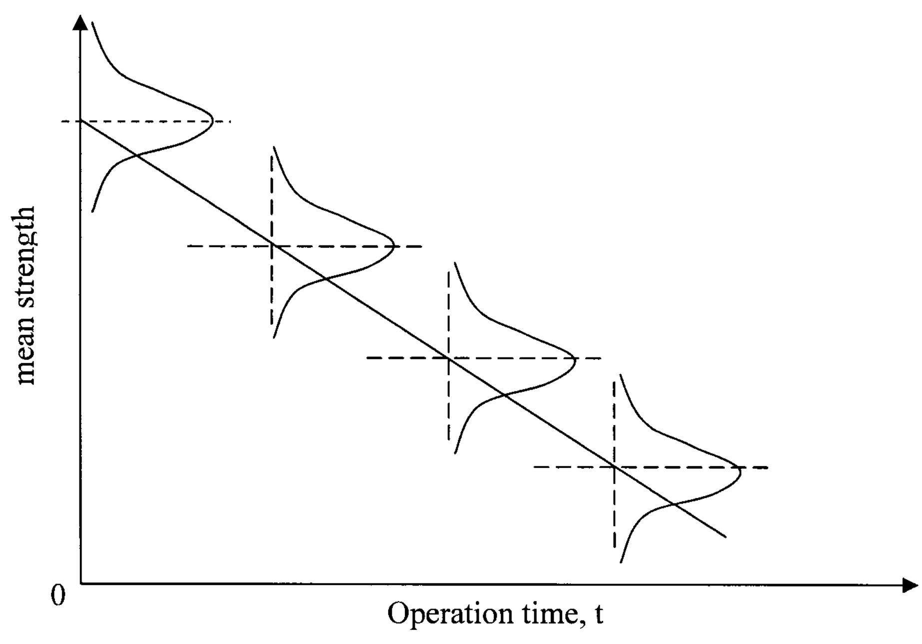

Fig. 2.7 – Mean strength changes with time.

where

D = damage in decimals,

n_i = number of cycles experienced at stress level "i",

N_i = number of cycles to failure at stress level "i",

and

m = total number of stress levels.

Following Miner's work, several damage models have been proposed to predict the residual strength of a fatigued structure. Wahl [47, p. 2] proposed a residual strength equation for fiberglass laminate based on Miner's rule. Cesare and Sues [48, p. 8] introduced a probabilistic material degradation model that considers thermal fatigue, creep, and high cycle mechanical fatigue effects. Xin and his co-workers [49, p. 836] established a damage model by using a tensile bar and considering its normal strain, and elastic limit strain. Rodin [50, p.1] compares Kachanov's continuum damage mechanics model for different cases. Schaff and his co-worker [51, pp.128-157; 52, pp. 158-181] developed a strength-based wear-out model to predict the residual strength of composite laminate by assuming that the residual strength distribution follows a two-parameter Weibull distribution. These models have been used in different cases. Curtis and Davies [53, p. 8] reviewed the past major works on fatigue life prediction, including damage models.

However, there are two major issues that Miner's rule, or its derivative models mentioned above, missed to consider. Firstly, none of the models considers the interaction between the different kinds of stresses, and most of the models even only considered one kind of stress with different levels. Secondly, no model considers the effect of the loading sequence. In reality, a structure or a product may experience many kinds of stresses acting simultaneously, such as thermal and vibration, and the contribution to strength loss due to these stresses interacts with each other. On top of that, different loading sequences will cause different damage. We can prove that the damage caused by the same load, but applied at different time will be different. The only exception is when the time to failure distribution follows the exponential distribution.

In this dissertation, a new model is proposed which considers multiple stresses, their interactions, and the loading sequence effects.

The proposed damage model has the similar format as Miner's rule but with different implications. The model is

$$D = \sum_{i=1}^{m} C_i \cdot \left(\frac{t_{i1eq}}{T_{i1}} \right)^{v(i)}, \tag{2-35}$$

where

D = damage,

m = number of different stresses,

C_i = interaction coefficient between stresses, to be obtained by testing,

t_{i1eq} = equivalent time at the 1st stress level for the ith kind of stress if the total operation time under a different stress level for the ith stress is t (see Fig. 2-8), the 1st stress level is the level to be used as the basis to convert all the other stress levels,

T_{i1} = mean time between failures of the product when it is under stress level 1 for the i^{th} kind of stress, or reliable life for a given reliability level,

and

v(i) = nonlinear degradation exponent for the i^{th} kind of stress, v(i) < 1 means a great loss of strength in the early stage of fatigue, v(i) = 1 means linear loss of strength, and v(i) > 1 means little loss of strength in the early stage and great loss at the later stage. It needs to be determined from tests.

Figure 2.8 illustrates an example of a stress profile for the i^{th} kind of stress.

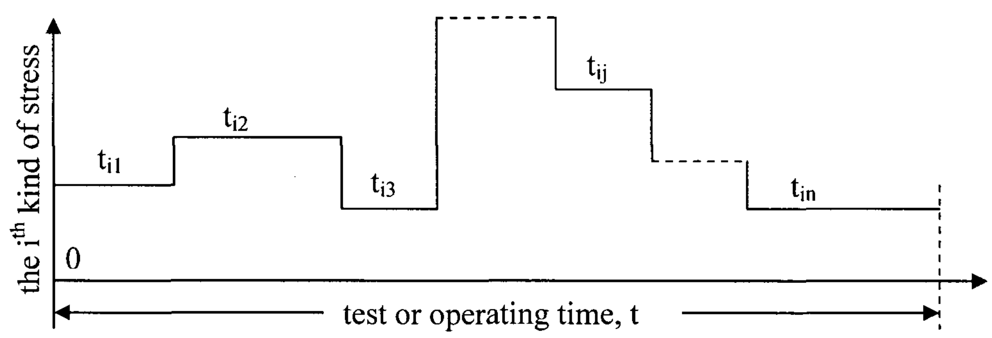

Fig. 2.8 - An example of a stress profile for the i^{th} kind of stress.

From Fig. 2.8, we see $t = t_{i1} + t_{i2} + \cdots + t_{ij} + \cdots + t_{in}$. It should be noted that t_{ik} (k = 1, …, n(i)) can be at the same stress level with t_{ij} (j = 1, …,n(i)), for $k \neq j$. Also, it should be noted that n(i) may be different for different kinds of stresses. We cannot directly use "t" to find the damage since it involves different stress levels. Therefore, we need to find out the equivalent time for "t" if the product is operated only at Stress Level 1 instead of at different stress levels. Which stress level is chosen to be the basis for the conversion is arbitrary. The reason of choosing Stress Level 1 in this dissertation is for the sake of convenience and simplicity.

The basic idea of finding the equivalent time is based on the belief that the failure probability (or reliability) should be the same for the two times of operation at different stress levels to be equivalent.

There are two cases involved in the determination of the equivalent time. Case 1 is when the time to failure distribution for the product is known; Case 2 is when only the mean strength distribution is known.

2.3.1 When the Time to Failure Distribution for the Product is Known

We assume that at each stress level, the time-to- failure follows a certain distribution with probability density function of $f_j(t)$, j = 1, ..., n(i). If we denote $t_{ij}^{(k)}$ as the equivalent time for t_{ij} at stress level k, then the problem becomes to find out

$$t_{i1eq} = t_{i1} + t_{i2}^{(1)} + t_{i3}^{(1)} + \cdots + t_{ij}^{(1)} + \cdots + t_{in}^{(1)} . \tag{2-36}$$

From Fig. 2.8 and using the equivalent time idea, we have

$$\int_0^{t_{i1}} f_1(t)dt = \int_0^{t_{i1}^{(2)}} f_2(t)dt , \tag{2-37}$$

$$\int_0^{t_{i1}+t_{i2}^{(1)}} f_1(t)dt = \int_0^{t_{i2}+t_{i1}^{(2)}} f_2(t)dt , \tag{2-38}$$

Solving Eq. (2-37) yields $t_{i1}^{(2)}$. Substituting it into Eq. (2-38) yields $t_{i2}^{(1)}$. Then, Fig. 2.8 can be equivalent to Fig. 2.9.

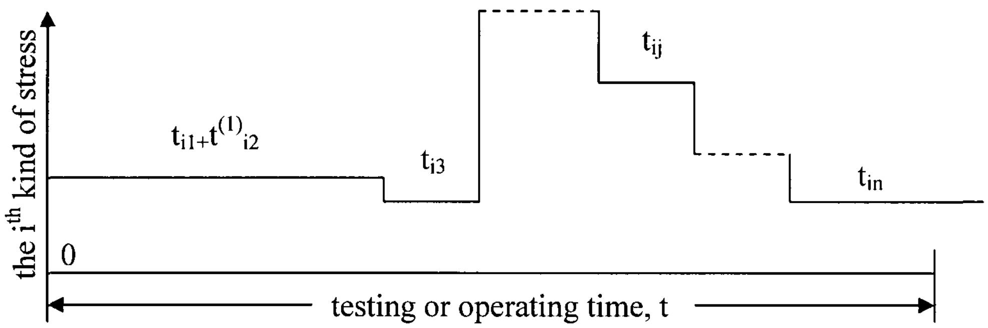

Fig. 2.9 – Equivalent diagram of Fig. 2.8 after t_{i2} has been converted to $t_{i2}^{(1)}$.

Repeating this process, we can have the following general equations:

$$\int_0^{t_{i1}+t_{i2}^{(1)}+\cdots+t_{i(j-1)}^{(1)}} f_1(t)\,dt = \int_0^{t^{(j)}_{i1+i2+\cdots+i(j-1)}} f_j(t)\,dt, \tag{2-39}$$

and

$$\int_0^{t_{i1}+t_{i2}^{(1)}+\cdots+t_{i(j-1)}^{(1)}+t_{ij}^{(1)}} f_1(t)\,dt = \int_0^{t^{(j)}_{i1+i2+\cdots+i(j-1)}+t_{ij}} f_j(t)\,dt. \tag{2-40}$$

Solving this system of equations, we can find t_{i1eq}.

T_{i1} can be found using mean value equation as

$$T_{i1} = \int_0^{\infty} t\, f_1(t)\,dt, \tag{2-41}$$

if the mean time between failures is used, or T_{i1} can be found from the generalized reliability equation [22, p. 198]

$$\ln R = -\int_0^{T_{i1}} \lambda(t)dt, \tag{2-42}$$

if the reliable life is used, where R is the given reliability, and $\lambda(t)$ is the failure rate.

Then, using Eq. (2-35), we can find the damage caused by the i^{th} kind of stress.

If the mean strength follows the exponential distribution, we can prove that the contribution of different stress levels to the damage of the strength is independent of the time when the stress is applied. For other distributions, the time when stress is applied will affect its contribution to the damage of the strength.

2.3.2 When the Mean Strength Distribution is Known

As we pointed out previously, the equivalent time calculation requires that the reliability be the same. Then, using Eq. (2-6) yields

$$m_1 = \frac{\bar{S}_1 - \bar{s}_1}{\sqrt{\sigma_S^2 + \sigma_{s_1}^2}} = \frac{\bar{S}_2 - \bar{s}_2}{\sqrt{\sigma_S^2 + \sigma_{s_2}^2}}, \tag{2-43}$$

or

$$\bar{S}_2 = m_1 \cdot \sqrt{\sigma_S^2 + \sigma_{s_2}^2} + \bar{s}_2, \tag{2-44}$$

If we assume that the initial strength is S_I, then

$$\bar{S}_1 = S_I \left(1 - \frac{t_1}{\int_0^\infty t \cdot f_1(t) dt} \right), \tag{2-45}$$

and

$$\bar{S}_2 = S_I \left(1 - \frac{t_e}{\int_0^\infty t \cdot f_2(t) dt} \right), \tag{2-46}$$

where

f_i = pdf of the mean strength distribution, i =1, 2.

Then, substituting Eqs. (2-45) and (2-46) into Eq. (2-43) yields

$$t_e = \left[1 - \frac{1}{S_I}\left(\frac{\sqrt{\sigma_S^2 + \sigma_{s_2}^2}\left(\bar{S}_1 - \bar{s}_1\right)}{\sqrt{\sigma_S^2 + \sigma_{s_1}^2}} + \bar{s}_2\right)\right]\int_0^{\infty} t \cdot f_2(t)dt,$$

or

$$t_e = \left[1 - \frac{1}{S_I}\left(\sqrt{\sigma_S^2 + \sigma_{s_2}^2}\, m_1 + \bar{s}_2\right)\right]\int_0^{\infty} t \cdot f_2(t)dt. \quad (2\text{-}46)$$

For more than two stress levels, repeating the above steps, the equivalent time can be found. Then, using Eq. (2-35), we can find the damage.

CHAPTER 3

DEFLECTION AND STRESS RESPONSE OF LAMINATE BOARDS SUBJECTED TO VIBRATION AND THERMAL LOADS

3.1 Modeling of PCB Subjected to Vibration

In reality, the vibration is not directly exerted on the PCB, but on the chassis on which the PCB is installed. Also to reduce the effect of vibration on PCBs, a cushion is used between the PCB and the chassis. Therefore, when modeling a plate which is subjected to vibration, these conditions should be taken into account. Figure 3.1 illustrates a two-step model of a PCB subjected to vibration using a two degrees of freedom spring damper system.

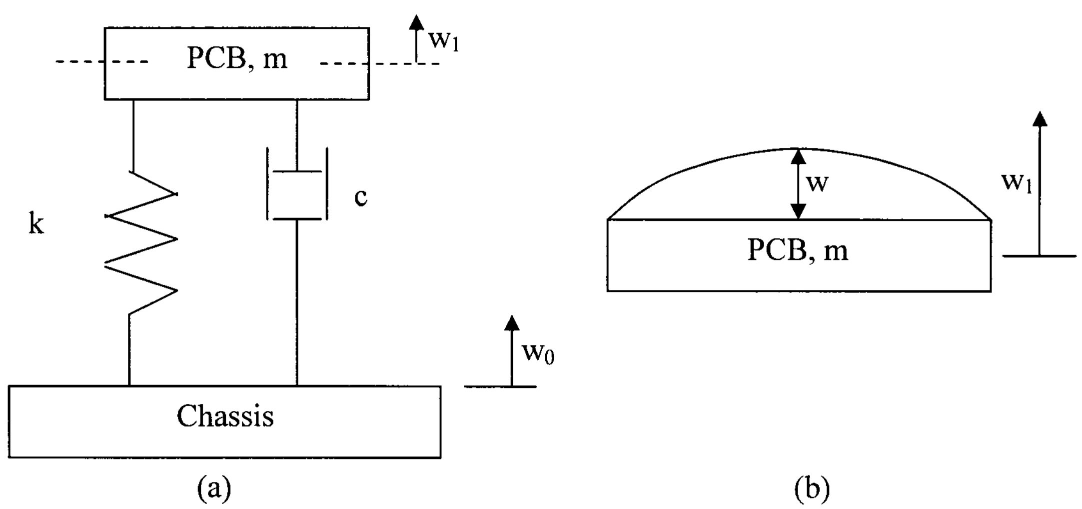

Fig. 3.1 - Two-step model of PCB subjected to vibration

The model illustrated in Fig. 3.1(a) is a standard one-degree of freedom system with a moving support [54, 521 pp.]. Its equation of motion is given by

$$m\,\ddot{w}_1 + k(w_1 - w_o) + c(\dot{w}_1 - \dot{w}_0) = 0\,, \tag{3-1}$$

where

w_0 = absolute displacement of the chassis,

w_1 = absolute displacement of the board,

$\ddot{w}_1$ and $\ddot{w}_0$ = second derivative of w_1 and w_0 with respect to time, respectively,

$\dot{w}_1$ and $\dot{w}_0$ = first derivative of w_1 and w_0 with respect to time, respectively,

k = spring constant,

c = coefficient of viscous damping,

and

m = mass of the board.

If we change the variable as $w^* = w_1 - w_0$, then, Eq.(3-1) becomes,

$$m(\ddot{w}^* + \ddot{w}_0) + c\,\dot{w}^* + k\,w^* = 0,$$

or

$$m\,\ddot{w}^* + c\,\dot{w}^* + k\,w^* = -m\,\ddot{w}_0.$$

Dividing both side by m yields

$$\ddot{w}^* + \frac{c}{m}\dot{w}^* + \frac{k}{m}w^* = -\ddot{w}_0. \tag{3-2}$$

Using the notations

$p^2 = \frac{k}{m}$, and $2\eta = \frac{c}{m}$, where p is the circular natural frequency of vibration,

we obtain the following standard form of the vibration equation:

$$\ddot{w}^* + 2\eta\,\dot{w}^* + p^2 w^* = -\ddot{w}_0. \tag{3-3}$$

The solution of Eq.(3-3) includes two parts, one is homogeneous solution; the other is a particular solution.

The homogeneous solution of the Eq. (3-3) can be found from any vibration book, or

$$w_H^* = e^{-\eta t}(C_1 \cos(p_d t) + C_2 \sin(p_d t)), \tag{3-4}$$

where

$p_d = \sqrt{p^2 - \eta^2}$, angular frequency of damped vibration.

The particular solution of the Eq. (3-3) can be found using Duhamel's integral method [54, p.98] [55, p. 67]

$$w_P^* = \frac{e^{-\eta t}}{p_d} \int_{-\infty}^{t} e^{\eta t'}(-\ddot{w}_0(t'))\sin(p_d(t-t'))\,dt',$$

or

$$w_P^* = -\frac{e^{-\eta t}}{p_d} \int_{-\infty}^{t} e^{\eta t'}\ddot{w}_0(t')\sin(p_d(t-t'))\,dt', \tag{3-5}$$

For the homogeneous solution given in Eq. (3-4), we see that when t becomes large, this term is died out. Therefore, the dominating term for vibration is the particular solution given by Eq. (3-5). Thus, we will just take the particular solution as the solution of Eq. (3-3) for this dissertation. Then,

$$w^*(t) = -\frac{e^{-\eta \cdot t}}{p_d} \int_{-\infty}^{t} e^{\eta \cdot t'}\ddot{w}_0(t')\sin(p_d(t-t'))\,dt'. \tag{3-6}$$

Denote

$$h(t) = \frac{e^{-\eta \cdot t}}{p_d}\sin(p_d t). \tag{3-7}$$

It is easy to prove that Eq. (3-7) is actually the solution of Eq. (3-3) when $-\ddot{w}(t)$ is a delta function.

Then, Eq. (3-6) becomes

$$w^*(t) = -\int_{-\infty}^{t} \ddot{w}_0(t')\, h(t-t')\, dt' . \tag{3-8}$$

Changing variable $t - t' = \tau$, and considering that $dt' = -d\tau$, Eq. (3-8) becomes

$$w^*(t) = -\int_{0}^{\infty} \ddot{w}_0(t-\tau)\, h(\tau) d\tau . \tag{3-9}$$

Next, let's find the moments of $w^*(t)$, since they will be used for the reliability computation.

The mean value of $w^*(t)$ is

$$E\left(w^*(t)\right) = -\int_{0}^{\infty} E\left(\ddot{w}_0(t-\tau)\right)\, h(\tau)\, d\tau . \tag{3-10}$$

In practice, vibration in many cases is a stationary process. For example, when a PCB is installed in a vehicle which drives on the road, the excitation can be considered as a stationary process [56, 166 pp.]. Thus, we can assume that $-\ddot{w}(t)$ is a stationary process. Therefore,

$$\mu(t+\tau) = \mu(t),\ K_{XX}(t_1 + r, t_2 + r) = K_{XX}(t_1, t_2),$$

where

$\mu(\bullet)$ = mean value function,

and

$K_{XX}(\bullet)$ = auto-covariance function of the stochastic process.

Using this relation in Eq. (3-10) yields

$$E(w^*) = -\int_0^\infty E(\ddot{w}_0(t-\tau))\,h(\tau)\,d\tau,$$

$$= -E(\ddot{w}_0(t))\int_0^\infty h(\tau)\,d\tau,$$

or

$$E(w^*) = -\frac{E(\ddot{w}_0(t))}{p^2}. \tag{3-11}$$

From the stochastic derivative [55, p. 38], we know

$$E(\dot{w}^*) = \frac{d(E(w^*))}{dt} = 0,$$

since $-\ddot{w}(t)$ is a stationary process.

The auto-correlation of $w^*(t)$ is [55, p. 71]

$$R_{w^*w^*}(\tau) = E[w^*(t+\tau)\,w^*(t)] = \int_0^\infty\int_0^\infty R_{\ddot{w}_0\ddot{w}_0}(\tau + r_2 - r_1)\,h(r_1)\,h(r_2)\,dr_1\,dr_2\,, \tag{3-12}$$

Similarly, the auto-correlation of $\dot{w}^*(t)$ is

$$R_{\dot{w}^*\dot{w}^*}(\tau) = E[\dot{w}^*(t+\tau)\,\dot{w}^*(t)] = \int_0^\infty\int_0^\infty R_{\ddot{w}_0\ddot{w}_0}(\tau + r_2 - r_1)\,\dot{h}(r_1)\,\dot{h}(r_2)\,dr_1\,dr_2\,, \tag{3-13}$$

and the cross-correlation of $w^*(t)$ and $\dot{w}^*(t)$ is

$$R_{w^*\dot{w}^*}(\tau) = E[w^*(t+\tau)\,\dot{w}^*(t)] = \int_0^\infty\int_0^\infty R_{\ddot{w}_0\ddot{w}_0}(\tau + r_2 - r_1)\,h(r_1)\,\dot{h}(r_2)\,dr_1\,dr_2\,, \tag{3-14}$$

and

$$R_{\dot{w}^* w^*}(\tau) = E\left[w^*(t+\tau)\,\dot{w}^*(t)\right] = \int_0^\infty\int_0^\infty R_{\ddot{w}_0\ddot{w}_0}(\tau + r_2 - r_1)\,\dot{h}(r_1)\,h(r_2)\,dr_1\,dr_2\ . \tag{3-15}$$

It can be proved that $R_{w^*\dot{w}^*}(\tau) = -R_{\dot{w}^* w^*}(\tau)$.

Next let us find the moment of $\ddot{w}_1(t)$.

We know that

$$\ddot{w}_1(t) = \ddot{w}^*(t) + \ddot{w}_0(t) = -(2\,\eta\,\dot{w}^* + p^2 w^*)\,.$$

Then,

$$E(\ddot{w}_1(t)) = -2\,\eta\,E\left(\dot{w}^*\right) - p^2 E(w^*) = E(\ddot{w}_0(t))\,. \tag{3-16}$$

Therefore, we see that $\ddot{w}_1(t)$ is also a stationary process. The auto-covariance of $\ddot{w}_1(t)$ is

$$\begin{aligned}
G_{\ddot{w}_1\ddot{w}_1}(\tau) &= E\left[\left(\ddot{w}_1(t+\tau) - \mu_{\ddot{w}_1}(t+\tau)\right)\left(\ddot{w}_1(t) - \mu_{\ddot{w}_1}(t)\right)\right] \\
&= E\left[\left(\ddot{w}_1(t+\tau)\,\ddot{w}_1(t)\right)\right] - \left[E(\ddot{w}_0)\right]^2, \\
&= E(4\,\eta^2\,\dot{w}^*(t+\tau)\,\dot{w}^*(t) + 2\,\eta\,p^2(w^*(t+\tau)\,\dot{w}^*(t) + \dot{w}^*(t+\tau)\,w^*(t)) \\
&\quad + p^4 w^*(t+\tau)\,w^*(t)) - \left[E(\ddot{w}_0)\right]^2, \\
&= 4n^2 E\left[\dot{w}^*(t+\tau)\,\dot{w}^*(t)\right] + 2\,\eta\,p^2\left[E\left\{w^*(t+\tau)\,\dot{w}^*(t)\right\} + E\left\{\dot{w}^*(t+\tau)\,w^*(t)\right\}\right] \\
&\quad p^4 E\left[w^*(t+\tau)\,w^*(t)\right] - \left[E(\ddot{w}_0)\right]^2,
\end{aligned}$$

or

$$G_{\ddot{w}_1\ddot{w}_1}(\tau) = 4\,\eta^2\,R_{\dot{w}^*\dot{w}^*}(\tau) + p^4\,R_{w^*w^*}(\tau) - \left[E(\ddot{w}_0)\right]^2, \tag{3-17}$$

where $R_{w^*w^*}(\tau)$ and $R_{\dot{w}^*\dot{w}^*}(\tau)$ are given by Eqs. (3-12) and (3-13), respectively.

In Eq. (3-17), the auto-covariance gives the variance when τ is zero. Then,

$$\sigma^2_{\ddot{w}_1} = G_{\ddot{w}_1\ddot{w}_1}(0) = 4\,\eta^2\,R_{\dot{w}^*\dot{w}^*}(0) + p^4\,R_{w^*w^*}(0) - \left[E(\ddot{w}_0)\right]^2. \tag{3-18}$$

In this dissertation, we consider the vibration is an ideal white noise excitation and a stationary process. Then,

$$R_{\ddot{w}_0 \ddot{w}_0}(\tau) = 2\,\pi\, S_0\, \delta(\tau)\,, \tag{3-19}$$

and

$$E(\ddot{w}_0) = 0. \tag{3-20}$$

Substituting Eq. (3-19) into Eqs. (3-12), (3-13), (3-14), and (3-15) yields

$$\begin{aligned}
R_{w^* w^*}(\tau) &= \int_0^\infty \int_0^\infty R_{\ddot{w}_0 \ddot{w}_0}(\tau + r_2 - r_1)\, h(r_1)\, h(r_2)\, dr_1\, dr_2, \\
&= 2\,\pi\, S_0 \int_0^\infty \int_0^\infty \delta(\tau + r_2 - r_1)\, h(r_1)\, h(r_2)\, dr_1\, dr_2, \\
&= 2\,\pi\, S_0 \int_0^\infty h(r_1) \left[\int_0^\infty h(r_2)\, \delta[r_2 - (r_1 - \tau)]\, dr_2 \right] dr_1, \\
&= 2\,\pi\, S_0 \int_0^\infty h(r_1)\, h(r_1 - \tau)\, dr_1,
\end{aligned}$$

or

$$R_{w^* w^*}(\tau) = 2\,\pi\, \mathrm{S}_0 \int_0^\infty h(r)\, h(r - \tau)\, dr, \tag{3-21}$$

where h(r) is defined in Eq. (3-7).

To reach this result, we used the property of the delta function,

$$\int_a^b f(x)\, \delta(x - x_0) = \begin{cases} f(x_0), & a < x_0 < b \\ 0, & \text{otherwise,} \end{cases}$$

and change the dummy variable.

Similarly, we can get

$$R_{\dot{w}^*\dot{w}^*}(\tau) = \int_0^\infty\int_0^\infty R_{\ddot{w}_0\ddot{w}_0}(\tau + r_2 - r_1)\,\dot{h}(r_1)\,\dot{h}(r_2)\,dr_1\,dr_2,$$

or

$$R_{\dot{w}^*\dot{w}^*}(\tau) = 2\,\pi\,S_0\int_0^\infty \dot{h}(r)\,\dot{h}(r-\tau)\,dr, \tag{3-22}$$

$$R_{w^*\dot{w}^*}(\tau) = \int_0^\infty\int_0^\infty R_{\ddot{w}_0\ddot{w}_0}(\tau + r_2 - r_1)\,h(r_1)\,\dot{h}(r_2)\,dr_1\,dr_2,$$

or

$$R_{w^*\dot{w}^*}(\tau) = 2\,\pi\,S_0\int_0^\infty h(r)\,\dot{h}(r-\tau)\,dr, \tag{3-23}$$

and

$$R_{\dot{w}^*w^*}(\tau) = \int_0^\infty\int_0^\infty R_{\ddot{w}_0\ddot{w}_0}(\tau + r_2 - r_1)\,\dot{h}(r_1)\,h(r_2)\,dr_1\,dr_2,$$

or

$$R_{\dot{w}^*w^*}(\tau) = 2\,\pi\,S_0\int_0^\infty \dot{h}(r)\,h(r-\tau)\,dr. \tag{3-24}$$

The integrals involved in Eqs. (3-21), (3-22), (3-23), and (3-24) can be found easily [55, 509 pp.]. Then, Eqs. (3-21) – (3-24) become

$$R_{w^*w^*}(\tau) = \frac{\pi\,S_0}{2\,\eta\,p^2}e^{-\eta|\tau|}\left[\cos(p_d\tau) + \frac{\eta}{p_d}\sin(p_d|\tau|)\right], \tag{3-25}$$

$$R_{\dot{w}^*\dot{w}^*}(\tau) = \frac{\pi\,S_0}{2\,\eta}e^{-\eta|\tau|}\left[\cos(p_d\tau) - \frac{\eta}{p_d}\sin(p_d|\tau|)\right], \tag{3-26}$$

$$R_{w^* \dot{w}^*}(\tau) = \frac{\pi S_0}{2\eta\, p_d} e^{-\eta|\tau|} \sin(p_d \tau), \tag{3-27}$$

and

$$R_{\dot{w}^* w^*}(\tau) = -R_{\dot{w}^* w^*}(\tau) = -\frac{\pi S_0}{2\eta\, p_d} e^{-\eta|\tau|} \sin(p_d \tau). \tag{3-28}$$

Substituting Eqs. (3-20), (3-25) and (3-26) into Eq. (3-18) yields

$$G_{\ddot{w}_1 \ddot{w}_1}(\tau) = R_{\ddot{w}_1 \ddot{w}_1}(\tau) = 4\eta^2\, R_{\dot{w}^* \dot{w}^*}(\tau) + p^4\, R_{w^* w^*}(\tau),$$

or

$$G_{\ddot{w}_1 \ddot{w}_1}(\tau) = 2\eta\, \pi\, S_0\, e^{-\eta|\tau|} \left[\frac{4\eta^2 + p^2}{4\eta^2} \cos(p_d \tau) + \frac{1}{4\eta} \sin(p_d |\tau|) \right]. \tag{3-29}$$

Then, the variance of $\ddot{w}_1(t)$ is obtained by letting $\tau = 0$, which gives

$$\sigma^2_{\ddot{w}_1 \ddot{w}_1} = \frac{4\eta^2 + p^2}{2\eta} \pi\, S_0. \tag{3-30}$$

Since $2\eta = c/m$ and $p^2 = k/m$, Eq. (3-30) becomes

$$\sigma^2_{\ddot{w}_1 \ddot{w}_1} = \frac{\left(\frac{c}{m}\right)^2 + \frac{k}{m}}{\frac{c}{m}} \pi\, S_0 = \frac{c^2 + k\, m}{c\, m} \pi\, S_0. \tag{3-31}$$

3.2 The Deflection and the Stress Determination of the PCB Subjected to Vibration and Thermal Loads

3.2.1 Deflection Determination

For a thin laminate composite board, shown in Fig. 3.2, the equation of motion governing deflection of an orthotropic laminate is given by

$$D_{11}\frac{\partial^4 w}{\partial x^4}+2(D_{12}+2D_{22})\frac{\partial^4 w}{\partial x^2 \partial y^2}+D_{66}\frac{\partial^4 w}{\partial y^4}+c_1\dot{w}+I_0\ddot{w}=-I_0\ddot{w}_1\,, \tag{3-32}$$

where

D_{ij} = bending stiffness, $D_{ij} = \frac{1}{3}\sum_{k=1}^{N} Q_{ij}\left(z_{k+1}^3 - z_k^3\right)$,

Q_{ij} = lamina stiffness, they are given by

$$Q_{11} = \frac{E_1}{1-v_{12}\,v_{21}},\ Q_{12} = \frac{v_{12}\,E_2}{1-v_{12}\,v_{21}},\ Q_{22} = \frac{E_2}{1-v_{12}\,v_{21}},\ \text{and}\ Q_{66} = G_{12}\,,$$

I_0 = mass moments of inertia, $I_0 = \sum_{k=1}^{L} \rho^{(k)}(z_{k+1} - z_k)$, $\rho^{(k)}$ is mass density of the k^{th} layer, L is the total number of layers,

c_1 = damping coefficient of the PCB,

w = deflection of the midplane of the board,

and

w_1 = absolute displacement of the board support due to vibration as investigated in Section 3.2.1.

Eq. (3-32) is a forced composite laminate vibration equation. A similar equation has been widely used in describing the motion of a plate under free and forced vibration or static bending. Many methods have been developed to solve this kind of equation. The most commonly used methods of solving Eq. (3-32) type of an equation are the Navier method, the Levy method and the Rayleigh-Rize method based on the boundary condition of the board. The Navier method is used when all edges of the board are simply supported. The Levy method is used when two opposite edges are

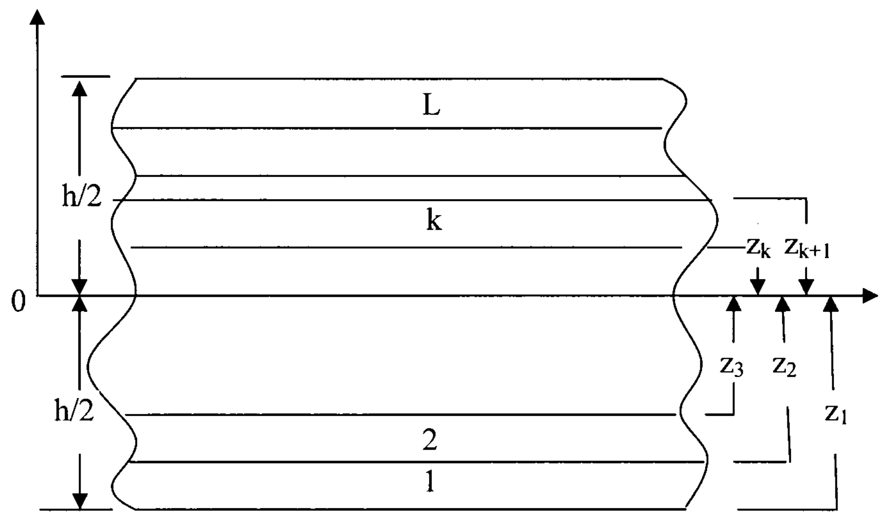

Fig. 3.2 - Coordinate system and layer numbering for laminate composite board.

simply supported, while the remaining two edges are not. The Rayleigh-Ritz method can be used to determine the approximate solution for more general boundary conditions. These three methods are widely used in plate, shell, and laminated plate applications, such as [57, 560 pp.], [58, 492 pp.], [59, 782 pp], [60, 153 pp.], and [61, 210 pp.]. In this dissertation, we are assuming that the four edges of the PCB are simply supported. Therefore, the Navier method will be used to solve Eq. (3-32). For a simply supported laminated plate, the boundary conditions are given by

$$x = 0,\ \text{and}\ x = a,\ w = 0\ \text{and}\ M_x = -D_{11}\frac{\partial^2 w}{\partial x^2} - D_{12}\frac{\partial^2 w}{\partial y^2} = 0, \tag{3-33a}$$

$$y = 0,\ \text{and}\ y = b,\ w = 0\ \text{and}\ M_y = -D_{12}\frac{\partial^2 w}{\partial x^2} - D_{22}\frac{\partial^2 w}{\partial y^2} = 0. \tag{3-33b}$$

Using the Navier method and assuming the solution of Eq. (3-32) is

$$w(x,y,t)=\sum_{m=1}^{\infty}\sum_{n=1}^{\infty}\sin(\alpha\, x)\sin(\beta\, y)\;\phi(t), \tag{3-34}$$

where

$$\alpha=\frac{m\pi}{a},$$

and

$$\beta=\frac{n\pi}{b}.$$

Substituting Eq. (3-34) into Eq. (3-32) yields

$$\sum_{m=1}^{\infty}\sum_{n=1}^{\infty}\left\{\left[D_{11}\alpha^4+2(D_{12}+2D_{66})\alpha^2\beta^2+D_{22}\beta^4\right]\phi(t)+c_1\dot{\phi}(t)+I_0\ddot{\phi}(t)\right\}\sin(\alpha x)\sin(\beta y)=-I_0\ddot{w}_1$$

Denote

$$\xi\,=\,D_{11}\alpha^4\,+\,2(D_{12}\,+\,2D_{66})\alpha^2\beta^2\,+\,D_{22}\beta^4\,.$$

Using orthogonal relations yield

$$I_0\,\ddot{\phi}(t)+c_1\,\dot{\phi}(t)+\xi\,\phi(t)=-\frac{4}{a\,b}\int_0^a\!\!\int_0^b I_0\;\ddot{w}_1\,\sin(\alpha\, x)\sin(\beta\, y)\,dx\,dy.$$

Since $\int_0^a\sin(\alpha\, x)\,dx=\frac{a}{m\,\pi}\left[1-(-1)^m\right]$, and $\int_0^b\sin(\beta\, y)\,dy=\frac{b}{n\pi}\left[1-(-1)^n\right]$, then

$$I_0\,\ddot{\phi}(t)+c_1\,\dot{\phi}(t)+\xi\,\phi(t)=-\frac{4\,I_0\,\ddot{w}_1}{m\,n\,\pi^2}\left[1-(-1)^m\right]\left[1-(-1)^n\right].$$

Dividing this equation by I_0 on both sides yields

$$\ddot{\phi}(t)+\frac{c_1}{I_0}\dot{\phi}(t)+\frac{\xi}{I_0}\phi(t)=-\frac{4\,\ddot{w}_1}{m\,n\,\pi^2}\left[1-(-1)^m\right]\left[1-(-1)^n\right]. \tag{3-35}$$

This is the standard forced vibration equation. Comparing it with Eq. (3-3) yields the frequency of vibration, or

$$p_{mn}^2 = \frac{\xi}{I_0} = \frac{D_{11}\,\alpha^4 + 2\,(D_{12} + 2\,D_{66})\alpha^2\beta^2 + D_{22}\,\beta^4}{I_0},$$

or

$$p_{mn}^2 = \frac{\pi^4}{I_0\,b^4}\left[D_{11}\,m^4\left(\frac{b}{a}\right)^4 + 2\,(D_{12} + 2\,D_{22})\,m^2\,n^2\left(\frac{b}{a}\right)^2 + D_{22}\,n^4\right]. \tag{3-36}$$

This equation is the same as the derivation given in [59, p. 315]. In a PCB design, the designers should avoid the forced vibration frequency close to these frequencies, or resonance will occur, which in turn will cause serious reliability problems. In this dissertation, we are assuming that no resonance will occur.

Equation (3-35) can be solved the same way as Eq. (3-3) but with

$$p^2 = p_{mn}^2,\quad 2\,\eta = \frac{c_1}{I_0},\ \text{and}\ \ddot{w}_0 = \frac{4\,\ddot{w}_1}{m\,n\,\pi^2}\left[1-(-1)^m\right]\left[1-(-1)^n\right].$$

Then, the solution of Eq. (3-35) is obtained using the Duhamel integral

$$\phi(t) = -\int_0^\infty h_{mn}(\tau)\left[A_{mn}\ \ddot{w}_1(t-\tau)\right]\,d\tau, \tag{3-37}$$

where

$$h_{mn}(\tau) = \frac{e^{-\eta_b\tau}}{p_{dbmn}}\sin\left(p_{dbmn}\tau\right),$$

$$p_{dbmn}^2 = p_{mn}^2 - \eta_b^2,$$

$$\eta_b = {c_1}/{2I_0},$$

and

$$A_{mn} = \frac{4}{m\,n\,\pi^2}\left[1-(-1)^m\right]\left[1-(-1)^n\right].$$

Considering that A_{mn} =0 for m or n is even, then

$$A_{mn} = \begin{cases} \dfrac{16}{m\,n\,\pi^2} & \text{for m and n odd,} \\ 0 & \text{for m or n even.} \end{cases} \tag{3-38}$$

Substituting Eqs. (3-37) and (3-38) into Eq. (3-34) yields

$$w(x,y,t) = -\frac{16}{\pi^2}\sum_{m=1,3,5,...}^{\infty}\sum_{n=1,3,5,...}^{\infty}\frac{\sin(\alpha\,x)\sin(\beta\,y)}{m\,n}\int_0^{\infty} h_{mn}(\tau)\,\ddot{w}_1(t-\tau)\,d\tau\,. \tag{3-39}$$

We know that the maximum deflection occurs at the center of the PCB, then

$$w_{\max}(x,y,t) = w(a/2, b/2, t),$$

or

$$w_{\max}(x,y,t) = -\frac{16}{\pi^2}\sum_{m=1,3,5,...}^{\infty}\sum_{n=1,3,5,...}^{\infty}\frac{(-1)^{\frac{m+n-2}{2}}}{m\,n}\int_0^{\infty} h_{mn}(\tau)\,\ddot{w}_1(t-\tau)\,d\tau. \tag{3-40}$$

Next, let's find the mean and the variance of w. From the previous equation, we see that the deflection of the PCB is a random process not a deterministic one. We need to use the same method when we try to find the mean and variance of $\ddot{w}_1$.

As previously, we also assume that the response of the PCB is a stationary process based on the reason discussed previously. Then,

$$E[w(x,y,t)] = -\frac{16}{\pi^2}E[\ddot{w}_1]\sum_{m=1,3,5,...}^{\infty}\sum_{n=1,3,5,...}^{\infty}\frac{\sin(\alpha\,x)\sin(\beta\,y)}{m\,n}\int_0^{\infty} h_{mn}(\tau)\,d\tau\,, \tag{3-41}$$

$$E[w_{\max}(x,y,t)] = -\frac{16}{\pi^2} E[\ddot{w}_1] \sum_{m=1,3,5,\dots}^{\infty} \sum_{n=1,3,5,\dots}^{\infty} \frac{(-1)^{\frac{m+n-2}{2}}}{m\,n} \int_0^{\infty} h_{mn}(\tau)\,d\tau. \tag{3-42}$$

From Eqs.(3-16) and (3-20), we know

$$E(\ddot{w}_1(t)) = E(\ddot{w}_0(t)) = 0.$$

Then,

$$E[w(x,y,t)] = 0,$$

and

$$E[w_{\max}(x,y,t)] = 0.$$

Therefore, the variance of w(x,y,t) can be found through the auto-correlation relation,

$$\begin{aligned} G_{ww}(\tau) &= R_w(\tau) = E\left[w(x,y,t+\tau)w(x,y,t)\right], \\ &= E\left[\left(-\frac{16}{\pi^2}\sum_{m=1,3,5,\dots}^{\infty}\sum_{n=1,3,5,\dots}^{\infty}\frac{\sin\left(\frac{m\,\pi\,x}{a}\right)\sin\left(\frac{n\,\pi\,y}{b}\right)}{m\,n}\int_0^{\infty} h_{mn}(r_1)\,\ddot{w}_1(t+\tau-r_1)\,dr\right)\right. \\ &\quad \left.\cdot\left(-\frac{16}{\pi^2}\sum_{i=1,3,5,\dots}^{\infty}\sum_{j=1,3,5,\dots}^{\infty}\frac{\sin\left(\frac{i\,\pi\,x}{a}\right)\sin\left(\frac{j\,\pi\,y}{b}\right)}{i\,j}\int_0^{\infty} h_{ij}(r_2)\,\ddot{w}_1(t-r_2)\,dr\right)\right], \end{aligned}$$

or

$$\begin{aligned} G_{ww}(\tau) = \frac{256}{\pi^4}\sum_{m=1,3,5,\dots}^{\infty}\sum_{n=1,3,5,\dots}^{\infty}\sum_{i=1,3,5,\dots}^{\infty}\sum_{j=1,3,5,\dots}^{\infty} &\frac{\sin\left(\frac{m\,\pi\,x}{a}\right)\sin\left(\frac{n\,\pi\,y}{b}\right)\sin\left(\frac{i\,\pi\,x}{a}\right)\sin\left(\frac{j\,\pi\,y}{b}\right)}{m\,n\,i\,j} \\ &\cdot E\left[\int_0^{\infty}\int_0^{\infty} h_{mn}(r_1)\,\ddot{w}_1(t+\tau-r_1)\,h_{ij}(r_2)\,\ddot{w}_1(t-r_2)\,dr_1\,dr_2\right]. \end{aligned}$$

Note that

$$E[\ddot{w}_1(t+\tau-r_1)\ddot{w}_1(t-r_2)] = R_{\ddot{w}_1\ddot{w}_1}(\tau+r_2-r_1).$$

Then,

$$G_{ww}(\tau) = \frac{256}{\pi^4}\sum_{m=1,3,5,\ldots}^{\infty}\sum_{n=1,3,5,\ldots}^{\infty}\sum_{i=1,3,5,\ldots}^{\infty}\sum_{j=1,3,5,\ldots}^{\infty}\frac{\sin\left(\frac{m\pi x}{a}\right)\sin\left(\frac{n\pi y}{b}\right)\sin\left(\frac{i\pi x}{a}\right)\sin\left(\frac{j\pi y}{b}\right)}{m\,n\,i\,j}$$
$$\cdot\int_0^{\infty}\int_0^{\infty} h_{mn}(r_1)\,h_{ij}(r_2)\,R_{\ddot{w}_1\ddot{w}_1}(\tau+r_2-r_1)\,dr_1\,dr_2,$$

$$\sigma_w^2 = G_{ww}(0),$$

or

$$\sigma_w^2 = \frac{256}{\pi^4}\sum_{m=1,3,5,\ldots}^{\infty}\sum_{n=1,3,5,\ldots}^{\infty}\sum_{i=1,3,5,\ldots}^{\infty}\sum_{j=1,3,5,\ldots}^{\infty}\frac{\sin\left(\frac{m\pi x}{a}\right)\sin\left(\frac{n\pi y}{b}\right)\sin\left(\frac{i\pi x}{a}\right)\sin\left(\frac{j\pi y}{b}\right)}{m\,n\,i\,j}$$
$$\cdot\int_0^{\infty}\int_0^{\infty} h_{mn}(r_1)\,h_{ij}(r_2)\,R_{\ddot{w}_1\ddot{w}_1}(r_2-r_1)\,dr_1\,dr_2, \tag{3-43}$$

and

$$\sigma_{w_{\max}}^2 = G_{ww}(0)\Big|_{x=a/2,\,y=b/2},$$

or

$$\sigma_{w_{\max}}^2 = \frac{256}{\pi^4}\sum_{m=1,3,5,\ldots}^{\infty}\sum_{n=1,3,5,\ldots}^{\infty}\sum_{i=1,3,5,\ldots}^{\infty}\sum_{j=1,3,5,\ldots}^{\infty}\frac{(-1)^{\frac{m+n+i+j-4}{2}}}{m\,n\,i\,j}$$
$$\cdot\int_0^{\infty}\int_0^{\infty} h_{mn}(r_1)\,h_{ij}(r_2)\,R_{\ddot{w}_1\ddot{w}_1}(r_2-r_1)\,dr_1\,dr_2. \tag{3-44}$$

For an ideal white noise process, we have found $R_{\ddot{w}_1\ddot{w}_1}(r_2-r_1)$ and is given in

Eq. (3-29). Then, the variance given in Eqs. (3-43) and (3-44) can be computed. Appendix E gives the closed form of the double integral involved in Eqs. (3-43) and (3-44). We will not give the equation here since it is too complex, readers, who are interested in it, can read Appendix E for the detailed derivation.

3.2.2 Stress Determination

The classical laminated plate theory (CLPT) and Suhir's type method (see Appendix G) will be used in this dissertation to determine the stress in the PCB subjected to vibration and thermal loads. The classical laminated plate theory is an extension of the classical plate theory, which is most useful when the ratio of the plate dimension to the thickness of the plate is greater than 20. That is the case for PCBs. For other cases, a higher order laminated plate theory should be used, such as the First-Order Shear Deformation Laminated Plate Theory (FSDT). The basic assumptions in the classical laminated plate theory are:

1. Straight lines perpendicular to the midplane before deformation remain straight after deformation.
2. The transverse normals do not experience elongation (i.e., inextensible).
3. The transverse normals rotate such that they remain perpendicular to the mid-surface after deformation.

Reddy [59, 782 pp.] determined the stress of an orthotropic composite plate utilizing this theory. For the k^{th} layer, the in-plane stresses are given by

$$\begin{Bmatrix} s_{xx} \\ s_{yy} \\ s_{xy} \end{Bmatrix}^{(k)} = \begin{bmatrix} Q_{11} & Q_{12} & 0 \\ Q_{12} & Q_{22} & 0 \\ 0 & 0 & Q_{66} \end{bmatrix}^{(k)} \begin{Bmatrix} -z\dfrac{\partial^2 w}{\partial x^2} - \alpha_x \Delta T \\ -z\dfrac{\partial^2 w}{\partial y^2} - \alpha_y \Delta T \\ -2z\dfrac{\partial^2 w}{\partial x \partial y} - 2\alpha_{xy}\Delta T \end{Bmatrix}$$

$$= \mathrm{z}\sum_{m=1}^{\infty}\sum_{n=1}^{\infty} W_{mn} \begin{Bmatrix} \left(Q_{11}^{(k)}\alpha^2 + Q_{12}^{(k)}\beta^2\right)\sin(\alpha\, x)\sin(\beta\, y) \\ \left(Q_{12}^{(k)}\alpha^2 + Q_{22}^{(k)}\beta^2\right)\sin(\alpha\, x)\sin(\beta\, y) \\ -2\, Q_{66}^{(k)}\,\alpha\,\beta\cos(\alpha\, x)\cos(\beta\, y) \end{Bmatrix} - \qquad (3\text{-}45)$$

$$\text{-}\begin{Bmatrix} \mathrm{Q}_{11}^{(\mathrm{k})}\,\alpha_x + Q_{12}^{(ki)}\,\alpha_y \\ \mathrm{Q}_{12}^{(\mathrm{k})}\,\alpha_x + Q_{22}^{(k)}\,\alpha_y \\ 2\,Q_{66}\,\alpha_{xy} \end{Bmatrix}\Delta T,$$

and the interlaminar stresses due to vibration are given by

$$s_{xz,vib}^{(k)}(x,y,z_{k+1}) = -\sum_{m=1}^{\infty}\sum_{n=1}^{\infty}\left(\sum_{p=1}^{k}\frac{\left(z_{k+1}^2 - z_p^2\right)}{2}C_{1mn}^{(p)}\right)W_{mn}\cos(\alpha\, x)\sin(\beta\, y), \qquad (3\text{-}46)$$

$$s_{yz,vib}^{(k)}(x,y,z_{k+1}) = -\sum_{m=1}^{\infty}\sum_{n=1}^{\infty}\left(\sum_{p=1}^{k}\frac{\left(z_{k+1}^2 - z_p^2\right)}{2}C_{2mn}^{(p)}\right)W_{mn}\sin(\alpha\, x)\cos(\beta\, y), \qquad (3\text{-}47)$$

$$s_{zz,vib}^{(k)}(z_{k+1}) = \sum_{m=1}^{\infty}\sum_{n=1}^{\infty}\left[\left(\frac{z_{k+1}^3}{6} - \frac{z_{k+1}\cdot z_k^2}{2}\right)\left(-\alpha\, C_{1mn}^{(k)} - \beta\, C_{2mn}^{(k)}\right) + C_{3mn}^{(k)}\right]W_{mn}\sin(\alpha\, x)\sin(\beta\, y),$$

(3-48)

where

$$C_{1mn}^{(k)} = \alpha^3\, Q_{11}^{(k)} + \alpha\,\beta^2\left(2\,Q_{66}^{(k)} + Q_{12}^{(k)}\right),$$

$$C_{2mn}^{(k)} = \beta^3\, Q_{11}^{(k)} + \alpha^2\,\beta\left(2\,Q_{66}^{(k)} + Q_{12}^{(k)}\right),$$

and

$C_{3mn}^{(k)}$ are the coefficients of W_{mn} in the term of $\varepsilon_{mn}^{(k)}$.

$\varepsilon_{mn}^{(k)}$ can be found as follows:

$$\varepsilon_{mn}^{(1)} = \frac{h^3}{24}\left(-\alpha\, C_{1mn}^{(1)} - \beta\, C_{2mn}^{(1)}\right) W_{mn}, \tag{3-49}$$

and

$$\begin{aligned} \varepsilon_{mn}^{(k)} = \varepsilon_{mn}^{(k-1)} &+ z_k\left(\frac{z_k^2}{6} - \frac{z_{k-1}^2}{2}\right)\left(\alpha\, C_{1mn}^{(k-1)} + \beta\, C_{2mn}^{(k-1)}\right) W_{mn} \\ &+ \frac{z_k^3}{3}\left(\alpha\, C_{1mn}^{(k)} + \beta\, C_{2mn}^{(k)}\right) W_{mn}, \end{aligned} \tag{3-50}$$

$$\alpha = \frac{m\pi}{a},$$

$$\beta = \frac{n\pi}{b},$$

a, b = length and width of the board, respectively,

Q_{ij} = as defined previously,

and

$$W_{mn} = -\frac{16}{m\,n\,\pi^2}\int_0^\infty h_{mn}(\tau)\,\ddot{w}_1(t-\tau)\,d\tau .$$

Since the interfacial failure is the major failure mode of the PCB, only the interfacial stresses will be considered in this dissertation. The maximum interfacial stresses due to vibration are then obtained as

$$s_{xz,\max,vib}^{(k)}(x,y,z_{k+1}) = -\sum_{m=1}^{\infty}\sum_{n=1,3,5,\ldots}^{\infty}\left(\sum_{p=1}^{k}\frac{\left(z_{k+1}^2 - z_p^2\right)}{2} C_{1mn}^{(p)}\right) W_{mn}(-1)^{\frac{n-1}{2}}, \tag{3-51}$$

$$s_{yz,\max,vib}^{(k)}(x,y,z_{k+1}) = -\sum_{m=1,3,5,\ldots}^{\infty}\sum_{n=1}^{\infty}\left(\sum_{p=1}^{k}\frac{\left(z_{k+1}^2 - z_p^2\right)}{2} C_{2mn}^{(p)}\right) W_{mn}(-1)^{\frac{m-1}{2}}, \tag{3-52}$$

and

$$s_{zz,\max,vib}^{(k)}(x,y,z_{k+1}) = -\sum_{m=1}^{\infty}\sum_{n=1}^{\infty}\left[\left(\frac{z_{k+1}^3}{6} - \frac{z_{k+1}\cdot z_k^2}{2}\right)\left(-\alpha\, C_{1mn}^{(k)} - \beta\, C_{2mn}^{(k)}\right) + C_{3mn}^{(k)}\right] W_{mn}(-1)^{\frac{m+n-2}{2}}.$$

(3-53)

The interfacial stresses induced by temperature change can be obtained as follows:

The maximum shear stress in the interface between the kth and the (k+1)th layer is given by

$$\tau_k = -k'\,T_k \tanh(k'\,l), \qquad (3\text{-}54)$$

and the maximum peeling stress between the kth and the (k+1)th layer is given by

$$p_k = -\frac{1}{2}k'^2\, T_k \sum_{j=k+1}^{m} h_j, \qquad (3\text{-}55)$$

where

τ_i = maximum shear stress in the interface between the kth and the (k+1)th layer, it gives the shear stress in the x or y direction, depending on what value of l is used,

$$k'^2 = \frac{3}{4}\frac{\sum_{i=1}^{m} g_i}{\sum_{i=1}^{m} h_i^2 g_i},$$

m = total number of layers,

$$T_k = \sum_{j=k}^{m} F_j,$$

$$F_j = \frac{\left(\sum_{j=1}^{m}\left(\frac{d-b_j}{g_j}\right)\right)\cdot\left(\sum_{k=1}^{j} h_k - \frac{h_j}{2}\right)}{\left[\sum_{i=1}^{m} f_i - \left(\sum_{j=1}^{m}\left(\frac{c-a_j}{g_j}\right)\right)\cdot\left(\sum_{k=1}^{j} h_k - \frac{h_j}{2}\right)\right]}\left(\frac{c-a_j}{g_j}\right) + \frac{d-b_j}{g_j},$$

$$c = \frac{\sum_{j=1}^{m} a_j / g_j}{\sum_{j=1}^{m} 1/g_j},$$

$$d = \frac{\sum_{j=1}^{m} b_j / g_j}{\sum_{j=1}^{m} 1/g_j},$$

$$a_j = \sum_{i=1}^{j} h_i - \frac{h_1 + h_j}{2},$$

$$b_j = \alpha_j\, \Delta T_j - \alpha_1\, \Delta T_1,$$

$$g_i(E_i, h_i, \nu_i) = \frac{1-\nu_i}{E_i\, h_i},$$

and

$$f_i(E_i, h_i, \nu_i) = \frac{E_i\, h_i^3}{12\,(1-\nu_i)}.$$

Appendix F gives the derivation of these equations.

Combining the vibration stress and the thermal stress yields the interfacial stresses between layers, or

$$s_{xz,\max}^{(k)}(x, y, z_{k+1}) = -\sum_{m=1}^{\infty}\sum_{n=1,3,5,\ldots}^{\infty}\left(\sum_{p=1}^{k}\frac{\left(z_{k+1}^2 - z_p^2\right)}{2} C_{1mn}^{(p)}\right) W_{mn}(-1)^{\frac{n-1}{2}} - k'\, T_k \tanh(k'\, l), \quad (3\text{-}56)$$

$$s_{yz,\max}^{(k)}(x,y,z_{k+1}) = -\sum_{m=1,3,5,\ldots}^{\infty}\sum_{n=1}^{\infty}\left(\sum_{p=1}^{i}\frac{\left(z_{k+1}^2 - z_p^2\right)}{2}C_{2mn}^{(p)}\right)W_{mn}(-1)^{\frac{m-1}{2}} - k'\,T_k \tanh(k'\,l),$$

(3-57)

and

$$s_{zz,\max}^{(k)}(x,y,z_{k+1}) = -\sum_{m=1}^{\infty}\sum_{n=1}^{\infty}\left[\left(\frac{z_{k+1}^2}{6} - \frac{z_{k+1}\cdot z_k^2}{2}\right)\left(-\alpha\, C_{1mn}^{(k)} - \beta\, C_{2mn}^{(k)}\right) + C_{3mn}^{(k)}\right]W_{mn}(-1)^{\frac{m+n-2}{2}}$$
$$-\frac{1}{2}k'^2\,T_k\sum_{j=k+1}^{m}h_j.$$

(3-58)

Since for a > b, the shear stress in the y direction is more sever, without losing generality, we can use this stress with the normal stress in the z direction to quantify the reliability of a PCB.

Then, the means of each interfacial stress are given by

$$E(s_{yz,\max}^{(k)}) = -k'\,T_k \tanh(k'\,l), \tag{3-59}$$

and

$$E(s_{zz}^{(k)}) = -\frac{1}{2}k'^2\,T_k\sum_{j=k+1}^{m}h_j, \tag{3-60}$$

due to

$$\begin{aligned} E\{W_{mn}\} &= -\frac{16}{m\,n\,\pi^2}\int_0^{\infty}h_{mn}(\tau)\,E\{\ddot{w}_1(t-\tau)\}\,d\tau \\ &= E\{\ddot{w}_1(t)\}\cdot\left[-\frac{16}{m\,n\,\pi^2}\int_0^{\infty}h_{mn}(\tau)\,d\tau\right] = 0, \end{aligned} \tag{3-61}$$

since $\ddot{w}_1$ is a stationary process.

The variance of each stress is given by

$$\sigma_{yz,\max}^{(k)^2} = \frac{256}{\pi^4} \sum_{m=1,3,5,\dots}^{\infty} \sum_{n=1}^{\infty} \sum_{i=1,3,5,\dots}^{\infty} \sum_{j=1}^{\infty} \frac{(-1)^{\frac{m+i-2}{2}}}{m\,n\,i\,j} \cdot \left(\sum_{p=1}^{k} \left(\frac{z_{k+1}^2 - z_p^2}{2} C_{2mn}^{(p)} \right) \right)$$
$$\cdot \left(\sum_{p=1}^{k} \left(\frac{z_{k+1}^2 - z_p^2}{2} C_{2ij}^{(p)} \right) \right) \cdot \int_0^{\infty} h_{mn}(r_1)\, h_{ij}(r_2)\, R_{\ddot{w}_1 \ddot{w}_1}(r_2 - r_1)\, dr_1\, dr_2, \tag{3-62}$$

and

$$\sigma_{zz,\max}^{(k)^2} = \frac{256}{\pi^4} \sum_{m=1,3,5,\dots}^{\infty} \sum_{n=1,3,5,\dots}^{\infty} \sum_{i=1,3,5,\dots}^{\infty} \sum_{j=1,3,5,\dots}^{\infty} \frac{(-1)^{\frac{m+n+i+j-4}{2}}}{m\,n\,i\,j} \cdot$$
$$\cdot \left[\left(\frac{z^3}{6} - \frac{z \cdot z_k^2}{2} \right) \left(-\frac{m\pi}{a} C_{1mn}^{(k)} - \frac{n\pi}{b} C_{2mn}^{(k)} \right) + C_{3mn}^{(k)} \right] \cdot$$
$$\cdot \left[\left(\frac{z^3}{6} - \frac{z \cdot z_k^2}{2} \right) \left(-\frac{i\pi}{a} C_{1ij}^{(k)} - \frac{j\pi}{b} C_{2ij}^{(k)} \right) + C_{3ij}^{(k)} \right] \tag{3-63}$$
$$\cdot \int_0^{\infty} h_{mn}(r_1)\, h_{ij}(r_2)\, R_{\ddot{w}_1 \ddot{w}_1}(r_2 - r_1)\, dr_1\, dr_2 .$$

CHAPTER 4

DETERMINATION OF THE TEMPERATURE DISTRIBUTION OF THE PCB

To evaluate the reliability of a PCB, we first need to find out the temperature distribution on the board, because all the stress calculations of the package are related to it. Figure 4.1 depicts a laminated PCB with the heat sources located on the top of the board.

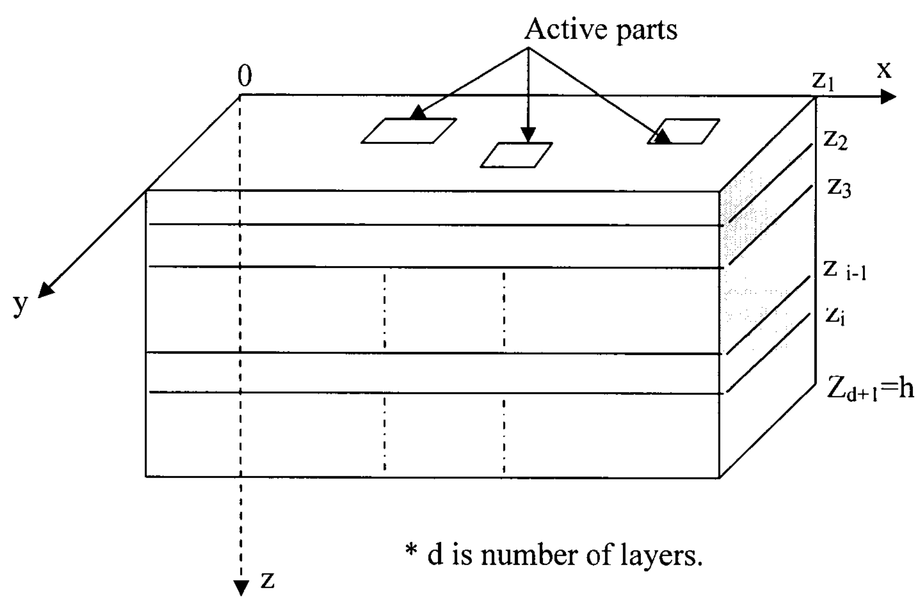

Fig. 4.1 – Laminated PCB with heat source on the top.

The temperature distribution of the laminated PCB can be found by solving a Partial Differential Equations (PDE) for each heat source, and then use the superposition theory to obtain the temperature distribution of the board due to all of the heat sources.

For any heat source (active part) "j" on the PCB, (j = 1, …, N), where N is the total number of active parts on the PCB, the following systems of PDEs need to be solved to find the temperature distribution in the board.

$$\kappa_i\left(\frac{\partial^2\theta_i^{(j)}(x,y,z,t)}{\partial x^2}+\frac{\partial^2\theta_i^{(j)}(x,y,z,t)}{\partial y^2}+\frac{\partial^2\theta_i^{(j)}(x,y,z,t)}{\partial z^2}\right)$$
$$+\frac{\kappa_i\, Q_i^{(j)}}{k_i}=\frac{\partial\theta_i^{(j)}(x,y,z,t)}{\partial t},\quad z_i\le z\le z_{i+1}, i=1,2,3,\ldots,d, \tag{4-1a}$$

with boundary conditions (BC):

$$\begin{aligned}
&x=0,a, && \frac{\partial\theta_i^{(j)}(x,y,z,t)}{\partial x}=0,\\
&y=0,b, && \frac{\partial\theta_i^{(j)}(x,y,z,t)}{\partial y}=0,\\
&z=0, && \mathrm{k}_1\cdot\frac{\partial\theta_1^{(j)}(x,y,z,t)}{\partial z}=h_1\,\theta_1^{(j)},\\
&z=z_d, && \mathrm{k}_\mathrm{d}\cdot\frac{\partial\theta_d^{(j)}(x,y,z,t)}{\partial z}=-h_d\,\theta_{d1}^{(j)},
\end{aligned} \tag{4-1b}$$

and initial condition

$$\theta_i^{(j)}(x,y,z,0)=0, \tag{4-1c}$$

where

k_i = isotropic thermal conductivity for layer i,

κ_i = thermal diffusivity for the ith layer,

$\theta_i^{(j)}(x,y,z)$ = temperature change in the ith layer due to heat source "j". We will use $\theta_i^{(j)}$ instead of $\theta_i^{(j)}(x,y,z)$ hereafter.

$Q_i^{(j)}$ = heat energy per unit volume generated per unit time by heat source j.

For the electronic parts on the PCB, since it works all the time after it is turned on and its position does not change with time, it can be expressed by

$$Q_i^{(j)} = \begin{cases} Q_1^{(j)} \cdot \delta(x - x_j) \cdot \delta(y - y_j) \cdot \delta(z - 0) & \text{for } i = 1, \\ 0 & \text{for } i = 2 \ldots d, \end{cases}$$

δ is Dirac delta function,

and

h_1, h_d = convection coefficient of the top surface of the 1st layer and bottom surface of the d th layer.

In addition to the above boundary conditions and initial condition, between two layers, the following conditions should be satisfied:

$$\theta_i^{(j)}(z_i) = \theta_{i+1}^{(j)}(z_i),$$

and

$$k_i \left.\frac{\partial \theta_i^{(j)}}{\partial z}\right|_{z_i} = k_{i+1} \left.\frac{\partial \theta_{i+1}^{(j)}}{\partial z}\right|_{z_i}. \qquad i = 2, \ldots, d\text{-}1. \tag{4-2}$$

By solving Eqs. (4-1), and (4-2), we can obtain the temperature distribution of the board due to the j th active parts. The temperature distribution of the whole board can be found through superposition. It should be noted that there are two assumptions made to reach the above equations: 1. Each layer is isotropic. 2. Considering the thickness of each layer is too thin relative to the width and length of the board, the insulated condition is assumed at x and y direction as shown in Fig. 4.1.

Solving the above system of PDEs is achievable but very complicated and time-consuming. Therefore, in this dissertation, a simplified method will be employed to obtain the temperature distribution of the board. However, to be complete, Appendix G gives the solution of the system of PDEs given in Eqs. (4-1) and (4-2).

In this simplified method, instead of solving a system of PDEs, only one PDE needs to be solved. It is given by

$$k_x \frac{\partial^2 \theta^{(j)}}{\partial x^2} + k_y \frac{\partial^2 \theta^{(j)}}{\partial y^2} + k_z \frac{\partial^2 \theta^{(j)}}{\partial z^2} + Q^{(j)} = c\rho \frac{\partial \theta^{(j)}}{\partial t} \ . \tag{4-3a}$$

Boundary conditions:

$$\begin{aligned} x &= 0, a, & \frac{\partial \theta^{(j)}}{\partial x} &= 0, \\ y &= 0, b, & \frac{\partial \theta^{(j)}}{\partial y} &= 0, \\ z &= 0, & \mathrm{k_z} \cdot \frac{\partial \theta^{(j)}}{\partial z} &= h_1 \theta^{(j)}, \\ z &= h, & \mathrm{k_z} \cdot \frac{\partial \theta^{(j)}}{\partial z} &= -h_2 \theta^{(j)}. \end{aligned} \tag{4-3b}$$

Initial condition:

$$\theta^{(j)} = 0 , \tag{4-3c}$$

where

$\theta^{(j)}$ = temperature change of the board due to heat source "j",

k_i = thermal conductivity in the i direction, i = x, y, z,

$Q^{(j)}$ = as defined above for 1st layer,

c = specific heat (the heat energy that must be supplied to a unit mass of a substance to raise its temperature one unit),

and

ρ = mass density (mass per unit volume).

This PDE can be solved using eigenfunction expansion method. Then, the resulting temperature due to source ‘j’ at any point of the board is given by

$$\begin{aligned}\theta^{(j)} &= \sum_{m=0}^{\infty}\sum_{n=0}^{\infty}\sum_{l=0}^{\infty}\frac{b_{mnl}}{c\,\rho\,(\alpha_m^2+\beta_n^2+\gamma_l^2)}\phi_m(x)\,\varphi_n(y)\,\psi_l(z) - \\ &\sum_{m=0}^{\infty}\sum_{n=0}^{\infty}\sum_{l=0}^{\infty}\frac{e^{-(\alpha_m^2+\beta_n^2+\gamma_l^2)t}\cdot b_{mnl}}{c\,\rho\,(\alpha_m^2+\beta_n^2+\gamma_l^2)}\phi_m(x)\,\varphi_n(y)\,\psi_l(z),\end{aligned} \tag{4-4}$$

where

$$\phi_m(x) = \cos\left(\frac{\alpha_m}{\sqrt{\omega_x}}x\right) = \cos\left(\frac{m\pi}{a}x\right),\quad \alpha_{\mathrm{m}} = \frac{m\pi\sqrt{\omega_x}}{a},\quad m = 1,\dots,\infty,$$

$$\varphi_n(y) = \cos\left(\frac{\beta_n}{\sqrt{\omega_y}}y\right) = \cos\left(\frac{n\pi}{b}y\right),\quad \beta_{\mathrm{n}} = \frac{n\pi\sqrt{\omega_y}}{b}, n = 1,\dots,\infty,$$

$$\psi_l(z) = \frac{k_z\cdot\gamma_l}{\sqrt{\omega_z}h_1}\cos\left(\frac{\gamma_l}{\sqrt{\omega_z}}z\right) + \sin\left(\frac{\gamma_l}{\sqrt{\omega_z}}z\right),\qquad l = 1,\dots,\infty,$$

γ_l = eigenvalues for the z variable, is computed using the following equation:

$$\tan\left(\frac{\gamma_l}{\sqrt{\omega_z}}h\right) = \frac{k_z^2\,\gamma_l^2 - h_1\,h_2\,\omega_z}{k_z\,\gamma_l\,\sqrt{\omega_z}\,(h_1+h_2)},$$

$$b_{mnl}(t) = \frac{Q^{(j)}}{N_{mnl}}\cos\left(\frac{m\pi}{a}x_j\right)\cos\left(\frac{n\pi}{b}y_j\right)\left(\frac{k_z\,\gamma_l}{\sqrt{\omega_z}h_1}\right),$$

and

$$N_{mnl} = \frac{ab}{4}\left[\frac{k_z^2\,\gamma_l^2\,h + k_z h_1 \omega_z + h\,h_1^2\,\omega_z}{2\,h_1^2\,\omega_z} + \left(\frac{k_z^2\,\gamma_l^2 - h_1^2\,\omega_z}{4\,h_1^2\,\sqrt{\omega_z}\,\gamma_l}\right)\cdot\right.$$
$$\left.\sin\left(\frac{2\,\gamma_l\,h}{\sqrt{\omega_z}}\right) - \frac{k_z}{2\,h_1}\cos\left(\frac{2\,\gamma_l\,h}{\sqrt{\omega_z}}\right)\right].$$

As we discussed in the temperature profile, we are more concerned about temperature at steady state. Then, Eq. (4-4) becomes

$$\theta^{(j)} = \sum_{m=1}^{\infty}\sum_{n=1}^{\infty}\sum_{l=1}^{\infty}\frac{Q^{(j)}\cos\left(\frac{m\,\pi}{a}x_j\right)\cos\left(\frac{n\,\pi}{b}y_j\right)\left(-\frac{k_z\,\gamma_l}{\sqrt{\omega_z}\,h_1}\right)}{c\,\rho\,(\alpha_m^2+\beta_n^2+\gamma_l^2)\,N_{mnl}}\cdot\phi_m(x)\cdot\varphi_n(y)\cdot\psi_l(z)\,. \quad (4\text{-}5)$$

Then, at any location, the temperature change will be

$$\theta(x,y,z) = \sum_{j=1}^{N}\theta^{(j)},$$

or

$$\theta(x,y,z) = \sum_{j=1}^{N}\sum_{m=1}^{\infty}\sum_{n=1}^{\infty}\sum_{l=1}^{\infty}\frac{\left(\frac{k_z\,\gamma_l}{\sqrt{\omega_z}\,h_1}\right)\phi_m(x)\,\varphi_n(y)\,\psi_l(z)}{c\,\rho\,(\alpha_m^2+\beta_n^2+\gamma_l^2)\,N_{mnl}}Q^{(j)}\cos\left(\frac{m\,\pi}{a}x_j\right)\cos\left(\frac{n\,\pi}{b}y_j\right). \quad (4\text{-}6)$$

Appendix G details the process of solving this PDE.

CHAPTER 5

RELIABILITY QUANTIFICATION METHODOLOGY

5.1 Introduction

To evaluate a PCB's reliability, finding out each section's failure modes and reliability is a must. In this dissertation, two failure modes of the board, five failure modes of interconnects, and one failure mode (popcorn) of the module plus the failures of the parts will be considered to quantify the PCB's reliability. For the summary and the categories of all the possible failure modes and failure mechanisms of electronic packaging, see Tummala [62, ;63, 967 pp.], Lau [64, 409 pp.], and Dasgupta [65, pp. 531-536; 66, pp. 149-154; 67, pp. 168-174; 68, pp. 328-335; 69, pp. 489-495; 70, pp. 9-16; and 71, pp. 548-555].

5.2 Failure modes of the Board

Theoretically, a laminated board can fail in many ways, such as delamination, bending, buckling, and others. However, only delamination and excessive deflection failure modes will be covered in this dissertation since other failure modes have not been encountered in normal PCB use conditions to my knowledge.

Delamination failure occurs when inter-layer stress caused by thermal load and vibration exceeds its strength. Therefore the performance function is given by

$$Z_1 = S(t) - s, \tag{5-1}$$

where

Z_1 = performance function of the delamination failure mode,

S(t) = time dependent strength,

and

s = stress caused by temperature variation and vibration.

As we already know a PCB is a multilayered composite body. Therefore, it experiences not only normal stresses but also interfacial shearing and peeling (transverse normal) stresses. While normal stresses in each layer are responsible for the ultimate and fatigue strength of each layer, it is the shearing and peeling stresses which are mostly responsible for the failure of the board.

The strength is assumed to follow a normal distribution with a constant standard deviation and time dependent mean. The stresses, as stated above, are the shear and peeling stresses. In this case, we will use the maximum one to compute the reliability of the board.

The mean of the performance function is

$$\overline{Z}_1 = \overline{S}(t) - \overline{s}, \tag{5-2}$$

and the variance of the performance function is

$$\sigma_{Z_1}^2 = \sigma_{S(t)}^2 + \sigma_s^2. \tag{5-3}$$

Then, the reliability of this failure mode is computed using Eqs. (2-6) and (2-7), or

$$R_1 = \Phi(m) = \Phi\left(\frac{\overline{Z}_1}{\sigma_{Z_1}}\right). \tag{5-4}$$

An excessive deflection failure mode occurs when the board's deflection at any point plus the height of the part, plus the height of lead or solder joint exceed a specified value. This value normally is the clearance between the top/bottom board and the top/bottom surface of the electronic box. Figure 5.1 illustrates one of these situations. To simplify the problem, we assume that all parts are located only on the top side of the board and that lead height or solder joint height does not change during board deflection. In reality, there are some boards with parts mounted on both sides, and a little change of lead or solder joint height may occur.

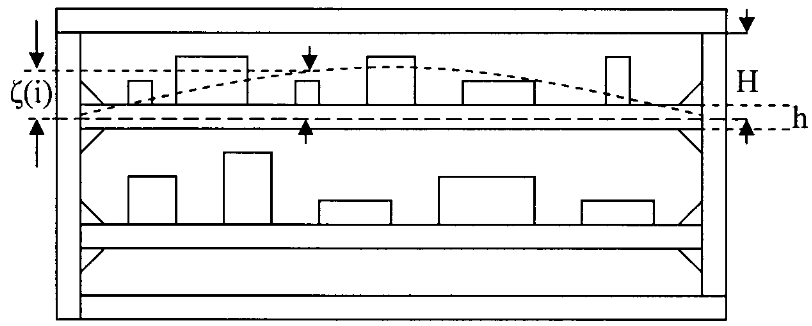

Fig. 5.1 – Illustration of a PCB in the electronic box.

If we denote the coordinates of part "*i*" on the board as (x_i, y_i, z_i) and its height as h_i as shown in Fig. 1.2, the thickness of the board as h, and the clearance between the board and the top side of the box (without loss of generality, we only consider the top side of the box, the bottom side can be treated in the same way) as H as shown in Fig. 5.1, the relative movement between the board and the box as w^*, and the deflection of the board at point (x_i, y_i, z_i) as ζ(i), then the performance function for the deflection failure mode is given by

$$Z_2 = H - \frac{1}{2}h - \max(\xi(i) + h_i) - w^* . \tag{5-5}$$

If $Z_2 < 0$, then failure will occur. On the other hand, if $Z_2 \geq 0$, the board will not fail. In the design of the electronic box, we can use max (ζ(i)) + max(h_i) instead of max(ζ(i)+h$_i$) in Eq. (5-5) because this is more conservative. Then, Eq. (5-5) becomes

$$Z_2 = H - \tfrac{1}{2}h - w_{\max} + h_{i\max} - w^*, \tag{5-6}$$

where

w_{max} = maximum deflection of the board,

and

h_{imax} = maximum height of the parts on the board.

The mean of Z_2 is given by

$$\overline{Z}_2 = H - \frac{1}{2}h - \overline{w}_{\max} + h_{i\max} - \overline{w}^* \tag{5-7}$$

or

$\overline{Z}_2 = H - \frac{1}{2}h + h_{i\max}$ since w_{max} and w^* are both stationary Gaussian processes with a mean of zero as discussed before.

The variance of Z_2 can be found using its definition, or

$$\begin{aligned} \sigma_{Z_2}^2 &= E\left[\left(Z_2 - \overline{Z}_2\right)^2\right] = E\left[\left(w_{\max} + w^*\right)^2\right], \\ &= E\left(w_{\max}^2\right) + E\left(w^{*2}\right) + 2\,E\left(w_{\max} w^*\right), \end{aligned} \tag{5-8}$$

Since the mean of w_{max} and w^* are both zero, then from Eq. (3-44),

$$E\left(w_{\max}^2\right) = \sigma_{w_{\max}}^2 = G_{ww}(0)\Big|_{x = a/2,\, y = b/2},$$

or

$$E\left(w_{\max}^2\right)=\frac{256}{\pi^4}\sum_{m=1,3,5,\ldots}^{\infty}\sum_{n=1,3,5,\ldots}^{\infty}\sum_{i=1,3,5,\ldots}^{\infty}\sum_{j=1,3,5,\ldots}^{\infty}\frac{(-1)^{\frac{m+n+i+j-4}{2}}}{m\,n\,i\,j} \cdot\int_0^{\infty}\int_0^{\infty}h_{mn}(r_1)\,h_{ij}(r_2)\,R_{\ddot{w}_1\ddot{w}_1}(r_2-r_1)\,dr_1\,dr_2, \tag{5-9}$$

and from Eq. (3-21)

$$E(w^{*2})=R_{w^*w^*}(0)=\int_0^{\infty}\int_0^{\infty}R_{\ddot{w}_0\ddot{w}_0}(r_2-r_1)\,h(r_1)\,h(r_2)\,dr_1\,dr_2. \tag{5-10}$$

$$E\left(w_{\max}w^*\right)=-\frac{16}{\pi^2}\sum_{m=1,3,5,\ldots}^{\infty}\sum_{n=1,3,5\ldots}^{\infty}\frac{(-1)^{\frac{m+n-2}{2}}}{mn}\int_0^{\infty}h_{mn}(r)\,E\left[\ddot{w}_1(t-r)\,w^*(t)\right]dr,$$

or

$$E\left(w_{\max}w^*\right)=\frac{16}{\pi^2}\sum_{m=1,3,5\ldots}^{\infty}\sum_{n=1,3,5,\ldots}^{\infty}\frac{(-1)^{\frac{m+n-2}{2}}}{m\,n}\int_0^{\infty}h_{mn}(r)\left[2\,\eta\,R_{\dot{w}^*w^*}(r)+p^2\,R_{w^*w^*}(r)\right]dr, \tag{5-11}$$

where $\ddot{w}_1(t)=\ddot{w}^*(t)+\ddot{w}_0(t)=-(2\,\eta\,\dot{w}^*+p^2\,w^*)$ has been used in reaching the above equation.

It can be shown that

$$2\,\eta\int_0^{\infty}h_{mn}(r)\,R_{\dot{w}^*w^*}(r)\,dr=\frac{\pi\,S_0(\eta_b+\eta)}{2\,p_{dbmn}\,p_d}\left[\frac{1}{(\eta_b+\eta)^2+(p_{dbmn}-p_d)^2}-\frac{1}{(\eta_b+\eta)^2+(p_{dbmn}+p_d)^2}\right] \tag{5-12}$$

and

$$p^2 \int_0^\infty h_{mn}(r)\, R_{\dot{w}\dot{w}}(r)\, dr = \frac{\pi \cdot S_0}{4 p_{dbmn} \cdot p_d} \left[\frac{p_{dbmn} - p_d + \dfrac{\eta(\eta_b + \eta)}{p_d}}{(\eta_b + \eta)^2 + (p_{dbmn} - p_d)^2} \right. \\ \left. + \frac{p_{dbmn} + p_d - \dfrac{\eta(\eta_b + \eta)}{p_d}}{(\eta_b + \eta)^2 + (p_{dbmn} + p_d)^2} \right]. \tag{5-13}$$

Substituting Eqs.(5-9), (5-10) and (5-11) into Eq. (5.8) yields the variance of the performance function Z_2.

Then, the reliability of the board related to deflection failure mode can be computed using Eqs. (2-6) and (2-7).

It can be seen, from the two performance functions, that these two failure modes are not independent since they both involve the same distributed variable, namely, the deflection of the board. Therefore, we need to compute their coefficient of correlation before we can calculate the reliability of the whole board. The coefficient of correlation can be found as follows. From the definition of the coefficient of correlation, we have

$$\rho_{12} = \frac{E\left[\left(Z_1 - \bar{Z}_1\right)\left(Z_2 - \bar{Z}_2\right)\right]}{\sigma_{Z_1} \sigma_{Z_2}} . \tag{5-14}$$

Regardless of whether the shear stress or the peeling stress is used for the delamination failure mode, we can generally denote its performance function as

$$Z_1 = S - s = S - (s_{vir} + s_{th}), \tag{5-15}$$

where

s_{vir} = stress caused by vibration,

and

s_{th} = stress caused by thermal load.

From previous work, we know $\bar{s}_{vir} = 0$, then

$$Z_1 - \bar{Z}_1 = S - (s_{vir} + s_{th}) - (\bar{S} - s_{th}) = (S - \bar{S}) - s_{vir}. \tag{5-16}$$

Similarly,

$$Z_2 - \bar{Z}_2 = -w_{\max} - w^*. \tag{5-17}$$

Substituting Eqs. (5-16) and (5-17) into Eq. (5-14) yields

$$\rho = \frac{E\left[\left(Z_1 - \bar{Z}_1\right)\left(Z_2 - \bar{Z}_2\right)\right]}{\sigma_{Z_1}\sigma_{Z_2}},$$
$$= \frac{E\left\{\left[\left(S - \bar{S}\right) - s_{vir}\right]\left[-w_{\max} - w^*\right]\right\}}{\sigma_{Z_1}\sigma_{Z_2}},$$

or

$$\rho = \frac{E\left[s_{vir} w_{\max}\right] + E\left[s_{vir} w^*\right]}{\sigma_{Z_1}\sigma_{Z_2}}. \tag{5-18}$$

If s_{vir} is the shear stress given by Eq. (3-57), then

$$E\left[s_{vir}\, w_{\max}\right] = \frac{256}{\pi^4} \sum_{m=1,3,5...}^{\infty} \sum_{n=1,3,5,...}^{\infty} \sum_{i=1,3,5,...}^{\infty} \sum_{j=1,3,5...}^{\infty} \frac{(-1)^{\frac{m+i+j-1}{2}}}{m\,n\,i\,j} \cdot \left(\sum_{p=1}^{k}\left(\frac{z^2 - z_p^2}{2} C_{2mn}^{(p)}\right)\right) \cdot \int_0^{\infty} h_{mn}(r_1)\, h_{ij}(r_2)\, R_{\ddot{w}_1\ddot{w}_1}(r_2 - r_1)\, dr_1\, dr_2. \tag{5-19}$$

In deriving this relation, we used $E(W_{mn})=0$.

Similarly,

$$E\left[s_{vir}w^*\right]=\frac{16}{\pi^2}\sum_{m=1,3,5\ldots}^{\infty}\sum_{n=1,3,5,\ldots}^{\infty}\left(\sum_{i=1}^{k}\left(\frac{z^2-z_i^2}{2}C_{2mn}^{(i)}\right)\right)\cdot\frac{(-1)^{\frac{m-1}{2}}}{m\,n}$$
$$\cdot\int_0^{\infty}h_{mn}(r_1)\,E\left[\ddot{w}_1(t-r_1)\,w^*(t)\right]dr_1,$$
$$=\frac{16}{\pi^2}\sum_{m=1,3,5\ldots}^{\infty}\sum_{n=1,3,5,\ldots}^{\infty}\left(\sum_{i=1}^{k}\left(\frac{z^2-z_i^2}{2}C_{2mn}^{(i)}\right)\right)\cdot\frac{(-1)^{\frac{m-1}{2}}}{m\,n}$$
$$\cdot\int_0^{\infty}h_{mn}(r_1)\left[2\eta\,R_{\dot{w}^*w^*}+p^2\,R_{w^*w^*}\right]dr_1. \tag{5-20}$$

Similarly, if the peeling stress is the dominant stress, then

$$E\left[s_{vir}w_{\max}\right]=\frac{256}{\pi^4}\sum_{m=1,3,5\ldots}^{\infty}\sum_{n=1,3,5,\ldots}^{\infty}\sum_{i=1,3,5,\ldots}^{\infty}\sum_{j=1,3,5\ldots}^{\infty}\frac{(-1)^{\frac{m+n+i+j-4}{2}}}{m\,n\,i\,j}\cdot$$
$$\cdot\left[\left(\frac{z^3}{6}-\frac{z\cdot z_k^2}{2}\right)\left(-\alpha\,C_{1mn}^{(k)}-\beta\,C_{2mn}^{(k)}\right)+C_{3mn}^{(k)}\right]\cdot$$
$$\cdot\int_0^{\infty}h_{mn}(r_1)\,h_{ij}(r_2)\,R_{\ddot{w}_1\ddot{w}_1}(r_2-r_1)\,dr_1\,dr_2, \tag{5-21}$$

and

$$E\left[s_{vir}w^*\right]=\frac{16}{\pi^2}\sum_{m=1,3,5\ldots}^{\infty}\sum_{n=1,3,5,\ldots}^{\infty}\left[\left(\frac{z^3}{6}-\frac{z\cdot z_k^2}{2}\right)\left(-\alpha\,C_{1mn}^{(k)}-\beta\,C_{2mn}^{(k)}\right)+C_{3mn}^{(k)}\right]\cdot$$
$$\cdot\frac{(-1)^{\frac{m+n-2}{2}}}{m\,n}\cdot\int_0^{\infty}h_{mn}(r_1)\left[2\eta\,R_{\dot{w}^*w^*}+p^2\,R_{w^*w^*}\right]dr_1. \tag{5-22}$$

Then, using Eq. (5-18) yields the correlation coefficient.

The reliability of the board is obtained using Eq. (2-29), or

$$R=\int_0^{\rho}w(-m_1,-m_2,r)\,dr+\Phi(m_1)\Phi(m_2). \tag{5-23}$$

5.3 Failure Modes of Interconnects

5.3.1 Introduction

There are mainly two kinds of interconnection techniques between the parts and the board, namely the insertion-mount and the surface-mount technology (SMT). Within the insertion-mount, the plate/pin through hole and the pin grid array interconnects are included. Within the surface mount technology, leaded or leadless technologies are used. Most of the leaded interconnects have the forms "J" bend or gull-wing, and are commonly used in Small Outline Transistors (SOT), Small Outline Integrated Circuits (SOIC), and Plastic Leaded Chip Carriers (PLCC); the leadless interconnect is typically used on the PCB with a stand-off and attached to the board by a solder fillet [72, pp.147-153]. Recently, the trends of employing interconnect techniques have changed from through hole to leaded surface mount and on to the leadless solder ball arrays [73, pp. 231-244] due to economic factors, which require denser packages with a larger number of connections. In this dissertation, all three kinds of the interconnect technologies will be discussed.

Solder joint, as the major part of all three interconnect technologies, serves two important purposes in the surface mount interconnect technology; i.e., electrical connections and mechanical supports. In the plate-through-hole technology, the pins serve as the mechanical support and the solder joints serve as the electronic connection. Therefore, solder joint reliability is very important to the reliable performance of a PCB. In the past years, extensive research has been conducted to study the solder joint reliability issues, and among them, a large portion of the studies are focused on the solder joint's fatigue life prediction, from which many empirical models are proposed [3, pp. 347-353; 74, pp.317-322; 75, pp. 423-432; 76, 123-128; 77, pp. 51-54; 78, pp. 279-285; 79, pp. 48-54; 80, pp. 1-10; 81, pp. 18-23; 82, pp. 398-405; 83, pp. 85-90; 84, pp. 212-220; 85, pp. 103-112; 86, pp. 559-570, 87, pp. 553-558; 88, pp. 179-182; 89, pp. 200-206; 90, pp. 120-125; 91, pp. 351-355]. Some of these models are fatigue-based models, which are based on the Coffin-Mason equation with some modifications; some of them are energy-based models, while others are damage-based models. Clattebraugh and Charles [92, 39 pp.], Yeo, Lee, and Pang [93, pp. 107-114], Desai and Whitenack [94, pp. 19-33], and Lee, et al [73, pp. 231-244] reviewed and compared these models. Lee, et al [73, pp. 231-244] even discussed two application scenarios of these models and gave a general procedure for choosing appropriate models. Some of these models have been applied in some products and achieved encouraging results [95, 28 pp.;96, pp. 499-506; 97, pp. 847-855; 98, pp. 257-266; 99, pp. 104-109; 100, pp. 903-908; 101, pp. 6-12; 102, pp. 438-443; 103, pp. 3-14; 104, pp. 961-971; 105, pp. 147-154; 106, pp. 184-189, etc.]. Other solder joint related research include studies on creep deformation, creep-fatigue damage/interaction of solder joints [107, pp. 727-735; 108, pp. 229-234; 109, pp. 794-798, etc.], solder joint mechanical properties [110, pp. 64-67; 111, pp. 129-134, etc.], the effect of the solder joints' shape, size, and geometry on the solder joint's reliability [112, pp. S19-2-1-S19-2-8; 113, pp. 57-62, etc.]. Liu, C. [114, pp. 44-50], and Borgesen, P., et al, [115, pp. 272-283] discussed the solder joints' shape design. Stoyanov, S. et al [116, pp. 178-186] discussed the solder joints' reliability optimization based on underfill materials (E and CTE) and the joint's geometry parameters.

With the pressure of "green" products and approaching the effective date of banning the lead-containing products, including solder joints, lead-free solder joint research has become a new, hot topic in electronic industries. So far, the effect of using lead-free solder joints on solder joint reliability is unclear. Syed, A. [117, pp. 143-147] and Lee, S. R. and Lui, B. H. W. [118, pp. 82-89] reported that reliability is improved using lead-free solder joint, while Schubert, A. et al, [119, pp. 90-96] found that the degree of the improvement is package-related. For a more compliant package board, such as PBGA, the reliability might be improved, but for package types with high CTE mismatch with the board, such as LCCC assembled on FR-4, the reliability might be decreased. One thing we are sure of now is that there are many challenges ahead, such as the tin whisker problem, new infrastructure to be built, higher solder joint reflow temperature effect, etc. Solberg [120, pp. 10-14] studied different alloy compositions of lead-free solder joints, their melting temperature and the resulting effects. Xiao, L., et al [121, pp. 145-151] researched on the characterization of mechanical properties of lead-free solders and found that lead-free solder joints have better tensile strength in general. Mutoh Y. et al [122, pp. 37-45] studied the fatigue crack growth behavior of lead-bearing and lead-free solders and found that the lead-free solder joints have a better fatigue crack growth resistance than lead-bearing solder joints. In terms of predicting fatigue life, there are no signs indicating that the past methods are not acceptable. Lau, J., et al [123, pp. S42-2-1-S42-2-13; 124, pp. 403-410], and Lau, J. H. and Lee. S. R. [125, pp. 55-63] studied a lead-free solder joint, 95.5 Sn-3.9 Ag-0.6 Cu using the old methods, and obtained sound results.

The primary disadvantage for using empirical models to quantify fatigue life of solder joints is that it requires strain, or energy release rate data from the testing or Finite Element Methods. This is sometimes difficult to obtain, especially in the early design stages. Another disadvantage of using the above models is that different models are likely to give different answers, and thus it is hard for the designers to determine which model to choose. Third disadvantages of using the above model is that only one solder joint fatigue life can be obtained, the whole board interconnect fatigue life, especially the reliability, and the failure rate, cannot be found. For these three reasons, in this dissertation, the MSSI method will be used to quantify the three interconnects' reliability.

5.3.2 Surface Mount Interconnect

5.3.2.1 Leadless Solder Joints

A leadless solder joint is the most commonly used interconnect method in the current electronic industry. The common leadless surface mount packages include Leadless Ceramic Chip Carriers (LCCC), Leadless Chip Capacitor (LCC), and Leadless Chip Resistors (LCR). The two common forms of the joint are given in Fig. 5.2. Ball Grid Array (BGA) packages belong to this type.

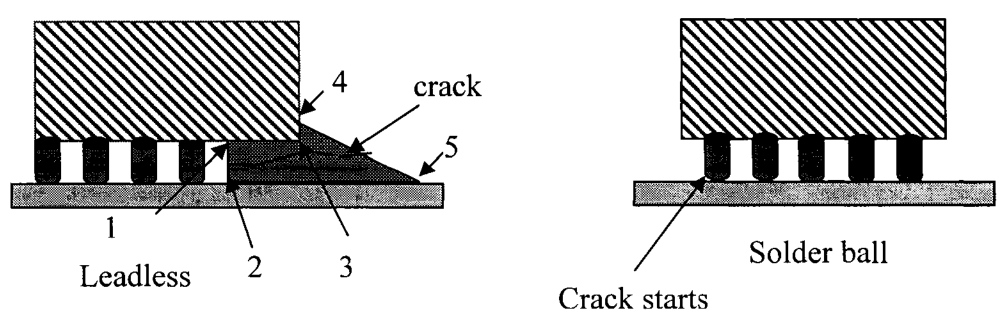

Fig. 5.2 – Examples of leadless solder joints.

The major failure mode of this type of interconnect is cracking due to thermal and mechanical stresses caused by mismatched CTE between modules and the board during thermal cycling and vibration. The crack pattern, path, and location depend on the fatigue resistance of the solders, the strength of the interface, and the location of the stress concentration, etc. Lau, J. H. and Pao, Y-H. [64] found that there are five potential locations where cracks can start for this kind of an interconnect (see Fig. 5.2). Most of the time, the crack starts from Location 3 (primary crack start location) and Location 1 (secondary crack start location) and moves through the solder [99, pp. 104-109]. For the Ball Grid Array (BGA) interconnects, the crack initiates and grows in the solder ball near the attached board/substrate. Also, cracks have been found starting from the outer edge and growing towards the inside solder ball. Shear force appears to be the driven force for leadless interconnect failures.

The shear stress experienced by the solder ball in this interconnect can be treated as the shear stress generated in the interface of two layers since the solder ball is very stiff [126, 291 pp.]. Using this idea, we can model this interconnect as a three layer sandwich. The top layer is module, second layer is solder joint and the third layer is the board. Enger [126] treats the component and board plus solder ball together as a bi-metal thermostat, and obtains an equation for thermal load. For our three-layer model, the stress generated in the solder ball is computed using Eq. (3-57):

$$s^{(solder)}_{yz,\max,vib}(x,y,z_2) = -\sum_{m=1,3,5,\ldots}^{\infty}\sum_{n=1}^{\infty}\frac{\left(z_2^2 - z_1^2\right)}{2}C^{(1)}_{2mn}\cdot W_{mn}(-1)^{\frac{m-1}{2}} - k'\cdot T_1\tanh(k'\cdot l), \quad (5\text{-}24)$$

where

$$C^{(1)}_{2mn} = \beta^3 Q^{(1)}_{11} + \alpha^2 \beta \left(2 \cdot Q^{(1)}_{66} + Q^{(1)}_{12}\right),$$

and

$$W_{mn} = -\frac{16}{m \cdot n \cdot \pi^2} \int_0^\infty h_{mn}(\tau) \ddot{w}_1 (t - \tau) d\tau .$$

It should be noted the stress computed using Eq. (5-24) is for the case when the solder joint is a "solder layer". Thus, for the solder joint without underfill, we need to use a factor to adjust what we get from Eq. (5-24). This factor can be found as follows:

$$C_1 = \frac{4\, s_m}{N\, d_s^2\, \pi}, \tag{5-25}$$

where

N = total number of solder joints in the module,

s_m = area of the module,

and

d_s = diameter of each solder joint (consider the solder joint is a cylinder).

Using this factor yields the stress experienced by solder joints as

$$s^{(solder)}_{yz,\max,vib}(x, y, z_2) = -C_1 \sum_{m=1,3,5,\ldots}^{\infty} \sum_{n=1}^{\infty} \frac{\left(z_2^2 - z_1^2\right)}{2} C^{(1)}_{2mn} W_{mn} (-1)^{\frac{m-1}{2}} - C_1 k' T_1 \tanh(k'l). \tag{5-26}$$

Since any solder joint failing will cause the interconnect to fail, the average stress experienced by each solder joint needs to be determined, which is

$$s_{yz,\max}^{(one-joint)}(x,y,z_2) = -\frac{4s_m}{N^2 d_s^2 \pi} \sum_{m=1,3,5,\ldots}^{\infty} \sum_{n=1}^{\infty} \frac{\left(z_2^2 - z_1^2\right)}{2} C_{2mn}^{(1)} W_{mn} (-1)^{\frac{m-1}{2}} - \frac{4 \cdot s_m}{N^2 d_s^2 \pi} k' \cdot T_1 \tanh(k' \cdot l). \tag{5-27}$$

Since the maximum solder joint stress will occur on the corner solder joints of the module, another adjustment factor should be also utilized, which is

$C = \sqrt{2}$ for a square module, for other shapers this is an approximation.

Then, the maximum stress in a solder joint is given by

$$s_{yz,\max}^{(corner-joint)}(x,y,z_2) = -\frac{4\sqrt{2} \cdot s_m}{N^2 d_s^2 \pi} \sum_{m=1,3,5,\ldots}^{\infty} \sum_{n=1}^{\infty} \frac{\left(z_2^2 - z_1^2\right)}{2} C_{2mn}^{(1)} W_{mn} (-1)^{\frac{m-1}{2}} - \frac{4\sqrt{2} \cdot s_m}{N^2 d_s^2 \pi} k' \cdot T_1 \tanh(k' \cdot l). \tag{5-28}$$

The mean and the variance of this stress are

$$\bar{s}_{yz,\max}^{(corner-joint)}(x,y,z_2) = -\frac{4\sqrt{2}\, s_m}{N^2\, d_s^2\, \pi} k'\, T_1 \tanh(k'\, l), \tag{5-29}$$

and

$$\sigma_{solder}^2 = -\frac{8{,}192}{N^4\, d_s^4\, \pi^6} \frac{\left(z_2^2 - z_1^2\right)^2}{4} \sum_{m=1,3,5,\ldots}^{\infty} \sum_{n=1}^{\infty} \sum_{i=1,3,5,\ldots}^{\infty} \sum_{j=1}^{\infty} C_{2mn}^{(1)}\, C_{2ij}^{(1)} \frac{(-1)^{\frac{m+i-2}{2}}}{m\, n\, i\, j} \cdot \int_0^{\infty} h_{mn}(r_1)\, h_{ij}(r_2)\, R_{\ddot{w}_1 \ddot{w}_1}(r_2 - r_1)\, dr_1\, dr_2. \tag{5-30}$$

Then, the performance function for this failure mode is

$$Z_3 = S_{solder} - s_{yz,\max}^{(corner-joint)}. \tag{5-31}$$

The reliability of the corner joint can be found using Eqs. (2-6) and (2-7) as

$$R_{solder}^{corner} = \Phi\left(\frac{\overline{Z}_3}{\sigma_{Z_3}}\right).$$

The reliability of this interconnect is

$$R_{leadless} = \left(R_{solder}^{(corner)}\right)^N,$$

where N is the number of solder joints in the leadless package.

5.3.2.2 Leaded Solder Joints

The second surface mount interconnect is the leaded solder joint, which have been used for over 35 years. There are two major shapes for leaded solder joints, namely J-lead and the Gull Wing formation. The common packages using leaded solder joints include Plastic Leaded Chip Carrier (PLCC), Small Outline J-leaded (SOJ) packages, Small Outline Gull-Wing Packages (SOP), and Thin Small Outline Packages (TSOP). Figure 5.3 illustrates these two forms of solder joints. Figure 5.4 depicts two packages using J-lead and Gull-Wing interconnections.

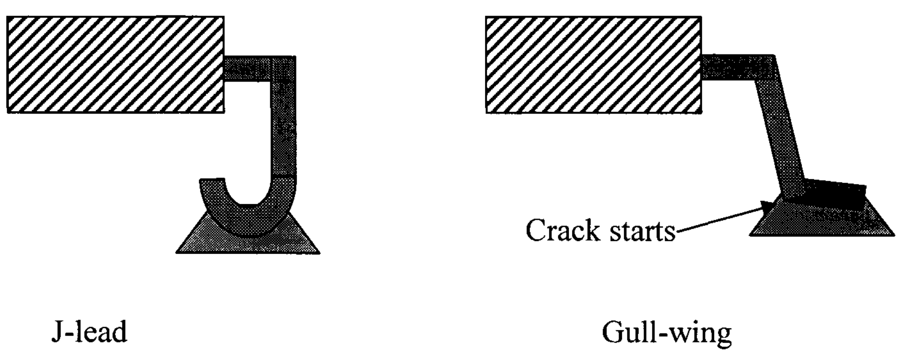

Fig. 5.3 – illustration of leaded solder joint.

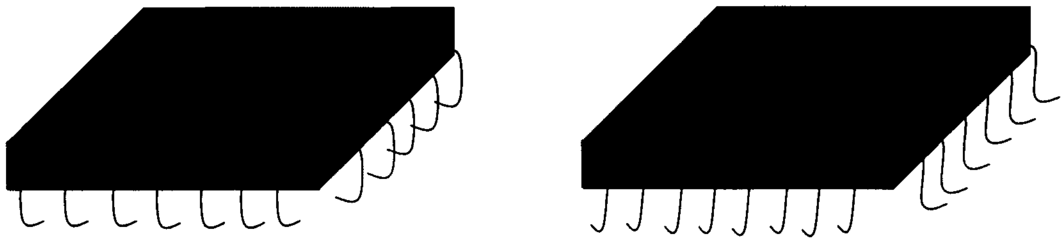

J-lead package

Gull-wing package

Fig. 5.4 – illustration of leaded package.

The failure mode for this type of interconnect is crack starting at the outside of the solder joint and tending to separate it from the lead [126]. The crack for the Gull-Wing leads, for example, normally starts from the heel where the lead bends to form the foot (see Fig. 5.3). Unlike leadless interconnects, the failures are due to shear loading, for leaded interconnects, the normal (peeling) forces appear to be the driving force for the crack formation and growth.

As in the leadless case, the stress that the solder joint and the lead wire experience also includes two parts, one is due to vibration, and the other is due to thermal load. But unlike in the leadless case, we cannot assume that module, lead wire and the board are treated as a three-layer structure since the lead wire is easier to bend. For this interconnect, the stress generated due to vibration can be found by [127]

$$s_{lead}^{(vib)} = \frac{E_w}{N\,L_w}\frac{\delta}{1+\dfrac{L_m^3}{3E_m\,I_m}\dfrac{N\,A_w\,E_w}{L_w}}, \tag{5-32}$$

where

E_W = wire modulus of elasticity,

E_m = module modulus of elasticity,

L_w = length of the lead wire,

L_m = half length of the module,

I_m = moment of inertia of the module,

N = total number of lead wires,

A_w = area of lead wire,

and

$$\delta = w_{\max} - w(\frac{a-l}{2}, \frac{b}{2}),$$
$$= -\frac{16}{\pi^2} \sum_{m=1,3,5,\ldots}^{\infty} \sum_{n=1,3,5,\ldots}^{\infty} \left(\frac{(-1)^{\frac{m+n-2}{2}}}{mn} - \frac{(-1)^{\frac{n-1}{2}} \sin\left(\frac{m\pi}{a}\frac{a-l}{2}\right)}{mn} \right) \cdot \tag{5-33}$$
$$\cdot \int_0^{\infty} h_{mn}(\tau) \ddot{w}_1(t-\tau) d\tau.$$

Figure 5.5 illustrates the strain generated in the lead wire.

The peeling stress for each lead wire due to the thermal stress can be found by treating the lead as a plane frame beam on an elastic foundation. It is given by [126, p. 206]

$$s_{lead}^{(th)} = \frac{E_w\, I_w \sin(2\beta)}{A_w\, L_w^{\;3}} (6 - \frac{A_w\, L_w^{\;2}}{2\, I_w})\, \Delta u\,, \tag{5-34}$$

where

$\Delta u = \alpha_w\, \Delta T_w\, a + \alpha_{beam}\, \Delta T_{beam}\, b - \alpha_b\, \Delta T_b\, (a + b + l\cos\beta)$, this equation is a little different with that given in [126],

I_w = moment of inertia of the lead wire,

and

β = angle between the lead wire and the solder pad.

Figure 5.6 illustrates the schematic of this plane frame.

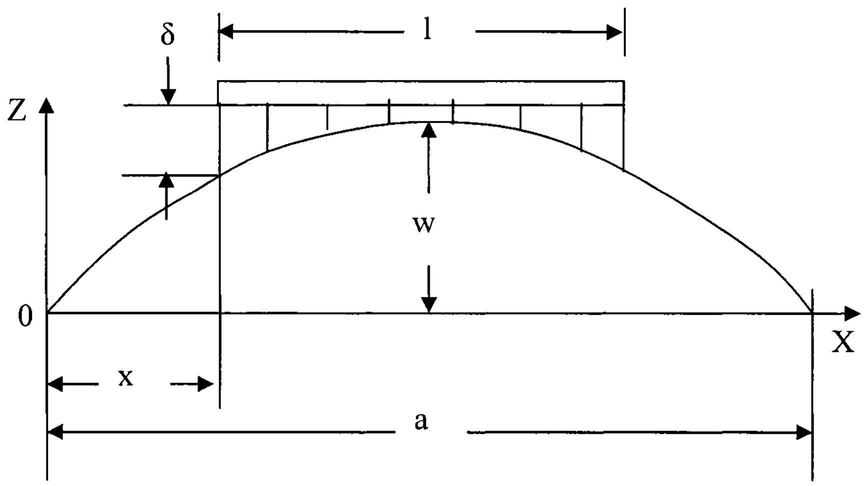

Fig.5.5 - Strain generated in the lead wire when the PCB is subjected to vibration.

Since the corner lead wire will experience the highest stress, the "a" value in the expression of Δu should be half of the diagonal length of the module. Combining Eqs. (5-32) and (5-34) and considering the maximum stress occurs when these two stresses in the same direction, yield

$$s_{lead} = s_{lead}^{(vib)} + s_{lead}^{(th)}, \tag{5-35}$$

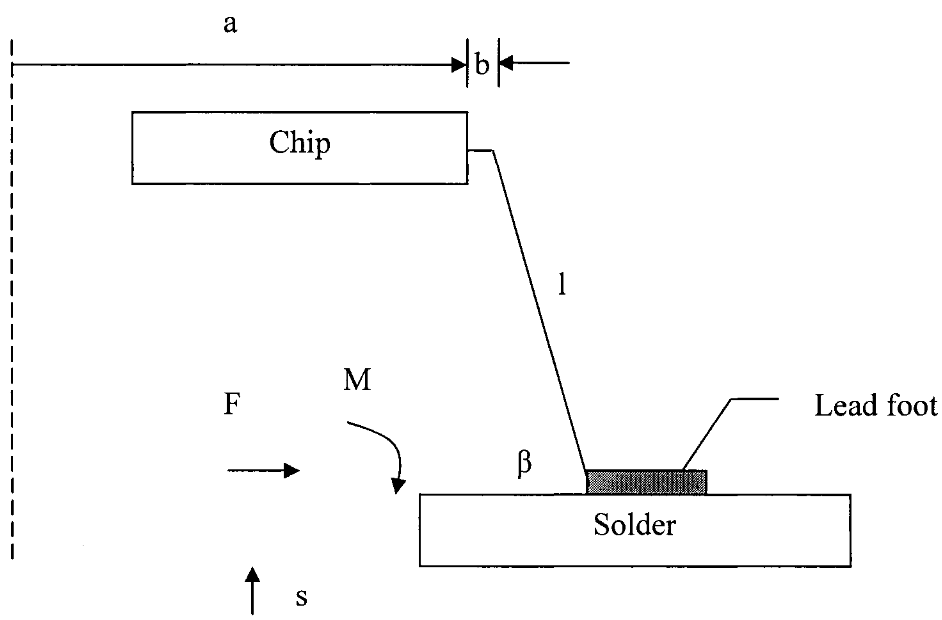

Fig. 5.6 - Schematic of SMT lead force, and moment subjected to thermal stress.

Then, the mean of the stress is

$$
\begin{aligned}
E(s_{lead}) &= \frac{E_w\, I_w \sin(2\,\beta)}{A_w\, L_w^{\ 3}}(6-\frac{A_w\, L_w^{\ 2}}{2\, I_w})\,\Delta\bar{u}, \\
&= \frac{E_w\, I_w \sin(2\,\beta)}{A_w\, L_w^{\ 3}}(6-\frac{A_w\, L_w^{\ 2}}{2\, I_w})\cdot\big[\alpha_m\,\Delta T_m\, a+\alpha_{beam}\,\Delta T_{beam}\, b, \\
&\quad -\alpha_b\,\Delta T_b(a+b+l\cos\beta)\big] \\
&\approx -\frac{E_w\, I_w}{A_w\, L_w^{\ 3}}(6-\frac{A_w\, L_w^{\ 2}}{2 I_w})\,(\alpha_m-\alpha_b)\,\Delta T\, a.
\end{aligned}
\tag{5-36}
$$

The last term is obtained by assuming $\beta = 90$ degrees, the temperature change for module and board are the same, and $b = 0$.

The variance of the stress is

$$\sigma^2_{s_{lead}} = \frac{256}{N^2 \pi^4} \left[\frac{E_w}{L_w} \frac{1}{1 + \frac{L_m^3}{3E_m I_m} \frac{N A_w E_w}{L_w}} \right]^2 \sum_{m=1,3,5,...}^{\infty} \sum_{n=1,3,5,...}^{\infty} \cdot$$

$$\sum_{i=1,3,5,...}^{\infty} \sum_{j=1,3,5,...}^{\infty} \left(\frac{(-1)^{\frac{m+n-2}{2}}}{m\,n} - \frac{(-1)^{\frac{n-1}{2}} \sin\left(\frac{m\,\pi}{a} \frac{a-l}{2} \right)}{m\,n} \right) \cdot$$

$$\cdot \left(\frac{(-1)^{\frac{i+j-2}{2}}}{i\,j} - \frac{(-1)^{\frac{j-1}{2}} \sin\left(\frac{i\,\pi}{a} \frac{a-l}{2} \right)}{i\,j} \right) \tag{5-37}$$

$$\cdot \int_0^{\infty} h_{mn}(r_1)\, h_{ij}(r_2)\, R_{\ddot{w}_1 \ddot{w}_1}(r_2 - r_1)\, dr_1\, dr_2 .$$

Then, the performance function for this interconnect is

$$Z_4 = S_{solder} - s_{c-solder} . \tag{5-38}$$

Thus, the reliability for the corner lead can be computed using Eqs. (2-6) and (2-7).

The interconnect reliability of the whole leaded module can be found as follows:

$$R_{solder} = \left(R_{c-solder} \right)^N , \tag{5-39}$$

where

R_{c-lead} = reliability of corner lead in the leaded package,

and

N = number of leads in the leaded package.

5.3.3 Insertion-Mount Interconnect

The common insertion-mount packages include the Dual In-line packages (DIP), the Pin Grid Array packages (PGA), Plate Through Hole (PTH) packages, Can packages, and the axial discrete capacitors and resistors. This type of interconnect is used less and less recently due to the high density package requirement, but since via is still one of the most important interconnect methods for the transmission line on different layers, study of this interconnect reliability is still needed. Figure 5.7 illustrates a plate/pin through hole and a pin grid array interconnects.

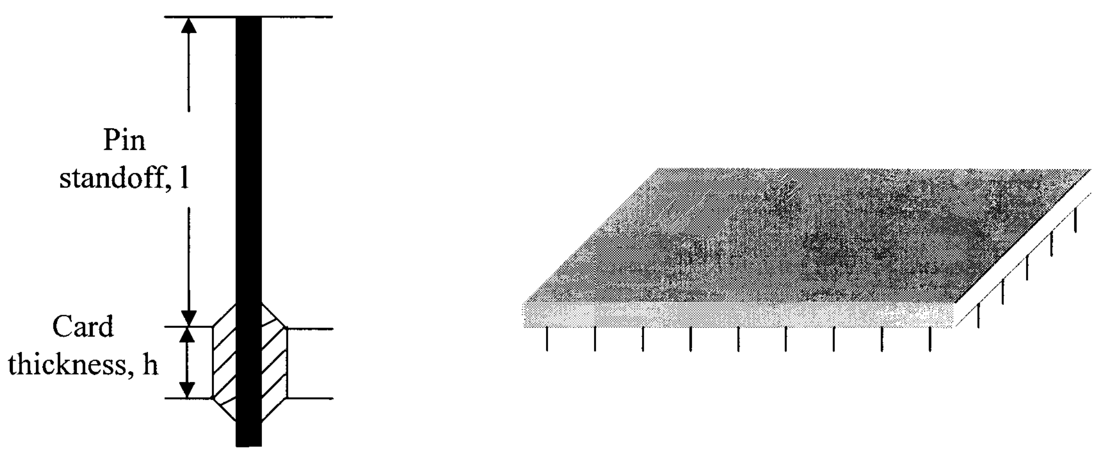

Plate/pin through hole

Pin grid array

Fig. 5.7 – illustration of plate/pin-through hole and pin grid array.

5.3.3.1 Plate/Pin Through Hole Interconnect

The failure modes for the plate/pin through hole are mainly cracks in the solder joints, and cracking of the copper plating or barrel. [128, pp.506-511] [129, pp. 865-872], and [130, pp.30-37] discuss other failure modes and give the effects of many factors on the reliability of the PTH interconnect. There are some other failure modes occurring in

Plate/pin through holes, such as delamination between the board and the barrel, pad corner crack, and pad delamination. However, in this dissertation, only the first two failure modes are considered.

First let's analyze the crack failure mode of the solder joint. The stresses causing this failure include two parts, one is due to thermal load, and the other is due to vibration. The stress caused in one lead wire by thermal load is given by [126, p. 94]

$$s_{solder}^{(th)} = \frac{A_w E_w}{60 \pi c h L_w^2}\left[18(u-u_1)^2 - 3\theta L_w (u-u_1) + 2\theta^2 L_w^2\right], \tag{5-40}$$

where

A_w = area of the lead wire,

E_w = modulus of the lead wire,

c = radius of the lead wire,

L_w = length of the lead wire outside of the board,

$u = (\alpha_m - \alpha_b)\Delta T r$,

r = diagonal length of the module,

$u_1 = \dfrac{3u(\gamma+1)}{(\gamma+1)^3+2}$,

$\gamma = \lambda h = \left(\dfrac{E_s c (b-c)}{E_l I}\right)^{1/4} h$,

b = radius of the hole,

E_s = modulus of the solder joint,

I_w = moment inertia of the lead wire,

and

$$\theta = \frac{6\,u\,\gamma}{L_w\,(\gamma+1)^3 + 2\,L_w}.$$

The stress caused by vibration can be found using the same equation given in Eq.(5-32). We know the maximum stress occurs when vibration induced stress and thermal induced stress are in the same direction; therefore, the maximum stress experienced by the corner solder joint is

$$s_{solder}^{(pth/pin)} = s_{solder}^{(vib)} + s_{solder}^{(th)}\,. \tag{5-41}$$

The mean and variance of this stress are given as follows

$$E\left(s_{solder}^{(pth/pin)}\right) = \bar{s}_{solder}^{(th)}, \tag{5-42}$$

and

$$\begin{aligned}\sigma_{s_{solder}}^2 = {} & \frac{256}{N^2\,\pi^4}\left[\frac{E_w}{L_w}\,\frac{1}{1+\dfrac{L_m^3}{3E_m\,I_m}\,\dfrac{N\,A_w\,E_w}{L_w}}\right]^2 \sum_{m=1,3,5,\ldots}^{\infty}\ \sum_{n=1,3,5,\ldots}^{\infty} \\ & \cdot \sum_{i=1,3,5,\ldots}^{\infty}\ \sum_{j=1,3,5,\ldots}^{\infty}\left(\frac{(-1)^{\frac{m+n-2}{2}}}{m\,n} - \frac{(-1)^{\frac{n-1}{2}}\sin\left(\dfrac{m\,\pi}{a}\,\dfrac{a-l}{2}\right)}{m\,n}\right) \\ & \cdot \left(\frac{(-1)^{\frac{i+j-2}{2}}}{i\,j} - \frac{(-1)^{\frac{j-1}{2}}\sin\left(\dfrac{i\,\pi}{a}\,\dfrac{a-l}{2}\right)}{i\,j}\right) \\ & \cdot \int_0^{\infty} h_{mn}(r_1)\,h_{ij}(r_2)\,R_{\ddot{w}_1\ddot{w}_1}(r_2-r_1)\,dr_1\,dr_2.\end{aligned} \tag{5-43}$$

Then, the performance function for this failure mode is

$$Z_5 = S_{solder} - s_{solder}^{(pth/pin)}, \tag{5-44}$$

$$\overline{Z}_5 = \overline{S}_{solder} - \overline{s}_{solder}^{(pth/pin)}, \tag{5-45}$$

and

$$\sigma_{z_5}^2 = \sigma_{S_{solder}}^2 + \sigma_{s_{solder}}^2. \tag{5-46}$$

Then, the reliability of the corner solder joint is computed using Eqs. (2-6) and (2-7), or

$$R_{c-pin} = \Phi\left(\frac{\overline{Z}_5}{\sigma_{Z_5}}\right). \tag{5-47}$$

The reliability of the pin connection is then computed by

$$R_{pin-con} = \left(R_{c-pin}\right)^N, \tag{5-48}$$

where

R_{c-pin} = reliability of the corner pin in the PTH package,

and

N = number of the pins in the PTH package.

The reliability index for the pin connection is computed using the inverse normal distribution; i.e,

$$m_5 = \Phi^{-1}\left(R_{pin-con}^{(j)}\right). \tag{5-49}$$

Next let's analyze the copper barrel cracking failure mode. The stress in the barrel due to vibration can be found by equaling it to the peeling stress given in Eq. (3-53).

The stress in the barrel due to the thermal load is given by [128, pp. 506-511]

$$s_{barrel}^{(th)} = \frac{(\alpha_b - \alpha_{ba})\Delta T\, E_{ba}\, t_r}{1 + \dfrac{E_{ba}\, t_{ba}}{E_b\,(r_1 - r_0)\,F(\zeta)}}, \tag{5-50}$$

where

$$t_r = \frac{t_{ba}}{t_{bm}\left(1 + \frac{0.75\log(r_1 / r_0)}{(1+\zeta)}\right)},$$

$$\zeta = (r_1 - r_0)\sqrt[4]{\frac{6E_b}{E_{pad}t_{pad}^3 h}},$$

$$F(\zeta) = \zeta\frac{1+\cos^2(\zeta)/\cosh^2(\zeta)}{\tanh(\zeta)+\sin(\zeta)\cos(\zeta)/\cosh^2(\zeta)},$$

α_b, α_{ba} = CTE of the board and the barrel, respectively,

E_{pad} = modulus of the pad,

E_b = modulus of the board,

E_{ba} = modulus of the barrel,

t_{ba} = average thickness of the barrel,

t_{bm} = minimum thickness of the barrel,

t_{pad} = thickness of the pad,

r_1 = pad radius or r_0+e, whichever is greater, $e = \frac{\pi}{2}\sqrt{\frac{E_{pad}\, t_{pad}^3\, h}{6\, E_b}}$,

r_0 = hole radius,

and

h = thickness of the board.

Other stress equations are due to Oien's work [131, pp. 121-128] and Marks's work [10, p. 421]. Refer to related literature for further information.

Then, the stress experienced by a barrel in a plate/pin through hole is given by

$$s_{barrel}^{(pth/pin)} = s_{barrel}^{(vib)} + s_{barrle}^{(th)}. \tag{5-51}$$

The mean and variance of this stress are given by

$$E\left(s_{barrel}^{(pth/pin)}\right) = \bar{s}_{barrel}^{(th)},$$

and

$$\begin{aligned}\sigma_{barrel}^{2} = \frac{256}{\pi^4} \sum_{m=1,3,5,...}^{\infty} \sum_{n=1,3,5,...}^{\infty} \sum_{i=1,3,5,...}^{\infty} \sum_{j=1,3,5,...}^{\infty} \frac{(-1)^{\frac{m+n+i+j-4}{2}}}{m\,n\,i\,j}\cdot \\ \cdot\left[\left(\frac{z^3}{6}-\frac{z\cdot z_k^2}{2}\right)\left(-\frac{m\pi}{a}C_{1mn}^{(k)}-\frac{n\pi}{b}C_{2mn}^{(k)}\right)+C_{3mn}^{(k)}\right]\cdot \\ \cdot\left[\left(\frac{z^3}{6}-\frac{z\cdot z_k^2}{2}\right)\left(-\frac{i\pi}{a}C_{1ij}^{(k)}-\frac{j\pi}{b}C_{2ij}^{(k)}\right)+C_{3ij}^{(k)}\right] \\ \cdot\int_0^{\infty} h_{mn}(r_1)\,h_{ij}(r_2)\,R_{\ddot{w}_1\ddot{w}_1}(r_2-r_1)\,dr_1\,dr_2.\end{aligned} \tag{5-52}$$

The performance function for the barrel failure mode is given by

$$Z_6 = S_{barrel} - s_{barrel}^{(pth/pin)}. \tag{5-53}$$

Thus, the reliability of one of the barrel in the plate/pin through hole interconnect can be computed using Eqs. (2-6) and (2-7), or

$$R_{barrel}^{(i)} = \Phi\left(\frac{\bar{Z}_6}{\sigma_{Z_6}}\right), \tag{5-54}$$

where

$R_{barrel}^{(i)}$ = reliability of the ith barrel in the PTH package.

If there are a total of N pins in the plate/pin-through hole module, then the reliability of the interconnect for each plate/pin through hole module due to barrel failure can be found by

$$R_{barrel} = \left(R_{barrel}^{(n)}\right)^N. \tag{5-55}$$

Then, the reliability index for this failure mode is found through the inverse normal distribution; i.e.,

$$m_6 = \Phi^{-1}\left(R_{barrel}\right). \tag{5-56}$$

It should be noted that the two failure modes of Pin/Plate Through Hole are not independent, we need to compute their correlation coefficient before we can find the reliability of this interconnect.

To simplify the derivation, let's denote the two performance functions as

$$Z_5 = S_5 - s_5^{vib} - s_5^{th},$$

and

$$Z_6 = S_6 - s_6^{vib} - s_6^{th},$$

with the means of

$$\overline{Z}_5 = \overline{S}_5 - s_5^{th},$$

and

$$\overline{Z}_6 = \overline{S}_6 - s_6^{th},$$

and the variances of

$$\sigma_{Z_5}^2 = \sigma_{S_5}^2 + \sigma_{s}^2,$$

and

$$\sigma_{Z_6}^2 = \sigma_{S_6}^2 + \sigma_{s_6}^2.$$

Then, the correlation coefficient is

$$\rho_{56} = \frac{E[(Z_5 - \bar{Z}_5)(Z_6 - \bar{Z}_6)]}{\sigma_{Z_5}\,\sigma_{Z_6}} = \frac{E[(S_5 - \bar{S}_5 - s_5^{vir})(S_6 - \bar{S}_6 - s_6^{vir})]}{\sigma_{Z_5}\,\sigma_{Z_6}}. \tag{5-57}$$

Since

$$E[(S_5 - \bar{S}_5 - s_5^{vir})(S_6 - \bar{S}_6 - s_6^{vir})] = E[(S_5 - \bar{S}_5)(S_6 - \bar{S}_6)] - E[(S_5 - \bar{S}_5)s_6^{vir}]$$
$$- E[(S_6 - \bar{S}_6)s_5^{vir}] + E(s_5^{vir} s_6^{vir}),$$

or

$$E[(S_5 - \bar{S}_5 - s_5^{vir})(S_6 - \bar{S}_6 - s_6^{vir})] = E(s_5^{vir} s_6^{vir}),$$

because S_5 and S_6 are independent, and $E(S_i - \bar{S}_i) = 0$. Then, Eq. (5-57) becomes

$$\rho_{56} = \frac{E[s_5^{vib} s_6^{vib}]}{\sigma_{Z_5}\,\sigma_{Z_6}}. \tag{5-58}$$

This equation can be generalized as

$$\rho_{ij} = \frac{E[s_i^{vib} s_j^{vib}]}{\sigma_{Z_i}\,\sigma_{Z_j}}. \tag{5-59}$$

It can be used for our computation of the whole PCB's reliability.

For the Plate Through Hole case,

$$E\left(s_5^{vir} s_6^{vir}\right) = \frac{256}{\pi^4} \frac{E_w}{N L_w} \frac{1}{1 + \frac{L_m^3}{3 E_m I_m} \frac{N A_w E_w}{L_w}} \cdot$$

$$\sum_{m=1,3,5,..}^{\infty} \sum_{n=1,3,5,...}^{\infty} \sum_{i=1,3,5,...}^{\infty} \sum_{j=1,3,5,...}^{\infty} \left[\left(\frac{(-1)^{\frac{m+n-2}{2}}}{m n} - \frac{(-1)^{\frac{n-1}{2}} \sin\left(\frac{m \pi}{a} \frac{a-l}{2} \right)}{m n} \right) \right. \cdot \tag{5-60}$$

$$\cdot \left(\left(\frac{z^3}{6} - \frac{z \cdot z_k^2}{2} \right) \left(-\alpha\, C_{1mn}^{(k)} - \beta\, C_{2mn}^{(k)} \right) + C_{3mn}^{(k)} \right) \frac{1}{i\, j}$$

$$\cdot \int_0^{\infty} h_{mn}(r_1)\, h_{ij}(r_2)\, R_{\ddot{w}_1 \ddot{w}_1}(r_2 - r_1)\, dr_1\, dr_2,$$

Then, using Eq. (2-29), we can quantify the reliability of the PTH interconnect from

$$R_{pth/pin} = \int_0^{\rho_{56}} w(-m_5, -m_6, r)\, dr + \Phi(m_5) \cdot \Phi(m_6), \tag{5-61}$$

where

m_5 and m_6 = reliability index for pin connection and barrel, respectively.

They are given by Eqs. (5-49) and (5-56)

5.3.3.2 Pin Grid Array (PGA)

The failure mode of the Pin Grid Array interconnect is solder joint crack. It is the same as the PTH case except it does not have barrel failure. Therefore, the reliability of this interconnect can be found using the same method as in the PTH case, using Eqs. (5-41) - (5-48) to compute the reliability of the PGA interconnect.

5.4 Failure Modes of the Parts on the PCB

There are many kinds of parts mounted on the PCB. Some of them are active parts, and some are passive parts; some of them are in the package form, some are discrete parts;

some of them are in plastic packages, some are not. In the plastic package, some are in ball grid array, some are in pin grid array, some are chip scale package; etc. Beelen-Hendrikx and Verguld [132, pp. 24-32] discussed the application trends of different package types in electronic packaging and assembly for portable consumer products. The variety of parts on the board makes quantification of the parts-on-board's reliability very difficult since different kinds of packages, or parts, have different failure modes. For example, for plastic package, delamination/crack caused by the popcorn effect is one of the major failure mode [133, pp. 269-273; 5, 56-65; 6, pp. 301-308; 134, pp. 392-399, etc.], while for TAB-bonded chips, the major failure modes are the fracture of the lead [135, pp. 856-864], and other failure modes such as corrosion [136, pp. 1105-1116; 137, pp. 86-92]. The failure modes of other kinds of packages or parts have also been studied by many researchers [138, pp. 97-103; 139, pp. 286-290; 140, pp. 84-87, 141, pp. 457-463; 142, pp. 399-404; 143, pp. 83-87; 144, pp. 93-97, 145, pp. 341-346; and 146, pp. 122-127]. Engel [147, pp. 262-267] introduced wear-out modes and mechanisms. Li [148, pp. 339-353; 149, pp. 2-10] introduced creep and aging failure mechanisms, respectively. Therefore, it is hard and not reasonable to quantify the reliability of the parts-on-board by considering all of the failure modes.

In this dissertation, a modified MIL-HDBK-217 type method will be employed to quantify the parts-on-board reliability. The basic idea of this method is as follows: for discrete parts, their reliability is computed directly using the MIL-HDBK-217 type of method, and for parts in package form, their reliability will be computed by considering both chip failures and packaging part failures. For example, for the package shown in

Fig.5.8, the chip reliability will be computed using the MIL-HDBK-217 type method while packaging part reliability will be computed using the MSSI method. To simplify the reliability quantification, the following assumptions are made for the modified MIL-HDBK-217 type method:

1. The MIL-HDBK-217 type method is applicable for discrete parts and chips inside the package.
2. Chips and packaging part failures are independent.
3. All packages on the PCB are plastic packages. This is a reasonable assumption since plastic packages are the most promising technology in terms of cost and performance for future microelectronics [150, pp. 401-404]. Only delamination/crack failure modes caused by the popcorn effect will be considered for packaging parts. It should be noted that even though we assume all packages are plastic for the sake of simplicity, the method introduced in this section is applicable to any other kind of packages.

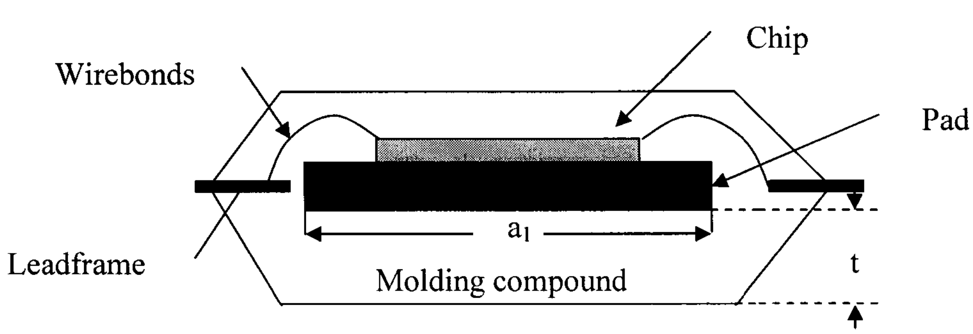

Fig. 5.8 – Schematic of a plastic package.

5.4.1 Discrete Parts and Chip Failure Modes

The failure modes of discrete parts and chips have been discussed previously. Its reliability will be computed using the MIL-HDBK-217 type method, denoted as $R_{chip}^{(i)}$, i = 1, …, P, where P is the number of parts in the package form, and $R_{dis-part}^{(j)}$, j =1, …, M-P, and M is the total number of parts on the board.

5.4.2 Failure Modes Caused by the Popcorn Effect

The popcorn phenomenon is a very severe problem for plastic-encapsulated packages. Its main effect is that it causes the packages to crack either right away during the reflow process or after it is delivered to customers. The latter case is in general more severe and important, and it is our research interest because if the package failed during the reflow, the manufacturers can discard the package. However, if the packages do not fail during the reflow, but are damaged, then the damaged packages will be delivered to the customers. If these packages are used in safety-related applications, their failures may cause great losses; if these packages fail in the early stage, then the manufacturers will have to pay much due to the warranty. Therefore, both the manufacturers and the customers want to know when this package will fail, and at a certain time what the reliability is. In fact, some failure modes caused by delamination have been found in the consumer's electronic products in the market [132, pp. 269-273].

The basic process of a popcorn is as follows [5, pp. 56-65; 6, pp. 301-308]: During the reflow process, the package is subjected to a very high temperature, normally between 220-240 °C for the lead-tin solder (it might increase a little for a lead-free solder joint, to around 260 °C), at this high temperature, delamination between the die pad and the molding compound (MC) interface or other interfaces may occur due to the thermal stress caused by mismatch of the coefficients of thermal expansion (CTE) between different materials; then the moisture inside the molding compound (absorbed during regular storage condition or operation) is diffused into the delaminated gap, vaporized, and expanded abruptly. When the stress caused by the vapor pressure is higher than the critical interfacial adhesion strength of the molding compound, the plastic package will be cracked or damaged. Figure 5.9 illustrates a schematic of a plastic encapsulated package where popcorn may cause the cracks. This agrees with Ho's survey [132, 269-273] on delamination failures on some consumers' electronic products, such as cell phones, VCRs, discmans, etc.

Based on the locations where the cracks occur, some researchers categorized the popcorn into different modes [5, pp. 56-65; 6, pp. 301-308; and 7, pp. 362-367]. For reliability quantification purposes, it is not necessary to differentiate these modes.

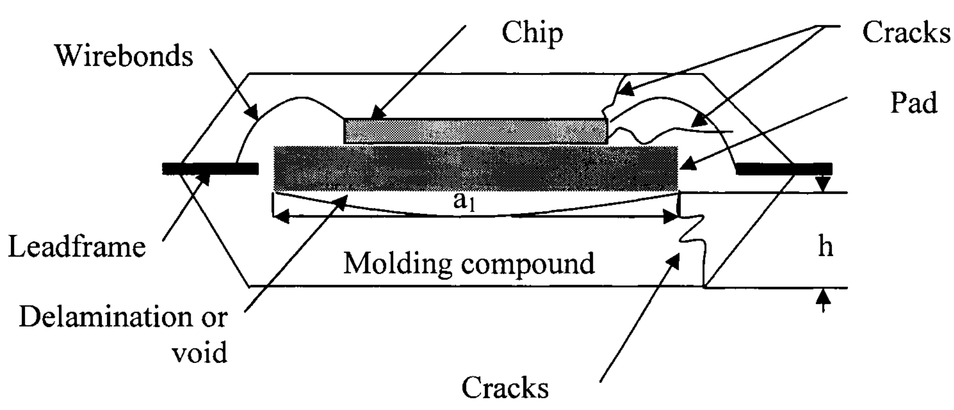

Fig. 5.9 – Illustration of popcorn caused failure modes.

The reliability in terms of this failure mode can be quantified based on the failure process of popcorn-caused failure modes discussed previously. There are three contributors to this type of failure. The first is the thermal stresses due to Coefficient of Thermal Expansion (CTE) mismatch; the second is vapor stress generated during the reflow; the third is the vapor stress generated during normal usage. The initial reliability of the package can be found by considering the first two processes. It is one minus the product of the probability of delamination and the unreliability after reflow. The reliability at any time after reflow will be a little complicated to compute since the reflow condition and the operating conditions are different, the conditional reliability or equivalent reliability concept should be used to compute the reliability of the package at any time. The initial reliability of the chip due to the popcorn effect is computed by

$$R_p = 1 - P_{th} \cdot F_{re}(t_{re}). \tag{5-62}$$

The reliability of the chip due to popcorn effect at any time after reflow is given by

$$R_p = 1 - P_{th} F_{re}(t_{re}) F_{op}(t \mid t_{re}) = 1 - P_{th} F_{re}(t_{re}) \frac{F_{op}(t + t_{re}^{(eq)})}{F_{re}(t_{re})},$$

or

$$R_p = 1 - P_{th} F_{op}(t + t_{re}^{(eq)}), \tag{5-63}$$

where

P_{th} = probability that delamination will occur,

$F_{re}(t_{re})$ = unreliability of the package after t_{re} hours of reflow,

$F_{op}(t|t_{re})$ = conditional unreliability of the package at t hours after reflow,

$t_{re}^{(eq)}$ = equivalent time for t_{re} at normal usage condition,

and

$F_{op}(t+t_{re}^{(eq)})$ = unreliability for a mission time $t+t_{re}^{(eq)}$ when considering a mission starting from the beginning of the reflow.

P_{th} , $F_{re}(t_{re})$, and $F_{op}(t+t_{re}^{(eq)})$ can be found using the MSSI method as follows:

$$P_{th} = P(s_{th} > S_{ad}), \tag{5-64}$$

$$F_{re}(t_{re}) = P(s_{re} > S_{\text{mod}}(t_{re}^{(re)})), \tag{5-65}$$

and

$$F_{op}(t+t_{re}^{(eq)}) = P(s_{op} > S_{\text{mod}}(t+t_{re}^{eq})), \tag{5-66}$$

where

s_{th} = thermal stress,

S_{ad} = adhesion strength,

$S_{\text{mod}}(t_{re}^{(re)})$ = molding compound strength at the end of reflow,

s_{re} = vapor induced stress during the reflow process,

$S_{\text{mod}}(t+t_{re}^{(eq)})$ = molding compound strength at time $t+t_{re}^{(eq)}$,

and

s_{op} = vapor induced stress at normal use condition.

The thermal stress inducing the delamination failure mode can be found through bi-metal thermostat stress analysis. Suhir [151, pp. 657-660; 152, pp. 595-

600] and many others, such as [153, pp. 349-353] and [154, pp. 393-399], have investigated these stresses, Glaser, J. C. [155, pp. 24-29] compared Suhir's method with other methods and concluded that Suhir's method provides fairly good results. The thermal stress from Suhir's research includes two stresses, one is shear stress, and the other one is peeling stress, and they are given by [151, pp. 657-660]

$$\tau_{\max} = \frac{\Delta\alpha\,\Delta T}{\sqrt{\lambda\,\kappa}}\tanh(k\,a)\,, \tag{5-67}$$

and

$$p_{\max} = \frac{\mu}{\kappa}\Delta\alpha\,\Delta T, \tag{5-68}$$

where

$$\lambda = \frac{1}{12}\left(\frac{h_1^2}{D_1} + \frac{h_2^2}{D_2} + \frac{3\,(h_1 + h_2)^2}{D_1 + D_2}\right),$$

$D_i = \dfrac{E_i\,h_i^2}{12\,(1 - v_i^2)}$, i = 1, 2, flexural rigidities of the pad and the molding compound, respectively,

a = half length of the pad,

h_i = thickness of the pad and the molding compound, respectively, i = 1, 2,

$$\kappa = \frac{2\,(1 + v_1)}{3\,E_1}h_1 + \frac{2\,(1 + v_2)}{3\,E_2}h_2\,,$$

$$k = \sqrt{\frac{\lambda}{\kappa}}\,,$$

and

$$\mu = \frac{h_2\, D_1 - h_1\, D_2}{2\,(D_1 + D_2)}.$$

Considering that both stresses will contribute to the delamination failure, we use the following equation to compute the thermal stress:

$$s_{th} = \sqrt{\tau_{\max}^2 + p_{\max}^2} = \sqrt{\frac{\tanh^2(k\,a)}{\lambda\,\kappa} + \frac{\mu^2}{\kappa^2}}\Delta\alpha\,\Delta T\,. \tag{5-69}$$

The performance function for the delamination failure mode is then obtained from

$$Z_{del} = S_{ad} - s_{th}. \tag{5-70}$$

Then, the minimum distance method can be used to find out the probability of the delamination.

Next, we need to find the reliability expressed by Eq. (5-62) or (5-63). It should be noted that the mean strength distribution parameters for the reflow and the operation will be different in most cases. Therefore, to find the reliability at any time after reflow, Eqs. (2-37)-(2-40) or (2-46) should be employed to find the equivalent time.

The vapor pressure stress generated inside the package can be found using Eq. (5-71) [156, 10 pp.].Other equations can be found from the following related papers: [6, p. 302], [157, p. 38], [158, pp. 31-38], [159, pp. 204-210], and [160, pp. 129-132]. Thus,

$$s_m = 6\,K\,P_{H_2O,Cavity}(T)\left(\frac{a_1}{t}\right)^2 \tag{5-71}$$

where

s_m = stress generated inside the package,

K = shape parameter, = 0.5 for a square pad,

$P_{H_2O,Cavity}(T)$ = pressure inside the cavity,

a_l= length of the pad,

and

t = thickness of the molding compound.

$P_{H_2O,Cavity}(T)$ can be found using following equation:

$$P_{H_2O,Cavity}(T) = RH_0 \; P_{sat,H_2O}(T_0)\, e^{-\frac{Q_s}{K}\left(\frac{1}{T_0}-\frac{1}{T}\right)}, \tag{5-72}$$

where

RH_0 = relative humidity at temperature T_0,

$P_{sat,H_2O}(T_0)$ = saturation pressure at temperature T_0, which can be found using Figure 5-10,

Q_s = 0.1 eV,

and

K = Boltzmann's Constant, 8.617385×10^{-5} eV/K.

Then, the performance function related to the moisture failure is

$$Z_{mo} = S - s_m,$$

where

S = strength of the molding compound at any time of interest. As we stated before it has to be computed using the corresponding equations given in Chapter 2.

The reliability related to the moisture failure mode can be found using the Minimum Distance Method.

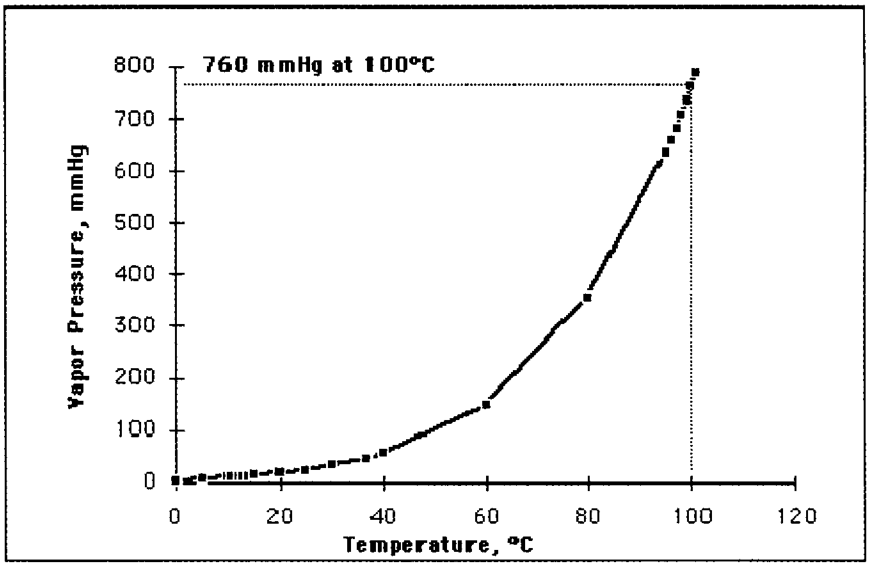

Fig. 5.10 - Saturated vapor pressure for water
(http://hyperphysics.phyastr.gsu.edu/hbase/kinetic/watvap.html)

Finally, the reliability related to the popcorn effect can be found using Eqs. (5-62) or (5-63), depending on what reliability is of interest.

The reliability of parts mounted on the board is equal to the reliability of the chips in the package times the reliability of the popcorn effect failure mode, and times the reliability of the discrete parts on the board, which is given by

$$R_{part} = \prod_{i=1}^{P} R_{chip}^{(i)} R_{p}^{(i)} \prod_{j=1}^{M-P} R_{dis-parts}^{(j)}, \tag{5-73}$$

where

R_{part} = reliability of all parts mounted on the board,

i = index number of packages on the board,

j = index number of discrete parts on the board,

$R_{chip}^{(i)}$ = reliability of the chip in the ith package,

$R_{p}^{(i)}$ = reliability of the packaging part due to popcorn effect in the ith package,

and

$R_{dis-parts}^{(j)}$ = reliability of the jth discrete part.

Table 5.1 illustrates an example of parts reliability quantification using Bellcore method.

Table 5.1 Example of reliability prediction using the Bellcore method.

Example of Reliability Prediction

MODEL NO.: MAIN MODULE

MTBF calculated, BellCore Technical Reference TR-332, Issue 6, December 1997
"Reliability Prediction Procedure for Electronic Equipment"

PART NUMBER Main Module DATE: 2/18/2004

MTBF = 5.0 Years

FIT = 23007.22
Ambient Temperature = Head-end Distribution and Customer Premises
Environmental Factor = 2 1=Gnd Fixed-Controlled; 2 = Gnd Fixed un-controlled,
Operating Temperature = 40 °C

Motorola PN	QTY	Failure Rate (FIT)	Temp Curve	Elec. Curve	Elec. Stress	Quality Level	Oper. Temp	FIT
506444-001-00	10	3	10		0.5	2	40	60.0
106115-002-00	2	150			0.5	2	40	600.0
110090-220-00	1	1	1	H	0.5	2	40	2.0
119010-015-00	1	2	7		0.5	2	40	4.0
119010-021-00	1	2	7		0.5	2	40	4.0
119020-048-00	2	4	7		0.5	2	40	16.0
123647-700-00	99	1	1	H	0.5	2	40	198.0
123672-117-00	3	1	1	H	0.5	2	40	6.0
123673-697-00	1	1	1	H	0.5	2	40	2.0
125101-303-00	1	0.5	3	C	0.5	2	40	1.0
125102-212-00	2	0.5	3	C	0.5	2	40	2.0
125144-991-00	1	0.5	3	C	0.5	2	40	1.0
127020-103-00	8	0.5	3		0.5	2	40	8.0
138194-000-00	1	9	3	E	0.5	2	40	18.0
157996-071-00	4	0.5	3		0.5	2	40	4.0
185223-000-00	6	0.6	7		0.5	2	40	7.2
404023-001-00	2	4	6		0.5	2	40	16.0
404589-001-00	2	0.5	3		0.5	2	40	2.0
407710-001-00	1	3.2	7		0.5	2	40	6.4
412599-001-00	9	1	3	G	0.5	2	40	18.0
413656-001-00	1	50	3	C	0.5	2	40	100.0
413992-001-00	3	1.036			0.5	2	40	6.2
414237-001-00	1	2.8	7		0.5	2	40	5.6
414705-001-00	1	5			0.5	2	40	10.0
414706-001-00	3	5			0.5	2	40	30.0
463027-001-00	27	4	1	H	0.5	2	40	216.0
463027-003-00	40	4	1	H	0.5	2	40	320.0
463027-005-00	4	4	1	H	0.5	2	40	32.0
464882-038-00	4	0.5	3	C	0.5	2	40	4.0
465119-001-00	34	0.5	3	C	0.5	2	40	34.0
465119-026-00	5	0.5	3	C	0.5	2	40	5.0
465119-038-00	20	0.5	3	C	0.5	2	40	20.0
465119-048-00	10	0.5	3	C	0.5	2	40	10.0
465119-050-00	1	0.5	3	C	0.5	2	40	1.0
465119-053-00	12	0.5	3	C	0.5	2	40	12.0
467066-311-00	1	0.5	3	C	0.5	2	40	1.0
467066-331-00	1	0.5	3	C	0.5	2	40	1.0
467066-335-00	5	0.5	3	C	0.5	2	40	5.0
467066-385-00	3	0.5	3	C	0.5	2	40	3.0
467639-001-00	32	1	1	H	0.5	2	40	64.0
467727-001-00	5	3.94			0.5	2	40	39.4
467983-001-00	43	1	1	H	0.5	2	40	86.0

CHAPTER 6

APPLICATION OF THE RELIABILITY QUANTIFICATION METHOD TO A 4-SIGNAL-LAYERED PCB

In this Chapter, a comprehensive example will be solved to demonstrate the application of the reliability quantification method proposed in this dissertation.

Example 6-1

An electronic component manufacturer wants to design a new PCB, which will be used in a vibration and thermal environment. The management wants to know the reliability of the product before its design is fixed for production. The PCB has 4 signal layers with 3 active IC packages and one passive package with the same dimensions of $0.013\times0.013\times0.00051$ m^3 mounted on the PCB of $0.15\times0.0635\times0.001354$ m^3. The details of each IC and passive package are as follows:

- IC No. 1 is a plastic package, located at x = 0.02 m, y = 0.03 m and generates a power of 0.2 w/m^3. The coordinate system is shown in Fig. 4-1. It uses leadless Surface Mount Technology (SMT) with a total of 52 solder joints. Each solder joint is 0.00028 m high and the diameter is 0.002 m. The molding compound is made of epoxy with a Young's modulus of 15.5 GPa, the Poisson's ratio of 0.25, and CTE of 15.0 ppm/°C. The pad material is ceramic with a Young's modulus of 275.8 GPa, Poisson's ratio of 0.22, and CTE of 1.6 ppm/°C. The thickness of the molding compound is 0.0008 ± 0.00006 m, the thickness of the pad is 0.0004 ± 0.00003 m, the half length of the pad is 0.015 ± 0.0003 m, and the width is 0.03 ± 0.0003 m. The strength of the adhesion is normally distributed with the initial mean 40 MPa and the standard deviation of 1 MPa, and the strength of the molding compound follows the normal distribution with the initial mean of 60 MPa and the standard deviation of 8 MPa. The mean strength of the molding compound is degraded with time and follows the equation of $e^{-0.001t}$ for reflow condition, and $e^{-0.0001t}$ for normal use condition. The standard deviations for both strengths are constant. The reflow time is 200 s at the temperature of 230°C. The storage temperature for the package before it is reflowed is 150°C with a standard deviation of 20°C. The ambient temperature is assumed to be 25°C. The relative humidity is 85%, and the saturated vapor pressure at 25°C is 3167.73 Pa. The normal use condition is 50°C with a standard deviation of 5°C.

- IC No.2 is a ceramic package, locates at x = 0.075 m, y = 0.03 m, and generates a power of 0.2 w/m^3. It uses leaded SMT with 52 Kovar lead wire. The height of lead wire is 0.00218 m and the diameter is 0.000203 m.
- IC No. 3 is also a ceramic package, locates at x = 0.13 m, y = 0.03 m, and generates a power 0.4 w/m^3. It uses the PGA technology with Kovar pins. The stand-off of the pin is 0.00157 m, the diameter is 0.000203 m and the hole's diameter is 0.000382 m.
- The passive module is mounted on the PCB using a Plate-Through Hole (PTH) technology.

The laminated PCB is shown in Fig. 6.1, and the material property and other needed data for this application are given in Table 6.1. Assuming that the vibration is an ideal white noise vibration with a power spectral density of 20.6 m^2/S^3. Find the following:

1. The temperature distribution of the board. It is known that the density of the board is 2850 kg/m^3, the thermal conductivity is 17 w/m°C in the x-y direction, and 0.2 w/m°C in the z direction, the convective heat transfer coefficient for top and bottom of the surface is 5, and the specific heat is 1,300.
2. The Reliability of the laminated board at time t =0, 1,000 hr, and 5,000 hr. Assuming that the interfacial shear strength between each layer of the laminated board is normally distributed with the initial strength of 48.75 MPa, the standard deviation of 3.895 MPa, and its mean value follows an exponential distribution with parameter of γ = 100 hr, η = 10,000 hr, and that the interfacial peeling strength is also normally distributed with the initial mean strength of 70 MPa, and the standard deviation of 3 MPa., and its mean follows the Weibull distribution with parameters of $\beta = 2$, η = 1,000 hr, and $\gamma = 0$. Assuming that the highest module on the board is 0.005 m, and the clearance requirement is 0.01m.
3. The Reliability of the interconnect between the IC No.1 and the board. The strength of the solder joint is normally distributed with the mean of 36.85 MPa and the standard deviation of 5 MPa.
4. The Reliability of the interconnect between the IC No. 2 and the board.
5. The Reliability of the interconnect between the IC No.3 and the board.

6. The Reliability of the interconnect between the passive package and board. It is given that α_b=28.98 ppm/°C, α_{ba}=17 ppm/°C, ΔT=20 °C, E_{ba} = 124 GPa, t_{ba} = 0.00004 m, t_{bm} =0.000015 m, t_{pad} = 0.00005 m, r_l = 0.0006 m, r_0= 0.0003 m, E_b = 4.0 GPa, E_{pad} = 90 GPa, and the mean yield strength of the barrel is 100 MPa and the standard deviation is 10 MPa.
7. The Reliability Quantification of the Plastic Package No.1 due to the popcorn effect at time 0, 1,000 hr, and 5,000 hr.
8. The Reliability of the whole PCB considering all of the failure modes.

Table 6.1 - Material data used in Example 6-1.

material	Cu	Epoxy-Glass	Cu-clad Invar	Kovar	Board	Solder joint	Module
Modulus (GPa)	124	2.7	200	138		13.8	300
Poisson ratio	0.328	0.35	0.3		0.39	0.35	0.3
CTE	17	39.6	3			25	3.5
Density kg/m^3	8,900	1,450	4,260		2,85 0		
Damping , NS/m					1.53E4 for board 200 for cushion		
Spring constant, N/m					400,000 for support cushion		

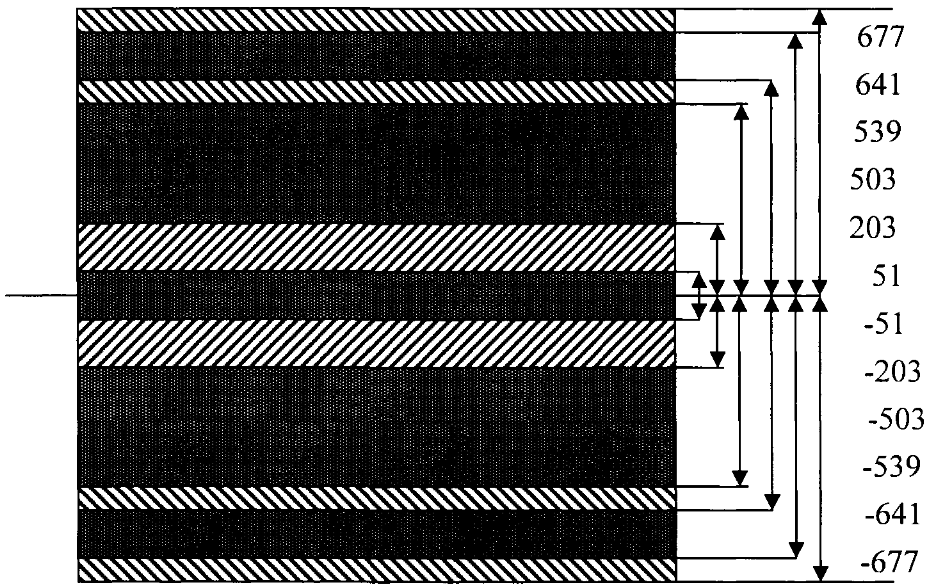

Fig. 6.1 - Illustration of a laminated PCB.

Copper (signal layers).

Epoxy glass.

Copper clad invar.

Unit: $\times 10^{-6}$ m.

Solution to Example 6-1

1. Temperature distribution of the board

First let's find out the material property data for the board. The in-plane modulus and the CTE are computed from

$$E_x = E_y = \frac{\sum_{i=1}^{3} h_i E_i}{\sum_{i=1}^{3} h_i} = \frac{4 \times 36 \times 124 + 906 \times 2.7 + 304 \times 200}{1{,}354} = 59.90 \text{ GPa},$$

and

$$\alpha_x = \alpha_y = \frac{\sum_{i=1}^{3} h_i \, \alpha_i \, E_i}{\sum_{i=1}^{3} h_i \, E_i} = \frac{144 \times 17 \times 124 + 906 \times 39.6 \times 2.7 + 304 \times 3 \times 200}{144 \times 124 + 906 \times 2.7 + 304 \times 200},$$

or

$$\alpha_x = \alpha_y = 7.19 \text{ ppm/C}.$$

The z direction modulus and CTE can be found using a constant stress model of

$$E_z = \frac{h}{\frac{h_1}{E_1} + \frac{h_2}{E_2} + \frac{h_3}{E_3}} = 4.00 \text{ GPa},$$

and

$$\alpha_z = \frac{\sum_{i=1}^{3} h_i \, \alpha_i}{\sum_{i=1}^{3} h_i} = 28.98 \text{ ppm/°C}.$$

The temperature distribution of the board can be found using Eq. (4-6). Figure 6.2 is a slice plotting of the temperature distribution of the board, the slice positions are at x = 0.01 m, 0.05 m, 0.08 m, 0.13 m, y = 0.03 m, and z = 0 m, and -0.001 m. Figure 6.3 illustrates the contour plotting of the temperature distribution on the top surface of the board. Appendix H gives the Matlab codes for this example.

For reliability purpose, the maximum temperature difference is the main concern. From the computation result, we see that the maximum temperature difference is about 20 °C and is on the top of the board. This result will be used to compute the following reliability.

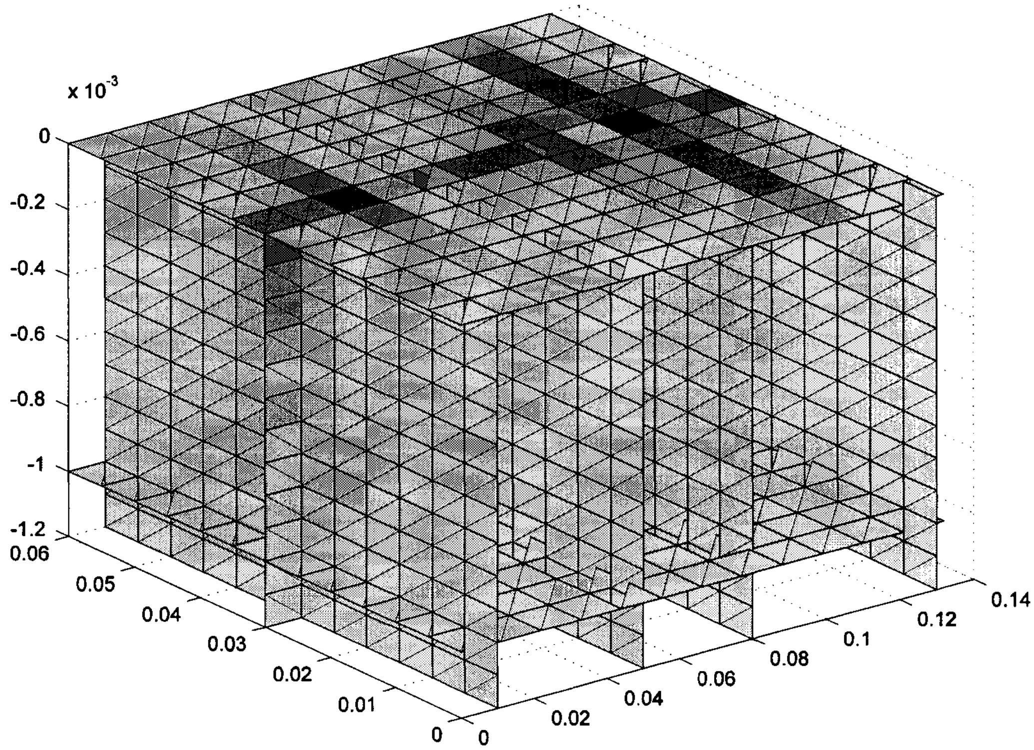

Fig .6.2 - Slice plotting of the temperature distribution of the board.

2. Reliability quantification of the board

As we discussed in Section 5.2, two failure modes will be considered for the reliability quantification of the board. The first failure mode is the lamination failure mode, and the second failure mode is excessive deflection failure mode. First we need to compute the plane stress-reduced stiffnesses for each layer.

For the copper layers,

$$Q_{11}^{(cu)} = Q_{22}^{(cu)} = \frac{E}{1-v^2} = \frac{124}{1-0.328^2} = 138.95\,GPa,$$

$$Q_{12}^{(cu)} = vQ_{11}^{(cu)} = 45.58\,GPa\,,$$

and

$$Q_{66}^{(cu)} = \frac{E}{2(1+v)} = \frac{124}{2(1+0.328)} = 46.69\,GPa.$$

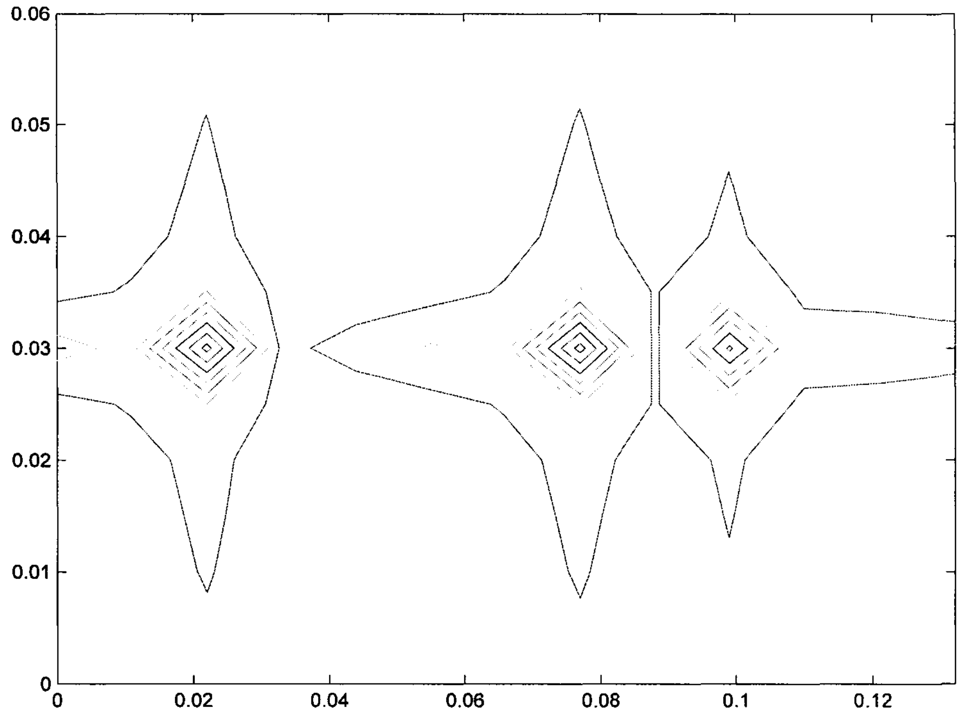

Fig. 6.3 - Contour plotting of the temperature distribution on the top of the board.

For the Epoxy -glass layer,

$$Q_{11}^{(eg)} = Q_{22}^{(eg)} = \frac{E}{1-v^2} = \frac{2.7}{1-0.35^2} = 3.08\,GPa,$$

$$Q_{12}^{(eg)} = vQ_{11}^{(eg)} = 1.08\,GPa\,,$$

and

$$Q_{66}^{(eg)} = \frac{E}{2(1+v)} = \frac{2.7}{2(1+0.35)} = 10\,GPa.$$

For Copper clad invar layer,

$$Q_{11}^{(cli)} = Q_{22}^{(cli)} = \frac{E}{1-v^2} = \frac{200}{1-0.3^2} = 219.78\,GPa,$$

$$Q_{12}^{(cli)} = v\, Q_{11}^{(cli)} = 65.93\, GPa\,,$$

and

$$Q_{66}^{(cli)} = \frac{E}{2\,(1+v)} = \frac{200}{2\,(1+0.3)} = 76.92\, GPa.$$

Next we need to find the bending stiffnesses of the board. Using Eq. (3-32) yields

$$\begin{aligned} D_{11} = D_{22} &= \frac{1}{3}\sum_{k=1}^{11} Q_{11}^{(k)}\left(z_{k+1}^3 - z_k^3\right) = \frac{1}{3} Q_{11}^{(cu)}(z_2^3 - z_1^3 + z_4^3 - z_3^3 + z_{10}^3 - z_9^3 + z_{12}^3 - z_{11}^3) \\ &+ \frac{1}{3} Q_{11}^{(eg)}(z_3^3 - z_2^3 + z_5^3 - z_4^3 + z_7^3 - z_6^3 + z_9^3 - z_8^3 + z_{11}^3 - z_{10}^3) \\ &+ \frac{1}{3} Q_{11}^{(eg)}(z_6^3 - z_5^3 + z_8^3 - z_7^3), \\ &= \frac{1}{3} \times 138.95 \times 1.52482608 \times 10^{-1} + \frac{1}{3} \times 3.08 \times 4.51629306 \times 10^{-1} \\ &+ \frac{1}{3} \times 219.78 \times 0.16465552 \times 10^{-1}, \end{aligned}$$

or

$$D_{11} = D_{22} = 8.732\, Pa - m^3,$$

$$\begin{aligned} D_{12} &= \frac{1}{3}\sum_{k=1}^{11} Q_{12}^{(k)}\left(z_{k+1}^3 - z_k^3\right) = \frac{1}{3} Q_{12}^{(cu)}(z_2^3 - z_1^3 + z_4^3 - z_3^3 + z_{10}^3 - z_9^3 + z_{12}^3 - z_{11}^3) \\ &+ \frac{1}{3} Q_{12}^{(eg)}(z_3^3 - z_2^3 + z_5^3 - z_4^3 + z_7^3 - z_6^3 + z_9^3 - z_8^3 + z_{11}^3 - z_{10}^3) \\ &+ \frac{1}{3} Q_{12}^{(eg)}(z_6^3 - z_5^3 + z_8^3 - z_7^3), \\ &= \frac{1}{3} \times 45.58 \times 1.52482608 \times 10^{-1} + \frac{1}{3} \times 1.08 \times 4.51629306 \times 10^{-1} \\ &+ \frac{1}{3} \times 65.93 \times 0.16465552 \times 10^{-1}, \end{aligned}$$

or

$$D_{12} = 2.841\, Pa - m^3,$$

and

$$D_{66} = \frac{1}{3}\sum_{k=1}^{11} Q_{66}^{(k)}\left(z_{k+1}^3 - z_k^3\right) = \frac{1}{3}Q_{66}^{(cu)}(z_2^3 - z_1^3 + z_4^3 - z_3^3 + z_{10}^3 - z_9^3 + z_{12}^3 - z_{11}^3)$$
$$+\frac{1}{3}Q_{66}^{(eg)}(z_3^3 - z_2^3 + z_5^3 - z_4^3 + z_7^3 - z_6^3 + z_9^3 - z_8^3 + z_{11}^3 - z_{10}^3)$$
$$+\frac{1}{3}Q_{66}^{(eg)}(z_6^3 - z_5^3 + z_8^3 - z_7^3),$$
$$= \frac{1}{3}\times 46.69 \times 1.52482608 \times 10^{-1} + \frac{1}{3}\times 10 \times 4.51629306 \times 10^{-1}$$
$$+\frac{1}{3}\times 76.92 \times 0.16465552 \times 10^{-1},$$

or

$$D_{66} = 4.301\, Pa - m^3.$$

The mass moment of inertia is

$$I_0 = \sum_{k=1}^{L} \rho^{(k)}(z_{k+1} - z_k) = 8{,}900 \times 4 \times 36 \times 10^{-6} + 1{,}450 \times 906 \times 10^{-6}$$
$$+ 4{,}260 \times 152 \times 2 \times 10^{-6},$$

or

$$I_0 = 3.89\ \text{kg/m}^2.$$

The mass of the board is

$$m = \rho \cdot V = 2{,}850 \cdot 0.000012896 = 0.0368\ \text{kg}.$$

Then,

$$p = \sqrt{\frac{k}{m}} = \sqrt{\frac{400{,}000}{0.0368}} = 3{,}296.9,$$

$$\eta = \frac{c}{2m} = \frac{200}{2 \times 0.0368} = 2{,}717.4,$$

$$p_d = \sqrt{p^2 - \eta^2} = 1{,}866.9\,,$$

and

$$\eta_b = \frac{c_1}{I_0} = \frac{15{,}300}{2 \times 3.89} = 1{,}966.6\,.$$

Now we are ready to compute the reliability of the board.

Using Eqs. (3-59) and (3-60), the maximum mean shear stress and peeling stress can be computed as

$$\bar{s}^{(11)}_{yz,\max} = 20.8\,MPa\,,$$

and

$$\bar{s}^{(11)}_{zz} = 41.5 \text{ MPa.}$$

Table 6.2 lists the calculation results using Eqs. (3-59) and (3-60).

Using Eq. (3-62) yields the variance of the shear stress as

$$\sigma^{(k)^2}_{yz,\max} = \frac{256}{\pi^4} \sum_{m=1,3,5,\ldots}^{\infty} \sum_{n=1}^{\infty} \sum_{i=1,3,5,\ldots}^{\infty} \sum_{j=1}^{\infty} \frac{(-1)^{\frac{m+i-2}{2}}}{m \cdot n \cdot i \cdot j} \cdot \left(\sum_{p=1}^{k} \left(\frac{z^2 - z_p^2}{2} C^{(p)}_{2mn} \right) \right) \cdot \left(\sum_{p=1}^{k} \left(\frac{z^2 - z_p^2}{2} C^{(p)}_{2ij} \right) \right) \cdot \int_0^{\infty} h_{mn}(r_1) \cdot h_{ij}(r_2) \cdot R_{\ddot{w}_1 \ddot{w}_1}(r_2 - r_1) \cdot dr_1 dr_2$$

Using Matlab yields,

$$\sigma^{(11)}_{yz,\max} = 0.91\,MPa\,.$$

Then, the reliability of the board due to the shear stress is computed as follows: At t = 0, the strength follows the normal distribution with the mean 48.75 MPa and standard deviation of 3.895 MPa. Then, the reliability is

$$R(t=0)=\Phi\left(\frac{48.75-20.8}{\sqrt{3.895^2+0.91^2}}\right)=\Phi(6.99)=0.9_{11}8625\,.$$

To compute the reliability of the board at t =1,000 hr. First we need to find the damage of the mean strength due to the usage. From the given data, we know that the mean value of the mean strength distribution is 10,000+100 = 10,100. The damage to the mean strength after 1,000 hr usage is

$$D_{m}=\frac{1{,}000}{10{,}100}=0.0990099\,.$$

Then, the residual mean strength is computed as

$$\overline{S}_r=48.75(1-D)=43.92\ \text{MPa},$$

and the reliability of the board at 1,000 hr is computed as

$$R(t=1{,}000)=\Phi\left(\frac{43.92-20.8}{\sqrt{3.895^2+0.91^2}}\right)=\Phi(5.780)=0.9_{8}62649687\,.$$

Similarly, at t = 5,000 hr, the damage is computed as

$$D_{m}=\frac{5{,}000}{10{,}100}=0.495\,.$$

Then, the residual mean strength is

$$\overline{S}_r=48.75(1-D)=24.62\ \text{MPa},$$

and the reliability of the board is

$$R(t=5{,}000)=\Phi\left(\frac{24.62-20.8}{\sqrt{3.895^2+0.91^2}}\right)=\Phi(0.955)=0.8302\,.$$

Table 6.2 - Computations of the shear and peeling stress.

No. of layer	h_i	E_i	f_i	CTE	a_i	b_i	g_i	a_i/g_i	$1/g_i$	b_i/g_i
1	3.60E-05	1.24E+11	0.000717	1.70E-05	0.00E+00	0.00E+00	1.51E-07	0.00E+00	6.64E+06	0.00E+00
2	1.02E-04	2.70E+09	0.000367	3.96E-05	6.90E-05	0.000452	2.36E-06	2.92E+01	4.24E+05	1.92E+02
3	3.60E-05	1.24E+11	0.000717	1.70E-05	1.38E-04	0	1.51E-07	9.17E+02	6.64E+06	0.00E+00
4	3.00E-04	2.70E+09	0.009346	3.96E-05	3.06E-04	0.000452	8.02E-07	3.81E+02	1.25E+06	5.63E+02
5	1.52E-04	2.00E+11	0.083614	3.00E-06	5.32E-04	-0.00028	2.30E-08	2.31E+04	4.34E+07	-1.22E+04
6	1.02E-04	2.70E+09	0.000367	3.96E-05	6.59E-04	0.000452	2.36E-06	2.79E+02	4.24E+05	1.92E+02
7	1.52E-04	2.00E+11	0.083614	3.00E-06	7.86E-04	-0.00028	2.30E-08	3.41E+04	4.34E+07	-1.22E+04
8	3.00E-04	2.70E+09	0.009346	3.96E-05	1.01E-03	0.000452	8.02E-07	1.26E+03	1.25E+06	5.63E+02
9	3.60E-05	1.24E+11	0.000717	1.70E-05	1.18E-03	0	1.51E-07	7.84E+03	6.64E+06	0.00E+00
10	1.02E-04	2.70E+09	0.000367	3.96E-05	1.25E-03	0.000452	2.36E-06	5.29E+02	4.24E+05	1.92E+02
11	3.60E-05	1.24E+11	0.000717	1.70E-05	1.32E-03	0	1.51E-07	8.76E+03	6.64E+06	0.00E+00
sum			0.189893				9.33E-6			

Table 6.2 - Computations of the shear and peeling stress – continued.

No. of layer	$(d-b_i)/g_i$	$(c-a_i)/g_i$	Sum of ($h1-h_i$)-hj/2	F_i	$(h_i\text{^}2)*g_i$	Sum of h_j	T_j	Shear (x=0.15)	Shear (y=0.0635)	Peeling (x=0.15)
1	-1.28E+03	4.38E+03	1.80E-05	-1.28E+03	1.95E-16	1.32E-03	-5.32E+01	3.00E+05	3.00E+05	1.12E+06
2	-2.73E+02	2.50E+02	8.70E-05	-2.73E+02	2.46E-14	1.22E-03	1.23E+03	-6.93E+06	-6.93E+06	-2.38E+07
3	-1.28E+03	3.46E+03	1.56E-04	-1.28E+03	1.95E-16	1.18E-03	1.50E+03	-8.47E+06	-8.47E+06	-2.82E+07
4	-8.04E+02	4.40E+02	3.24E-04	-8.03E+02	7.22E-14	8.80E-04	2.78E+03	-1.57E+07	-1.57E+07	-3.89E+07
5	3.78E+03	5.52E+03	5.50E-04	3.79E+03	5.32E-16	7.28E-04	3.58E+03	-2.02E+07	-2.02E+07	-4.15E+07
6	-2.73E+02	-4.59E-14	6.77E-04	-2.73E+02	2.46E-14	6.26E-04	-2.08E+02	1.18E+06	1.18E+06	2.08E+06
7	3.78E+03	-5.52E+03	8.04E-04	3.76E+03	5.32E-16	4.74E-04	6.48E+01	-3.66E+05	-3.66E+05	-4.89E+05
8	-8.04E+02	-4.40E+02	1.03E-03	-8.06E+02	7.22E-14	1.74E-04	-3.69E+03	2.08E+07	2.08E+07	1.02E+07
9	-1.28E+03	-3.46E+03	1.20E-03	-1.30E+03	1.95E-16	1.38E-04	-2.89E+03	1.63E+07	1.63E+07	6.34E+06
10	-2.73E+02	-2.50E+02	1.27E-03	-2.75E+02	2.46E-14	3.60E-05	-1.58E+03	8.94E+06	8.94E+06	9.08E+05
11	-1.28E+03	-4.38E+03	1.34E-03	-1.31E+03	1.95E-16	3.60E-05				
sum	9.03E-01	0.0			2.2E-13					

c = 6.59E-04, d=-1.93E-04, k = 5,641.458.

The variance of the peeling stress is obtained using Eq. (3-63), or

$$\sigma_{zz,\max}^{(k)^2} = \frac{256}{\pi^4} \sum_{m=1,3,5,\ldots}^{\infty} \sum_{n=1,3,5,\ldots}^{\infty} \sum_{i=1,3,5,\ldots}^{\infty} \sum_{j=1,3,5,\ldots}^{\infty} \frac{(-1)^{\frac{m+n+i+j-4}{2}}}{m\, n\, i\, j} \cdot$$

$$\cdot \left[\left(\frac{z^3}{6} - \frac{z \cdot z_k^2}{2} \right) \left(-\frac{m\pi}{a} C_{1mn}^{(k)} - \frac{n\pi}{b} C_{2mn}^{(k)} \right) + C_{3mn}^{(k)} \right] \cdot$$

$$\cdot \left[\left(\frac{z^3}{6} - \frac{z \cdot z_k^2}{2} \right) \left(-\frac{i\pi}{a} C_{1ij}^{(k)} - \frac{j\pi}{b} C_{2ij}^{(k)} \right) + C_{3ij}^{(k)} \right]$$

$$\cdot \int_0^{\infty} h_{mn}(r_1)\, h_{ij}(r_2)\, R_{\ddot{w}_1 \ddot{w}_1}(r_2 - r_1)\, dr_1\, dr_2 ,$$

Using Matlab yields,

$$\sigma_{zz,\max}^{(11)} = 0.0091\, MPa .$$

Then, the reliability due to this stress is computed as follows:

At t = 0, the strength follows the normal distribution with the mean of 70 MPa and the standard deviation of 3 MPa. Then, the reliability is

$$R(t=0) = \Phi\left(\frac{70 - 41.5}{\sqrt{3^2 + 0.0091^2}} \right) = \Phi(9.49996) \approx 1 .$$

Similarly as in the case of the shear stress, to compute the reliability at t =1,000 hr, first we need to find the damage to the mean strength due to usage. From the given data, the mean value of the mean strength distribution is computed as

$$\overline{m} = 0 + \eta \cdot \Gamma(1 + \frac{1}{\beta}) = 10{,}000\Gamma(1.5) = 8{,}862.3 .$$

Then, the damage to the mean strength is

$$D_m = \frac{1{,}000}{8{,}862.3} = 0.1128 .$$

Then, the residual mean strength is computed as

$$\bar{S}_r = 70(1-D) = 62.104 \text{ MPa},$$

and the reliability is computed as

$$R(t=1{,}000) = \Phi\left(\frac{62.104-41.5}{\sqrt{3^2+0.0091^2}}\right) = \Phi(6.868) = 0.9_{11}67446.$$

Similarly at t = 5,000 hr, the damage is

$$D_m = \frac{5{,}000}{8{,}862.3} = 0.5642.$$

Then, the residual mean strength is computed as

$$\bar{S}_r = 70(1-D) = 30.506 \text{ MPa},$$

and the reliability is

$$R(t=5{,}000) = \Phi\left(\frac{30.506-41.5}{\sqrt{3^2+0.0091^2}}\right) = \Phi(-3.664) = 0.00012.$$

From the above, it can be seen that the failure of the delamination is due to shear stress at the beginning of the use, but the peeling stress becomes important later. We will use the shear stress to compute the reliability of the board at the beginning of the usage.

Next we compute the reliability of the board due to the excessive deflection. From Eq. (5-7), the mean of the performance function for this failure mode is

$$\bar{Z}_2 = H - \frac{1}{2}h - h_{\max} = 0.05 - \frac{1}{2}\times 0.001354 - 0.01 = 0.039323 \text{ m}.$$

The variance of Z_2 is computed using Eq. (5-8), or

$$\sigma_{Z_2}^2 = E\left(w_{\max}^2\right) + E\left(w^{*2}\right) + 2E\left(w_{\max}w^*\right).$$

Using Eqs. (5-9), (5-10) and (5-11) yields

$$E\left(w_{\max}^2\right)=\frac{256}{\pi^4}\sum_{m=1,3,5,\ldots}^{\infty}\sum_{n=1,3,5,\ldots}^{\infty}\sum_{i=1,3,5,\ldots}^{\infty}\sum_{j=1,3,5,\ldots}^{\infty}\frac{(-1)^{\frac{m+n+i+j-4}{2}}}{m\,n\,i\,j}$$
$$\cdot\int_0^{\infty}\int_0^{\infty}h_{mn}(r_1)\,h_{ij}(r_2)\,R_{\ddot{w}_1\ddot{w}_1}(r_2-r_1)\,dr_1\,dr_2,$$

or

$$E\left(w_{\max}^2\right)=4.3029\times10^{-5},$$

$$E(w^{*2})=\int_0^{\infty}\int_0^{\infty}R_{\ddot{w}_0\ddot{w}_0}(r_2-r_1)\,h(r_1)\,h(r_2)\,dr_1\,dr_2=2.3429\times10^{-21},$$

and

$$E\left(w_{\max}w^*\right)=\frac{16}{\pi^2}\sum_{m=1}^{\infty}\sum_{n=1}^{\infty}\frac{(-1)^{\frac{m+n-2}{2}}}{m\,n}\int_0^{\infty}h_{mn}(r)\left[2\,\eta\,R_{\dot{w}^*w^*}(r)+p^2\,R_{w^*w^*}(r)\right]dr,$$

or

$$E\left(w_{\max}w^*\right)=1.4414\times10^{-9}.$$

Then, the standard deviation of Z_2 is given by

$$\sigma_{Z_2}=\sqrt{4.3029\times10^{-5}+2.3429\times10^{-21}+1.4414\times10^{-9}}=0.00656,$$

and the reliability of the board in the deflection failure mode is

$$R_2=\Phi\left(\frac{\overline{Z}_2}{\sigma_{Z_2}}\right)=\Phi\left(\frac{0.039323}{0.00656}\right)=\Phi(5.994)=0.9_8 8976.$$

To find the reliability of the board, we need to consider both failure modes together. Since these two failure modes are dependent, the correlation coefficient should be determined before the reliability can be quantified. Using Eq. (5-18) yields

$$\rho = \frac{E[s_{vir} w_{\max}] + E[s_{vir} w^*]}{\sigma_{Z_1}\, \sigma_{Z_2}},$$

where the vibration stress is the shear stress.

From Eqs. (5-19) and (5-20),

$$E[s_{vir} w_{\max}] = \frac{256}{\pi^4} \sum_{m=1,3,5\ldots}^{\infty} \sum_{n=1,3,5,\ldots}^{\infty} \sum_{i=1,3,5,\ldots}^{\infty} \sum_{j=1,3,5\ldots}^{\infty} \frac{(-1)^{\frac{m+i+j-1}{2}}}{m\, n\, i\, j}$$
$$\cdot \left(\sum_{p=1}^{k} \left(\frac{z^2 - z_p^2}{2} C_{2mn}^{(p)} \right) \right) \cdot \int_0^{\infty} h_{mn}(r_1)\, h_{ij}(r_2)\, R_{\ddot{w}_1 \ddot{w}_1}(r_2 - r_1)\, dr_1\, dr_2,$$

$$E[s_{vir} w^*] = \frac{16}{\pi^2} \sum_{m=1,3,5\ldots}^{\infty} \sum_{n=1,3,5,\ldots}^{\infty} \left(\sum_{i=1}^{k} \left(\frac{z^2 - z_i^2}{2} C_{2mn}^{(i)} \right) \right) \cdot \frac{(-1)^{\frac{m-1}{2}}}{m\, n}$$
$$\cdot \int_0^{\infty} h_{mn}(r_1) \left[2\eta\, R_{\dot{w}^* w^*} + p^2\, R_{w^* w^*} \right] dr_1.$$

Using Matlab yields

$$E[s_{vir} w_{\max}] = 23.3442,$$

and

$$E[s_{vir} w^*] = 0.0457.$$

We also know that

$$\sigma_{Z_1} = \sqrt{3.895^2 + 0.91^2} = 4\,\text{MPa}$$

Then, the correlation coefficient is

$$\rho = \frac{23.3442 + 0.0457}{4 \times 10^6 \times 0.00656} = 0.0008913.$$

At t = 0 hr, using Eq. (2-29) yields

$$R = \int_0^{\rho} w(\text{-}6.99, \text{-}5.994, r)\, dr + \Phi(6.99) \cdot \Phi(5.994),$$

or

$$R = 0.9_8 897492 .$$

At t = 1,000 hr, using Eq. (2-29) yields

$$R = \int_0^{\rho} w(\text{-}6.25, \text{-}5.994, r)\, dr + \Phi(6.25)\Phi(5.994),$$

or

$$R = 0.9_8 77107$$

It should be noted that at t = 5,000 hr, we have to use the peeling stress to compute the correlation coefficient and then use Eq. (2-29) to compute the reliability.

3. Reliability quantification of the leadless interconnects

As we discussed in Section 5.3, this kind of interconnects can be treated as a three-layer board, the stress in the interface between the first layer and the second layer can be treated as the shear stress experienced by the solder joints.

From Eq. (5-29), the mean shear stress is

$$\bar{s}_{yz,\max}^{(corner-jo\,\text{int})}(x, y, z_2) = -\frac{4\sqrt{2} s_m}{N^2 d_s^2 \pi} \mathrm{k}' \, \mathrm{T_1} \tanh(\mathrm{k}' \, \mathrm{l}).$$

The area of the module is computed as

$$s_m = 0.000169 \, \mathrm{m}^2.$$

Then, the mean of the stress for the corner joint is computed as

$$\bar{s}_{yz,\max}^{(corner-jo\,\text{int})}(x, y, z_2) = 0.111 \, MPa.$$

Table 6.3 Results of shear stress computation for leadless solder joint interconnect.

No. of layer	h_i	E_i	f_i	CTE	a_i	b_i	g_i	a_i/g_i	b_i/g_i
1	0.001354	5.99E10	20.31289	7.19E-6	0	0	7.52E-9	0	0
2	0.00028	1.38E10	0.038838	2.5E-5	0.000817	0.0003562	1.68E-7	4.86E3	2.12E3
3	0.00051	3.00E11	4.737536	3.5E-6	0.001212	-0.0000738	4.58E-9	2.65E5	-1.61E4
Sum			25.08926				1.80E-7	2.70E5	-1.40E4

Table 6.3 Results of shear stress computation for leadless solder joint interconnect- Continued

<table>
<tr><th>No. of layer</th><th>$1/g_i$</th><th>$(c-a_i)/g_i$</th><th>$(d-b_i)/g_i$</th><th>$\sum_{k=1}^{j} h_k - h_j/2$</th><th>$F_j$</th><th>$T_i$</th><th>Shear stress</th></tr>
<tr><td rowspan="2">1</td><td rowspan="2">1.33E8</td><td rowspan="2">1.004E5</td><td rowspan="2">-5212.77</td><td rowspan="2">0.000677</td><td rowspan="2">-3971.97</td><td></td><td></td></tr>
<tr><td rowspan="2">-1797.46</td><td rowspan="2">3.939 MPa</td></tr>
<tr><td rowspan="2">2</td><td rowspan="2">5.94E6</td><td rowspan="2">-369.05</td><td rowspan="2">-1886.90</td><td rowspan="2">0.001494</td><td rowspan="2">-1897.05</td></tr>
<tr><td rowspan="2">2174.51</td><td rowspan="2">-4.765 MPa</td></tr>
<tr><td rowspan="2">3</td><td rowspan="2">2.19E8</td><td rowspan="2">-99781.7</td><td rowspan="2">7554.59</td><td rowspan="2">0.001889</td><td rowspan="2">4071.56</td></tr>
<tr><td></td><td></td></tr>
<tr><td>Sum</td><td>3.57E8</td><td>249.25</td><td>454.92</td><td></td><td></td><td></td><td></td></tr>
</table>

$c = 7.55$ E-4, $d = -3.92$E-5, $k' = 2{,}191.1736$.

Table 6.3 gives the results of the shear stress computations.

The variance of the stress is computed using Eq. (5-30), or

$$\sigma^2_{solder} = \frac{8{,}192}{N^4 d_s^4 \pi^6} \frac{\left(z_2^2 - z_1^2\right)^2}{4} \sum_{m=1,3,5,\ldots}^{\infty} \sum_{n=1}^{\infty} \sum_{i=1,3,5,\ldots}^{\infty} \sum_{j=1}^{\infty} C^{(1)}_{2mn} C^{(1)}_{2ij} \frac{(-1)^{\frac{m+i-2}{2}}}{m\,n\,i\,j}$$

$$\cdot \int_0^{\infty} h_{mn}(r_1)\, h_{ij}(r_2)\, R_{\ddot{w}_1 \ddot{w}_1}(r_2 - r_1)\, dr_1\, dr_2 .$$

Using Matlab yields,

$$\sigma_{solder} = 0.48\, MPa .$$

Then, the reliability of each solder joint is

$$R = \Phi\left(\frac{38.64 - 0.111}{\sqrt{5^2 + 0.48^2}}\right) = \Phi(7.670) = 0.9_{14}15 .$$

Then, this interconnects reliability is computed as

$R_{inter} = \left(0.9_{14}15\right)^{52} = 0.9_{12}555$, which has an equivalent reliability index of 7.145.

4. Reliability quantification of the leaded solder joint

For a ceramic module, we know α_m=3.5ppm/°C from Table 6.1, and E_w=300 GPa, L_w = 0.00218 m and d_w = 0.000203 m from the given data. The moment of inertia for the lead wire is computed as

$$I_w = \frac{\pi\, d_w^4}{64} = 8.336 \times 10^{-17} .$$

The area of the wire is

$$A_w = \pi \left(\frac{d_w}{2}\right)^2 = 3.2 \times 10^{-8} .$$

Then, the mean stress on the lead wire is

$$E\left(s_{lead}\right)=-\frac{E_w\, I_w}{A_w\, L_w^{\;3}}(6-\frac{A_w\, L_w^{\;2}}{2\, I_w})\cdot\left(\alpha_m-\alpha_b\right)\Delta\overline{T}\; a,$$

or

$$\begin{aligned}E\left(s_{lead}\right)&=-\frac{E_w\, I_w}{A_w\, L_w^{\;3}}(6-\frac{A_w\, L_w^{\;2}}{2\, I_w})\cdot\left(\alpha_m-\alpha_b\right)\Delta\overline{T}\; a,\\ &=9.169\; MPa,\end{aligned}$$

and

$$\begin{aligned}\sigma^2_{s_{lead}} = &\frac{256}{\pi^4\, N^2}\left[\frac{E_w}{L_w}\frac{1}{1+\dfrac{L_m^3}{3\, E_m\, I_m}\dfrac{N\, A_w\, E_w}{L_w}}\right]^2 \sum_{m=1,3,5,\ldots}^{\infty}\sum_{n=1,3,5,\ldots}^{\infty}\cdot\\
&\sum_{i=1,3,5,\ldots}^{\infty}\sum_{j=1,3,5,\ldots}^{\infty}\left(\frac{\left(-1\right)^{\frac{m+n-2}{2}}}{m\, n}-\frac{\left(-1\right)^{\frac{n-1}{2}}\sin\left(\dfrac{m\,\pi}{a}\dfrac{a-l}{2}\right)}{m\, n}\right)\cdot\\
&\cdot\left(\frac{\left(-1\right)^{\frac{i+j-2}{2}}}{i\, j}-\frac{\left(-1\right)^{\frac{j-1}{2}}\sin\left(\dfrac{i\,\pi}{a}\dfrac{a-l}{2}\right)}{i\, j}\right)\\
&\cdot\int_0^{\infty} h_{mn}(r_1)\, h_{ij}(r_2)\, R_{\ddot{w}_1\ddot{w}_1}(r_2-r_1)\, dr_1\, dr_2.\end{aligned}$$

Using Matlab yields

$$\sigma_{\text{leaded}}=3.4131\times10^{-5}\ \text{Pa}.$$

Therefore, the stress experienced by the corner solder joint is also 9.169 MPa with a standard deviation of 3.4131×10^{-5} Pa. Since the strength of the solder joint is 40 MPa with a standard deviation of 5 MPa, then the reliability of the corner solder joint is computed using Eqs. (2-6) and (2-7) as,

$$R_{leaded}^{(corner)} = \Phi\left(\frac{40-9.169}{\sqrt{5^2+3.4131^2\times 10^{-10}}}\right) = \Phi(6.1666) = 0.9_9 6498046,$$

then, the reliability of this interconnect is

$$R_{leaded} = 0.9_9 6498046^{52} = 0.9999999817898378,$$

which is the equivalent of m = 5.5074.

5. Reliability quantification of PGA package No.3 interconnect

From the given data, we have $A_w = \pi\left(\frac{d_w}{2}\right)^2 = \pi\left(\frac{0.000203}{2}\right)^2 = 3.2\times 10^{-8}$,

$I_w = \frac{\pi\, d_w^4}{64} = \frac{\pi\times 0.000203^4}{64} = 8.336\times 10^{-17}$, E_w=300 GPa, L_w = 0.00218 m, α_m=3.5 ppm/°C, α_b=7.19 ppm/°C, d_w = 0.000203 m, c= $d_2/2$ = 0.0001015, b=0.000382 m, E_s = 13.8 GPa, and $r = \sqrt{2}\times 0.0013 = 0.00184$ m. Then,

$$u = (\alpha_m - \alpha_b)\Delta T\, r = 1.35792\times 10^{-7}\, m,$$

$$\gamma = \left(\frac{E_s c(b-c)}{E_w I_w}\right)^{1/4} h = 0.0852,$$

$$u_1 = \frac{3\,u\,(\gamma+1)}{(\gamma+1)^3+2} = 2.08\times 10^{-7},$$

and

$$\theta = \frac{6\,u\,\gamma}{L_w(\gamma+1)^3+2L_w} = 9.714\times 10^{-6}.$$

Then, using Eq. (5-40) yields

$$s_{solder}^{(th)} = \frac{A_w\, E_w}{60\,\pi\, c\, h\, L_w^{\;2}}\left[18\,(u-u_1)^2 - 3\,\theta\, L_w (u-u_1) + 2\,\theta^2\, L_w^{\;2}\right],$$

$$= \frac{3.2\times10^{-8}\cdot 300\times10^{9}}{60\cdot\pi\cdot 0.0001015\cdot 0.001354\cdot 0.00218^2}$$

$$\Big[18\cdot\left(1.35792\cdot10^{-7} - 2.08\cdot10^{-7}\right)^2 - 3\cdot 9.714\times10^{-6}$$

$$\left(1.35792\cdot10^{-7} - 2.08\cdot10^{-7}\right) + 2\cdot 9.714^2\times10^{-12}\times 0.00218^2,$$

$$= \frac{9600}{1.2311155\cdot10^{-10}}\left[9.3852\times10^{-14} + 2.1043\times10^{-12} + 8.9689\times10^{-12}\right],$$

or

$$s_{solder}^{(th)} = 870.78\ \text{Pa}.$$

Then,

$$E\left(s_{solder}^{(pth/pin)}\right) = \bar{s}_{solder}^{(th)} = 870.78\ \text{Pa}.$$

Since the vibration stress is the same as in the case for leaded case, we can use the result from Case 4; i.e,

$$\sigma_{\text{leaded}} = 3.4131\times10^{-5}\ \text{Pa}.$$

Therefore, the reliability of the corner solder joint for the PGA package is

$$R_{pga}^{(corner)} = \Phi\left(\frac{40 - 870.78\times10^{-6}}{\sqrt{5^2 + 3.4131^2\times10^{-10}}}\right) = \Phi(7.999) = 0.9_{15}3.$$

For this package, there are 52 pins; then,

$$R_{pga} = 0.9_{15}3^{52} = 0.9_{13}654.$$ which is equivalent to m = 7.4892.

6. Reliability quantification of Plate Through Hole interconnect

There are two failure modes involved in this reliability quantification; one is related to the failure of the solder joint; the other is related to the barrel failure. Since we assume all the dimensions are the same as the package No.3, the reliability of the solder joint will be the same for this package. Therefore, we have

$$R_{PTH}^{(solder)} = 0.9_{13}654,$$

and

$$\sigma_{Z_5} = \sqrt{5^2 + 3.4131^2 \times 10^{-10}} \approx 5 \text{ MPa.}$$

Next, let's find the reliability of the PTH due to the barrel failure mode. From the given data, we know α_b=28.98 ppm/°C, α_{ba}=17 ppm/°C, ΔT=20, E_{ba} = 124 GPa, t_{ba} = 0.00004 m, t_{bm} =0.000015 m, t_{pad} = 0.00005 m, r_1 = 0.0006 m, r_0= 0.0003 m, E_b = 4.0 GPa, and E_{pad} = 90 GPa; then,

$$e = \frac{\pi}{2}\sqrt{\frac{E_{pad}\, t_{pad}^3\, h}{6\, E_b}} = \frac{\pi}{2}\sqrt{\frac{90\times 10^9 \cdot 0.00005^3 \cdot 0.001354}{6\times 4.0\times 10^9}} = 2.798\times 10^{-10} < r_1 - r_0,$$

so we use r_1 in the calculation of

$$\zeta = (r_1 - r_0)\sqrt[4]{\frac{6E_b}{E_{pad}\, t_{pad}^3\, h}} = (0.0006 - 0.0003)\sqrt[4]{\frac{6\cdot 4\times 10^9}{90\times 10^9 0.00005^3 0.001354}} = 1.358,$$

$$t_r = \frac{t_{ba}}{t_{bm}\left(1 + \dfrac{0.75\log(r_1/r_0)}{(1+\zeta)}\right)} = \frac{0.00004}{0.000015\left(1 + \dfrac{0.75\log(0.0006/0.0003)}{1+1.358}\right)} = 2.43365,$$

and

$$F(\zeta) = \zeta\frac{1+\cos^2(\zeta)/\cosh^2(\zeta)}{\tanh(\zeta)+\sin(\zeta)\cos(\zeta)/\cosh^2(\zeta)} = 1.358\frac{1+0.211^2/2.073^2}{0.876+0.2064/2.073^2} = 1.485.$$

Then, using Eq. (5-50) yields the mean stress on the barrel, or

$$s_{barrel}^{(th)} = \frac{(\alpha_b - \alpha_{ba})\Delta T\, E_{ba}\, t_r}{1 + \dfrac{E_{ba}\, t_{ba}}{E_b(r_1 - r_0)F(\zeta)}} = \frac{(28.98 - 17)10^{-6} \cdot 20 \cdot 124 \times 10^9 \cdot 2.43365}{1 + \dfrac{124 \cdot 0.00004}{4 \times 0.0003 \cdot 1.485}},$$

or

$$s_{barrel}^{(th)} = 19.11\,\text{MPa}.$$

The standard deviation of the stress is the same as in Case 2; i.e.,

$$\sigma_{zz,\max}^{(11)} = 0.0091\,MPa\,.$$

Then, the reliability of this interconnect due to the barrel failure mode is

$$R_{barrel} = \Phi\left(\frac{100 - 19.11}{\sqrt{10^2 + 0.0091^2}}\right) = \Phi(8.089) = 0.9_{15}7\,,$$

with

$$\sigma_{Z_6} = \sqrt{10^2 + 0.0091^2} \approx 10\ \text{MPa}.$$

Next, we need to find the reliability of this interconnect considering both failure modes.

First we need to find the correlation coefficient between the two failure modes.

Using Eq. (5-60) and Matlab yields

$$E\left(s_5^{vir} s_6^{vir}\right) = 6{,}745.34\,.$$

Then, using Eq. (5-58) yields

$$\rho_{56} = \frac{E\left[s_5^{vib} s_6^{vib}\right]}{\sigma_{Z_5}\sigma_{Z_6}} = \frac{6745.34}{5 \times 10 \times 10^{12}} = 1.34 \times 10^{-10}\,.$$

We see the correlation coefficient is very small, we conclude these two failure modes have not interacted very strongly, by using Eq. (5-61) yields the reliability of this interconnect, or

$$R_{PTH} = \int_0^{\rho} w(-7.999, -8.089, r)\, dr + \Phi(7.999)\Phi(8.089),$$

or

$$R_{PTH} = 0.9_{15}0\,.$$

7. Reliability quantification of the Popcorn Effect

As we know the delamination failure mode is due to the storage condition. So, from the given data, we can compute the delamination probability using Eqs. (5-67) and (5-68), or

$\Delta\alpha = 15 - 1.6 = 13.4$ ppm/°C,

$\Delta T = 150^{\circ}C$ with a standard deviation of 20°C ,

$$D_1 = \frac{E_1\, h_1^3}{12(1-v_1^2)} = \frac{15.5\times 10^9\, h_1^3}{12(1-0.25^2)} = 1.38\times 10^9\, h_1^3\,,$$

$$D_2 = \frac{E_2\, h_2^3}{12(1-v_2^2)} = \frac{275.8\times 10^9\, h_2^3}{12(1-0.22^2)} = 2.42\times 10^{10}\, h_2^3\,,$$

h_1 = 0.0008±0.00006 m, which means that the mean value of h_1 is 0.0008 m and the standard deviation is 0.00002 m,

h_2 = 0.0004±0.00003 m, which means that the mean value of h_2 is 0.0004 m and standard deviation is 0.00001 m,

$$\lambda = \frac{1}{12}\left(\frac{h_1^2}{D_1} + \frac{h_2^2}{D_2} + \frac{3(h_1+h_2)^2}{D_1+D_2}\right),$$
$$= \frac{1}{12}\left(\frac{h_1^2}{1.38\times10^9} + \frac{h_2^2}{2.42\times10^{10}} + \frac{3(h_1+h_2)^2}{2.558\times10^{10}}\right),$$

or

$$\lambda = 6.04\times10^{-11}h_1^2 + 3.44\times10^{-12}h_2^2 + 1.30\times10^{-11}(h_1+h_2)^2,$$

$$\kappa = \frac{2(1+\nu_1)}{3E_1}h_1 + \frac{2(1+\nu_2)}{3E_2}h_2,$$
$$= \frac{2(1+0.25)}{3\times15.5\times10^9}h_1 + \frac{2(1+0.22)}{3\times275.8\times10^9}h_2,$$

or

$$\kappa = 5.38\times10^{-11}h_1 + 2.95\times10^{-12}h_2,$$

$$k = \sqrt{\frac{\lambda}{\kappa}} = \sqrt{\frac{6.04\times10^{-11}h_1^2 + 3.44\times10^{-12}h_2^2 + 1.30\times10^{-11}(h_1+h_2)^2}{5.38\times10^{-11}h_1 + 2.95\times10^{-12}h_2}},$$

or

$$k = \sqrt{\frac{60.4h_1^2 + 3.44h_2^2 + 13.0(h_1+h_2)^2}{53.8h_1 + 2.95h_2}},$$

$$\mu = \frac{h_2\cdot D_1 - h_1\cdot D_2}{2(D_1+D_2)} = \frac{1.38\times10^9 h_1^3 h_2 - 2.42\times10^{10} h_2^3 h_1}{2(1.38\times10^9 h_1^3 + 2.42\times10^{10} h_2^3)},$$

or

$$\mu = \frac{1.38h_1^3h_2 - 24.2h_2^3h_1}{2.76h_1^3 + 48.4h_2^3},$$

and

a =0.015±0.0003 m, which means the mean is 0.015 m and the standard deviation is 0.0001 m.

Using Eq. (5-69) yields the stress for the delamination failure mode, or

$$s_{th} = \sqrt{\frac{\tanh^2(ka)}{\lambda\kappa} + \frac{\mu^2}{\kappa^2}}\Delta\alpha\Delta T,$$

$$= \left[\frac{\tanh^2\left(\sqrt{\frac{60.4h_1^2 + 3.44h_2^2 + 13.0(h_1+h_2)^2}{53.8h_1 + 2.95h_2}}a\right)}{\left(6.04\times10^{-11}h_1^2 + 3.44\times10^{-12}h_2^2 + 1.30\times10^{-11}(h_1+h_2)^2\right)\left(5.38\times10^{-11}h_1 + 2.95\times10^{-12}h_2\right)} + \left(\frac{1.38h_1^3h_2 - 24.2h_2^3h_1}{\left(5.38\times10^{-11}h_1 + 2.95\times10^{-12}h_2\right)\left(2.76h_1^3 + 48.4h_2^3\right)}\right)^2\right]^{1/2} \Delta T\cdot 13.4\times10^{-6}.$$

Then, using Eq. (5-70) yields the performance function for the delamination failure mode

$$Z_{del} = S_{ad} - s_{th} = \overline{S} + \sigma_S\, x_1 - f(s_{th}),$$

where $f(s_{th})$ is the equation of s_{th} when each distributed variable written in the form of $\mu + \sigma\cdot u$, where, μ is the mean value of the variable and σ is the standard deviation of the variable, u is the standard normal variable.

Then, using the Minimum Distance Method and Matlab, we find that the design point is

$x_1 = 0.2048$,

$x_2 = 0.1978$,

$x_3 = 0.006849$,

$x_4 = -0.1649$,

and

$x_5 = -6.1637$,

where

x_1 = normal variable of the strength,

x_2 = normal variable of h_1,

x_3 = normal variable of h_2,

x_4 = normal variable of a,

and

x_5= normal variable of ΔT.

Then, the reliability index is

$$m = \sqrt{x_1^2 + x_2^2 + x_3^2 + x_4^2 + x_5^2} = 6.1725,$$

and the probability of the delamination not occurring is

$$R_d = \Phi(m) = 0.9_9 6639074.$$

Next we will compute the reliability after reflow. The initial reliability is equal to one minus the probability of delamination times the probability of compound fail. From the given data, we have

T = 230°C with standard deviation of 10°C,

a_1 = 0.01 m with standard deviation of 0.0002 m,

h_1 = 0.0008 m with standard deviation of 0.00002 m,

Q_s = 0.1 eV,

and

K = 8.617385×10^{-5} eV/K.

Then,

$$P_{H_2O,Cavity}(T) = RH_0\ P_{sat,H_2O}(T_0)\, e^{\frac{Q_s}{K}\left(\frac{1}{T_0}-\frac{1}{T}\right)},$$

$$= 0.85 \times 3167.73 e^{\frac{0.1}{8.617385\times10^{-5}}\left(\frac{1}{298}-\frac{1}{273+T}\right)},$$

$$= 2692.57\,\mathrm{e}^{1160.44\left(\frac{1}{298}-\frac{1}{273+T}\right)}.$$

Using Eq. (5-71) yields

$$s_m = 6\,\kappa\, P_{H_2O,Cavity}(T)\left(\frac{a_1}{h_1}\right)^2,$$

$$= 6 \times 0.5 \times 2{,}692.57\,\mathrm{e}^{1160.44\left(\frac{1}{298}-\frac{1}{273+T}\right)}\left(\frac{a_1}{h_1}\right)^2,$$

or

$$s_m = 8077.71\,\mathrm{e}^{1160.44\left(\frac{1}{298}-\frac{1}{273+T}\right)}\left(\frac{a_1}{h_1}\right)^2,$$

where

s_m = bending stress generated inside the package,

κ = shape parameter, 0.5 for a square pad,

$P_{H_2O,Cavity}(T)$ = pressure inside the cavity at the temperature T,

a_l = length of the pad,

h_l = thickness of the molding compound,

and

RH_0 = relative humidity at temperature T_0.

The mean strength of the molding compound at the end of reflow is computed as

$$S_{res} = S_0 e^{-0.5\cdot 200/3{,}600},$$

or

$S_{res} = 58.36$ MPa.

Then, the performance function for the molding compound failure is

$$Z_m = 58.36 + 8 \times x(1) - f(s),$$

where f(s) is the equation of s_m when each distributed variable is written in the form $\mu + \sigma\, u$, where, μ is the mean of the variable and σ is the standard deviation of the variable, u is the standard normal variable.

Using the Minimum Distance Method and Matlab yields the design point as

$x_1 = -7.2332$,

$x_2 = 0.0205$,

$x_3 = 0.0089$,

and

$x_4 = -0.0112$,

where

x_1 = normal variable of strength,

x_2 = normal variable of T,

x_3 = normal variable of a,

and

x_4 = normal variable of h_1.

Then, the reliability index is

$$m = \sqrt{x_1^2 + x_2^2 + x_3^2 + x_4^2} = 7.2332,$$

and reliability of the molding compound at the end of the reflow is

$$R_m = \Phi(7.2332) = 0.9_{12}7641.$$

Therefore, the plastic package reliability related to the popcorn effect at t = 0 (meaning when it is first delivered to the customers) is computed as

$$R = 1-(1-R_d)(1-R_m) = 0.9_{17}6636715.$$

To find the reliability of the package at 1,000 hr, we need to find the cumulative damage of the molding compound at 1,000 hr. Since the stress at the reflow and normal use condition is different, we need to use the equivalent theory to find the cumulative damage. First let's find the equivalent time of 200 sec. of the reflow condition to the normal use condition. The mean of the stress under the normal use conditions is

$$s_{normal} = 8{,}077.71\mathrm{e}^{1160.44\left(\frac{1}{298}-\frac{1}{273+T}\right)}\left(\frac{a_1}{h_1}\right)^2,$$

where T is normal use condition temperature. Using the Taylor Series Expansion Method,

$$\bar{s}_{normal} = 8{,}077.71\mathrm{e}^{1{,}160.44\left(\frac{1}{298}-\frac{1}{273+50}\right)}\left(\frac{\bar{a}}{\bar{h}_1}\right)^2,$$

or

$$\bar{s}_{normal} = 1.706\ \text{MPa},$$

and the variance of the stress is

$$\sigma_s^2 = \left(8{,}077.71 e^{1{,}160.44\left(\frac{1}{298}-\frac{1}{273+T}\right)} \left(\frac{\bar{a}_1}{\bar{h}_1}\right)^2 \left(\frac{1{,}160.44}{(273+T)^2}\right) \right)^2 \sigma_T^2 +$$

$$+ \left(8{,}077.71 e^{1{,}160.44\left(\frac{1}{298}-\frac{1}{273+T}\right)} \left(\frac{2\,\bar{a}_1}{\bar{h}_1^2}\right) \right)^2 \sigma_a^2 +$$

$$+ \left(8{,}077.71 e^{1160.44\left(\frac{1}{298}-\frac{1}{273+T}\right)} \left(\frac{-2\,\bar{a}_1^{\,2}}{\bar{h}_1^3}\right) \right)^2 \sigma_{h_1}^2,$$

$$= 57{,}618{,}898.98 + 4{,}657{,}251{,}206 + 7{,}276{,}955{,}009,$$

$$= 1.1991825 \times 10^{10},$$

or the standard deviation is

$$\sigma_s = 0.1095\ \text{MPa}.$$

Then, using Eq. (2-43) yields

$$6.1725 = \frac{60\, e^{-0.0001\, t_e} - 1.706}{\sqrt{8^2 + 0.1095^2}},$$

and solving this equation yields

t_e = 1,607.44 hr.

Then, the reliability of the package for 1,000 hr can be computed as follows: The residual strength of the molding compound at 1,000 hr will be

$$S_{res} = S_0 e^{-0.0001\,(1{,}000+1{,}607.44)},$$

or

$$S_{res} = 46.23\ \text{MPa},$$

and the performance function for the molding compound failure is

$$Z_m = 46.23 + 8 \times x(1) - f(s),$$

where $f(s)$ is the equation of s_m when each distributed variable is written in the form of $\mu + \sigma u$, where, μ is the mean of the variable and σ is the standard deviation of the variable, u is the standard normal variable. It should be noted that since the use condition is changed, the stress also will be changed. Then, using the Minimum Distance Method yields the design point as

$x_1 = -5.7617,$

$x_2 = 0.5555,$

$x_3 = 0.0020,$

and

$x_4 = -0.0025,$

where

x_1 = normal variable of strength,

x_2 = normal variable of T,

x_3 = normal variable of a,

and

x_4 = normal variable of h_1.

Then, the reliability index is computed as

$$m = \sqrt{x_1^2 + x_2^2 + x_3^2 + x_4^2} = 5.7617,$$

and reliability of the molding compound at the end of 1,000 hr is computed as

$$R_m = \Phi(5.7617) = 0.9_8 58364544.$$

Therefore, the plastic package reliability related to the popcorn effect at 1,000 hr is

$$
\begin{aligned}
R &= 1-(1-R_d)(1-R_m), \\
&= 1-(1-0.9_9 6639074)\,(1-0.9_8 58364544), \\
&= 0.9_{15} 55003618.
\end{aligned}
$$

At the 5,000 hr, the residual strength is computed as

$$
\begin{aligned}
S_{res} &= S_0 e^{-0.0001\cdot(5,000+1,607.44)}, \\
&= 30.99\ \text{MPa},
\end{aligned}
$$

then, the reliability of the molding compound at 5,000 hr is computed similarly as for the 1,000-hr case, the design points are

x_1 = -3.8567,

x_2 = 0.5555,

x_3 = 0.0013,

x_4 = -0.0017,

and

$$m = \sqrt{x_1^2 + x_2^2 + x_3^2 + x_4^2} = 3.8567,$$

and the reliability of the molding compound at 5,000 hr is computed as

$$R_m = \Phi(3.8567) = 0.9999425359652917.$$

Then, the reliability of the plastic package at 5,000 hr. is computed from

$$
\begin{aligned}
R &= 1-(1-R_d)(1-R_m), \\
&= 1-(1-0.9_9 6639074)\,(1-0.9999425359652917),. \\
&= 0.9_{13} 807.
\end{aligned}
$$

8. Reliability quantification of the whole PCB considering all failure modes

To find the reliability of the whole PCB, we need to consider the dependence among 7 failure modes. To be clear, let's restate the 7 failure modes as follows:

Failure mode 1: Failure due to the board delamination, and

performance function $Z_1 = S_1 - s_1^{vib} - s_1^{th}$ and $\sigma_{Z_1} = 4$ MPa.

Failure mode 2: Failure due to the excessive board deflection, and

performance function: $Z_2 = H - \frac{1}{2}h - w_{\max} + h_{i\max} - w^*$ and

$\sigma_{Z2} = 0.00656$,

Failure mode 3: Failure of the leadless interconnect, and

performance function: $Z_3 = S_3 - s_3^{vib} - s_3^{th}$, and $\sigma_{Z_3} = 5.02$ MPa,

Failure mode 4: Failure of leaded interconnect, and

performance function: $Z_4 = S_4 - s_4^{vib} - s_4^{th}$, and $\sigma_{Z_4} = 5$ MPa,

Failure mode 5: Failure of PGA interconnect, and

performance function: $Z_5 = S_5 - s_5^{vib} - s_5^{th}$, and $\sigma_{Z_5} = 5$ MPa.

Failure mode 6: Failure due to the PTH solder joint, and

performance function: $Z_6 = S_6 - s_6^{vib} - s_6^{th}$, $\sigma_{Z_6} = 5$ MPa,

Failure mode 7: Failure due to the PTH barrel failing, and

performance function: $Z_7 = S_7 - s_7^{vib} - s_7^{th}$, and $\sigma_{Z_7} = 10$ MPa,

Failure mode 8: Failure mode due to the popcorn effect. This mode is independent of the other failure modes.

From previous calculations or using Eq. (5-59), we find that

ρ_{12}=0.0008913, ρ_{13}=0.3740 , ρ_{14}= 3.8915×10^{-8}, ρ_{15}=3.8915×10^{-8}, ρ_{16}=3.8915×10^{-8},

ρ_{17}= 5.0421×10^{-4}, ρ_{23}=0.0128, ρ_{24}= 4.795×10^{-6}, ρ_{25}=4.795×10^{-6}, ρ_{26}= 4.795×10^{-6},

ρ_{27} = 2.942×10^{-6}, ρ_{34} = 4.5696×10^{-8}, ρ_{35} = 4.5696×10^{-8}, ρ_{36} = 4.5696×10^{-8}, ρ_{37} = 5.9401×10^{-4}, ρ_{45} = 1.3652×10^{-18}, ρ_{46} = 1.3652×10^{-18}, ρ_{47} = 1.34×10^{-10}, ρ_{56} = 1.3652×10^{-18}, ρ_{57} = 1.34×10^{-10}, and ρ_{67} = 1.34×10^{-10}.

Then, using Eq. (2-27) yields

$$P(F_1 \cap F_2) = \int_0^{0.0008913} w(-6.99,-5.994,r)\,dr + \Phi(-6.99)\Phi(-5.994) = 1.463\times10^{-21},$$

$$P(F_1 \cap F_3) = \int_0^{0.3740} w(-6.99,-7.145,r)\,dr + \Phi(-6.99)\Phi(-7.145) = 4.797\times10^{-19},$$

$$P(F_1 \cap F_4) = \int_0^{\rho} w(-6.99,-5.5074,r)\,dr + \Phi(-6.99)\Phi(-5.5074) = 2.5027\times10^{-20},$$

$$P(F_1 \cap F_5) = \int_0^{\rho} w(-6.99,-7.4892,r)\,dr + \Phi(-6.99)\Phi(-7.4892) = 4.762\times10^{-26},$$

$$P(F_1 \cap F_6) = \int_0^{\rho} w(-6.99,-7.4892,r)\,dr + \Phi(-6.99)\Phi(-7.4892) = 4.762\times10^{-26},$$

$$P(F_1 \cap F_7) = \int_0^{\rho} w(-6.99,-8.089,r)\,dr + \Phi(-6.99)\Phi(-8.089) = 4.258\times10^{-28},$$

$$P(F_2 \cap F_3) = \int_0^{\rho} w(-5.994,-7.145,r)\,dr + \Phi(-5.994)\Phi(-7.145) = 8.098\times10^{-22}$$

$$P(F_2 \cap F_4) = \int_0^{\rho} w(-5.994,-5.5074,r)\,dr + \Phi(-5.994)\Phi(-5.5074) = 1.846\times10^{-17}$$

$$P(F_2 \cap F_5) = \int_0^{\rho} w(-5.994,-7.4892,r)\,dr + \Phi(-5.994)\Phi(-7.4892) = 3.548\times10^{-23},$$

$$P(F_2 \cap F_6) = \int_0^{\rho} w(-5.994,-7.4892,r)\,dr + \Phi(-5.994)\Phi(-7.4892) = 3.548 \times 10^{-23},$$

$$P(F_2 \cap F_7) = \int_0^{\rho} w(-5.994,-8.089,r)\,dr + \Phi(-5.994)\Phi(-8.089) = 3.080 \times 10^{-25},$$

$$P(F_3 \cap F_4) = \int_0^{\rho} w(-7.145,-5.5074,r)\,dr + \Phi(-7.145)\Phi(-5.5074) = 8.194 \times 10^{-21},$$

$$P(F_3 \cap F_5) = \int_0^{\rho} w(-7.145,-7.4892,r)\,dr + \Phi(-7.145)\Phi(-7.4892) = 1.559 \times 10^{-26},$$

$$P(F_3 \cap F_6) = \int_0^{\rho} w(-7.145,-7.4892,r)\,dr + \Phi(-7.145)\Phi(-7.4892) = 1.559 \times 10^{-26},$$

$$P(F_3 \cap F_7) = \int_0^{\rho} w(-7.145,-8.089,r)\,dr + \Phi(-7.145)\Phi(-8.089) = 1.402 \times 10^{-28},$$

$$P(F_4 \cap F_5) = \int_0^{\rho} w(-5.5074,-7.4892,r)\,dr + \Phi(-5.5074)\Phi(-7.4892) = 6.309 \times 10^{-22},$$

$$P(F_4 \cap F_6) = \int_0^{\rho} w(-5.5074,-7.4892,r)\,dr + \Phi(-5.5074)\Phi(-7.4892) = 6.309 \times 10^{-22},$$

$$P(F_4 \cap F_7) = \int_0^{\rho} w(-5.5074,-8.089,r)\,dr + \Phi(-5.5074)\Phi(-8.089) = 1.150 \times 10^{-26},$$

$$P(F_5 \cap F_6) = \int_0^{\rho} w(-7.4892,-7.4892,r)\,dr + \Phi(-7.4892)\Phi(-7.4892) = 1.200 \times 10^{-27},$$

$$P(F_5 \cap F_7) = \int_0^{\rho} w(-7.4892,-8.089,r)\,dr + \Phi(-7.4892)\Phi(-8.089) = 1.042 \times 10^{-29},$$

and

$$P(F_6 \cap F_7) = \int_0^{\rho} w(-7.4892,-8.089,r)\,dr + \Phi(-7.4892)\Phi(-8.089) = 1.042 \times 10^{-29}.$$

Using Eqs. (2-23) and (2-24) yields

$$R_U = P(Z_1 \geq 0) - \sum_{i=2}^{k} \max\left\{ P(Z_i < 0) - \sum_{j=1}^{i-1} P[(Z_i < 0) \cap (Z_j < 0)],\ 0 \right\},$$

or

$$R_U = 0.9_7 807671659,$$

and

$$R_L = 1 - \sum_{i=1}^{k} P(Z_i < 0) + \sum_{i=2}^{k} \max_{j<i} \; P\left[(Z_i < 0) \cap (Z_j < 0)\right],$$
$$= 1 - 1.9234 \times 10^{-8} + 1.8942 \times 10^{-17},$$

or

$$R_L = 0.9_7 807657917.$$

Then,

$$R = \frac{1}{2}\left(R_U + R_L\right) = \frac{1}{2}\left(0.9_7 807671659 + 0.9_7 807657917\right),$$

or

$$R = 0.9_7 807664788.$$

Then, the reliability of the whole PCB at time zero is

$$R_{board} = R \cdot R_8 = 0.9_7 807664788 \cdot 0.9_9 6636715 = 0.9_7 804301503.$$

It is worth to point out that all of the correlation coefficients computed previously are very small except $\rho_{13} = 0.3740$; therefore, the reliability when considering the first 7 failure modes can be computed by assuming all of the failure modes are independent except the Failure Modes 1 and 3. Then, the reliability is computed by

$$R = R_{1,3} \, R_2 R_4 R_5 R_6 R_7 = 0.9_7 807657914,$$

where

$R_{1,3}$ = reliability by considering Failure Modes 1 and 3 dependent.

We see it is very close to what we get when considering all of the failure modes are dependent, which gives $R = 0.9_7807664788$. Therefore, in engineering, it might be good enough to use the latter method since it is much simple for the calculation of the reliability.

CHAPTER 7

CONTRIBUTIONS AND FUTURE RESEARCH

Reliability Quantification is one of the most important tasks in Reliability Engineering. During design, development, and operational phases, this information can be very valuable. In the past, MIL-HDBK-217, Bellcore, and other methods have been used for reliability quantification, but the lack of accuracy, slow pace of updating the data base, etc., make these methods less attractive, and researchers are starting to seek new and sound methods.

In this dissertation, the reliability of the PCB under vibration and thermal load is investigated. An effective method to quantify the reliability of PCB is proposed. Using this method, the designers can check if their design meets the reliability goal at the early product development stage thus avoiding the costly later stage design changes.

7.1 Contributions

1. A modified Stress-Strength Interference (MSSI) method has been proposed.

   In the conventional Stress-Strength Interference (SSM) method, the stress and the strength are both treated as distributed variables with constant parameters. It means that the stress and the strength are both distributed, but their parameters are constant. This assumption, in reality, is rarely true since the strength will be degraded with time in almost all products even though the stress can be considered to be a distributed variable with constant parameters in most of the cases as long as the operational condition stays unchanged. To reflect this situation, a Modified Stress-Strength Interference (MSSI) method has been proposed. In this method, besides assuming that both the stress and the strength are distributed, the mean of the strength is also assumed to be distributed. The damage of the strength can be reflected on the reduction (damage) of the mean strength. To quantify the damage of the mean strength, a damage model is proposed by considering the interaction between the different kinds of the stresses. For each stress type, the damage can be found by computing the ratio of the operation time and the mean value of the mean strength distribution. For the case where more than one stress level is involved in one type of stress, an equivalent time calculation method is proposed so that the single stress method can be used after time conversion. Using the MSSI, the designers not only can find the initial reliability of their design, like SSIM does, but also can find the reliability of the product at any operation time. This is especially important for those users whose products are safety related, or the maintenance cost is a big concern.

2. A multiple failure modes method being proposed to quantify the reliability of a PCB.

   A PCB is a fairly complex product and includes many parts and failure modes. In this dissertation, to easily quantify its reliability, a PCB is divided into three parts: the laminated board, the interconnect between the board and the modules, and the modules and parts mounted on the board.

   (a) In quantifying the reliability of the board, two failure modes are considered. One is the delamination failure mode; the other is the excessive deflection failure mode. Delamination failure mode has not been studied by any researcher to my knowledge, since so far all research on PCBs assumes it is an isotropic solid plate, and ignores the fact that it is actually a composite laminate board. The excessive deflection failure mode occurs when the PCB is installed in an electronic box in which excessive deflection of the PCBs can cause contact between the PCB and the enclosure of the box thus causing a short circuit or other damage to the PCB or the product. For these two failure modes, the stresses induced by vibration and thermal loads are computed first, and then the MSSI is used to compute the reliability related to each failure mode. Since these two failure modes are not independent, the final reliability of the board is computed by considering them as bivariate normal variables.

(b) In quantifying the reliability of the interconnects, three kinds of interconnects are investigated. The first is the surface mount leadless interconnect. For this interconnect, the failure mode of the solder joint due to shear stress is studied. The solder balls are first treated as a solder layer such that a layered stress equation can be used to find the stress experienced by the solder ball. Then, two adjustment factors are proposed to adjust the error caused by treating the solder ball as a solder layer. Its reliability is then computed using the MSSI method. The second kind of interconnect is the surface mounted leaded interconnect. For this interconnect, the peeling failure of the solder joint was investigated and its reliability was calculated using the MSSI method. The third type of interconnect includes two forms of interconnects, Pin Grid Array (PGA) and Plate Through Hole. For the PGA interconnect, the same failure mode as SM leaded interconnect was studied and its reliability was computed using the MSSI method. For the Plate/Pin Through Hole (PTH) interconnect, two failure modes are considered. One is the failure due to the peeling failure of the solder joint; the other is the failure due to the barrel cracking. These two failure modes are not independent, so a dependent reliability quantification method is utilized to find the reliability of this interconnect.

(c) In quantifying the reliability of the modules and parts, a focus is put on the reliability quantification of the Popcorn effect, one of the most challenging problems in plastic package. In this dissertation, a reliability model based on the Popcorn mechanism is proposed. A three-step method is used to compute the reliability of the plastic package related to the Popcorn effect. The first step is to compute the probability that a package will delaminate due to thermal load during storage or other situations; the second step is to compute the probability that this package will fail due to high stress during reflow. One minus the product of these two probabilities gives the initial reliability of the plastic package related to the Popcorn effect. The third step is used when computing the reliability of the product after it is delivered to the customer. To compute this reliability, an equivalent time calculation method is proposed. Using this method, one can convert the time between reflow stress and the operation stress, so that the single stress reliability quantification method can be used. Then, the reliability of the package at any time after it is delivered to the customer can be found.

3. Temperature distribution on the PCB was computed by solving a Partial Differential Equation (PDE).

    The temperature distribution of the board determines the stress in the board and elsewhere. A PDE equation is solved to find the temperature distribution of the board. Considering the operation profile of most of the electronic equipment, only the steady state temperature distribution is found. The maximum temperature is then used as the basis to compute the stress on the board since that is the most sever case which the board will experience. Also using this temperature to compute the reliability gives us a conservative result.

4. Failure modes dependence has been considered in the computation of the reliability.

    In this dissertation, 8 failure modes are considered. Except the failure mode due to the popcorn effect, all failure modes are not independent. A dependent reliability quantification method is used to compute the reliability of the PCB.

5. The reliability quantification method was applied to a PCB under "ideal white noise" conditions.

   In this example, all different interconnects are considered, the reliability of the board at times 0, 1,000 hr, and 5,000 hr are computed. The reliabilities of SM leadless, leaded, PGA and PTH interconnects are computed using the proposed method. The plastic package reliability related to the Popcorn effect is computed at times 0, 1,000 hr, and 5,000 hr. The equivalent time method is used to convert the reflow time to the equivalent time at normal use conditions. The reliability of the whole PCB is then computed using the dependent reliability quantification method.

7.2 Recommendations for Future Research

As we stated previously, a PCB is a fairly complex electronic component; it includes many failure modes and can experience many different environmental conditions. To further improve the method proposed in this dissertation, following works may need to be conducted:

1. More environmental conditions need to be considered.

   Space environment is one of the choices. As we know, in the current space aircraft and vehicles, there are many PCBs in their electronic equipment. The PCB's failure may cause the whole system to malfunction, fail, even cause the mission to abort. Therefore, improving the PCB's reliability in a space environment becomes very important. Another environmental condition that needs to be considered might be humidity, since this environment may cause failure due to corrosion.

2. More failure modes need to be considered.

   In this dissertation, 8 major failure modes of PCBs are considered to compute the reliability of the PCB. In reality, many other failure modes can occur in the PCB. For example, a lead wire in the package can be broken, corrode, etc.

3. Optimization of the PCB's design should be combined with this work.

   One of the most important tasks for a designer is to come up with the optimal design. If the method proposed in this dissertation can be combined with an optimization tool, the designers can reach an optimized design at the early stage. For example, by considering the performance requirement, reliability requirement and cost availability, the designer can easily determine the optimized design concept without any difficulty.

4. Development of related software to simplify the calculations.

   From the application example, it can be seen that calculating the reliability, especially when many dependent failure modes are involved, is very time consuming. If software can be developed, or current software can add some functions proposed in this dissertation, the application of this method will be much easier and more attractive.

APPENDIX A

DERIVATION OF EQ. (2-5)

We know for any normal distribution with mean μ and variance σ^2, its CDF is given by

$$F(z) = \int_{-\infty}^{z} f(t)\,dt = \int_{-\infty}^{z} \frac{1}{\sqrt{2\pi}\,\sigma} \exp\left(-\frac{1}{2}\left(\frac{t-\mu_z}{\sigma_z}\right)^2 \right) dt. \qquad \text{(A-1)}$$

Making the changes of the variable $u = (t-\mu_z)/\sigma_z$, and $dt = \sigma_z\,du$, then

$$F(z) = \int_{-\infty}^{(z-\mu_z)/\sigma_z} \frac{1}{\sqrt{2\pi}\,\sigma} e^{-\frac{1}{2}u^2}\,\sigma\,du,$$

or

$$F(z) = \int_{-\infty}^{(z-\mu_z)/\sigma_z} \frac{1}{\sqrt{2\pi}} e^{-\frac{1}{2}u^2}\,du. \qquad \text{(A-2)}$$

Comparing Eq. (A-2) with the definition of the cdf of the standard normal distribution given above, and realizing $R(t) = 1 - F(t)$, we get

$$R(z) = \int_{z}^{\infty} f(t)\,dt = 1 - \Phi\left(\frac{z-\mu_z}{\sigma_z} \right). \qquad \text{(A-3)}$$

APPENDIX B

PROOF OF THE RELIABILITY INDEX GEOMETRIC EXPRESSION

From Eq. (2-8), we know the performance function is given by

$$Z(u,v) = \bar{S} - \bar{s} + \sigma_S\, u - \sigma_s\, \mathrm{v}. \tag{B-1}$$

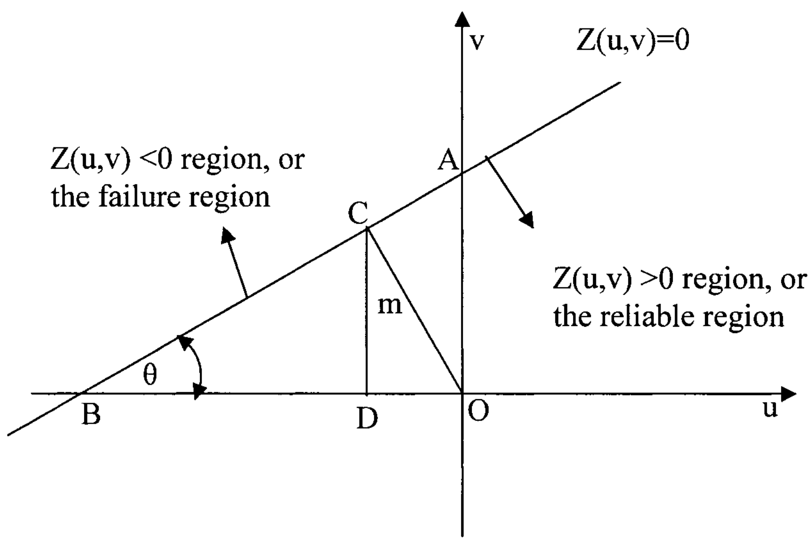

Fig. B-1 Illustration of the geometric expression of the reliability index.

Then, in Fig. B-1

$$AO = \frac{\bar{S} - \bar{s}}{\sigma_s}, \text{ and } BO = -\frac{\bar{S} - \bar{s}}{\sigma_S},$$

and

$$\tan\theta = \frac{|AO|}{|BO|} = \frac{\sigma_S}{\sigma_s}. \tag{B-2}$$

From trigonometry, we know

$$\sin\theta = \frac{\tan\theta}{\sqrt{1 + \tan^2\theta}}. \tag{B-3}$$

Substituting (B-2) into (B-3) yields

$$\sin\theta = \frac{\dfrac{\sigma_S}{\sigma_s}}{\sqrt{1+\left(\dfrac{\sigma_S}{\sigma_s}\right)^2}} = \frac{\sigma_S}{\sqrt{\sigma_S^2+\sigma_s^2}},$$

from Fig. B-1. Therefore,

$$m = CO = |BO|\sin\theta = \frac{\bar{S}-\bar{s}}{\sigma_S}\frac{\sigma_S}{\sqrt{\sigma_S^2+\sigma_s^2}} = \frac{\bar{S}-\bar{s}}{\sqrt{\sigma_S^2+\sigma_s^2}}.$$

Next let's find out the coordinates of point C. From trigonometry,

$$|BC| = |BO|\cos\theta = |BO|\frac{1}{\sqrt{1+\tan^2\theta}} = \frac{\bar{S}-\bar{s}}{\sigma_S}\frac{1}{\sqrt{1+\left(\dfrac{\sigma_S}{\sigma_s}\right)^2}},$$

or

$$|BC| = \frac{\sigma_s}{\sigma_S}\frac{\bar{S}-\bar{s}}{\sqrt{\sigma_S^2+\sigma_s^2}} = \frac{\sigma_s}{\sigma_S}m.$$

Therefore, the x-coordinate of C is

$$x_c = -|CO|\cdot\sin\theta = -m\cdot\frac{\sigma_S}{\sqrt{\sigma_S^2+\sigma_s^2}},$$

and the y-coordinate of C is

$$y_c = |CO|\cdot\cos\theta = m\cdot\frac{\sigma_s}{\sqrt{\sigma_S^2+\sigma_s^2}}.$$

APPENDEX C
CODE FOR EXAMPLE 2-3

C.1 Code for optimization

OBJECTIVE FUNCTION

```
function f = objfun(x)
f = (x(1).^2+x(2).^2)^0.5;
```

CONSTRAIN FUNCTION

```
function [c, ceq] = confuneq(x)
% Nonlinear inequality constraints
c = [];
% Nonlinear equality constraints
ceq = 30+5*x(1)+10*x(2)+x(1)*x(2);
```

MAIN CODE

```
clear all
close all
%objective = @(x) x(1)^2+x(2)^2;
x0 = [0,0];          % Make a starting guess at the solution
options = optimset('LargeScale','off');
[x,fval] = fmincon(@objfun,x0,[],[],[],[],[],[],...
  @confuneq,options)
[c,ceq] = confuneq(x) % Check the constraint values at x
```

C.2 CODE FOR MONTE CARLO SIMULATION

```
clear all
close all
for i=1:10
   m=0;
   for j=1:10000
      a(j)=5+1*randn;
      b(j)=10+1*randn;
      c=20;
      g(j)=a(j)*b(j)-c;
      if g(j)>0
          m=m+1;
      end
   end
      R(i)=m/10000
end
```

APPENDIX D

PROOF OF BIVARIATE NORMAL INTEGRAL EQUATION

From Section 2.2, we know the CDF of a bivariate normal distribution is

$$\Phi = \int_{-\infty}^{-m_1}\int_{-\infty}^{-m_2} \frac{1}{2\pi\sqrt{1-\rho^2}} \exp\left(-\frac{u^2 - 2\,\rho\, u\, v + v^2}{2\,(1-\rho^2)}\right) du\, dv. \qquad \text{(D-1)}$$

Let's denote $w(u, v, \rho) = \dfrac{1}{2\pi\sqrt{1-\rho^2}} \exp\left(-\dfrac{u^2 - 2\rho\, u\, v + v^2}{2\,(1-\rho^2)}\right)$, then

$$\begin{aligned}
\frac{\partial w}{\partial \rho} &= \frac{1}{2\pi}\left(\frac{-\rho}{\sqrt{1-\rho^2}\left(1-\rho^2\right)}\right)\exp\left(-\frac{u^2 - 2\rho\, u\, v + v^2}{2(1-\rho^2)}\right) + \\
&\quad + \frac{1}{2\pi\sqrt{1-\rho^2}} \exp\left(-\frac{u^2 - 2\rho\, u\, v + v^2}{2(1-\rho^2)}\right)\left(\frac{1}{2}\right) \\
&\quad \cdot\left(-\frac{-2\,u\, v(1-\rho^2) - (u^2 - 2\rho\, u\, v + v^2)(-2\rho)}{(1-\rho^2)^2}\right), \\
&= \frac{1}{2\pi}\left(\frac{-\rho}{\sqrt{1-\rho^2}\left(1-\rho^2\right)}\right)\exp\left(-\frac{u^2 - 2\rho\, u\, v + v^2}{2(1-\rho^2)}\right) + \\
&\quad + \frac{1}{2\pi\sqrt{1-\rho^2}} \exp\left(-\frac{u^2 - 2\rho\, u\, v + v^2}{2(1-\rho^2)}\right)\left(\frac{u\, v + \rho^2\, u\, v - \rho\, u^2 - \rho\, v^2}{(1-\rho^2)^2}\right),
\end{aligned}$$

$$\begin{aligned}
\frac{\partial w}{\partial v} &= \frac{1}{2\pi\sqrt{1-\rho^2}} \exp\left(-\frac{u^2 - 2\rho\, u\, v + v^2}{2(1-\rho^2)}\right)\left(-\frac{-2\,\rho\, u + 2\, v}{2(1-\rho^2)}\right), \\
&= \frac{1}{2\pi\sqrt{1-\rho^2}} \exp\left(-\frac{u^2 - 2\rho\, u\, v + v^2}{2(1-\rho^2)}\right)\left(\frac{v - \rho\, u}{(1-\rho^2)}\right),
\end{aligned}$$

$$\frac{\partial^2 w}{\partial u \partial v} = \frac{\partial}{\partial u}\left(\frac{\partial w}{\partial v}\right) = \frac{1}{2\pi\sqrt{1-\rho^2}} \exp\left(-\frac{u^2 - 2\rho\, uv + v^2}{2(1-\rho^2)}\right)\left(\frac{-\rho}{(1-\rho^2}\right)$$

$$+\frac{1}{2\pi\sqrt{1-\rho^2}} \exp\left(-\frac{u^2 - 2\rho\, uv + v^2}{2(1-\rho^2)}\right)\left(\frac{v-\rho u}{1-\rho^2}\right)\left(\frac{u-\rho v}{1-\rho^2}\right),$$

$$= \frac{1}{2\pi}\left(\frac{-2\rho}{\sqrt{1-\rho^2}\left(1-\rho^2\right)}\right)\exp\left(-\frac{u^2 - 2\rho\, uv + v^2}{2(1-\rho^2)}\right) +$$

$$+\frac{1}{2\pi\sqrt{1-\rho^2}} \exp\left(-\frac{u^2 - 2\rho\, uv + v^2}{2(1-\rho^2)}\right)\left(\frac{uv + \rho^2 uv - \rho u^2 - \rho v^2}{(1-\rho^2)^2}\right).$$

We see that

$$\frac{\partial w}{\partial \rho} = \frac{\partial^2 w}{\partial u \partial v}.$$

Then,

$$\frac{\partial \Phi}{\partial \rho} = \int_{-\infty}^{-m_1}\int_{-\infty}^{-m_2} \frac{\partial w}{\partial \rho}\, du\, dv,$$

$$= \int_{-\infty}^{-m_1}\int_{-\infty}^{-m_2} \frac{\partial^2 w}{\partial u \partial v}\, du\, dv,$$

$$= w(-m_1, -m_2, \rho),$$

$$\int_0^{\rho} \frac{\partial \Phi}{\partial \rho}\, d\rho = \int_0^{\rho} w(-m_1, -m_2, \rho)\, d\rho.$$

Consider $\int_0^{\rho} \frac{\partial \Phi}{\partial \rho} d\rho = \Phi - \Phi(\rho = 0)$. Then,

$$\Phi = \int_0^{\rho} w(-m_1, -m_2, \rho) d\rho + \Phi(0).$$

From Eq. (D-1),

$$\Phi(0) = \int_{-\infty}^{-m_1}\int_{-\infty}^{-m_2} \frac{1}{2\pi\sqrt{1-\rho^2}} \exp\left(-\frac{u^2 - 2\rho uv + v^2}{2(1-\rho^2)}\right) dudv,$$

$$= \int_{-\infty}^{-m_1}\int_{-\infty}^{-m_2} \frac{1}{2\pi} \exp\left(-\frac{u^2 + v^2}{2}\right) dudv,$$

$$= \int_{-\infty}^{-m_1} \frac{1}{\sqrt{2\pi}} \exp\left(-\frac{1}{2}u^2\right) du \int_{-\infty}^{-m_2} \frac{1}{\sqrt{2\pi}} \exp\left(-\frac{1}{2}v^2\right) dv,$$

$$= \Phi(-m_1)\Phi(-m_2),$$

Then,

$$\Phi = \int_0^{\rho} w(-m_1, -m_2, \rho) d\rho + \Phi(-m_1)\Phi(-m_2).$$

APPENDIX E

THE CLOSED FORM OF INTEGRAL $\int_0^\infty\int_0^\infty h_{mn}(r_1)\, h_{ij}(r_2)\, R_{\ddot{w}_1\ddot{w}_1}(r_2-r_1)\, dr_1\, dr_2$

Denote $I=\int_0^\infty\int_0^\infty h_{mn}(r_1)\, h_{ij}(r_2)\, R_{\ddot{w}_1\ddot{w}_1}(r_2-r_1)\, dr_1\, dr_2$

From Eq. (3-37) we know

$$h_{mn}(r_1)=\frac{e^{-\eta_b r_1}}{p_{dbmn}}\sin\left(p_{dbmn}r_1\right),$$

$$h_{ij}(r_2)=\frac{e^{-\eta_b r_2}}{p_{dbij}}\sin\left(p_{dbij}r_2\right),$$

and Eq. (3-29)

$$R_{\ddot{w}_1\ddot{w}_1}(r_2-r_1)=2\,\eta\,\pi\, S_0 e^{-\eta|r_2-r_1|}\left[\frac{4\eta^2+p^2}{4\eta^2}\cos\left(p_d(r_2-r_1)\right)+\frac{1}{4\eta}\sin\left(p_d|r_2-r_1|\right)\right].$$

Let $A=\dfrac{\pi\, S_0\left(4\,\eta^2+p^2\right)}{2\eta}$, $B=\dfrac{\pi\, S_0}{2}$, then

$$R_{\ddot{w}_1\ddot{w}_1}(r_2-r_1)=\begin{cases}Ae^{-\eta(r_2-r_1)}\cos\left(p_d(r_2-r_1)\right)+Be^{-\eta(r_2-r_1)}\sin\left(p_d(r_2-r)\right) & r_2>r_1\\ Ae^{-\eta(r_1-r_2)}\cos\left(p_d(r_1-r_2)\right)+Be^{-\eta(r_1-r_2)}\sin\left(p_d(r_1-r_2)\right) & r_2<r_1\end{cases}.$$

Then, the integral I can be divided into two parts, part 1 (denoted as I_1) represents the case when $r_2 > r_1$; while part 2 (denoted as I_2) represents the case when $r_2 < r_2$.

Denote $p_{dbmn}=C$, and $p_{dbij}=D$, then,

$$\begin{aligned}I_1 &= \int_0^\infty\int_0^{r_2}\frac{A}{CD}e^{-\eta_b r_1}e^{-\eta_b r_2}e^{-\eta(r_2-r_1)}\sin(Cr_1)\sin(Dr_2)\cos\left(p_d(r_2-r_1)\right)dr_1\, dr_2\\ &+\int_0^\infty\int_0^{r_2}\frac{B}{CD}e^{-\eta_b r_1}e^{-\eta_b r_2}e^{-\eta(r_2-r_1)}\sin(Cr_1)\sin(Dr_2)\sin\left(p_d(r_2-r_1)\right)dr_1\, dr_2.\end{aligned} \qquad \text{(E-1)}$$

I_2 can be found by switching r_2 with r_1.

Denote

$$I_1(a)=\int_0^\infty\int_0^{r_2}\frac{A}{CD}e^{-\eta_b r_1}e^{-\eta_b r_2}e^{-\eta(r_2-r_1)}\sin(Cr_1)\sin(Dr_2)\cos\left(p_d(r_2-r_1)\right)dr_1\, dr_2, \qquad \text{(E-2)}$$

and

$$I_1(b)=\int_0^\infty\int_0^{r_2}\frac{B}{CD}e^{-\eta_b r_1}e^{-\eta_b r_2}e^{-\eta(r_2-r_1)}\sin(Cr_1)\sin(Dr_2)\sin(p_d(r_2-r_1))dr_1\,dr_2. \qquad \text{(E-3)}$$

Then,

$$I_1=I_1(a)+I_1(b).$$

Consider $\cos(p_d(r_2-r_1))=\cos(p_d r_2)\cos(p_d r_1)+\sin(p_d r_2)\sin(p_d r_1)$. Then,

$$\begin{aligned}
I_1(a)&=\int_0^\infty\int_0^{r_2}\frac{A}{CD}e^{-\eta_b r_1}e^{-\eta_b r_2}e^{-\eta(r_2-r_1)}\sin(Cr_1)\sin(Dr_2)\cos(p_d r_2)\cos(p_d r_1)dr_1\,dr_2\\
&+\int_0^\infty\int_0^{r_2}\frac{A}{CD}e^{-\eta_b r_1}e^{-\eta_b r_2}e^{-\eta(r_2-r_1)}\sin(Cr_1)\sin(Dr_2)\sin(p_d r_2)\sin(p_d r_1)dr_1\,dr_2,\\
&=\int_0^\infty\frac{A}{CD}e^{-(\eta+\eta_b)r_2}\sin(Dr_2)\cos(p_d r_2)\left[\int_0^{r_2}e^{(\eta-\eta_b)r_1}\sin(Cr_1)\cos(p_d r_1)dr_1\right]dr_2\\
&+\int_0^\infty\frac{A}{CD}e^{-(\eta+\eta_b)r_2}\sin(Dr_2)\sin(p_d r_2)\left[\int_0^{r_2}e^{(\eta-\eta_b)r_1}\sin(Cr_1)\sin(p_d r_1)dr_1\right]dr_2,\\
&=I_1(a1)+I_1(a2).
\end{aligned}$$

To simplify $I_1(A)$, let's first find out the following integrals. From a mathematics handbook, we have

$$\begin{aligned}
\int e^{ax}\sin(\alpha x)\sin(\beta x)&=\frac{e^{ax}[(\alpha-\beta)\sin(\alpha-\beta)x+a\cos(\alpha-\beta)x]}{2\left[a^2+(\alpha-\beta)^2\right]}\\
&-\frac{e^{ax}[(\alpha+\beta)\sin(\alpha+\beta)x+a\cos(\alpha+\beta)x]}{2\left[a^2+(\alpha+\beta)^2\right]},
\end{aligned} \qquad \text{(E-4a)}$$

and

$$\begin{aligned}
\int e^{ax}\sin(\alpha x)\cos(\beta x)&=\frac{e^{ax}[a\sin(\alpha-\beta)x-(\alpha-\beta)\cos(\alpha-\beta)x]}{2\left[a^2+(\alpha-\beta)^2\right]}\\
&+\frac{e^{ax}[a\cos(\alpha+\beta)x-(\alpha+\beta)\sin(\alpha+\beta)x]}{2\left[a^2+(\alpha+\beta)^2\right]}.
\end{aligned} \qquad \text{(E-4b)}$$

For $a < 0$,

$$E(a,\alpha,\beta)=\int_0^\infty e^{ax}\sin(\alpha x)\sin(\beta x)=\frac{-a}{2\left[a^2+(\alpha-\beta)^2\right]}+\frac{a}{2\left[a^2+(\alpha+\beta)^2\right]}, \tag{E-5a}$$

and

$$F(a,\alpha,\beta)=\int_0^\infty e^{ax}\sin(\alpha x)\cos(\beta x)=\frac{\alpha-\beta}{2\left[a^2+(\alpha-\beta)^2\right]}+\frac{\alpha+\beta}{2\left[a^2+(\alpha+\beta)^2\right]}. \tag{E-5b}$$

$$\begin{aligned}
\int e^{ax}\sin(\alpha x)\sin(\beta x)\cos(\gamma x)dx &= \int e^{ax}\sin(\alpha x)\left[\frac{\sin(\beta+\gamma)x+\sin(\beta-\gamma)x}{2}\right],\\
&=\frac{1}{2}\int \mathrm{e}^{ax}\sin(\alpha x)\sin(\beta+\gamma)xdx+\frac{1}{2}\int \mathrm{e}^{ax}\sin(\alpha x)\sin(\beta-\gamma)xdx,\\
&=\frac{1}{2}\left\{\frac{e^{ax}\left[(\alpha-\beta-\gamma)\sin(\alpha-\beta-\gamma)x+a\cos(\alpha-\beta-\gamma)x\right]}{2\left[a^2+(\alpha-\beta-\gamma)^2\right]}\right.\\
&\quad\left.-\frac{e^{ax}\left[(\alpha+\beta+\gamma)\sin(\alpha+\beta+\gamma)x+a\cos(\alpha+\beta+\gamma)x\right]}{2\left[a^2+(\alpha+\beta+\gamma)^2\right]}\right\}\\
&\quad+\frac{1}{2}\left\{\frac{e^{ax}\left[(\alpha-\beta+\gamma)\sin(\alpha-\beta+\gamma)x+a\cos(\alpha-\beta+\gamma)\right]}{2\left[a^2+(\alpha-\beta+\gamma)^2\right]}\right.\\
&\quad\left.-\frac{e^{ax}\left[(\alpha+\beta-\gamma)\sin(\alpha+\beta-\gamma)x+a\cos(\alpha+\beta-\gamma)x\right]}{2\left[a^2+(\alpha+\beta-\gamma)^2\right]}\right\},
\end{aligned} \tag{E-6a}$$

$$\begin{aligned}
\int e^{ax}\sin(\alpha x)\cos(\beta x)\cos(\gamma x)dx &= \int e^{ax}\sin(\alpha x)\left[\frac{\cos(\beta+\gamma)x+\cos(\beta-\gamma)x}{2}\right],\\
&=\frac{1}{2}\int \mathrm{e}^{ax}\sin(\alpha x)\cos(\beta+\gamma)xdx+\frac{1}{2}\int \mathrm{e}^{ax}\sin(\alpha x)\cos(\beta-\gamma)xdx,\\
&=\frac{1}{2}\left\{\frac{e^{ax}\left[a\sin(\alpha-\beta-\gamma)x-(\alpha-\beta-\gamma)\cos(\alpha-\beta-\gamma)x\right]}{2\left[a^2+(\alpha-\beta-\gamma)^2\right]}\right.\\
&\quad\left.+\frac{e^{ax}\left[a\sin(\alpha+\beta+\gamma)x-(\alpha+\beta+\gamma)\cos(\alpha+\beta+\gamma)x\right]}{2\left[a^2+(\alpha+\beta+\gamma)^2\right]}\right\}\\
&\quad+\frac{1}{2}\left\{\frac{e^{ax}\left[a\sin(\alpha-\beta+\gamma)x-(\alpha-\beta+\gamma)\cos(\alpha-\beta+\gamma)x\right]}{2\left[a^2+(\alpha-\beta+\gamma)^2\right]}\right.\\
&\quad\left.+\frac{e^{ax}\left[a\sin(\alpha+\beta-\gamma)x-(\alpha+\beta-\gamma)\cos(\alpha+\beta-\gamma)x\right]}{2\left[a^2+(\alpha+\beta-\gamma)^2\right]}\right\}.
\end{aligned} \tag{E-6b}$$

For a < 0,

$$G(a,\alpha,\beta,\gamma)=\int_0^\infty e^{ax}\sin(\alpha x)\sin(\beta x)\cos(\gamma x)dx$$

$$=-\frac{a}{4\left[a^2+(\alpha-\beta-\gamma)^2\right]}+\frac{a}{4\left[a^2+(\alpha+\beta+\gamma)^2\right]} \tag{E-7a}$$
$$-\frac{a}{4\left[a^2+(\alpha-\beta+\gamma)^2\right]}+\frac{a}{4\left[a^2+(\alpha+\beta-\gamma)^2\right]},$$

and

$$H(a,\alpha,\beta,\gamma)=\int_0^\infty e^{ax}\sin(\alpha x)\cos(\beta x)\cos(\gamma x)dx,$$

$$=\frac{\alpha-\beta-\gamma}{4\left[a^2+(\alpha-\beta-\gamma)^2\right]}+\frac{\alpha+\beta+\gamma}{4\left[a^2+(\alpha+\beta+\gamma)^2\right]} \tag{E-7b}$$
$$+\frac{\alpha-\beta+\gamma}{4\left[a^2+(\alpha-\beta+\gamma)^2\right]}+\frac{\alpha+\beta-\gamma}{4\left[a^2+(\alpha+\beta-\gamma)^2\right]}.$$

$$\int e^{ax}\sin(\alpha x)\sin(\beta x)\sin(\gamma x)dx=\int e^{ax}\sin(\alpha x)\left[\frac{\cos(\beta-\gamma)x-\cos(\beta+\gamma)x}{2}\right],$$

$$=\frac{1}{2}\int \mathrm{e}^{ax}\sin(\alpha x)\cos(\beta-\gamma)xdx-\frac{1}{2}\int \mathrm{e}^{ax}\sin(\alpha x)\cos(\beta+\gamma)xdx,$$

$$=\frac{1}{2}\left\{\frac{e^{ax}\left[a\sin(\alpha-\beta+\gamma)x-(\alpha-\beta+\gamma)\cos(\alpha-\beta+\gamma)x\right]}{2\left[a^2+(\alpha-\beta+\gamma)^2\right]}\right.$$
$$\left.+\frac{e^{ax}\left[a\sin(\alpha+\beta-\gamma)x-(\alpha+\beta-\gamma)\cos(\alpha+\beta-\gamma)x\right]}{2\left[a^2+(\alpha+\beta-\gamma)^2\right]}\right\}$$
$$-\frac{1}{2}\left\{\frac{e^{ax}\left[a\sin(\alpha-\beta-\gamma)x-(\alpha-\beta-\gamma)\cos(\alpha-\beta-\gamma)x\right]}{2\left[a^2+(\alpha-\beta-\gamma)^2\right]}\right.$$
$$\left.+\frac{e^{ax}\left[a\sin(\alpha+\beta+\gamma)x-(\alpha+\beta+\gamma)\cos(\alpha+\beta+\gamma)x\right]}{2\left[a^2+(\alpha+\beta+\gamma)^2\right]}\right\}.$$

For a < 0,

$$J(a,\alpha,\beta,\gamma)=\int_0^\infty e^{ax}\sin(\alpha x)\sin(\beta x)\sin(\gamma x)dx,$$

$$\begin{aligned}&=\frac{(\alpha-\beta+\gamma)}{4\left[a^2+(\alpha-\beta+\gamma)^2\right]}+\frac{(\alpha+\beta-\gamma)}{4\left[a^2+(\alpha+\beta-\gamma)^2\right]}\\&-\frac{(\alpha-\beta-\gamma)}{4\left[a^2+(\alpha-\beta-\gamma)^2\right]}-\frac{(\alpha+\beta+\gamma)}{4\left[a^2+(\alpha+\beta+\gamma)^2\right]}.\end{aligned}\tag{E-8}$$

Using Eq. (F-4b) yields

$$\begin{aligned}\int_0^r e^{(\eta-\eta_b)r_1}\sin(Cr_1)\cos(p_dr_1)dr_1 &=\frac{e^{(\eta-\eta_b)r_1}\left[(\eta-\eta_b)\sin(C-p_d)r_1-(C-p_d)\cos(C-p_d)r_1\right]}{2\left[(\eta-\eta_b)^2+(C-p_d)^2\right]}\Bigg|_0^{r_2}\\&+\frac{e^{(\eta-\eta_b)r_1}\left[(\eta-\eta_b)\sin(C+p_d)r_1-(C+p_d)\cos(C+p_d)r_1\right]}{2\left[(\eta-\eta_b)^2+(C+p_d)^2\right]}\Bigg|_0^{r_2},\\&=\frac{e^{(\eta-\eta_b)r_2}\left[(\eta-\eta_b)\sin(C-p_d)r_2-(C-p_d)\cos(C-p_d)r_2\right]}{2\left[(\eta-\eta_b)^2+(C-p_d)^2\right]}\\&+\frac{C-p_d}{2\left[(\eta-\eta_b)^2+(C-p_d)^2\right]}\\&+\frac{e^{(\eta-\eta_b)r_2}\left[(\eta-\eta_b)\sin(C+p_d)r_2-(C+p_d)\cos(C+p_d)r_2\right]}{2\left[(\eta-\eta_b)^2+(C+p_d)^2\right]}\\&+\frac{C+p_d}{2\left[(\eta-\eta_b)^2+(C+p_d)^2\right]}.\end{aligned}$$

Denote

$p_1=C-p_d$ and $p_2=C+p_d$. Then,

$$\begin{aligned}\int_0^r e^{(\eta-\eta_b)r_1}\sin(Cr_1)\cos(p_dr_1)dr_1 &=\frac{e^{(\eta-\eta_b)r_2}\left[(\eta-\eta_b)\sin(p_1r_2)-p_1\cos(p_1r_2)\right]}{2\left[(\eta-\eta_b)^2+p_1^2\right]}\\&+\frac{p_1}{2\left[(\eta-\eta_b)^2+p_1^2\right]}\\&+\frac{e^{(\eta-\eta_b)r_2}\left[(\eta-\eta_b)\sin(p_2r_2)-p_2\cos(p_2r_2)\right]}{2\left[(\eta-\eta_b)^2+p_2^2\right]}\\&+\frac{p_2}{2\left[(\eta-\eta_b)^2+p_2^2\right]}.\end{aligned}\tag{E-9a}$$

Similarly,

$$\int_0^r e^{(\eta-\eta_b)r_1}\sin(Cr_1)\sin(p_d r_1)dr_1 = \frac{e^{(\eta-\eta_b)r_2}\left[(\eta-\eta_b)\cos(p_1 r_2)+p_1\sin(p_1 r_2)\right]}{2\left[(\eta-\eta_b)^2+p_1^2\right]} - \frac{(\eta-\eta_b)}{2\left[(\eta-\eta_b)^2+p_1^2\right]} - \frac{e^{(\eta-\eta_b)r_2}\left[(\eta-\eta_b)\cos(p_2 r_2)+p_2\sin(p_2 r_2)\right]}{2\left[(\eta-\eta_b)^2+p_2^2\right]} + \frac{(\eta-\eta_b)}{2\left[(\eta-\eta_b)^2+p_2^2\right]}. \tag{E-9b}$$

Then,

$$\begin{aligned} I_1(a1) &= \int_0^\infty \frac{A}{CD}e^{-(\eta+\eta_b)r_2}\sin(Dr_2)\cos(p_d r_2)\frac{e^{(\eta-\eta_b)r_2}\left[(\eta-\eta_b)\sin(p_1 r_2)-p_1\cos(p_1 r_2)\right]}{2\left[(\eta-\eta_b)^2+p_1^2\right]}dr_2 \\ &+ \int_0^\infty \frac{A}{CD}e^{-(\eta+\eta_b)r_2}\sin(Dr_2)\cos(p_d r_2)\frac{p_1}{2\left[(\eta-\eta_b)^2+p_1^2\right]}dr_2 \\ &+ \int_0^\infty \frac{A}{CD}e^{-(\eta+\eta_b)r_2}\sin(Dr_2)\cos(p_d r_2)\frac{e^{(\eta-\eta_b)r_2}\left[(\eta-\eta_b)\sin(p_2 r_2)-p_2\cos(p_2 r_2)\right]}{2\left[(\eta-\eta_b)^2+p_2^2\right]}dr_2 \\ &+ \int_0^\infty \frac{A}{CD}e^{-(\eta+\eta_b)r_2}\sin(Dr_2)\cos(p_d r_2)\frac{p_2}{2\left[(\eta-\eta_b)^2+p_2^2\right]}dr_2, \\ &= I_1(a11)+I_1(a12)+I_1(a13)+I_1(a14). \end{aligned}$$

$$\begin{aligned} I_1(a11) &= \int_0^\infty \frac{A}{CD}e^{-(\eta+\eta_b)r_2}\sin(Dr_2)\cos(p_d r_2) \\ &\quad \frac{e^{(\eta-\eta_b)r_2}\left[(\eta-\eta_b)\sin(p_1 r_2)-p_1\cos(p_1 r_2)\right]}{2\left[(\eta-\eta_b)^2+p_1^2\right]}dr_2, \\ &= \frac{A(\eta-\eta_b)}{2CD\left[(\eta-\eta_b)^2+p_1^2\right]}\int_0^\infty e^{-2\eta_b r_2}\sin(Dr_2)\cos(p_d r_2)\sin(p_1 r_2)dr_2 \\ &\quad - \frac{Ap_1}{2CD\left[(\eta-\eta_b)^2+p_1^2\right]}\int_0^\infty e^{-2\eta_b r_2}\sin(Dr_2)\cos(p_d r_2)\cos(p_1 r_2)dr_2, \\ &= \frac{A(\eta-\eta_b)}{2CD\left[(\eta-\eta_b)^2+p_1^2\right]}G(-2\eta_b, D, p_1, p_d) \\ &\quad - \frac{Ap_1}{2CD\left[(\eta-\eta_b)^2+p_1^2\right]}H(-2\eta_b, D, p_1, p_d). \end{aligned} \tag{E-10a}$$

$$I_1(a12) = \int_0^\infty \frac{A}{CD} e^{-(\eta+\eta_b)r_2} \sin(Dr_2)\cos(p_d r_2) \frac{p_1}{2\left[(\eta-\eta_b)^2 + p_1^2\right]} dr_2$$

$$= \frac{Ap_1}{2CD\left[(\eta-\eta_b)^2 + p_1^2\right]} \int_0^\infty e^{-(\eta+\eta_b)r_2} \sin(Dr_2)\cos(p_d r_2) dr_2 \qquad \text{(E-10b)}$$

$$= \frac{Ap_1}{2CD\left[(\eta-\eta_b)^2 + p_1^2\right]} F(-(\eta-\eta_b), D, p_d).$$

$$I_1(a13) = \int_0^\infty \frac{A}{CD} e^{-(\eta+\eta_b)r_2} \sin(Dr_2)\cos(p_d r_2)$$

$$\cdot \frac{e^{(\eta-\eta_b)r_2}\left[(\eta-\eta_b)\sin(p_2 r_2) - p_2\cos(p_2 r_2)\right]}{2\left[(\eta-\eta_b)^2 + p_2^2\right]} dr_2,$$

$$= \frac{A(\eta-\eta_b)}{2CD\left[(\eta-\eta_b)^2 + p_2^2\right]} \int_0^\infty e^{-2\eta_b r_2} \sin(Dr_2)\cos(p_d r_2)\sin(p_2 r_2) dr_2 \qquad \text{(E-10c)}$$

$$- \frac{Ap_2}{2CD\left[(\eta-\eta_b)^2 + p_2^2\right]} \int_0^\infty e^{-2\eta_b r_2} \sin(Dr_2)\cos(p_d r_2)\cos(p_2 r_2) dr_2,$$

$$= \frac{A(\eta-\eta_b)}{2CD\left[(\eta-\eta_b)^2 + p_2^2\right]} G(-2\eta_b, D, p_2, p_d)$$

$$- \frac{Ap_2}{2CD\left[(\eta-\eta_b)^2 + p_2^2\right]} H(-2\eta_b, D, p_2, p_d),$$

and

$$I_1(a14) = \int_0^\infty \frac{A}{CD} e^{-(\eta+\eta_b)r_2} \sin(Dr_2)\cos(p_d r_2) \frac{p_2}{2\left[(\eta-\eta_b)^2 + p_2^2\right]} dr_2$$

$$= \frac{Ap_2}{2CD\left[(\eta-\eta_b)^2 + p_2^2\right]} \int_0^\infty e^{-(\eta+\eta_b)r_2} \sin(Dr_2)\cos(p_d r_2) dr_2 \qquad \text{(F-10d)}$$

$$= \frac{Ap_2}{2CD\left[(\eta-\eta_b)^2 + p_2^2\right]} F(-(\eta+\eta_b), D, p_d).$$

Next let's find $I_1(A2)$.

$$I_1(a2) = \int_0^\infty \frac{A}{CD} e^{-(\eta+\eta_b)r_2} \sin(Dr_2)\sin(p_d r_2) \cdot \left[\int_0^{r_2} e^{(\eta-\eta_b)r_1} \sin(Cr_1)\sin(p_d r_1) dr_1 \right] dr_2. \tag{E-11}$$

Substituting Eq. (E-4a) into Eq. (E-11) yields

$$\begin{aligned}
I_1(a2) = &\int_0^\infty \frac{A}{CD} e^{-(\eta+\eta_b)r_2} \sin(Dr_2)\sin(p_d r_2) \frac{e^{(\eta-\eta_b)r_2}\left[p_1 \sin(p_1 r_2) + (\eta-\eta_b)\cos(p_1 r_2)\right]}{2\left[(\eta-\eta_b)^2 + p_1^2\right]} dr_2 \\
&- \int_0^\infty \frac{A}{CD} e^{-(\eta+\eta_b)r_2} \sin(Dr_2)\sin(p_d r_2) \frac{\eta-\eta_b}{2\left[(\eta-\eta_b)^2 + p_1^2\right]} dr_2 \\
&- \int_0^\infty \frac{A}{CD} e^{-(\eta+\eta_b)r_2} \sin(Dr_2)\sin(p_d r_2) \frac{e^{(\eta-\eta_b)r_2}\left[p_2 \sin(p_2 r_2) + (\eta-\eta_b)\cos(p_2 r_2)\right]}{2\left[(\eta-\eta_b)^2 + p_2^2\right]} dr_2 \\
&+ \int_0^\infty \frac{A}{CD} e^{-(\eta+\eta_b)r_2} \sin(Dr_2)\sin(p_d r_2) \frac{\eta-\eta_b}{2\left[(\eta-\eta_b)^2 + p_2^2\right]} dr_2, \\
&= I_1(a21) + I_1(a22) + I_1(a23) + I_1(a24).
\end{aligned}$$

$$\begin{aligned}
I_1(a21) = &\frac{Ap_1}{2CD\left[(\eta-\eta_b)^2 + p_1^2\right]} \int_0^\infty e^{-2\eta_b r_2} \sin(Dr_2)\sin(p_d r_2)\sin(p_1 r_2) dr_2 \\
&+ \frac{A(\eta-\eta_b)}{2CD\left[(\eta-\eta_b)^2 + p_1^2\right]} \int_0^\infty e^{-2\eta_b r_2} \sin(Dr_2)\sin(p_d r_2)\cos(p_1 r_2) dr_2, \\
= &\frac{Ap_1}{2CD\left[(\eta-\eta_b)^2 + p_1^2\right]} J(-2\eta_b, D, p_d, p_1) \\
&+ \frac{A(\eta-\eta_b)}{2CD\left[(\eta-\eta_b)^2 + p_1^2\right]} G(-2\eta_b, D, p_d, p_1).
\end{aligned} \tag{E-12a}$$

$$\begin{aligned}
I_1(a22) &= -\int_0^\infty \frac{A}{CD} e^{-(\eta+\eta_b)r_2} \sin(Dr_2)\sin(p_d r_2) \frac{\eta-\eta_b}{2\left[(\eta-\eta_b)^2 + p_1^2\right]} dr_2 \\
&= -\frac{A(\eta-\eta_b)}{2CD\left[(\eta-\eta_b)^2 + p_1^2\right]} \int_0^\infty e^{-(\eta+\eta_b)r_2} \sin(Dr_2)\sin(p_d r_2) dr_2, \\
&= -\frac{A(\eta-\eta_b)}{2CD\left[(\eta-\eta_b)^2 + p_1^2\right]} E(-(\eta+\eta_b), D, p_d).
\end{aligned} \tag{E-12b}$$

$$I_1(a23) = -\frac{Ap_2}{2CD\left[(\eta-\eta_b)^2+p_2^2\right]}\int_0^\infty e^{-2\eta_b r_2}\sin(Dr_2)\sin(p_d r_2)\sin(p_2 r_2)dr_2$$

$$-\frac{A(\eta-\eta_b)}{2CD\left[(\eta-\eta_b)^2+p_2^2\right]}\int_0^\infty e^{-2\eta_b r_2}\sin(Dr_2)\sin(p_d r_2)\cos(p_2 r_2)dr_2, \qquad \text{(E-12c)}$$

$$= -\frac{Ap_2}{2CD\left[(\eta-\eta_b)^2+p_2^2\right]}J(-2\eta_b, D, p_d, p_2)$$

$$-\frac{A(\eta-\eta_b)}{2CD\left[(\eta-\eta_b)^2+p_2^2\right]}G(-2\eta_b, D, p_d, p_2).$$

$$I_1(a24) = \int_0^\infty \frac{A}{CD}e^{-(\eta+\eta_b)r_2}\sin(Dr_2)\sin(p_d r_2)\frac{\eta-\eta_b}{2\left[(\eta-\eta_b)^2+p_2^2\right]}dr_2$$

$$= \frac{A(\eta-\eta_b)}{2CD\left[(\eta-\eta_b)^2+p_2^2\right]}\int_0^\infty e^{-(\eta+\eta_b)r_2}\sin(Dr_2)\sin(p_d r_2)dr_2 \qquad \text{(E-12d)}$$

$$= \frac{A(\eta-\eta_b)}{2CD\left[(\eta-\eta_b)^2+p_2^2\right]}E(-(\eta+\eta_b), D, p_d).$$

Now we find $I_1(a)$. Let's find $I_1(b)$.

$$I_1(b) = \int_0^\infty\int_0^{r_2}\frac{B}{CD}e^{-\eta_b r_1}e^{-\eta_b r_2}e^{-\eta(r_2-r_1)}\sin(Cr_1)\sin(Dr_2)\sin(p_d(r_2-r_1))dr_1 dr_2.$$

Consider $\sin(p_d(r_2-r_1)) = \sin(p_d r_2)\cos(p_d r_1) - \cos(p_d r_2)\sin(p_d r_1)$, then

$$I_1(b) = \int_0^\infty\int_0^{r_2}\frac{B}{CD}e^{-\eta_b r_1}e^{-\eta_b r_2}e^{-\eta(r_2-r_1)}\sin(Cr_1)\sin(Dr_2)\sin(p_d r_2)\cos(p_d r_1)dr_1 dr_2$$

$$-\int_0^\infty\int_0^{r_2}\frac{B}{CD}e^{-\eta_b r_1}e^{-\eta_b r_2}e^{-\eta(r_2-r_1)}\sin(Cr_1)\sin(Dr_2)\cos(p_d r_2)\sin(p_d r_1)dr_1 dr_2,$$

$$= \int_0^\infty \frac{B}{CD}e^{-(\eta+\eta_b)r_2}\sin(Dr_2)\sin(p_d r_2)\left[\int_0^{r_2}e^{(\eta-\eta_b)r_1}\sin(Cr_1)\cos(p_d r_1)dr_1\right]dr_2 \qquad \text{(E-13)}$$

$$-\int_0^\infty \frac{B}{CD}e^{-(\eta+\eta_b)r_2}\sin(Dr_2)\cos(p_d r_2)\left[\int_0^{r_2}e^{(\eta-\eta_b)r_1}\sin(Cr_1)\sin(p_d r_1)dr_1\right]dr_2,$$

$$= I_1(b1) - I_1(b2).$$

First let's compute $I_1(b1)$. Using Eq. (9a) yields

$$I_1(b1) = \int_0^\infty \frac{B}{CD} e^{-(\eta+\eta_b)r_2} \sin(Dr_2)\sin(p_d r_2)$$
$$\cdot \frac{e^{(\eta-\eta_b)r_2}\left[(\eta-\eta_b)\sin(p_1 r_2) - p_1\cos(p_1 r_2)\right]}{2\left[(\eta-\eta_b)^2 + p_1^2\right]} dr_2$$
$$+ \int_0^\infty \frac{B}{CD} e^{-(\eta+\eta_b)r_2} \sin(Dr_2)\sin(p_d r_2) \frac{p_1}{2\left[(\eta-\eta_b)^2 + p_1^2\right]} dr_2$$
$$+ \int_0^\infty \frac{B}{CD} e^{-(\eta+\eta_b)r_2} \sin(Dr_2)\sin(p_d r_2) \tag{E-14}$$
$$\cdot \frac{e^{(\eta-\eta_b)r_2}\left[(\eta-\eta_b)\sin(p_2 r_2) - p_2\cos(p_2 r_2)\right]}{2\left[(\eta-\eta_b)^2 + p_2^2\right]} dr_2$$
$$+ \int_0^\infty \frac{B}{CD} e^{-(\eta+\eta_b)r_2} \sin(Dr_2)\sin(p_d r_2) \frac{p_2}{2\left[(\eta-\eta_b)^2 + p_2^2\right]} dr_2,$$
$$= I_1(b11) + I_1(b12) + I_1(b13) + I_1(b14).$$

$$I_1(b11) = \int_0^\infty \frac{B}{CD} e^{-(\eta+\eta_b)r_2} \sin(Dr_2)\sin(p_d r_2)$$
$$\frac{e^{(\eta-\eta_b)r_2}\left[(\eta-\eta_b)\sin(p_1 r_2) - p_1\cos(p_1 r_2)\right]}{2\left[(\eta-\eta_b)^2 + p_1^2\right]} dr_2,$$
$$= \frac{B(\eta-\eta_b)}{2CD\left[(\eta-\eta_b)^2 + p_1^2\right]} \int_0^\infty e^{-2\eta_b r_2} \sin(Dr_2)\sin(p_d r_2)\sin(p_1 r_2) dr_2 \tag{E-15a}$$
$$- \frac{Bp_1}{2CD\left[(\eta-\eta_b)^2 + p_1^2\right]} \int_0^\infty e^{-2\eta_b r_2} \sin(Dr_2)\sin(p_d r_2)\cos(p_1 r_2) dr_2,$$
$$= \frac{B(\eta-\eta_b)}{2CD\left[(\eta-\eta_b)^2 + p_1^2\right]} J(-2\eta_b, D, p_d, p_1)$$
$$- \frac{Bp_1}{2CD\left[(\eta-\eta_b)^2 + p_1^2\right]} G(-2\eta_b, D, p_d, p_1).$$

$$I_1(b12) = \int_0^\infty \frac{B}{CD} e^{-(\eta+\eta_b)r_2} \sin(Dr_2)\sin(p_d r_2) \frac{p_1}{2\left[(\eta-\eta_b)^2 + p_1^2\right]} dr_2,$$
$$= \frac{Bp_1}{2CD\left[(\eta-\eta_b)^2 + p_1^2\right]} \int_0^\infty e^{-(\eta+\eta_b)r_2} \sin(Dr_2)\sin(p_d r_2) dr_2, \tag{F-15b}$$
$$= \frac{Bp_1}{2CD\left[(\eta-\eta_b)^2 + p_1^2\right]} E\left(-(\eta-\eta_b), D, p_d\right).$$

$$I_1(b13) = \int_0^\infty \frac{B}{CD} e^{-(\eta+\eta_b)r_2} \sin(Dr_2)\sin(p_d r_2)$$
$$\cdot \frac{e^{(\eta-\eta_b)r_2}\left[(\eta-\eta_b)\sin(p_2 r_2) - p_2\cos(p_2 r_2)\right]}{2\left[(\eta-\eta_b)^2 + p_2^2\right]} dr_2,$$
$$= \frac{B(\eta-\eta_b)}{2CD\left[(\eta-\eta_b)^2 + p_2^2\right]} \int_0^\infty e^{-2\eta_b r_2} \sin(Dr_2)\sin(p_d r_2)\sin(p_2 r_2) dr_2$$
$$- \frac{Bp_2}{2CD\left[(\eta-\eta_b)^2 + p_2^2\right]} \int_0^\infty e^{-2\eta_b r_2} \sin(Dr_2)\sin(p_d r_2)\cos(p_2 r_2) dr_2, \tag{E-15c}$$
$$= \frac{B(\eta-\eta_b)}{2CD\left[(\eta-\eta_b)^2 + p_2^2\right]} J(-2\eta_b, D, p_d, p_2)$$
$$- \frac{Bp_2}{2CD\left[(\eta-\eta_b)^2 + p_2^2\right]} G(-2\eta_b, D, p_d, p_2).$$

$$I_1(b14) = \int_0^\infty \frac{B}{CD} e^{-(\eta+\eta_b)r_2} \sin(Dr_2)\sin(p_d r_2) \frac{p_2}{2\left[(\eta-\eta_b)^2 + p_2^2\right]} dr_2,$$
$$= \frac{Bp_2}{2CD\left[(\eta-\eta_b)^2 + p_2^2\right]} \int_0^\infty e^{-(\eta+\eta_b)r_2} \sin(Dr_2)\sin(p_d r_2) dr_2, \tag{E-15d}$$
$$= \frac{Bp_2}{2CD\left[(\eta-\eta_b)^2 + p_2^2\right]} E(-(\eta+\eta_b), D, p_d).$$

Next let's find $I_1(B2)$.

$$I_1(b2) = \int_0^\infty \frac{B}{CD} e^{-(\eta+\eta_b)r_2} \sin(Dr_2)\cos(p_d r_2)$$
$$\cdot\left[\int_0^{r_2} e^{(\eta-\eta_b)r_1} \sin(Cr_1)\sin(p_d r_1)dr_1\right]dr_2,$$
$$= \int_0^\infty \frac{B}{CD} e^{-(\eta+\eta_b)r_2} \sin(Dr_2)\cos(p_d r_2)$$
$$\cdot\frac{e^{(\eta-\eta_b)r_2}\left[p_1 \sin(p_1 r_2) + (\eta-\eta_b)\cos(p_1 r_2)\right]}{2\left[(\eta-\eta_b)^2 + p_1^2\right]}dr_2$$
$$-\int_0^\infty \frac{B}{CD} e^{-(\eta+\eta_b)r_2} \sin(Dr_2)\cos(p_d r_2)\frac{\eta-\eta_b}{2\left[(\eta-\eta_b)^2 + p_1^2\right]}dr_2$$
$$-\int_0^\infty \frac{B}{CD} e^{-(\eta+\eta_b)r_2} \sin(Dr_2)\cos(p_d r_2)$$
$$\cdot\frac{e^{(\eta-\eta_b)r_2}\left[p_2 \sin(p_2 r_2) + (\eta-\eta_b)\cos(p_2 r_2)\right]}{2\left[(\eta-\eta_b)^2 + p_2^2\right]}dr_2$$
$$+\int_0^\infty \frac{B}{CD} e^{-(\eta+\eta_b)r_2} \sin(Dr_2)\cos(p_d r_2)\frac{\eta-\eta_b}{2\left[(\eta-\eta_b)^2 + p_2^2\right]}dr_2,$$
$$= I_1(b21) - I_1(b22) - I_1(b23) + I_1(b24).$$

$$I_1(b21) = \int_0^\infty \frac{B}{CD} e^{-(\eta+\eta_b)r_2} \sin(Dr_2)\cos(p_d r_2)$$
$$\cdot\frac{e^{(\eta-\eta_b)r_2}\left[p_1 \sin(p_1 r_2) + (\eta-\eta_b)\cos(p_1 r_2)\right]}{2\left[(\eta-\eta_b)^2 + p_1^2\right]}dr_2,$$
$$= \frac{Bp_1}{2CD\left[(\eta-\eta_b)^2 + p_1^2\right]}\int_0^\infty e^{-2\eta_b} \sin(Dr_2)\cos(p_d r_2)\sin(p_1 r_2)dr_2$$
$$+\frac{B(\eta+\eta_b)}{2CD\left[(\eta-\eta_b)^2 + p_1^2\right]}\int_0^\infty e^{-2\eta_b} \sin(Dr_2)\cos(p_d r_2)\cos(p_1 r_2)dr_2, \tag{E-16a}$$
$$= \frac{Bp_1}{2CD\left[(\eta-\eta_b)^2 + p_1^2\right]}G(-2\eta_b, D, p_1, p_d)$$
$$+\frac{B(\eta+\eta_b)}{2CD\left[(\eta-\eta_b)^2 + p_1^2\right]}H(-2\eta_b, D, p_1, p_d).$$

$$
\begin{aligned}
I_1(b22) &= \int_0^\infty \frac{B}{CD} e^{-(\eta+\eta_b)r_2} \sin(Dr_2)\cos\left(p_d r_2\right) \frac{\eta-\eta_b}{2\left[(\eta-\eta_b)^2+p_1^2\right]} dr_2, \\
&= \frac{B(\eta-\eta_b)}{2CD\left[(\eta-\eta_b)^2+p_1^2\right]} \int_0^\infty e^{-(\eta+\eta_b)r_2} \sin(Dr_2)\cos\left(p_d r_2\right) dr_2, \\
&= \frac{B(\eta-\eta_b)}{2CD\left[(\eta-\eta_b)^2+p_1^2\right]} F\left(-\left(\eta+\eta_b\right), D, p_d\right).
\end{aligned}
\tag{E-16b}
$$

$$
\begin{aligned}
I_1(b23) &= \int_0^\infty \frac{B}{CD} e^{-(\eta+\eta_b)r_2} \sin(Dr_2)\cos\left(p_d r_2\right) \\
&\quad \cdot \frac{e^{(\eta-\eta_b)r_2}\left[p_2 \sin(p_2 r_2) + \left(\eta-\eta_b\right)\cos(p_2 r_2)\right]}{2\left[(\eta-\eta_b)^2+p_2^2\right]} dr_2, \\
&= \frac{Bp_2}{2\left[(\eta-\eta_b)^2+p_2^2\right]} \int_0^\infty e^{-(\eta+\eta_b)r_2} \sin(Dr_2)\cos\left(p_d r_2\right)\sin(p_2 r_2) dr_2 \\
&\quad + \frac{B\left(\eta-\eta_b\right)}{2\left[(\eta-\eta_b)^2+p_2^2\right]} \int_0^\infty e^{-(\eta+\eta_b)r_2} \sin(Dr_2)\cos\left(p_d r_2\right)\cos(p_2 r_2) dr_2, \\
&= \frac{Bp_2}{2CD\left[(\eta-\eta_b)^2+p_2^2\right]} G\left(-\left(\eta+\eta_b\right), D, p_2, p_d\right) \\
&\quad + \frac{B\left(\eta-\eta_b\right)}{2CD\left[(\eta-\eta_b)^2+p_2^2\right]} H\left(-\left(\eta+\eta_b\right), D, p_2, p_d\right).
\end{aligned}
\tag{E-16c}
$$

$$
\begin{aligned}
I_1(b24) &= \int_0^\infty \frac{B}{CD} e^{-(\eta+\eta_b)r_2} \sin(Dr_2)\cos\left(p_d r_2\right) \frac{\eta-\eta_b}{2\left[(\eta-\eta_b)^2+p_2^2\right]} dr_2, \\
&= \frac{B(\eta-\eta_b)}{2CD\left[(\eta-\eta_b)^2+p_2^2\right]} \int_0^\infty e^{-(\eta+\eta_b)r_2} \sin(Dr_2)\cos\left(p_d r_2\right) dr_2, \\
&= \frac{B(\eta-\eta_b)}{2CD\left[(\eta-\eta_b)^2+p_2^2\right]} F\left(-\left(\eta+\eta_b\right), D, p_d\right).
\end{aligned}
\tag{E-16d}
$$

Denote

$\left(\eta-\eta_b\right)^2 + p_1^2 = p_3$ and $\left(\eta-\eta_b\right)^2 + p_1^2 = p_4$; then, using Eq. (E-10) and Eq. (E-12) yields

$$
I_1(a11) = \frac{A(\eta-\eta_b)}{2CDp_3} G(-2\eta_b, D, p_1, p_d) - \frac{Ap_1}{2CDp_3} H(-2\eta_b, D, p_1, p_d), \tag{E-17a}
$$

$$
I_1(a12) = \frac{Ap_1}{2CDp_3} F(-\left(\eta-\eta_b\right), D, p_d), \tag{E-17b}
$$

$$I_1(a13)=\frac{A(\eta-\eta_b)}{2CDp_4}G(-2\eta_b,D,p_2,p_d)-\frac{Ap_2}{2CDp_4}H(-2\eta_b,D,p_2,p_d), \quad \text{(E-17c)}$$

$$I_1(a14)=\frac{Ap_2}{2CDp_4}F(-(\eta+\eta_b),D,p_d). \quad \text{(E-17d)}$$

$$I_1(a21)=\frac{Ap_1}{2CDp_3}J(-2\eta_b,D,p_d,p_1)+\frac{A(\eta-\eta_b)}{2CDp_3}G(-2\eta_b,D,p_d,p_1), \quad \text{(E-17e)}$$

$$I_1(a22)=-\frac{A(\eta-\eta_b)}{2CDp_3}E(-(\eta+\eta_b),D,p_d), \quad \text{(E-17f)}$$

$$I_1(a23)=-\frac{Ap_2}{2CDp_4}J(-2\eta_b,D,p_d,p_2)-\frac{A(\eta-\eta_b)}{2CDp_4}G(-2\eta_b,D,p_d,p_2), \quad \text{(E-17g)}$$

$$I_1(a24)=\frac{A(\eta-\eta_b)}{2CDp_4}E(-(\eta+\eta_b),D,p_d). \quad \text{(E-17h)}$$

Using Eq. (E-15) and (E-16) yields

$$I_1(b11)=\frac{B(\eta-\eta_b)}{2CDp_3}J(-2\eta_b,D,p_d,p_1)-\frac{Bp_1}{2CDp_3}G(-2\eta_b,D,p_d,p_1), \quad \text{(E-17i)}$$

$$I_1(b12)=\frac{Bp_1}{2CDp_3}E(-(\eta-\eta_b),D,p_d), \quad \text{(E-17j)}$$

$$I_1(b13)=\frac{B(\eta-\eta_b)}{2CDp_4}J(-2\eta_b,D,p_d,p_2)-\frac{Bp_2}{2CDp_4}G(-2\eta_b,D,p_d,p_2), \quad \text{(E-17k)}$$

$$I_1(b14)=\frac{Bp_2}{2CDp_4}E(-(\eta+\eta_b),D,p_d). \quad \text{(E-17l)}$$

$$I_1(b21)=\frac{Bp_1}{2CDp_3}G(-2\eta_b,D,p_1,p_d)+\frac{B(\eta+\eta_b)}{2CDp_3}H(-2\eta_b,D,p_1,p_d), \quad \text{(E-17m)}$$

$$I_1(b22)=\frac{B(\eta-\eta_b)}{2CDp_3}F(-(\eta+\eta_b),D,p_d), \quad \text{(E-17n)}$$

$$I_1(b23)=\frac{Bp_2}{2CDp_4}G(-(\eta+\eta_b),D,p_2,p_d)+\frac{B(\eta-\eta_b)}{2CDp_4}H(-(\eta+\eta_b),D,p_2,p_d)$$

(E-17o)

$$I_1(b24)=\frac{B(\eta-\eta_b)}{2CDp_4}F\left(-(\eta+\eta_b),D,p_d\right), \tag{E-17p}$$

where

$$A=\frac{\pi\,S_0\left(4\eta^2+p^2\right)}{2\eta},$$

$$B=\frac{\pi S_0}{2},$$

$$C=p_{dbmn},$$

$$D=p_{dbij},$$

$$\eta=\frac{c}{2m},$$

$$\eta_b=\frac{c_1}{2I_0},$$

$$p_d=\sqrt{p^2-\eta^2},$$

$$p^2=\frac{k}{m},$$

$$p_1=C-p_d,$$

$$p_2=C+p_d,$$

$$p_3=(\eta-\eta_b)^2+(C-p_d)^2$$

$$p_4=(\eta-\eta_b)^2+(C+p_d)^2.$$

Then,

$$\begin{aligned}I_1&=I_1(a)+I_1(b),\\&=I_1(a11)+I_1(a12)+I_1(a13)+I_1(a14)\\&\quad+I_1(a21)+I_1(a22)+I_1(a23)+I_1(a24)\\&\quad+I_1(b11)+I_1(b12)+I_1(b13)+I_1(b14)\\&\quad+I_1(b21)-I_1(b22)-I_1(b23)+I_1(b24).\end{aligned} \tag{E-18}$$

Next let's find the integral I_2 when $r_1 > r_2$.

$$I_2 = \int_0^{\infty}\int_0^{r_1} \frac{A}{CD} e^{-\eta_b r_1} e^{-\eta_b r_2} e^{-\eta(r_1 - r_{21})} \sin(Cr_1)\sin(Dr_2)\cos(p_d(r_1 - r_2))dr_1 dr_2$$

$$+ \int_0^{\infty}\int_0^{r_2} \frac{B}{CD} e^{-\eta_b r_1} e^{-\eta_b r_2} e^{-\eta(r_1 - r_2)} \sin(Cr_1)\sin(Dr_2)\sin(p_d(r_1 - r_2))dr_1 dr_2, \tag{E-19}$$

$$= I_2(a) + I_2(b).$$

Consider $\cos(p_d(r_1 - r_2)) = \cos(p_d r_2)\cos(p_d r_1) + \sin(p_d r_2)\sin(p_d r_1)$, then

$$I_2(a) = \int_0^{\infty}\int_0^{r_1} \frac{A}{CD} e^{-\eta_b r_1} e^{-\eta_b r_2} e^{-\eta(r_1 - r_2)} \sin(Cr_1)\sin(Dr_2)\cos(p_d r_2)\cos(p_d r_1)dr_1 dr_2$$

$$+ \int_0^{\infty}\int_0^{r_1} \frac{A}{CD} e^{-\eta_b r_1} e^{-\eta_b r_2} e^{-\eta(r_1 - r_2)} \sin(Cr_1)\sin(Dr_2)\sin(p_d r_2)\sin(p_d r_1)dr_1 dr_2,$$

$$= \int_0^{\infty} \frac{A}{CD} e^{-(\eta+\eta_b)r_1} \sin(Cr_1)\cos(p_d r_1)\left[\int_0^{r_1} e^{(\eta-\eta_b)r_2} \sin(Dr_2)\cos(p_d r_2)dr_2\right]dr_1 \tag{E-20}$$

$$+ \int_0^{\infty} \frac{A}{CD} e^{-(\eta+\eta_b)r_1} \sin(Cr_1)\sin(p_d r_1)\left[\int_0^{r_1} e^{(\eta-\eta_b)r_2} \sin(Dr_2)\sin(p_d r_2)dr_1\right]dr_2,$$

$$= I_1(a|C \leftrightarrow D),$$

where

$I_1(a|C \leftrightarrow D)$ means $I_2(a)$ has the same equation with $I_1(a)$ but with C and D exchanging position.

Similarly, we have

$$I_2(b) = I_1(b|C \leftrightarrow D)$$

APPENDIX F

DERIVATION OF INTERFACIAL STRESS DUE TO THERMAL LOAD

Figure F.1 illustrates a multilayer board.

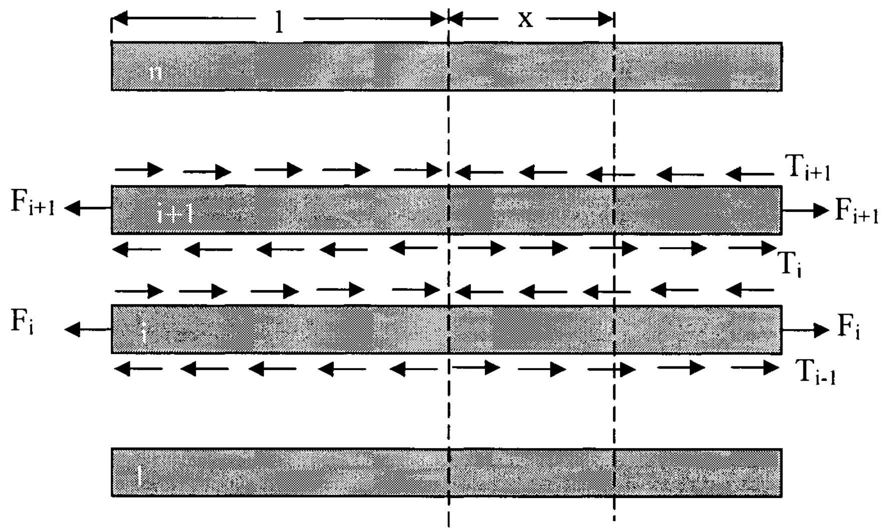

Fig F.1 Illustration of a multilayer board.

Considering each layer is thin and rigid, the radius of curvature is much larger than the thickness of the layer, we can assume that the radius of curvature of each layer is the same. The radius of curvature of the board is given by [162, p. 31]

$$\rho = \frac{D_i}{(1+\upsilon_i)M_i} = \frac{E_i h_i^3}{12(1-\upsilon_i)M_i},$$

where

ρ = radius of curvature,

D_i = flexural rigidity, $D_i = \dfrac{E_i h_i^3}{12(1-\upsilon_i^2)}$,

ν_i = Possion's ratio,

M_i = bending moment of i^{th} layer,

and

h_i = thickness of i^{th} layer,

or

$$M_i = \frac{E_i h_i^3}{12(1-\nu_i)\rho} = \frac{f_i(E_i, h_i, \nu_i)}{\rho}, \tag{F-1}$$

where

$$f_i(E_i, h_i, \nu_i) = \frac{E_i h_i^3}{12(1-\nu_i)}.$$

The equilibrium of total forces and moments yield [162, p. 31]

$$\sum_{i=1}^{m} F_i = 0, \tag{F-2}$$

and

$$\sum_{i=1}^{m} M_i - \sum_{j=1}^{m} F_j (\sum_{k=1}^{j} h_k - \frac{h_j}{2}) = 0. \tag{F-3}$$

The last equation is obtained based on the strain compatibility condition; i.e., the strain in each layer should be the same. This equation consists of three parts, the thermal expansion part, the part due to the elongation from the fore applied and the bending part.

$$\alpha_i \Delta T_i + \frac{F_i(1-\nu_i)}{E_i h_i} - \frac{h_i}{2\rho} = \alpha_{i+1} \Delta T_{i+1} + \frac{F_{i+1}(1-\nu_{i+1})}{E_{i+1} h_{i+1}} + \frac{h_{i+1}}{2\rho}.$$

Denoting $g_i(E_i, h_i, \nu_i) = \frac{1-\nu_i}{E_i h_i}$ and rearranging above equation yields

$$g_i F_i - g_{i+1} F_{i+1} - \frac{h_i + h_{i+1}}{2\rho} = \alpha_{i+1} \Delta T_{i+1} - \alpha_i \Delta T_i.$$

Summarizing this equation from 1 to j-1 yields,

$$g_1 F_1 - g_j F_j - \frac{2\sum_{i=1}^{j} h_i - (h_1 + h_j)}{2\rho} = \alpha_j \Delta T_j - \alpha_1 \Delta T_1,$$

or

$$F_j = \frac{1}{g_j} \left(g_1 F_1 - \frac{2\sum_{i=1}^{j} h_i - (h_1 + h_j)}{2\rho} - \left(\alpha_j \Delta T_j - \alpha_1 \Delta T_1\right) \right). \tag{F-4}$$

Denote $a_j = \sum_{i=1}^{j} h_i - \frac{h_1 + h_j}{2}$, $b_j = \alpha_j \Delta T_j - \alpha_1 \Delta T_1$ and considering $\sum_{j=1}^{m} F_j = 0$, we have

$$g_1 F_1 \sum_{j=1}^{m} \frac{1}{g_j} - \frac{1}{\rho} \sum_{j=1}^{m} \frac{a_j}{g_j} - \sum_{j=1}^{m} \frac{b_j}{g_j} = 0 .$$

Solving this equation yields

$$g_1 F_1 = \frac{1}{\rho} \frac{\sum_{j=1}^{m} a_j / g_j}{\sum_{j=1}^{m} 1/g_j} + \frac{\sum_{j=1}^{m} b_j / g_j}{\sum_{j=1}^{m} 1/g_j} .$$

Denote $c = \frac{\sum_{j=1}^{m} a_j / g_j}{\sum_{j=1}^{m} 1/g_j}$, $d = \frac{\sum_{j=1}^{m} b_j / g_j}{\sum_{j=1}^{m} 1/g_j}$ and plug the above equation into (F-4) yields

$$F_j = \frac{1}{g_j} \left(\frac{c}{\rho} + d - \frac{a_j}{\rho} - b_j \right) = \frac{1}{\rho} \left(\frac{c - a_j}{g_j} \right) + \frac{d - b_j}{g_j} . \tag{F-5}$$

Substituting equations (F-4) and (F-5) into (F-3) yields

$$\frac{1}{\rho} \sum_{i=1}^{m} f_i - \sum_{j=1}^{m} \left[\frac{1}{\rho} \left(\frac{c - a_j}{g_j} \right) + \frac{d - b_j}{g_j} \right] \left[\sum_{k=1}^{j} h_k - \frac{h_j}{2} \right] = 0 ,$$

or

$$\frac{1}{\rho} = \frac{\left(\sum_{j=1}^{m} \left(\frac{d - b_j}{g_j} \right) \right) \cdot \left(\sum_{k=1}^{j} h_k - \frac{h_j}{2} \right)}{\left[\sum_{i=1}^{m} f_i - \left(\sum_{j=1}^{m} \left(\frac{c - a_j}{g_j} \right) \right) \cdot \left(\sum_{k=1}^{j} h_k - \frac{h_j}{2} \right) \right]} .$$

Substitute this value into (F-5), and find the force

$$F_j = \frac{\left(\sum_{j=1}^{m} \left(\frac{d - b_j}{g_j} \right) \right) \cdot \left(\sum_{k=1}^{j} h_k - \frac{h_j}{2} \right)}{\left[\sum_{i=1}^{m} f_i - \left(\sum_{j=1}^{m} \left(\frac{c - a_j}{g_j} \right) \right) \cdot \left(\sum_{k=1}^{j} h_k - \frac{h_j}{2} \right) \right]} \left(\frac{c - a_j}{g_j} \right) + \frac{d - b_j}{g_j} .$$

The corresponding stresses in the j^{th} layer is given by

$$\sigma_j = \frac{F_j}{h_j}.$$

Then the shearing force acting in the i^{th} interface; i.e., in the interface between the i^{th} and $(i+1)^{th}$ layers, is [163, p.146]

$$T_i = \sum_{j=i}^{m} F_j .$$

Then, the distributed stresses in the i^{th} interface can be computed as follows:

The shear stress

$$\tau_i = -kT_i \frac{\sinh(kx)}{\cosh(kl)}, \tag{F-6}$$

and the peeling stress

$$p_i = -\frac{1}{2}k^2 T_i \frac{\cosh(kx)}{\cosh(kl)} \sum_{j=i+1}^{m} h_j , \tag{F-7}$$

where k is computed from

$$k^2 = \frac{3}{4} \frac{\sum_{i=1}^{m} g_i}{\sum_{i=1}^{m} h_i^2 g_i}.$$

The maximum values of these interfacial stresses occur at the edge of the board; therefore [163, p. 146]

$$\tau_{i\max} = -kT_i \tanh(kl), \tag{F-8}$$

and

$$p_{i\max} = -\frac{1}{2}k^2 T_i \sum_{j=i+1}^{m} h_j . \tag{F-9}$$

If there are only two layers, then it can be shown that the shear stress and the peeling stress are given by

$$\tau_{\max} = \frac{\Delta\alpha\Delta T}{\sqrt{\lambda\kappa}} \tanh(ka), \tag{F-10}$$

and

$$p_{\max} = \frac{\mu}{\kappa}\Delta\alpha\Delta T, \tag{F-11}$$

where

$$\lambda = \frac{1}{12}\left(\frac{h_1^2}{D_1} + \frac{h_2^2}{D_2} + \frac{3(h_1+h_2)^2}{D_1+D_2}\right),$$

$D_i = \dfrac{E_i h_i^2}{12(1-v_i^2)}$, i = 1, 2, the flexural rigidities of layer 1 and 2, respectively,

a = half length of plate,

h_i = thickness of layer 1 and 2, respectively, i = 1, 2,

$$\kappa = \frac{2(1+v_1)}{3E_1}h_1 + \frac{2(1+v_2)}{3E_2}h_2,$$

and

$$\mu = \frac{h_2 D_1 - h_1 D_2}{2(D_1 + D_2)}.$$

APPENDIX G

SOLUTION OF SYSTEM OF PDE GIVEN IN EQS. (4-1), (4-2) AND (4-3)

G.1 Solution to PDE given in Eq. (4-3)

First we rewrite Eq. (4-3) as follows and denote $\frac{k_i}{c\rho} = \omega_i$, i = x, y, z. Then,

$$\omega_x \frac{\partial^2 \theta^{(j)}}{\partial x^2} + \omega_y \frac{\partial^2 \theta^{(j)}}{\partial y^2} + \omega_z \frac{\partial^2 \theta^{(j)}}{\partial z^2} + \frac{1}{c\rho} Q^{(j)} = \frac{\partial \theta^{(j)}}{\partial t}. \tag{G-1}$$

Use the eigenfunction expansion and let

$$\theta^{(j)} = \sum_{m=0}^{\infty}\sum_{n=0}^{\infty}\sum_{l=0}^{\infty} a_{mnl}(t) \cdot \phi_m(x) \cdot \varphi_n(y) \cdot \psi_l(z), \tag{G-2}$$

and

$$Q^{(j)} = \sum_{m=0}^{\infty}\sum_{n=0}^{\infty}\sum_{l=0}^{\infty} b_{mnl}(t) \cdot \phi_m(x) \cdot \varphi_n(y) \cdot \psi_l(z), \tag{G-3}$$

where

a_{mnl}, b_{mnl} = time dependent coefficients,

and

$\phi_m(x), \varphi_n(y), \psi_l(z)$ = eigenfunctions of variables x, y and z, respectively.

Based on the boundary conditions given in Eq. (4-3b), we can get

$$\begin{aligned}
&\phi_m(x) = \cos\left(\frac{\alpha_m}{\sqrt{\omega_x}} x\right) = \cos\left(\frac{m\pi}{a} x\right), \quad \alpha_m = \frac{m\pi\sqrt{\omega_x}}{a}, \quad m = 0,\ldots,\infty, \\
&\varphi_n(y) = \cos\left(\frac{\beta_n}{\sqrt{\omega_y}} y\right) = \cos\left(\frac{n\pi}{b} y\right), \quad \beta_n = \frac{n\pi\sqrt{\omega_y}}{b}, n = 0,\ldots,\infty, \\
&\psi_l(z) = \frac{k_z \cdot \gamma_l}{\sqrt{\omega_z} h_1} \cos\left(\frac{\gamma_l}{\sqrt{\omega_z}} z\right) + \sin\left(\frac{\gamma_l}{\sqrt{\omega_z}} z\right), \qquad l = 0,\ldots,\infty,
\end{aligned} \tag{G-4}$$

where γ_l is computed using the following equation:

$$\tan\left(\frac{\gamma_l}{\sqrt{\omega_z}} h\right) = \frac{k_z^2 \gamma_l^2 - h_1 h_2 \omega_z}{k_z \gamma_l \sqrt{\omega_z}(h_1 + h_2)}.$$

Substituting Eqs. (G-2) and (G-3) into Eq. (G-1), and realizing that

$\omega_x \dfrac{d^2\phi_m}{dx^2} = -\alpha_m^2\phi_m$, $\omega_y \dfrac{d^2\varphi_n}{dy^2} = -\beta_n^2\varphi_n$, and $\omega_z \dfrac{d^2\psi_l}{dz^2} = -\gamma_l^2\psi_l$, yields

$$\frac{da_{mnl}(t)}{dt} + \left(\alpha_m^2 + \beta_n^2 + \gamma_l^2\right)a_{mnl}(t) = \frac{1}{c\rho} b_{mnl}(t). \tag{G-5}$$

Solving Eq. (G-5) yields

$$a_{mnl}(t) = c' e^{-(\alpha_m^2+\beta_n^2+\gamma_l^2)t} + \frac{1}{c\rho}\int_0^t d\tau \cdot e^{-(\alpha_m^2+\beta_n^2+\gamma_l^2)(t-\tau)} \cdot b_{mnl}(\tau). \tag{G-6}$$

Substituting Eq. (G-6) into Eq. (G-2) yields the temperature change due to source j, or

$$\begin{aligned} \theta^{(j)} &= \sum_{m=0}^{\infty}\sum_{n=0}^{\infty}\sum_{l=0}^{\infty} c' \cdot \phi_m(x) \cdot \varphi_n(y) \cdot \psi_l(z) \cdot e^{-(\alpha_m^2+\beta_n^2+\gamma_l^2)t} + \\ & \sum_{m=0}^{\infty}\sum_{n=0}^{\infty}\sum_{l=0}^{\infty} \frac{1}{c\rho}\int_0^t d\tau \cdot e^{-(\alpha_m^2+\beta_n^2+\gamma_l^2)(t-\tau)} \cdot b_{mnl}(t)\, \phi_m(x) \cdot \varphi_n(y) \cdot \psi_l(z). \end{aligned} \tag{G-7}$$

The coefficients of c' are zero since the initial condition given in Eq. (4-3c) is zero. The coefficient of b_{mnl} can be found through Eq. (G-3) by

$$\begin{aligned} b_{mnl}(t) &= \frac{1}{N_{mnl}} \int_0^a\int_0^b\int_0^h Q^{(j)} \cdot \phi_m(x') \cdot \varphi_n(y') \cdot \psi_l(z') dx'dy'dz', \\ &= \frac{1}{N_{mnl}} \int_0^a\int_0^b\int_0^h Q^{(j)} \delta(x - x_n) \cdot \delta(y - y_n) \cdot \delta(z - 0) \cdot \\ &\quad \phi_m(x') \cdot \varphi_n(y') \cdot \psi_l(z') dx'dy'dz', \end{aligned}$$

or

$$b_{mnl}(t) = \frac{Q^{(j)}}{N_{mnl}} \cos\left(\frac{m\pi}{a}x_j\right)\cos\left(\frac{n\pi}{b}y_j\right)\left(\frac{k_z\gamma_l}{\sqrt{\omega_z}h_1}\right),$$

where N_{mnl} is given by

$$N_{mnl} = \int_0^a\int_0^b\int_0^h \phi_m^2(x') \cdot \varphi_n^2(y') \cdot \psi_l^2(z') dx'dy'dz',$$

or

$$N_{mnl} = \frac{ab}{4}\left[\frac{k_z^2 \cdot \gamma_l^2 \cdot h + k_z h_1 \omega_z + h \cdot h_1^2 \omega_z}{2h_1^2 \omega_z} + \left(\frac{k_z^2 \gamma_l^2 - h_1^2 \omega_z}{4h_1^2 \sqrt{\omega_z}\gamma_l}\right) \cdot \right.$$
$$\left. \sin\left(\frac{2\gamma_l h}{\sqrt{\omega_z}}\right) - \frac{k_z}{2h_1}\cos\left(\frac{2\gamma_l h}{\sqrt{\omega_z}}\right)\right].$$

Then, the temperature change distribution of the board due to the j[th] source is given by (realizing $b_{mnl}(t)$ is time independent)

$$\theta^{(j)} = \sum_{m=0}^{\infty}\sum_{n=0}^{\infty}\sum_{l=0}^{\infty}\frac{1}{c\rho}\int_0^t d\tau \cdot e^{-(\alpha_m^2+\beta_n^2+\gamma_l^2)(t-\tau)} \cdot b_{mnl}(t)\,\phi_m(x)\cdot\varphi_n(y)\cdot\psi_l(z),$$
$$= \sum_{m=0}^{\infty}\sum_{n=0}^{\infty}\sum_{l=0}^{\infty}\frac{b_{mnl}}{c\rho(\alpha_m^2+\beta_n^2+\gamma_l^2)}(1-e^{-(\alpha_m^2+\beta_n^2+\gamma_l^2)t})\,\phi_m(x)\cdot\varphi_n(y)\cdot\psi_l(z),$$

or

$$\theta^{(j)} = \sum_{m=0}^{\infty}\sum_{n=0}^{\infty}\sum_{l=0}^{\infty}\frac{b_{mnl}}{c\rho(\alpha_m^2+\beta_n^2+\gamma_l^2)}\phi_m(x)\cdot\varphi_n(y)\cdot\psi_l(z) -$$
$$\sum_{m=0}^{\infty}\sum_{n=0}^{\infty}\sum_{l=0}^{\infty}\frac{e^{-(\alpha_m^2+\beta_n^2+\gamma_l^2)t}\cdot b_{mnl}}{c\rho(\alpha_m^2+\beta_n^2+\gamma_l^2)}\phi_m(x)\cdot\varphi_n(y)\cdot\psi_l(z). \tag{G-8}$$

As we discussed in the temperature profile, we are more concerned about temperature at steady state. Then, Eq. (G-8) becomes

$$\theta^{(j)} = \sum_{m=1}^{\infty}\sum_{n=1}^{\infty}\sum_{l=1}^{\infty}\frac{Q^{(j)}\cos\left(\frac{m\pi}{a}x_j\right)\cos\left(\frac{n\pi}{b}y_j\right)\left(\frac{k_z\gamma_l}{\sqrt{\omega_z}h_1}\right)}{c\rho(\alpha_m^2+\beta_n^2+\gamma_l^2)N_{mnl}}\cdot\phi_m(x)\cdot\varphi_n(y)\cdot\psi_l(z). \tag{G-9}$$

Then, at any location, the temperature change will be

$$\theta(x,y,z) = \sum_{j=1}^{N}\theta^{(j)},$$

or

$$\theta(x,y,z) = \sum_{m=1}^{\infty}\sum_{n=1}^{\infty}\sum_{l=1}^{\infty}\frac{\left(\frac{k_z\gamma_l}{\sqrt{\omega_z}h_1}\right)\phi_m(x)\cdot\varphi_n(y)\cdot\psi_l(z)}{c\rho(\alpha_m^2+\beta_n^2+\gamma_l^2)N_{mnl}}\cdot$$
$$\sum_{j=1}^{N}Q^{(j)}\cos\left(\frac{m\pi}{a}x_j\right)\cos\left(\frac{n\pi}{b}y_j\right). \tag{G-10}$$

If we use the Green function to express the temperature change, Eq. (G-7) becomes

$$\theta^{(j)} = \frac{1}{c\rho}\int_0^a\int_0^b\int_0^h\int_0^t d\tau \cdot G(x,y,z,t|x',y',z',\tau)\cdot Q^{(j)}(x',y',z',\tau)dx'dy'dz',$$

where the Green function is given by

$$G(x,y,z,t|x',y',z',\tau) = \sum_{m=1}^{\infty}\sum_{n=1}^{\infty}\sum_{l=1}^{\infty}\frac{1}{N_{mnl}}\phi_m(x)\phi_m(x')\varphi_n(y)\varphi_n(y')$$
$$\cdot\psi_l(z)\psi(z')e^{-\left(\alpha_m^2+\beta_n^2+\gamma_l^2\right)(t-\tau)}.$$

G.2 Solution to PDE given in Equations (4-1) and (4-2)

We use the eigenfunction expansion method. The solution is

$$\theta_i^{(j)} = \sum_{m=1}^{\infty}\sum_{n=1}^{\infty}\sum_{l=1}^{\infty}a_{mnl}(t)\cdot\phi_{im}^{(j)}(x)\cdot\varphi_{in}^{(j)}(y)\cdot\psi_{il}^{(j)}(z) \text{ in } z_i \le z \le z_{i+1}, i=1,\dots,d. \quad \text{(G-11)}$$

The heat source can be expanded as

$$\frac{\kappa_i}{k_i}Q_i^{(j)} = \sum_{m=1}^{\infty}\sum_{n=1}^{\infty}\sum_{l=1}^{\infty}b_{mnl}(t)\cdot\phi_{im}^{(j)}(x)\cdot\varphi_{in}^{(j)}(y)\cdot\psi_{il}^{(j)}(z), \quad \text{(G-12)}$$

where $a_{mnl}(t)$ and $b_{mnl}(t)$ are functions which are to be determined. $\phi_{im}^{(j)}(x)$, $\varphi_{in}^{(j)}(y)$, and $\psi_{il}^{(j)}(z)$ can be found through the following eigenvalue problems:

$$\kappa_i\cdot\frac{d^2\phi_{im}^{(j)}(x)}{dx^2}+\alpha_m^2\phi_{im}^{(j)}(x)=0, \text{ with BC: } x=0,a \quad \frac{d\phi_{im}^{(j)}(x)}{dx}=0, \quad \text{(G-13a)}$$

$$\kappa_i\frac{d^2\varphi_{in}^{(j)}(y)}{dy^2}+\beta_n^2\,\varphi_{in}^{(j)}(y)=0, \text{ with BC: } y=0,b \quad \frac{d\varphi_{in}^{(j)}(y)}{dy}=0, \quad \text{(G-13b)}$$

$$\kappa_i\cdot\frac{d^2\psi_{il}^{(j)}}{dz^2}+\gamma_l^2\psi_{il}^{(j)}(z)=0, \quad \text{(G-13c)}$$

with the following BCs

$$k_1\frac{d\psi_1^{(j)}(z=0)}{dz}=h_1\psi_1^{(j)}(z=0), \text{ for the top surface of the top layer}$$

$$\psi_i^{(j)}(z_{i+1}) = \psi_{i+1}^{(j)}(z_{i+1}),$$
$$k_i \left.\frac{d\psi_i^{(j)}}{dz}\right|_{z_{i+1}} = k_{i+1} \left.\frac{d\psi_{i+1}^{(j)}}{dz}\right|_{z_{i+1}}, \qquad \text{for i = 1,..,d-1} \qquad \text{(G-13d)}$$

and

$$k_d \frac{d\psi_d^{(j)}(z = z_d)}{dz} = -h_d \psi_d^{(j)}(z = z_d)$$, for the bottom surface of the dth layer.

Solving Equations (G-13a), (G-13b), and (G-13c) yields

$$\phi_{im}^{(j)}(x) = \cos\left(\frac{\alpha_m}{\sqrt{\kappa_i}} x\right) = \cos\left(\frac{m\pi}{a} x\right),\ \alpha_m = \frac{m\pi\sqrt{\kappa_i}}{a}, m = 1,\ldots,\infty.$$

Similarly,

$$\varphi_{in}^{(j)}(y) = \cos\left(\frac{\beta_n}{\sqrt{\kappa_i}} y\right) = \cos\left(\frac{n\pi}{b} y\right),\ \beta_n = \frac{n\pi\sqrt{\kappa_i}}{b}, n = 1,\ldots,\infty, \text{ and}$$

$$\psi_{il}^{(j)}(z) = A_{il}^{(j)} \cos\left(\frac{\gamma_l}{\sqrt{\kappa_i}} \cdot z\right) + B_{il}^{(j)} \sin\left(\frac{\gamma_l}{\sqrt{\kappa_i}} \cdot z\right). \qquad \text{(G-14)}$$

It should be noted that there are "d" solutions in the form of Eq. (G-14), which means that there are "2d" unknown coefficients, $A_{il}^{(j)}, B_{il}^{(j)}$ for i = 1, …, d. We need to find them through the boundary conditions given in Eq. (G-13d).

Applying the boundary conditions given in Eq. (G-13d) into Eq. (G-14) yields "2d" linear homogenous equations. One is at the top surface of first layer, one is at the bottom surface of dth layer, and 2d-2 are at the interface between layers.

At the outer boundary z_0

$$B_{1l}^{(j)} = \frac{h_1\sqrt{\kappa_1}}{\gamma_l k_1} A_{1l}^{(j)}. \qquad \text{(G-15a)}$$

At the interface, the following relations for the coefficients $A_{il}^{(j)}$, $B_{il}^{(j)}$ with $A_{(i+1)l}^{(j)}, B_{(i+1)l}^{(j)}$

$$\begin{pmatrix} A_{il}^{(j)} \\ B_{il}^{(j)} \end{pmatrix} = \begin{bmatrix} a_{11}(i) & a_{12}(i) \\ a_{21}(i) & a_{22}(i) \end{bmatrix} \begin{pmatrix} A_{(i+1)l}^{(j)} \\ B_{(i+1)l}^{(j)} \end{pmatrix}, \qquad \text{(G-15b)}$$

where

$$a_{11}(i) = \cos\left(\frac{\gamma_l}{\sqrt{\kappa_i}} z_{i+1}\right)\cos\left(\frac{\gamma_l}{\sqrt{\kappa_{i+1}}} z_{i+1}\right) + \frac{k_{i+1}}{k_i}\sqrt{\frac{\kappa_i}{\kappa_{i+1}}}\sin\left(\frac{\gamma_l}{\sqrt{\kappa_i}} z_{i+1}\right)\sin\left(\frac{\gamma_l}{\sqrt{\kappa_{i+1}}} z_{+1i}\right),$$

$$a_{12}(i) = \cos\left(\frac{\gamma_l}{\sqrt{\kappa_i}} z_{i+1}\right)\sin\left(\frac{\gamma_l}{\sqrt{\kappa_{i+1}}} z_{i+1}\right) - \frac{k_{i+1}}{k_i}\sqrt{\frac{\kappa_i}{\kappa_{i+1}}}\sin\left(\frac{\gamma_l}{\sqrt{\kappa_i}} z_{i+1}\right)\cos\left(\frac{\gamma_l}{\sqrt{\kappa_{i+1}}} z_{i+1}\right),$$

$$a_{21}(i) = \sin\left(\frac{\gamma_l}{\sqrt{\kappa_i}} z_{i+1}\right)\cos\left(\frac{\gamma_l}{\sqrt{\kappa_{i+1}}} z_{i+1}\right) - \frac{k_{i+1}}{k_i}\sqrt{\frac{\kappa_i}{\kappa_{i+1}}}\cos\left(\frac{\gamma_l}{\sqrt{\kappa_i}} z_{i+1}\right)\sin\left(\frac{\gamma_l}{\sqrt{\kappa_{i+1}}} z_{i+1}\right),$$

and

$$a_{22}(i) = \sin\left(\frac{\gamma_l}{\sqrt{\kappa_i}} z_{i+1}\right)\sin\left(\frac{\gamma_l}{\sqrt{\kappa_{i+1}}} z_{i+1}\right) + \frac{k_{i+1}}{k_i}\sqrt{\frac{\kappa_i}{\kappa_{i+1}}}\cos\left(\frac{\gamma_l}{\sqrt{\kappa_i}} z_{i+1}\right)\cos\left(\frac{\gamma_l}{\sqrt{\kappa_{i+1}}} z_{i+1}\right).$$

At the bottom surface of the d$^{\text{th}}$ layer

$$B_{dl}^{(j)} = \frac{k_d \cdot \frac{\gamma_l}{\sqrt{\kappa_d}}\sin\left(\frac{\gamma_l}{\sqrt{\kappa_d}} z_d\right) - h_d\cos\left(\frac{\gamma_l}{\sqrt{\kappa_d}} z_d\right)}{k_z\frac{\gamma_l}{\sqrt{\kappa_d}}\cos\left(\frac{\gamma_l}{\sqrt{\kappa_d}} z_d\right) + h_d\sin\left(\frac{\gamma_l}{\sqrt{\kappa_d}} z_d\right)} A_{dl}^{(j)}\ . \tag{G-15c}$$

When "2d" linear homogenous equations given in (G-15) are solved, the 2d unknown coefficients will be found in terms of one of them, say $A_{1l}^{(j)}$, since they are homogenous equations. Then, the resulting eigenfunctions $\psi_{il}^{(j)}(z)$ will all include the unknown coefficient $A_{1l}^{(j)}$, it will cancel out in the final solution.

In Eq. (G-15), there are unknown eigenvalues γ_l. Thus, an additional relation is needed to determine these eigenvalues. Ozisik, M. N. [166, pp.278-279] proposed the following method. The relationship to be used to calculate the eigenvalues is obtained from the condition that if the homogenous equations given in Eq. (G-15) should have nontrivial solution the determinant of the coefficients should be zero. If now we rewrite the above homogenous equations in the matrix form, we have

$$\begin{bmatrix} \frac{h_1\sqrt{\kappa_1}}{\gamma_l k_1} & -1 & 0 & 0 & \cdots & 0 & 0 & 0 & 0 & \cdots & 0 & 0 & 0 & 0 \\ -1 & 0 & a_{11}(1) & a_{12}(1) & \cdots & 0 & 0 & 0 & 0 & \cdots & 0 & 0 & 0 & 0 \\ 0 & -1 & a_{21}(1) & a_{22}(1) & \cdots & 0 & 0 & 0 & 0 & \cdots & 0 & 0 & 0 & 0 \\ 0 & 0 & 0 & 0 & \cdots & 0 & 0 & 0 & 0 & \cdots & 0 & 0 & 0 & 0 \\ 0 & 0 & 0 & 0 & \cdots & 0 & 0 & 0 & 0 & \cdots & 0 & 0 & 0 & 0 \\ \vdots & \vdots & \vdots & \vdots & \cdots & \vdots & \vdots & \vdots & \vdots & \cdots & \vdots & \vdots & \vdots & \vdots \\ 0 & 0 & 0 & 0 & \cdots & -1 & 0 & a_{11}(i) & a_{12}(i) & \cdots & 0 & 0 & 0 & 0 \\ 0 & 0 & 0 & 0 & \cdots & 0 & -1 & a_{21}(i) & a_{22}(i) & \cdots & 0 & 0 & 0 & 0 \\ \vdots & \vdots & \vdots & \vdots & \cdots & \vdots & \vdots & \vdots & \vdots & \cdots & \vdots & \vdots & \vdots & \vdots \\ 0 & 0 & 0 & 0 & \cdots & 0 & 0 & 0 & 0 & \cdots & 0 & 0 & 0 & 0 \\ 0 & 0 & 0 & 0 & \cdots & 0 & 0 & 0 & 0 & \cdots & 0 & 0 & 0 & 0 \\ 0 & 0 & 0 & 0 & \cdots & 0 & 0 & 0 & 0 & \cdots & -1 & 0 & a_{11}(d-1) & a_{12}(d-1) \\ 0 & 0 & 0 & 0 & \cdots & 0 & 0 & 0 & 0 & \cdots & 0 & -1 & a_{21}(d-1) & a_{22}(d-1) \\ 0 & 0 & 0 & 0 & \cdots & 0 & 0 & 0 & 0 & \cdots & 0 & 0 & a_d & -1 \end{bmatrix} \begin{bmatrix} A_{1l}^{(j)} \\ B_{1l}^{(j)} \\ A_{2l}^{(j)} \\ B_{2l}^{(j)} \\ \vdots \\ A_{il}^{(j)} \\ B_{il}^{(j)} \\ A_{(i+1)l}^{(j)} \\ B_{(i+1)l}^{(j)} \\ \vdots \\ A_{(d-1)l}^{(j)} \\ B_{(d-1)l}^{(j)} \\ A_{dl}^{(j)} \\ B_{dl}^{(j)} \end{bmatrix} = [\bar{0}]$$

where

$$a_d = \frac{k_d \cdot \frac{\gamma_l}{\sqrt{\kappa_d}} \sin\left(\frac{\gamma_l}{\sqrt{\kappa_d}} z_d\right) - h_d \cos\left(\frac{\gamma_l}{\sqrt{\kappa_d}} z_d\right)}{k_z \frac{\gamma_l}{\sqrt{\kappa_d}} \cos\left(\frac{\gamma_l}{\sqrt{\kappa_d}} z_d\right) + h_d \sin\left(\frac{\gamma_l}{\sqrt{\kappa_d}} z_d\right)}.$$

Then, the following transcendental equation should be solved, and its positive roots give the enginvalues, $\gamma_1 < \gamma_2 < \cdots < \gamma_l < \cdots$

$$\begin{vmatrix}
\frac{h_1\sqrt{\kappa_1}}{\gamma_l k_1} & -1 & 0 & 0 & \cdots & 0 & 0 & 0 & 0 & \cdots & 0 & 0 & 0 & 0 \\
-1 & 0 & a_{11}(1) & a_{12}(1) & \cdots & 0 & 0 & 0 & 0 & \cdots & 0 & 0 & 0 & 0 \\
0 & -1 & a_{21}(1) & a_{22}(1) & \cdots & 0 & 0 & 0 & 0 & \cdots & 0 & 0 & 0 & 0 \\
0 & 0 & 0 & 0 & \cdots & 0 & 0 & 0 & 0 & \cdots & 0 & 0 & 0 & 0 \\
0 & 0 & 0 & 0 & \cdots & 0 & 0 & 0 & 0 & \cdots & 0 & 0 & 0 & 0 \\
\vdots & \vdots & \vdots & \vdots & \cdots & \vdots & \vdots & \vdots & \vdots & \cdots & \vdots & \vdots & \vdots & \vdots \\
0 & 0 & 0 & 0 & \cdots & -1 & 0 & a_{11}(i) & a_{12}(i) & \cdots & 0 & 0 & 0 & 0 \\
0 & 0 & 0 & 0 & \cdots & 0 & -1 & a_{21}(i) & a_{22}(i) & \cdots & 0 & 0 & 0 & 0 \\
\vdots & \vdots & \vdots & \vdots & \cdots & \vdots & \vdots & \vdots & \vdots & \cdots & \vdots & \vdots & \vdots & \vdots \\
0 & 0 & 0 & 0 & \cdots & 0 & 0 & 0 & 0 & \cdots & 0 & 0 & 0 & 0 \\
0 & 0 & 0 & 0 & \cdots & 0 & 0 & 0 & 0 & \cdots & 0 & 0 & 0 & 0 \\
0 & 0 & 0 & 0 & \cdots & 0 & 0 & 0 & 0 & \cdots & -1 & 0 & a_{11}(d-1) & a_{12}(d-1) \\
0 & 0 & 0 & 0 & \cdots & 0 & 0 & 0 & 0 & \cdots & 0 & -1 & a_{21}(d-1) & a_{22}(d-1) \\
0 & 0 & 0 & 0 & \cdots & 0 & 0 & 0 & 0 & \cdots & 0 & 0 & a_d & -1
\end{vmatrix} = 0$$

For each of these eigenvalues there is the corresponding values of $A_{il}^{(j)}, B_{il}^{(j)}$ and $\psi_{il}^{(j)}(z)$. After we find these eigenvalues, coefficients and eigenfuctions, we can use eigenfunction expansion to solve Eq. (4-1).

Substituting equations (G-11) and (G-12) into Eq. (4-1), and realizing that

$\kappa_i \cdot \dfrac{d^2\phi_{im}^{(j)}(x)}{dx^2} + \alpha_m^2 \phi_{im}^{(j)}(x) = 0$, $\kappa_i \dfrac{d^2\varphi_{in}^{(j)}(y)}{dy^2} + \beta_n^2\, \varphi_{in}^{(j)}(y) = 0$, and

$\kappa_i \cdot \dfrac{d^2\psi_{il}^{(j)}}{dz^2} + \gamma_l^2 \psi_{il}^{(j)}(z) = 0$, yields

$$\sum_{m=1}^{\infty}\sum_{n=1}^{\infty}\sum_{l=1}^{\infty}\left[\frac{da_{mnl}(t)}{dt} + \left(\alpha_m^2 + \beta_n^2 + \gamma_l^2\right)a_{mnl}(t) - b_{mnl}(t)\right]\phi_{im}^{(j)}\varphi_{in}^{(j)}\psi_{il}^{(j)} = 0\,. \tag{G-16}$$

From this equation, we obtain the following ODE for the function $a_{mnl}(t)$:

$$\frac{da_{mnl}(t)}{dt} + \left(\alpha_m^2 + \beta_n^2 + \gamma_l^2\right)a_{mnl}(t) = b_{mnl}(t)\,. \tag{G-17}$$

Solving Eq. (G-17) yields

$$a_{mnl}(t) = c' e^{-(\alpha_m^2+\beta_n^2+\gamma_l^2)t} + \int_0^t d\tau \cdot e^{-(\alpha_m^2+\beta_n^2+\gamma_l^2)(t-\tau)} \cdot b_{mnl}(\tau)\,. \tag{G-18}$$

Substituting Eq. (G-18) into (G-11) yields the temperature distribution of the i$^{\text{th}}$ layer of the board subjected to heat source "j", which is

$$\theta_i^{(j)} = \sum_{m=1}^{\infty}\sum_{n=1}^{\infty}\sum_{l=1}^{\infty} c' \cdot \phi_{im}^{(j)}(x)\cdot\varphi_{in}^{(j)}(y)\cdot\psi_{il}^{(j)}(z)\cdot e^{-(\alpha_m^2+\beta_n^2+\gamma_l^2)t} + \sum_{m=1}^{\infty}\sum_{n=1}^{\infty}\sum_{l=1}^{\infty}\int_0^t d\tau\cdot e^{-(\alpha_m^2+\beta_n^2+\gamma_l^2)(t-\tau)}\cdot b_{mnl}(t)\,\phi_{im}^{(j)}(x)\cdot\varphi_{in}^{(j)}(y)\cdot\psi_{il}^{(j)}(z). \tag{G-19}$$

In this equation, there are two unknowns; i.e., c' and $b_{mnl}(t)$. Since the initial condition in each layer is zero, c' will be zero. To find the coefficient of $b_{mnl}(t)$, we consider the following orthogonality property [166, p. 292]:

$$\sum_{i=1}^{d}\frac{k_i}{\kappa_i}\int_0^a\int_0^b\int_{z_i}^{z_{i+1}}\phi_{im}^{(j)}(x)\phi_{im'}^{(j)}(x)\varphi_{in}^{(j)}(y)\varphi_{in'}^{(j)}(y)\psi_{il}^{(j)}(z)\psi_{il'}^{(j)}(z)dx\,dy\,dz = \begin{cases}0 & \text{for } n\neq n',\\ N_{mnl} & \text{for } n=n'.\end{cases}$$

Applying this orthogonality property to Eq. (G-12) by multiplying both sides by $\frac{k_i}{\kappa_i}\phi_{im'}^{(j)}\varphi_{in'}^{(j)}\psi_{il'}^{(j)}$ and integrating with respect to x (from 0 to a), y (from 0 to b), and z from z_i to z_{i+1}, and summing up the equalities over all values of i, yields

$$\begin{aligned} b_{mnl}(t) &= \frac{\sum_{i=1}^{d}\int_0^a\int_0^b\int_{z_i}^{z_{i+1}} Q_i^{(j)}\phi_{im}^{(j)}(x)\varphi_{in}^{(j)}(y)\psi_{il}^{(j)}(z)dxdydx}{N_{mnl}},\\ &= \frac{\int_0^a\int_0^b\int_{z_1}^{z_2} Q_1^{(j)}\delta(x-x_j)\delta(y-y_j)\delta(z-0)\phi_{im}^{(j)}(x)\varphi_{in}^{(j)}(y)\psi_{il}^{(j)}(z)dxdydx}{N_{mnl}},\\ &= \frac{Q_1^{(j)}\sin\left(\frac{m\pi}{a}x_j\right)\sin\left(\frac{n\pi}{b}y_j\right)}{N_{mnl}}, \end{aligned} \tag{G-20}$$

where the norm N_{mnl} is given as

$$\begin{aligned} N_{mnl} &= \sum_{i=1}^{d}\frac{k_i}{\kappa_i}\int_0^a\int_0^b\int_{z_i}^{z_{i+1}}\phi_{im}^2(x')\cdot\varphi_{in}^2(y')\cdot\psi_{il}^2(z')dx'dy'dz' \\ &= \frac{4}{ab}\sum_{i=1}^{d}\frac{k_i}{\kappa_i}\int_{z_i}^{z_{i+1}}\psi_{il}^{2(j)}(z)dz. \end{aligned} \tag{G-21}$$

Then, the temperature distribution of the ith layer due to the jth heat source is given as

$$\theta_i^{(j)} = \sum_{m=1}^{\infty}\sum_{n=1}^{\infty}\sum_{l=1}^{\infty}\int_0^t d\tau \cdot e^{-(\alpha_m^2+\beta_n^2+\gamma_l^2)(t-\tau)} \cdot b_{mnl}(t)\, \phi_{im}^{(j)}(x)\cdot\varphi_{in}^{(j)}(y)\cdot\psi_{il}^{(j)}(z),$$

$$= \sum_{m=1}^{\infty}\sum_{n=1}^{\infty}\sum_{l=1}^{\infty}\frac{b_{mnl}}{(\alpha_m^2+\beta_n^2+\gamma_l^2)}(1-e^{-\omega(\alpha_m^2+\beta_n^2+\gamma_l^2)t})\, \phi_{im}^{(j)}(x)\cdot\varphi_{in}^{(j)}(y)\cdot\psi_{il}^{(j)}(z),$$

$$= \sum_{m=1}^{\infty}\sum_{n=1}^{\infty}\sum_{l=1}^{\infty}\frac{b_{mnl}}{(\alpha_m^2+\beta_n^2+\gamma_l^2)}\phi_{im}^{(j)}(x)\cdot\varphi_{in}^{(j)}(y)\cdot\psi_{il}^{(j)}(z) - \tag{G-22}$$

$$\sum_{m=1}^{\infty}\sum_{n=1}^{\infty}\sum_{l=1}^{\infty}\frac{b_{mnl}}{(\alpha_m^2+\beta_n^2+\gamma_l^2)}e^{-\omega(\alpha_m^2+\beta_n^2+\gamma_l^2)t})\, \phi_{im}^{(j)}(x)\cdot\varphi_{in}^{(j)}(y)\cdot\psi_{il}^{(j)}(z),$$

where $b_{mnl}(t)$ is given in Eq. (G-20).

Then, the temperature distribution of the ith layer due to all of the heat sources is given by

$$\theta_i(x,y,z,t) = \sum_{j=1}^{N}\sum_{m=1}^{\infty}\sum_{n=1}^{\infty}\sum_{l=1}^{\infty}\frac{b_{mnl}}{(\alpha_m^2+\beta_n^2+\gamma_l^2)}\phi_{im}^{(j)}(x)\cdot\varphi_{in}^{(j)}(y)\cdot\psi_{il}^{(j)}(z) -$$

$$\sum_{j=1}^{N}\sum_{m=1}^{\infty}\sum_{n=1}^{\infty}\sum_{l=1}^{\infty}\frac{b_{mnl}}{(\alpha_m^2+\beta_n^2+\gamma_l^2)}e^{-\omega(\alpha_m^2+\beta_n^2+\gamma_l^2)t})\, \phi_{im}^{(j)}(x)\cdot\varphi_{in}^{(j)}(y)\cdot\psi_{il}^{(j)}(z).$$

APPENDIX H

MATLAB CODES FOR EXAMPLE 6-1

H.1 Matlab code for solving the PDE.

```
clear all
close all
a=0.15;
b=0.06350;
h=0.001354;
x=0:0.011:a;
y=0:0.005:b;
z=0:-0.0001:-h;
T=zeros (13,13,13);
kz=0.2; h1=5; h2=5; wz=8.32e-8; wx=7.07e-6; wy=7.07e-6; ch=1300; rou=2850;
gamm=[0.76 0.391883 1.20136801100198 2.00563038000417 2.80917207999
3.6124745219 4.415668375099999 5.218803790999 6.021904155999 6.82498184865];
gamm(11:501) = 6.82498184865;
q=[0.2 0.2 0.4];
x1= [0.02 0.075 0.1 ];
y1= [0.03 0.03 0.03];
for iy=1:13
  for ix=1:13
    for iz=1:13
      Ts = 0;
      for i = 1:3
        for m=0:20
          for n=0:20
            for l=0:20
            Ai=q(1,i)*cos((m*pi/a)*x1(1,i))*cos((n*pi/b)*y1(1,i));
            F=kz*gamm(1,l+1)/(sqrt(wz)*h1);
            phixy=cos((m*pi/a).*x(ix))*cos((n*pi/b).*y(iy));
            %phiy=cos((n*pi/b).*y(iy));
            phiz=(kz*gamm(1,l+1)/(sqrt(wz)*h1))*cos(gamm(1,l+1).*z(iz)/sqrt(wz))+
            sin(gamm(1,l+1).*z(iz)/sqrt(wz));
            Nmnl=(a*b/4)*((kz^2*gamm(1,l+1)^2*h+kz*h1*wz+h*h1^2*wz)/(2*h1^
            2*wz)+(kz^2*gamm(1,l+1)^2-
            h1^2*wz)*sin(2*gamm(1,l+1).*h/sqrt(wz))/(4*h1^2*sqrt(wz)*gamm(1,l+
            1))-kz*cos(2*gamm(1,l+1).*h/sqrt(wz))/(2*h1));
            denor=ch*rou*((m*pi*sqrt(wx)/a)^2+(n*pi*sqrt(wy)/b)^2+
            gamm(1,l+1)^2);
            Ts=Ts+phixy*phiz*Ai*F/(Nmnl*denor);
            end
```

```
            end
          end
        end
        T(iy,ix,iz)=Ts;
      end
    end
end
[x,y,z]=meshgrid(0:0.011:0.132,0:0.005:0.06,0:-0.0001:-0.0012);
xslice = [0.01, 0.05, 0.08, 0.13]; yslice = 0.030; zslice = [0, -0.0010];
slice(x,y,z,T,xslice,yslice,zslice);
colormap hsv
```

H.2 Subroutine for computation of the integral

$$I = \int_0^\infty\int_0^\infty h_{mn}(r_1)\, h_{ij}(r_2)\, R_{\ddot{w}_1\ddot{w}_1}(r_2 - r_1)\, dr_1\, dr_2$$

```
I = A*(eta-etab)*[computeG(-2*etab,D,p1,pd)+computeG(-
   2*etab,C,p1,pd)]/(2*C*D*p3)-A*p1*[computeH(-2*etab,D,p1,pd)+computeH(-
   2*etab,C,p1,pd)]/(2*C*D*p3)+...
   A*p1*[computeF(-(eta+etab),D,pd)+computeF(-(eta+etab),C,pd)]/(2*C*D*p3)+...
   A*(eta-etab)*[computeG(-2*etab,D,p2,pd)+computeG(-
   2*etab,C,p2,pd)]/(2*C*D*p4)-A*p2*[computeH(-2*etab,D,p2,pd)+computeH(-
   2*etab,C,p2,pd)]/(2*C*D*p4)+...
   A*p2*[computeF(-(eta+etab),D,pd)+computeF(-(eta+etab),C,pd)]/(2*C*D*p4)+...
   A*p1*[computeJ(-2*etab,D,pd,p1)+computeJ(-
   2*etab,C,pd,p1)]/(2*C*D*p3)+A*(eta-etab)*[computeG(-
   2*etab,D,pd,p1)+computeG(-2*etab,C,pd,p1)]/(2*C*D*p3)-...
   A*(eta-etab)*[computeE(-(eta+etab),D,pd)+computeE(-
   (eta+etab),C,pd)]/(2*C*D*p3)-...
   A*p2*[computeJ(-2*etab,D,pd,p2)+computeJ(-2*etab,C,pd,p2)]/(2*C*D*p4)-
   A*(eta-etab)*[computeG(-2*etab,D,pd,p2)+computeG(-
   2*etab,C,pd,p2)]/(2*C*D*p4)+...
   A*(eta-etab)*[computeE(-(eta+etab),D,pd)+computeE(-
   (eta+etab),C,pd)]/(2*C*D*p4)+...
   B*(eta-etab)*[computeJ(-2*etab,D,pd,p1)+computeJ(-
   2*etab,C,pd,p1)]/(2*C*D*p3)-B*p1*[computeG(-2*etab,D,pd,p1)+computeG(-
   2*etab,C,pd,p1)]/(2*C*D*p3)+...
   B*p1*[computeE(-(eta+etab),D,pd)+computeE(-(eta+etab),C,pd)]/(2*C*D*p3)+...
   B*(eta-etab)*[computeJ(-2*etab,D,pd,p2)+computeJ(-
   2*etab,C,pd,p2)]/(2*C*D*p4)-B*p2*[computeG(-2*etab,D,pd,p2)+computeG(-
   2*etab,C,pd,p2)]/(2*C*D*p4)+...
   B*p2*[computeE(-(eta+etab),D,pd)+computeE(-(eta+etab),C,pd)]/(2*C*D*p4)+...
```

```
B*p1*[computeG(-2*etab,D,p1,pd)+computeG(-
2*etab,C,p1,pd)]/(2*C*D*p3)+B*(eta-etab)*[computeH(-
2*etab,D,p1,pd)+computeH(-2*etab,C,p1,pd)]/(2*C*D*p3)-...
B*(eta-etab)*[computeF(-(eta+etab),D,pd)+computeF(-
(eta+etab),C,pd)]/(2*C*D*p3)-...
B*p2*[computeG(-(eta+etab),D,p2,pd)+computeG(-
(eta+etab),C,p2,pd)]/(2*C*D*p4)-B*(eta-etab)*[computeH(-
(eta+etab),D,p2,pd)+computeH(-(eta+etab),C,p2,pd)]/(2*C*D*p4)+...
B*(eta-etab)*[computeF(-(eta+etab),D,pd)+computeF(-
(eta+etab),C,pd)]/(2*C*D*p4);
```

H.3 Matlab code for computation of the standard deviation of the shear stress of the board.

```
%compute standard deviation of stress-syz-board
clear all
z=[-677e-6 -641e-6 -539e-6 -503e-6 -203e-6 -51e-6 51e-6 203e-6 503e-6 539e-6
641e-6];
Q11=[138.95e9 3.08e9 138.95e9 3.08e9 219.78e9 3.08e9 219.78e9 3.08e9 138.95e9
 3.08e9 138.95e9];
Q12=[45.58e9 1.08e9 45.58e9 1.08e9 65.93e9 1.08e9 65.93e9 1.08e9 45.58e9 1.08e9
 45.58e9];
Q66=[46.69e9 10e9 46.69e9 10e9 76.92e9 10e9 76.92e9 10e9 46.69e9 10e9 46.69e9];
S0=20.6;                 %power spectral density
eta=2717.4;              %c/m
etab=1966.6;             %c/I0
p=3296.9;                %k/m
pd=sqrt(p^2-eta^2);      %equal to sqrt(p^2-eta^2)
A=pi*S0*(4*eta^2+p^2)/(2*eta);
B=pi*S0/2;
D11=8.732;
D12=2.841;
D22=8.732;
D66=4.301;
I0=3.89;
a= 0.15;                 %length of board
b=0.0635;                %width of the board
sigma2syz=0;
for m=1:2:41
  for n=1:21
    for i=1:2:41
      for j=1:21
      sigmn=1.249093918e10*m^3+2.444744431e9*m^2*n;
```

```
            sigij=1.249093918e10*i^3+2.444744431e9*i^2*j;
            C = (pi^2/(sqrt(I0)*b^2))*sqrt(D11*m^4*(b/a)^4+2*(D12+2*D66)*
                m^2*n^2*(b/a)^2+D22*n^4);
            D= (pi^2/(sqrt(I0)*b^2))*sqrt(D11*i^4*(b/a)^4+2*(D12+2*D66)*
                i^2*j^2*(b/a)^2+D22*j^4);
            p1=C-pd;
            p2=C+pd;
            p3=p1^2+(eta-etab)^2;
            p4=p2^2+(eta-etab)^2;
           sigma2syz=sigma2syz+sigmn*sigij*(1/(m*n*i*j))*(256/pi^4)*((-
                      1)^((m+i-2)/2))*I;
          end
        end
      end
      end
      sigmasyz=sqrt(sigma2syz)
```

H.4 Matlab code for computation of the standard deviation of the peeling stress of the board.

```
%compute standard deviation of stress-szz-board
clear all
z=[-677e-6 -641e-6 -539e-6 -503e-6 -203e-6 -51e-6 51e-6 203e-6 503e-6 539e-6 641e-6];
Q11=[138.95e9 3.08e9 138.95e9 3.08e9 219.78e9 3.08e9 219.78e9 3.08e9 138.95e9
3.08e9 138.95e9];
Q12=[45.58e9 1.08e9 45.58e9 1.08e9 65.93e9 1.08e9 65.93e9 1.08e9 45.58e9 1.08e9
45.58e9];
Q66=[46.69e9 10e9 46.69e9 10e9 76.92e9 10e9 76.92e9 10e9 46.69e9 10e9 46.69e9];
S0=20.6;                    %power spectral density
eta=2717.4;                 %c/m
etab=1966.6;                %c/I0
p=3296.9;                   %k/m
pd=sqrt(p^2-eta^2);         %equal to sqrt(p^2-eta^2)
A=pi*S0*(4*eta^2+p^2)/(2*eta);
B=pi*S0/2;
D11=8.732;
D12=2.841;
D22=8.732;
D66=4.301;
I0=3.89;
a= 0.15;                    %length of board
b=0.0635;                   %width of the board
sigma2szz=0;
for m=1:2:41
```

```
  for n=1:2:41
    for i=1:2:41
      for j=1:2:41
      sigmn=1358570.847*m^4+42301174.52*n^4+28415140.64*m^2*n*2;
      sigij=1358570.847*i^4+42301174.52*j^4+28415140.64*i^2*j*2;
      C = (pi^2/(sqrt(I0)*b^2))*sqrt(D11*m^4*(b/a)^4+
           2*(D12+2*D66)*m^2*n^2*(b/a)^2+D22*n^4);
      D= (pi^2/(sqrt(I0)*b^2))*sqrt(D11*i^4*(b/a)^4+
           2*(D12+2*D66)*i^2*j^2*(b/a)^2+D22*j^4);
      p1=C-pd;
      p2=C+pd;
      p3=p1^2+(eta-etab)^2;
      p4=p2^2+(eta-etab)^2;
     sigma2szz=sigma2szz+sigmn*sigij*(1/(m*n*i*j))*
               (256/pi^4)*((-1)^((m+n+i+j-4)/2))*I;
    end
  end
end
end
sigmaszz=sqrt(abs(sigma2szz))
```

H.5 Matlab code for computation of the correlation coefficient of two failure modes of the board.

H.5.1 Mean value of the product of the shear stress and max. deflection.

```
%compute mean value of stress-syz with w_max
clear all
z=[-677e-6 -641e-6 -539e-6 -503e-6 -203e-6 -51e-6 51e-6 203e-6 503e-6 539e-6 641e-6];
Q11=[138.95e9 3.08e9 138.95e9 3.08e9 219.78e9 3.08e9 219.78e9 3.08e9 138.95e9
3.08e9 138.95e9];
Q12=[45.58e9 1.08e9 45.58e9 1.08e9 65.93e9 1.08e9 65.93e9 1.08e9 45.58e9 1.08e9
45.58e9];
Q66=[46.69e9 10e9 46.69e9 10e9 76.92e9 10e9 76.92e9 10e9 46.69e9 10e9 46.69e9];
S0=20.6;                    %power spectral density
eta=2717.4;                 %c/m
etab=1966.6;                %c/I0
p=3296.9;                   %k/m
pd=sqrt(p^2-eta^2);         %equal to sqrt(p^2-eta^2)
A=pi*S0*(4*eta^2+p^2)/(2*eta);
B=pi*S0/2;
D11=8.732;
D12=2.841;
D22=8.732;
```

```
D66=4.301;
I0=3.89;
a= 0.15;                    %length of board
b=0.0635;                   %width of the board
sigma2=0;
for m=1:2:41
  for n=1:2:41
    for i=1:2:41
      for j=1:2:41
      sigmn=((z(1,11)^2-z(1,1)^2)/2)*((n*pi/b)^3*Q11(1,1)+
            (m^2*n*pi^3/(a^2*b))*(2*Q66(1,1)+Q12(1,1)))...
            +((z(1,11)^2-z(1,2)^2)/2)*((n*pi/b)^3*Q11(1,2)+
            (m^2*n*pi^3/(a^2*b))*(2*Q66(1,2)+Q12(1,2)))...
             +((z(1,11)^2-z(1,3)^2)/2)*((n*pi/b)^3*Q11(1,3)+
            (m^2*n*pi^3/(a^2*b))*(2*Q66(1,3)+Q12(1,3)))...
            +((z(1,11)^2-z(1,4)^2)/2)*((n*pi/b)^3*Q11(1,4)+
            (m^2*n*pi^3/(a^2*b))*(2*Q66(1,4)+Q12(1,4)))...
            +((z(1,11)^2-z(1,5)^2)/2)*((n*pi/b)^3*Q11(1,5)+
            (m^2*n*pi^3/(a^2*b))*(2*Q66(1,5)+Q12(1,5)))...
            +((z(1,11)^2-z(1,6)^2)/2)*((n*pi/b)^3*Q11(1,6)+
            (m^2*n*pi^3/(a^2*b))*(2*Q66(1,6)+Q12(1,6)))...
            +((z(1,11)^2-z(1,7)^2)/2)*((n*pi/b)^3*Q11(1,7)+
            (m^2*n*pi^3/(a^2*b))*(2*Q66(1,7)+Q12(1,7)))...
             +((z(1,11)^2-z(1,8)^2)/2)*((n*pi/b)^3*Q11(1,8)+
            (m^2*n*pi^3/(a^2*b))*(2*Q66(1,8)+Q12(1,8)))...
            +((z(1,11)^2-z(1,9)^2)/2)*((n*pi/b)^3*Q11(1,9)+
            (m^2*n*pi^3/(a^2*b))*(2*Q66(1,9)+Q12(1,9)))...
            +((z(1,11)^2-z(1,10)^2)/2)*((n*pi/b)^3*Q11(1,10)+
            (m^2*n*pi^3/(a^2*b))*(2*Q66(1,10)+Q12(1,10)))...
            +((z(1,11)^2-z(1,11)^2)/2)*((n*pi/b)^3*Q11(1,11)+
            (m^3*n*pi^3/(a^2*b))*(2*Q66(1,11)+Q12(1,11)));
      C = (pi^2/(sqrt(I0)*b^2))*sqrt(D11*m^4*(b/a)^4+2*(D12+2*D66)*
          m^2*n^2*(b/a)^2+D22*n^4);
      D= (pi^2/(sqrt(I0)*b^2))*sqrt(D11*i^4*(b/a)^4+2*(D12+2*D66)*
          i^2*j^2*(b/a)^2+D22*j^4);
      p1=C-pd;
      p2=C+pd;
      p3=p1^2+(eta-etab)^2;
      p4=p2^2+(eta-etab)^2;
      sigma2=sigma2-sigmn*(1/(m*n*i*j))*(256/pi^4)*((-1)^((m+n+i+j-4)/2))*I;
    end
  end
end
end
```

mean=sigma2

H.5.2 Mean value of the product of the shear stress and w^* .

```
%compute E(s_vir*w*)
clear all
z=[-677e-6 -641e-6 -539e-6 -503e-6 -203e-6 -51e-6 51e-6 203e-6 503e-6 539e-6 641e-6];
Q11=[138.95e6 3.08e6 138.95e6 3.08e6 219.78e6 3.08e6 219.78e6 3.08e6 138.95e6
3.08e6 138.95e6];
Q12=[45.58e6 1.08e6 45.58e6 1.08e6 65.93e6 1.08e6 65.93e6 1.08e6 45.58e6 1.08e6
45.58e6];
Q66=[46.69e6 10e6 46.69e6 10e6 76.92e6 10e6 76.92e6 10e6 46.69e6 10e9 46.69e6];
a= 0.15;                    %length of board
b=0.0635;                   %width of the board
S0=20.6;                     %power spectral density
eta=2717.4;                  %c/m
etab=1966.6;                 %c/I0
p=3296.9;                    %k/m
pd=sqrt(p^2-eta^2);           %equal to sqrt(p^2-eta^2)
D11=8.732;
D12=2.841;
D22=8.732;
D66=4.301;
I0=3.89;                    %
a= 0.15;                    %length of board
b=0.0635;                   %width of the board
A=0;
for m=1:2:551
  for n=1:2:551
    C = (pi^2/(sqrt(I0)*b^2))*sqrt(D11*m^4*(b/a)^4+
        2*(D12+2*D66)*m^2*n^2*(b/a)^2+D22*n^4);
    p1=C-pd;
    p2=C+pd;
    p3=p1^2+(eta+etab)^2;
    p4=p2^2+(eta+etab)^2;
    A1=(pi*S0*(etab+eta)/(2*C*pd))*(1/p3-1/p4);
    A2=(pi*S0/(4*C*pd))*((p1+eta*(etab+eta)/pd)/p3+(p2-eta*(etab+eta)/pd)/p4);
    sigmn=((z(1,11)^2-z(1,1)^2)/2)*((n*pi/b)^3*Q11(1,1)+
          (m^2*n*pi^3/(a^2*b))*(2*Q66(1,1)+Q12(1,1)))...
          +((z(1,11)^2-z(1,2)^2)/2)*((n*pi/b)^3*Q11(1,2)+
          (m^2*n*pi^3/(a^2*b))*(2*Q66(1,2)+Q12(1,2)))...
          +((z(1,11)^2-z(1,3)^2)/2)*((n*pi/b)^3*Q11(1,3)+
          (m^2*n*pi^3/(a^2*b))*(2*Q66(1,3)+Q12(1,3)))...
          +((z(1,11)^2-z(1,4)^2)/2)*((n*pi/b)^3*Q11(1,4)+
```

```
          (m^2*n*pi^3/(a^2*b))*(2*Q66(1,4)+Q12(1,4)))...
          +((z(1,11)^2-z(1,5)^2)/2)*((n*pi/b)^3*Q11(1,5)+
          (m^2*n*pi^3/(a^2*b))*(2*Q66(1,5)+Q12(1,5)))...
        +((z(1,11)^2-z(1,6)^2)/2)*((n*pi/b)^3*Q11(1,6)+
          (m^2*n*pi^3/(a^2*b))*(2*Q66(1,6)+Q12(1,6)))...
        +((z(1,11)^2-z(1,7)^2)/2)*((n*pi/b)^3*Q11(1,7)+
          (m^2*n*pi^3/(a^2*b))*(2*Q66(1,7)+Q12(1,7)))...
        +((z(1,11)^2-z(1,8)^2)/2)*((n*pi/b)^3*Q11(1,8)+
          (m^2*n*pi^3/(a^2*b))*(2*Q66(1,8)+Q12(1,8)))...
        +((z(1,11)^2-z(1,9)^2)/2)*((n*pi/b)^3*Q11(1,9)+
          (m^2*n*pi^3/(a^2*b))*(2*Q66(1,9)+Q12(1,9)))...
        +((z(1,11)^2-z(1,10)^2)/2)*((n*pi/b)^3*Q11(1,10)+
          (m^2*n*pi^3/(a^2*b))*(2*Q66(1,10)+Q12(1,10)))...
        +((z(1,11)^2-z(1,11)^2)/2)*((n*pi/b)^3*Q11(1,11)+
          (m^3*n*pi^3/(a^2*b))*(2*Q66(1,11)+Q12(1,11)));
      A=A+(1/(m*n))*(16/pi^2)*((-1)^((m-1)/2))*sigmn*(A1+A2);
  end
end
```

H.6 Matlab code for computation of the stress standard deviation of the leadless solder joint interconnect.

```
%compute standard deviation of leadless solder joint
clear all
z=[-0.001494 -0.00014];
Q11=[138.95e6];
Q12=[45.58e6];
Q66=[46.69e6];
S0=20.6;                    %power spectral density
eta=2717.4;                 %c/m
etab=1966.6;                %c/I0
p=3296.9;                   %k/m
pd=sqrt(p^2-eta^2);         %equal to sqrt(p^2-eta^2)
A=pi*S0*(4*eta^2+p^2)/(2*eta);
B=pi*S0/2;
D11=8.732;
D12=2.841;
D22=8.732;
D66=4.301;
I0=3.89;
a= 0.15;                    %length of board
b=0.0635;                   %width of the board
sigma2solder=0;
for m=1:2:17
```

```
  for n=1:15
    for i=1:2:17
      for j=1:15
      sigmn=(n*pi/b)^3*Q11(1,1)+(m*pi/a)^2*(n*pi/b)*(2*Q66(1,1)+Q12(1,1));
      sigij=(j*pi/b)^3*Q11(1,1)+(i*pi/a)^2*(j*pi/b)*(2*Q66(1,1)+Q12(1,1));
      C = (pi^2/(sqrt(I0)*b^2))*sqrt(D11*m^4*(b/a)^4+
           2*(D12+2*D66)*m^2*n^2*(b/a)^2+D22*n^4);
      D= (pi^2/(sqrt(I0)*b^2))*sqrt(D11*i^4*(b/a)^4+
           2*(D12+2*D66)*i^2*j^2*(b/a)^2+D22*j^4);
      p1=C-pd;
      p2=C+pd;
      p3=p1^2+(eta-etab)^2;
      p4=p2^2+(eta-etab)^2;
      sigma2solder=sigma2solder+(8192/(52^4*0.002^4*pi^6*4))*
                         (z(1,2)^2-z(1,1)^2)^2*sigmn*sigij*(1/(m*n*i*j))*
                         ((-1)^((m+i-2)/2))*I;
    end
  end
end
end
sigmasolder=sqrt(sigma2solder)
```

H.7 Matlab code for computation of the standard deviation of the stress in the leaded solder joint.

```
%compute standard deviation of leaded solder vib stress
clear all
z=[-677e-6 -641e-6 -539e-6 -503e-6 -203e-6 -51e-6 51e-6 203e-6 503e-6 539e-6 641e-6];
Q11=[138.95e9 3.08e9 138.95e9 3.08e9 219.78e9 3.08e9 219.78e9 3.08e9 138.95e9
3.08e9 138.95e9];
Q12=[45.58e9 1.08e9 45.58e9 1.08e9 65.93e9 1.08e9 65.93e9 1.08e9 45.58e9 1.08e9
45.58e9];
Q66=[46.69e9 10e9 46.69e9 10e9 76.92e9 10e9 76.92e9 10e9 46.69e9 10e9 46.69e9];
S0=20.6;                    %power spectral density
eta=2717.4;                 %c/m
etab=1966.6;                %c/I0
p=3296.9;                   %k/m
pd=sqrt(p^2-eta^2);         %equal to sqrt(p^2-eta^2)
A=pi*S0*(4*eta^2+p^2)/(2*eta);
B=pi*S0/2;
D11=8.732;
D12=2.841;
D22=8.732;
D66=4.301;
```

```
I0=3.89;                    %
a= 0.15;                    %length of board
b=0.0635; %width of the board
L_m=0.0013; %length of the module
Aw=3.2e-8; %lead wire area
Ew=138e9; %modulus of lead wire
Em=300e9; % modulus of the module
Lw=0.000208; % length of lead wire
Im=8.336e-17; %moment inertia of lead wire
sigma2leaded=0;
for m=1:2:31
   for n=1:2:31
      for i=1:2:31
         for j=1:2:31
         ss=((L_m)^3*52*Aw*Ew)/(3*Em*Im*Lw);
         sigmn=(1/(m*n))*((-1)^((m+n-2)/2)-(-1)^((n-1)/2)*sin(m*pi*(a-L_m)/(2*a)));
         sigij=(1/(i*j))*((-1)^((i+j-2)/2)-(-1)^((j-1)/2)*sin(i*pi*(a-L_m)/(2*a)));
         C = (pi^2/(sqrt(I0)*b^2))*sqrt(D11*m^4*(b/a)^4+
              2*(D12+2*D66)*m^2*n^2*(b/a)^2+D22*n^4);
         D= (pi^2/(sqrt(I0)*b^2))*sqrt(D11*i^4*(b/a)^4+
              2*(D12+2*D66)*i^2*j^2*(b/a)^2+D22*j^4);
         p1=C-pd;
         p2=C+pd;
         p3=p1^2+(eta-etab)^2;
         p4=p2^2+(eta-etab)^2;
         sigma2leaded=sigma2leaded+sigmn*sigij*
                        (256/(pi^4*52^2))*((-1)^((m+i-2)/2))*I*(Ew/Lw)*(1/(1+ss));
      end
   end
end
end
sigmalead=sqrt(sigma2leaded)
```

H.8. Matlab code for computation of the correlation coefficient of the two failure modes in PTH interconnect

```
%compute mean of product of vib stress in leadwire and szz force
clear all
z=[-677e-6 -641e-6 -539e-6 -503e-6 -203e-6 -51e-6 51e-6 203e-6 503e-6 539e-6 641e-6];
Q11=[138.95e9 3.08e9 138.95e9 3.08e9 219.78e9 3.08e9 219.78e9 3.08e9 138.95e9
     3.08e9 138.95e9];
Q12=[45.58e9 1.08e9 45.58e9 1.08e9 65.93e9 1.08e9 65.93e9 1.08e9 45.58e9 1.08e9
     45.58e9];
Q66=[46.69e9 10e9 46.69e9 10e9 76.92e9 10e9 76.92e9 10e9 46.69e9 10e9 46.69e9];
```

```
S0=20.6;                        %power spectral density
eta=2717.4;                     %c/m
etab=1966.6;                    %c/I0
p=3296.9;                       %k/m
pd=sqrt(p^2-eta^2);             %equal to sqrt(p^2-eta^2)
A=pi*S0*(4*eta^2+p^2)/(2*eta);
B=pi*S0/2;
D11=8.732;
D12=2.841;
D22=8.732;
D66=4.301;
I0=3.89;
a= 0.15;                        %length of board
b=0.0635; %width of the board
L_m=0.0013; %length of the module
Aw=3.2e-8; %lead wire area
Ew=138e9; %modulus of lead wire
Em=300e9; % modulus of the module
Lw=0.00218; % length of lead wire
Im=8.336e-17; %moment inertia of lead wire
sigma2=0;
   for m=1:2:21
     for n=1:2:21
       for i=1:2:21
         for j=1:2:21
         ss=((L_m)^3*52*Aw*Ew)/(3*Em*Im*Lw);
         sigmn=(1/(m*n))*((-1)^((m+n-2)/2)-(-1)^((n-1)/2)*sin(m*pi*(a-L_m)/(2*a)));
         sigij=1358570.847*i^4+42301174.52*j^4+28415140.64*i^2*j*2;
         C = (pi^2/(sqrt(I0)*b^2))*sqrt(D11*m^4*(b/a)^4+
              2*(D12+2*D66)*m^2*n^2*(b/a)^2+D22*n^4);
         D= (pi^2/(sqrt(I0)*b^2))*sqrt(D11*i^4*(b/a)^4+
              2*(D12+2*D66)*i^2*j^2*(b/a)^2+D22*j^4);
         p1=C-pd;
         p2=C+pd;
         p3=p1^2+(eta-etab)^2;
         p4=p2^2+(eta-etab)^2;
         sigma2=sigma2+sigmn*sigij*(1/(i*j))*(256/(pi^4*52^2))
                   ((-1)^((m+i-2)/2))*I*(Ew/Lw)*(1/(1+ss));
       end
     end
   end
   end
   rou=sigma2/(5*10e12)
```

H.9 Matlab code for computation of the bivarite normal reliability.

```
clear all
close all
u = 7.4892; % m1 value
v = 8.089; % m2 value
rou = 5.4527e-10; % correlation coef. value
%uu = inline('(1/sqrt(1-r^2))*exp(-((u)^2-2*r*u*v+v^2)/(2*(1-r^2)))');
format long e
R=((1/(2*pi))*quad(@uu,0,rou) + normcdf(u)*normcdf(v))

Function
function x = uu(r)
u =7.4892;
v=8.089;
x=(1./sqrt(1.-r.^2))*exp(-(u^2-2*r.*u*v+v^2)/(2*(1.-r.^2)));
```

H.10 Matlab code for computation of the correlation coefficient.

H.10.1 Correlation coefficient between the failure modes 1 and 3.

```
%compute correlation coefficient of rou(1,3)
clear all
z=[-677e-6 -641e-6 -539e-6 -503e-6 -203e-6 -51e-6 51e-6 203e-6 503e-6 539e-6
641e-6];
Q11=[138.95e9 3.08e9 138.95e9 3.08e9 219.78e9 3.08e9 219.78e9 3.08e9 138.95e9
3.08e9 138.95e9];
Q12=[45.58e9 1.08e9 45.58e9 1.08e9 65.93e9 1.08e9 65.93e9 1.08e9 45.58e9 1.08e9
45.58e9];
Q66=[46.69e9 10e9 46.69e9 10e9 76.92e9 10e9 76.92e9 10e9 46.69e9 10e9 46.69e9];
S0=20.6;                    %power spectral density
eta=2717.4;                 %c/m
etab=1966.6;                %c/I0
p=3296.9;                   %k/m
pd=sqrt(p^2-eta^2);         %equal to sqrt(p^2-eta^2)
A=pi*S0*(4*eta^2+p^2)/(2*eta);
B=pi*S0/2;
D11=8.732;
D12=2.841;
D22=8.732;
D66=4.301;
I0=3.89;
a= 0.15;                    %length of board
b=0.0635;                   %width of the board
```

```
L_m=0.0013; %length of the module
Aw=3.2e-8; %lead wire area
Ew=138e9; %modulus of lead wire
Em=300e9; % modulus of the module
Lw=0.000208; % length of lead wire
Im=8.336e-17; %moment inertia of lead wire
z1=[-0.001494 -0.00014];
sigma2=0;
for m=1:2:41
  for n=1:21
    for i=1:2:41
      for j=1:21
      sigmn=((z(1,11)^2-z(1,1)^2)/2)*((n*pi/b)^3*Q11(1,1)+
            (m^2*n*pi^3/(a^2*b))*(2*Q66(1,1)+Q12(1,1)))...
            +((z(1,11)^2-z(1,2)^2)/2)*((n*pi/b)^3*Q11(1,2)+
            (m^2*n*pi^3/(a^2*b))*(2*Q66(1,2)+Q12(1,2)))...
            +((z(1,11)^2-z(1,3)^2)/2)*((n*pi/b)^3*Q11(1,3)+
            (m^2*n*pi^3/(a^2*b))*(2*Q66(1,3)+Q12(1,3)))...
            +((z(1,11)^2-z(1,4)^2)/2)*((n*pi/b)^3*Q11(1,4)+
            (m^2*n*pi^3/(a^2*b))*(2*Q66(1,4)+Q12(1,4)))...
            +((z(1,11)^2-z(1,5)^2)/2)*((n*pi/b)^3*Q11(1,5)+
            (m^2*n*pi^3/(a^2*b))*(2*Q66(1,5)+Q12(1,5)))...
            +((z(1,11)^2-z(1,6)^2)/2)*((n*pi/b)^3*Q11(1,6)+
            (m^2*n*pi^3/(a^2*b))*(2*Q66(1,6)+Q12(1,6)))...
            +((z(1,11)^2-z(1,7)^2)/2)*((n*pi/b)^3*Q11(1,7)+
            (m^2*n*pi^3/(a^2*b))*(2*Q66(1,7)+Q12(1,7)))...
            +((z(1,11)^2-z(1,8)^2)/2)*((n*pi/b)^3*Q11(1,8)+
            (m^2*n*pi^3/(a^2*b))*(2*Q66(1,8)+Q12(1,8)))...
            +((z(1,11)^2-z(1,9)^2)/2)*((n*pi/b)^3*Q11(1,9)+
            (m^2*n*pi^3/(a^2*b))*(2*Q66(1,9)+Q12(1,9)))...
            +((z(1,11)^2-z(1,10)^2)/2)*((n*pi/b)^3*Q11(1,10)+
            (m^2*n*pi^3/(a^2*b))*(2*Q66(1,10)+Q12(1,10)))...
            +((z(1,11)^2-z(1,11)^2)/2)*((n*pi/b)^3*Q11(1,11)+
            (m^3*n*pi^3/(a^2*b))*(2*Q66(1,11)+Q12(1,11)));
      sigij=(j*pi/b)^3*Q11(1,1)+(i*pi/a)^2*(j*pi/b)*(2*Q66(1,1)+Q12(1,1));
      C = (pi^2/(sqrt(I0)*b^2))*sqrt(D11*m^4*(b/a)^4+
          2*(D12+2*D66)*m^2*n^2*(b/a)^2+D22*n^4);
      D= (pi^2/(sqrt(I0)*b^2))*sqrt(D11*i^4*(b/a)^4+
          2*(D12+2*D66)*i^2*j^2*(b/a)^2+D22*j^4);
      p1=C-pd;
      p2=C+pd;
      p3=p1^2+(eta-etab)^2;
      p4=p2^2+(eta-etab)^2;
      sigma2=sigma2+sigmn*sigij*(1/(m*n*i*j))*
```

```
              (256/pi^4)*((-1)^((m+i-2)/2))*I*((z1(1,1)^2-z1(1,2)^2)/2);
      end
    end
  end
  end
roul_3=sigma2/(4*5.02e12)
```

H.10.2 Correlation coefficient between the failure modes 1 and 4.

```
%compute correlation coefficient of rou(1,4)
clear all
z=[-677e-6 -641e-6 -539e-6 -503e-6 -203e-6 -51e-6 51e-6 203e-6 503e-6 539e-6
641e-6];
Q11=[138.95e9 3.08e9 138.95e9 3.08e9 219.78e9 3.08e9 219.78e9 3.08e9 138.95e9
3.08e9 138.95e9];
Q12=[45.58e9 1.08e9 45.58e9 1.08e9 65.93e9 1.08e9 65.93e9 1.08e9 45.58e9 1.08e9
45.58e9];
Q66=[46.69e9 10e9 46.69e9 10e9 76.92e9 10e9 76.92e9 10e9 46.69e9 10e9 46.69e9];
S0=20.6;                %power spectral density
eta=2717.4;             %c/m
etab=1966.6;            %c/I0
p=3296.9;               %k/m
pd=sqrt(p^2-eta^2);     %equal to sqrt(p^2-eta^2)
A=pi*S0*(4*eta^2+p^2)/(2*eta);
B=pi*S0/2;
D11=8.732;
D12=2.841;
D22=8.732;
D66=4.301;
I0=3.89;
a= 0.15;                %length of board
b=0.0635;               %width of the board
L_m=0.0013;             %length of the module
Aw=3.2e-8;              %lead wire area
Ew=138e9;               %modulus of lead wire
Em=300e9;               % modulus of the module
Lw=0.000208;            % length of lead wire
Im=8.336e-17;           %moment inertia of lead wire
sigma2=0;
for m=1:2:41
  for n=1:21
    for i=1:2:41
      for j=1:2:41
      ss=((L_m)^3*52*Aw*Ew)/(3*Em*Im*Lw);
```

```
        sigmn=((z(1,11)^2-z(1,1)^2)/2)*((n*pi/b)^3*Q11(1,1)+
              (m^2*n*pi^3/(a^2*b))*(2*Q66(1,1)+Q12(1,1)))...
              +((z(1,11)^2-z(1,2)^2)/2)*((n*pi/b)^3*Q11(1,2)+
              (m^2*n*pi^3/(a^2*b))*(2*Q66(1,2)+Q12(1,2)))...
              +((z(1,11)^2-z(1,3)^2)/2)*((n*pi/b)^3*Q11(1,3)+
              (m^2*n*pi^3/(a^2*b))*(2*Q66(1,3)+Q12(1,3)))...
              +((z(1,11)^2-z(1,4)^2)/2)*((n*pi/b)^3*Q11(1,4)+
              (m^2*n*pi^3/(a^2*b))*(2*Q66(1,4)+Q12(1,4)))...
              +((z(1,11)^2-z(1,5)^2)/2)*((n*pi/b)^3*Q11(1,5)+
              (m^2*n*pi^3/(a^2*b))*(2*Q66(1,5)+Q12(1,5)))...
              +((z(1,11)^2-z(1,6)^2)/2)*((n*pi/b)^3*Q11(1,6)+
              (m^2*n*pi^3/(a^2*b))*(2*Q66(1,6)+Q12(1,6)))...
              +((z(1,11)^2-z(1,7)^2)/2)*((n*pi/b)^3*Q11(1,7)+
              (m^2*n*pi^3/(a^2*b))*(2*Q66(1,7)+Q12(1,7)))...
              +((z(1,11)^2-z(1,8)^2)/2)*((n*pi/b)^3*Q11(1,8)+
              (m^2*n*pi^3/(a^2*b))*(2*Q66(1,8)+Q12(1,8)))...
              +((z(1,11)^2-z(1,9)^2)/2)*((n*pi/b)^3*Q11(1,9)+
              (m^2*n*pi^3/(a^2*b))*(2*Q66(1,9)+Q12(1,9)))...
              +((z(1,11)^2-z(1,10)^2)/2)*((n*pi/b)^3*Q11(1,10)+
              (m^2*n*pi^3/(a^2*b))*(2*Q66(1,10)+Q12(1,10)))...
              +((z(1,11)^2-z(1,11)^2)/2)*((n*pi/b)^3*Q11(1,11)+
              (m^3*n*pi^3/(a^2*b))*(2*Q66(1,11)+Q12(1,11)));
        sigij=(1/(i*j))*((-1)^((i+j-2)/2)-(-1)^((j-1)/2)*sin(i*pi*(a-L_m)/(2*a)));
        C = (pi^2/(sqrt(I0)*b^2))*sqrt(D11*m^4*(b/a)^4+
            2*(D12+2*D66)*m^2*n^2*(b/a)^2+D22*n^4);
        D= (pi^2/(sqrt(I0)*b^2))*sqrt(D11*i^4*(b/a)^4+
            2*(D12+2*D66)*i^2*j^2*(b/a)^2+D22*j^4);
        p1=C-pd;
        p2=C+pd;
        p3=p1^2+(eta-etab)^2;
        p4=p2^2+(eta-etab)^2;
        sigma2=sigma2+sigmn*sigij*(1/(m*n))*
              (256/pi^4)*((-1)^((m-1)/2))*I*(1/(1+ss))*(Ew/(Lw*52));
      end
    end
  end
end
roul_4=sigma2/(4*5e12)
```

H.10.3 Correlation coefficient between the failure modes 1 and 7.

```
%compute correlation coefficient of rou(1,7)
clear all
z=[-677e-6 -641e-6 -539e-6 -503e-6 -203e-6 -51e-6 51e-6 203e-6 503e-6 539e-6
```

```
641e-6];
Q11=[138.95e9 3.08e9 138.95e9 3.08e9 219.78e9 3.08e9 219.78e9 3.08e9 138.95e9
3.08e9 138.95e9];
Q12=[45.58e9 1.08e9 45.58e9 1.08e9 65.93e9 1.08e9 65.93e9 1.08e9 45.58e9 1.08e9
45.58e9];
Q66=[46.69e9 10e9 46.69e9 10e9 76.92e9 10e9 76.92e9 10e9 46.69e9 10e9 46.69e9];
S0=20.6;                %power spectral density
eta=2717.4;             %c/m
etab=1966.6;            %c/I0
p=3296.9;               %k/m
pd=sqrt(p^2-eta^2);     %equal to sqrt(p^2-eta^2)
A=pi*S0*(4*eta^2+p^2)/(2*eta);
B=pi*S0/2;
D11=8.732;
D12=2.841;
D22=8.732;
D66=4.301;
I0=3.89;               %
a= 0.15;               %length of board
b=0.0635;              %width of the board
L_m=0.0013;            %length of the module
Aw=3.2e-8;             %lead wire area
Ew=138e9;              %modulus of lead wire
Em=300e9;              % modulus of the module
Lw=0.000208;           % length of lead wire
Im=8.336e-17;          %moment inertia of lead wire
sigma2=0;
for m=1:2:41
  for n=1:21
    for i=1:2:41
      for j=1:2:41
      sigmn=((z(1,11)^2-z(1,1)^2)/2)*((n*pi/b)^3*Q11(1,1)+
            (m^2*n*pi^3/(a^2*b))*(2*Q66(1,1)+Q12(1,1)))...
            +((z(1,11)^2-z(1,2)^2)/2)*((n*pi/b)^3*Q11(1,2)+
            (m^2*n*pi^3/(a^2*b))*(2*Q66(1,2)+Q12(1,2)))...
            +((z(1,11)^2-z(1,3)^2)/2)*((n*pi/b)^3*Q11(1,3)+
            (m^2*n*pi^3/(a^2*b))*(2*Q66(1,3)+Q12(1,3)))...
            +((z(1,11)^2-z(1,4)^2)/2)*((n*pi/b)^3*Q11(1,4)+
            (m^2*n*pi^3/(a^2*b))*(2*Q66(1,4)+Q12(1,4)))...
            +((z(1,11)^2-z(1,5)^2)/2)*((n*pi/b)^3*Q11(1,5)+
            (m^2*n*pi^3/(a^2*b))*(2*Q66(1,5)+Q12(1,5)))...
            +((z(1,11)^2-z(1,6)^2)/2)*((n*pi/b)^3*Q11(1,6)+
            (m^2*n*pi^3/(a^2*b))*(2*Q66(1,6)+Q12(1,6)))...
            +((z(1,11)^2-z(1,7)^2)/2)*((n*pi/b)^3*Q11(1,7)+
```

```
                (m^2*n*pi^3/(a^2*b))*(2*Q66(1,7)+Q12(1,7)))...
                +((z(1,11)^2-z(1,8)^2)/2)*((n*pi/b)^3*Q11(1,8)+
                (m^2*n*pi^3/(a^2*b))*(2*Q66(1,8)+Q12(1,8)))...
                +((z(1,11)^2-z(1,9)^2)/2)*((n*pi/b)^3*Q11(1,9)+
                (m^2*n*pi^3/(a^2*b))*(2*Q66(1,9)+Q12(1,9)))...
                +((z(1,11)^2-z(1,10)^2)/2)*((n*pi/b)^3*Q11(1,10)+
                (m^2*n*pi^3/(a^2*b))*(2*Q66(1,10)+Q12(1,10)))...
                +((z(1,11)^2-z(1,11)^2)/2)*((n*pi/b)^3*Q11(1,11)+
                (m^3*n*pi^3/(a^2*b))*(2*Q66(1,11)+Q12(1,11)));
         sigij=1358570.847*i^4+42301174.52*j^4+28415140.64*i^2*j*2;
         C = (pi^2/(sqrt(I0)*b^2))*sqrt(D11*m^4*(b/a)^4+
             2*(D12+2*D66)*m^2*n^2*(b/a)^2+D22*n^4);
         D= (pi^2/(sqrt(I0)*b^2))*sqrt(D11*i^4*(b/a)^4+
             2*(D12+2*D66)*i^2*j^2*(b/a)^2+D22*j^4);
         p1=C-pd;
         p2=C+pd;
         p3=p1^2+(eta-etab)^2;
         p4=p2^2+(eta-etab)^2;
         sigma2=sigma2+sigmn*sigij*(1/(m*n*i*j))*
                (256/pi^4)*((-1)^((m+i+j-3)/2))*I;
      end
   end
end
end
rou1_7=sigma2/(4*10e12)
```

H.10.4 Correlation coefficient between the failure modes 2 and 3.

H.10.4.1 Mean value of the product of the vibration stress and the max. deflection.

```
%compute mean value of rou2_3 w_max
clear all
z=[-677e-6 -641e-6 -539e-6 -503e-6 -203e-6 -51e-6 51e-6 203e-6 503e-6 539e-6
641e-6];
Q11=[138.95e9 3.08e9 138.95e9 3.08e9 219.78e9 3.08e9 219.78e9 3.08e9 138.95e9
3.08e9 138.95e9];
Q12=[45.58e9 1.08e9 45.58e9 1.08e9 65.93e9 1.08e9 65.93e9 1.08e9 45.58e9 1.08e9
45.58e9];
Q66=[46.69e9 10e9 46.69e9 10e9 76.92e9 10e9 76.92e9 10e9 46.69e9 10e9 46.69e9];
S0=20.6;                    %power spectral density
eta=2717.4;                 %c/m
etab=1966.6;                %c/I0
p=3296.9;                    %k/m
pd=sqrt(p^2-eta^2);         %equal to sqrt(p^2-eta^2)
```

```
A=pi*S0*(4*eta^2+p^2)/(2*eta);
B=pi*S0/2;
D11=8.732;
D12=2.841;
D22=8.732;
D66=4.301;
I0=3.89;
a= 0.15;                    %length of board
b=0.0635;                   %width of the board
z1=[-0.001494 -0.00014];
sigma2=0;
for m=1:2:41
  for n=1:21
    for i=1:2:41
      for j=1:21
      sigij=(j*pi/b)^3*Q11(1,1)+(i*pi/a)^2*(j*pi/b)*(2*Q66(1,1)+Q12(1,1));
      C = (pi^2/(sqrt(I0)*b^2))*sqrt(D11*m^4*(b/a)^4+
           2*(D12+2*D66)*m^2*n^2*(b/a)^2+D22*n^4);
      D= (pi^2/(sqrt(I0)*b^2))*sqrt(D11*i^4*(b/a)^4+
           2*(D12+2*D66)*i^2*j^2*(b/a)^2+D22*j^4);
      p1=C-pd;
      p2=C+pd;
      p3=p1^2+(eta-etab)^2;
      p4=p2^2+(eta-etab)^2;
      sigma2=sigma2-sigij*(1/(m*n*i*j))*
               (256/pi^4)*((-1)^((m+i-2)/2))*I*((z1(1,2)^2-z1(1,1)^2)/2);
    end
  end
end
end
mean=sigma2
```

H.10.4.2 Mean value of the product of the vibration stress and w^*.

```
%compute E(s_vir*w*)
clear all
z=[-677e-6 -641e-6 -539e-6 -503e-6 -203e-6 -51e-6 51e-6 203e-6 503e-6 539e-6
641e-6];
Q11=[138.95e6 3.08e6 138.95e6 3.08e6 219.78e6 3.08e6 219.78e6 3.08e6 138.95e6
3.08e6 138.95e6];
Q12=[45.58e6 1.08e6 45.58e6 1.08e6 65.93e6 1.08e6 65.93e6 1.08e6 45.58e6 1.08e6
45.58e6];
Q66=[46.69e6 10e6 46.69e6 10e6 76.92e6 10e6 76.92e6 10e6 46.69e6 10e9 46.69e6];
a= 0.15;                  %length of board
```

```
b=0.0635;               %width of the board
S0=20.6;                %power spectral density
eta=2717.4;             %c/m
etab=1966.6;            %c/I0
p=3296.9;               %k/m
pd=sqrt(p^2-eta^2);     %equal to sqrt(p^2-eta^2)
D11=8.732;
D12=2.841;
D22=8.732;
D66=4.301;
I0=3.89;
a= 0.15;                %length of board
b=0.0635;               %width of the board
z1=[-0.001494 -0.00014];
A=0;
for m=1:2:1551
  for n=1:551
    sigmn=(n*pi/b)^3*Q11(1,1)+(m*pi/a)^2*(n*pi/b)*(2*Q66(1,1)+Q12(1,1));
    C = (pi^2/(sqrt(I0)*b^2))*sqrt(D11*m^4*(b/a)^4+
        2*(D12+2*D66)*m^2*n^2*(b/a)^2+D22*n^4);
    p1=C-pd;
    p2=C+pd;
    p3=p1^2+(eta+etab)^2;
    p4=p2^2+(eta+etab)^2;
    A1=(pi*S0*(etab+eta)/(2*C*pd))*(1/p3-1/p4);
    A2=(pi*S0/(4*C*pd))*((p1+eta*(etab+eta)/pd)/p3+(p2-eta*(etab+eta)/pd)/p4);
    A=A+(1/(m*n))*(16/pi^2)*sigmn*((-1)^((m-1)/2))*
        (A1+A2)*((z1(1,2)^2-z1(1,1)^2)/2);
  end
end
A
```

H.10.5 Correlation coefficient between the failure modes 2 and 4.

H.10.5.1 Mean value of the product of the vibration stress and the max. deflection.

```
%compute mean value of stress-leadwire with w_max
clear all
z=[-677e-6 -641e-6 -539e-6 -503e-6 -203e-6 -51e-6 51e-6 203e-6 503e-6 539e-6
641e-6];
Q11=[138.95e9 3.08e9 138.95e9 3.08e9 219.78e9 3.08e9 219.78e9 3.08e9 138.95e9
3.08e9 138.95e9];
Q12=[45.58e9 1.08e9 45.58e9 1.08e9 65.93e9 1.08e9 65.93e9 1.08e9 45.58e9 1.08e9
45.58e9];
```

```
Q66=[46.69e9 10e9 46.69e9 10e9 76.92e9 10e9 76.92e9 10e9 46.69e9 10e9 46.69e9];
S0=20.6;                    %power spectral density
eta=2717.4;                 %c/m
etab=1966.6;                %c/I0
p=3296.9;                   %k/m
pd=sqrt(p^2-eta^2);         %equal to sqrt(p^2-eta^2)
A=pi*S0*(4*eta^2+p^2)/(2*eta);
B=pi*S0/2;
D11=8.732;
D12=2.841;
D22=8.732;
D66=4.301;
I0=3.89;
a= 0.15;                    %length of board
b=0.0635;                   %width of the board
L_m=0.0013;                 %length of the module
Aw=3.2e-8;                  %lead wire area
Ew=138e9;                   %modulus of lead wire
Em=300e9;                   % modulus of the module
Lw=0.000208;                % length of lead wire
Im=8.336e-17;               %moment inertia of lead wire
sigma2=0;
for m=1:2:41
  for n=1:2:41
    for i=1:2:41
      for j=1:2:41
      ss=((L_m)^3*52*Aw*Ew)/(3*Em*Im*Lw);
      sigmn=(1/(m*n))*((-1)^((m+n-2)/2)-(-1)^((n-1)/2)*sin(m*pi*(a-L_m)/(2*a)));
      C = (pi^2/(sqrt(I0)*b^2))*sqrt(D11*m^4*(b/a)^4+
           2*(D12+2*D66)*m^2*n^2*(b/a)^2+D22*n^4);
      D= (pi^2/(sqrt(I0)*b^2))*sqrt(D11*i^4*(b/a)^4+
           2*(D12+2*D66)*i^2*j^2*(b/a)^2+D22*j^4);
      p1=C-pd;
      p2=C+pd;
      p3=p1^2+(eta-etab)^2;
      p4=p2^2+(eta-etab)^2;
      sigma2=sigma2+sigmn*(1/(i*j))*
             (256/pi^4)*((-1)^((m+n+i+j-4)/2))*I*(1/(1+ss))*(Ew/(52*Lw));
    end
  end
end
end
rou2_4sleadwire_w_max=sigma2
```

H.10.5.2 Mean value of the product of the vibration stress and w^*.

```
%compute mean value of stress-leadwire with w*
clear all
z=[-677e-6 -641e-6 -539e-6 -503e-6 -203e-6 -51e-6 51e-6 203e-6 503e-6 539e-6
641e-6];
Q11=[138.95e9 3.08e9 138.95e9 3.08e9 219.78e9 3.08e9 219.78e9 3.08e9 138.95e9
3.08e9 138.95e9];
Q12=[45.58e9 1.08e9 45.58e9 1.08e9 65.93e9 1.08e9 65.93e9 1.08e9 45.58e9 1.08e9
45.58e9];
Q66=[46.69e9 10e9 46.69e9 10e9 76.92e9 10e9 76.92e9 10e9 46.69e9 10e9 46.69e9];
S0=20.6;                    %power spectral density
eta=2717.4;                 %c/m
etab=1966.6;                %c/I0
p=3296.9;                   %k/m
pd=sqrt(p^2-eta^2);         %equal to sqrt(p^2-eta^2)
A=pi*S0*(4*eta^2+p^2)/(2*eta);
B=pi*S0/2;
D11=8.732;
D12=2.841;
D22=8.732;
D66=4.301;
I0=3.89;
a= 0.15;                    %length of board
b=0.0635;                   %width of the board
L_m=0.0013;                 %length of the module
Aw=3.2e-8;                  %lead wire area
Ew=138e9;                   %modulus of lead wire
Em=300e9;                   % modulus of the module
Lw=0.000208;                % length of lead wire
Im=8.336e-17;               %moment inertia of lead wire
sigma2=0;
for m=1:2:41
  for n=1:2:41
      ss=((L_m)^3*52*Aw*Ew)/(3*Em*Im*Lw);
      sigmn=(1/(m*n))*((-1)^((m+n-2)/2)-(-1)^((n-1)/2)*sin(m*pi*(a-L_m)/(2*a)));
      C = (pi^2/(sqrt(I0)*b^2))*sqrt(D11*m^4*(b/a)^4+
          2*(D12+2*D66)*m^2*n^2*(b/a)^2+D22*n^4);
      D= (pi^2/(sqrt(I0)*b^2))*sqrt(D11*i^4*(b/a)^4+
          2*(D12+2*D66)*i^2*j^2*(b/a)^2+D22*j^4);
      p1=C-pd;
      p2=C+pd;
      p3=p1^2+(eta-etab)^2;
      p4=p2^2+(eta-etab)^2;
```

```
        A1=(pi*S0*(etab+eta)/(2*C*pd))*(1/p3-1/p4);
        A2=(pi*S0/(4*C*pd))*((p1+eta*(etab+eta)/pd)/p3+(p2-eta*(etab+eta)/pd)/p4);
        sigma2=sigma2+sigmn*(16/pi^2)*
                ((-1)^((m+n-2)/2))*(A1+A2)*(1/(1+ss))*(Ew/(52*Lw));
      end
    end
end
end
rou2_4sleadwire_w_star=-sigma2
```

H.10.6 Correlation coefficient between the failure modes 2 and 7.

H.10.6.1 Mean value of the product of the vibration stress and the max. deflection.

```
%compute mean value of stress-szz with w_max
clear all
z=[-677e-6 -641e-6 -539e-6 -503e-6 -203e-6 -51e-6 51e-6 203e-6 503e-6 539e-6
641e-6];
Q11=[138.95e9 3.08e9 138.95e9 3.08e9 219.78e9 3.08e9 219.78e9 3.08e9 138.95e9
3.08e9 138.95e9];
Q12=[45.58e9 1.08e9 45.58e9 1.08e9 65.93e9 1.08e9 65.93e9 1.08e9 45.58e9 1.08e9
45.58e9];
Q66=[46.69e9 10e9 46.69e9 10e9 76.92e9 10e9 76.92e9 10e9 46.69e9 10e9 46.69e9];
S0=20.6;                    %power spectral density
eta=2717.4;                 %c/m
etab=1966.6;                %c/I0
p=3296.9;                   %k/m
pd=sqrt(p^2-eta^2);         %equal to sqrt(p^2-eta^2)
A=pi*S0*(4*eta^2+p^2)/(2*eta);
B=pi*S0/2;
D11=8.732;
D12=2.841;
D22=8.732;
D66=4.301;
I0=3.89;
a= 0.15;                    %length of board
b=0.0635;                   %width of the board
sigma2=0;
for m=1:2:41
  for n=1:2:41
    for i=1:2:41
      for j=1:2:41
      sigmn=1358570.847*m^4+42301174.52*n^4+28415140.64*m^2*n*2;
```

```
        C = (pi^2/(sqrt(I0)*b^2))*sqrt(D11*m^4*(b/a)^4+
             2*(D12+2*D66)*m^2*n^2*(b/a)^2+D22*n^4);
        D= (pi^2/(sqrt(I0)*b^2))*sqrt(D11*i^4*(b/a)^4+
             2*(D12+2*D66)*i^2*j^2*(b/a)^2+D22*j^4);
        p1=C-pd;
        p2=C+pd;
        p3=p1^2+(eta-etab)^2;
        p4=p2^2+(eta-etab)^2;
        sigma2=sigma2+sigmn*(1/(m*n*i*j))*(256/pi^4)*((-1)^((m+n+i+j-4)/2))*I;
      end
    end
  end
end
rou2_7szz_w_max=sigma2
```

H.10.6.2 Mean value of the product of the vibration stress and w^*.

```
%compute E(s_vir*w*) for szz_w*
clear all
z=[-677e-6 -641e-6 -539e-6 -503e-6 -203e-6 -51e-6 51e-6 203e-6 503e-6 539e-6
641e-6];
Q11=[138.95e6 3.08e6 138.95e6 3.08e6 219.78e6 3.08e6 219.78e6 3.08e6 138.95e6
3.08e6 138.95e6];
Q12=[45.58e6 1.08e6 45.58e6 1.08e6 65.93e6 1.08e6 65.93e6 1.08e6 45.58e6 1.08e6
45.58e6];
Q66=[46.69e6 10e6 46.69e6 10e6 76.92e6 10e6 76.92e6 10e6 46.69e6 10e9 46.69e6];
a= 0.15;                    %length of board
b=0.0635;                   %width of the board
S0=20.6;                    %power spectral density
eta=2717.4;                 %c/m
p=3296.9;                   %k/m
pd=sqrt(p^2-eta^2);         %equal to sqrt(p^2-eta^2)
etab=1966.6;                %c/I0
I0=3.89;
D11=8.732;
D12=2.841;
D22=8.732;
D66=4.301;
A=0;
for m=1:2:149
  for n=1:2:149
    C = (pi^2/(sqrt(I0)*b^2))*sqrt(D11*m^4*(b/a)^4+
         2*(D12+2*D66)*m^2*n^2*(b/a)^2+D22*n^4);
    p1=C-pd;
```

```
      p2=C+pd;
      p3=p1^2+(eta+etab)^2;
      p4=p2^2+(eta+etab)^2;
      A1=(pi*S0*(etab+eta)/(2*C*pd))*(1/p3-1/p4);
      A2=(pi*S0/(4*C*pd))*((p1+eta*(etab+eta)/pd)/p3+(p2-eta*(etab+eta)/pd)/p4);
      sigmn=1358570.847*m^4+42301174.52*n^4+28415140.64*m^2*n*2;
      A=A+(1/(m*n))*(16/pi^2)*((-1)^((m+n-2)/2))*sigmn*(A1+A2);
   end
end
rou2_7_szz_w_star=A
```

H.10.7 Correlation coefficient between the failure modes 3 and 4.

```
%compute correlation coefficient of rou(3,4)
clear all
z=[-677e-6 -641e-6 -539e-6 -503e-6 -203e-6 -51e-6 51e-6 203e-6 503e-6 539e-6
641e-6];
Q11=[138.95e9 3.08e9 138.95e9 3.08e9 219.78e9 3.08e9 219.78e9 3.08e9 138.95e9
3.08e9 138.95e9];
Q12=[45.58e9 1.08e9 45.58e9 1.08e9 65.93e9 1.08e9 65.93e9 1.08e9 45.58e9 1.08e9
45.58e9];
Q66=[46.69e9 10e9 46.69e9 10e9 76.92e9 10e9 76.92e9 10e9 46.69e9 10e9 46.69e9];
S0=20.6;                %power spectral density
eta=2717.4;             %c/m
etab=1966.6;            %c/I0
p=3296.9;               %k/m
pd=sqrt(p^2-eta^2);     %equal to sqrt(p^2-eta^2)
A=pi*S0*(4*eta^2+p^2)/(2*eta);
B=pi*S0/2;
D11=8.732;
D12=2.841;
D22=8.732;
D66=4.301;
I0=3.89;
a= 0.15;                %length of board
b=0.0635;               %width of the board
L_m=0.0013;             %length of the module
Aw=3.2e-8;              %lead wire area
Ew=138e9;               %modulus of lead wire
Em=300e9;               % modulus of the module
Lw=0.000208;            % length of lead wire
Im=8.336e-17;           %moment inertia of lead wire
z1=[-0.001494 -0.00014];
sigma2=0;
```

```
for m=1:2:41
   for n=1:21
      for i=1:2:41
         for j=1:2:41
         ss=((L_m)^3*52*Aw*Ew)/(3*Em*Im*Lw);
         sigmn=(n*pi/b)^3*Q11(1,1)+(m*pi/a)^2*(n*pi/b)*(2*Q66(1,1)+Q12(1,1));
         sigij=(1/(i*j))*((-1)^((i+j-2)/2)-(-1)^((j-1)/2)*sin(i*pi*(a-L_m)/(2*a)));
         C = (pi^2/(sqrt(I0)*b^2))*sqrt(D11*m^4*(b/a)^4+
              2*(D12+2*D66)*m^2*n^2*(b/a)^2+D22*n^4);
         D= (pi^2/(sqrt(I0)*b^2))*sqrt(D11*i^4*(b/a)^4+
              2*(D12+2*D66)*i^2*j^2*(b/a)^2+D22*j^4);
         p1=C-pd;
         p2=C+pd;
         p3=p1^2+(eta-etab)^2;
         p4=p2^2+(eta-etab)^2;
         sigma2=sigma2+sigmn*sigij*(1/(m*n))*
                 (256/pi^4)*((-1)^((m-1)/2))*I*(1/(1+ss))*(Ew/(Lw*52))*((z1(1,1)^2-
                 z1(1,2)^2)/2);
      end
   end
end
end
rou3_4=sigma2/(5.02*5e12)
```

H.10.8 Correlation coefficient between the failure modes 3 and 7.

```
%compute correlation coefficient of rou(3,7)
clear all
z=[-677e-6 -641e-6 -539e-6 -503e-6 -203e-6 -51e-6 51e-6 203e-6 503e-6 539e-6
641e-6];
Q11=[138.95e9 3.08e9 138.95e9 3.08e9 219.78e9 3.08e9 219.78e9 3.08e9 138.95e9
3.08e9 138.95e9];
Q12=[45.58e9 1.08e9 45.58e9 1.08e9 65.93e9 1.08e9 65.93e9 1.08e9 45.58e9 1.08e9
45.58e9];
Q66=[46.69e9 10e9 46.69e9 10e9 76.92e9 10e9 76.92e9 10e9 46.69e9 10e9 46.69e9];
S0=20.6;                    %power spectral density
eta=2717.4;                 %c/m
etab=1966.6;                %c/I0
p=3296.9;                    %k/m
pd=sqrt(p^2-eta^2);         %equal to sqrt(p^2-eta^2)
A=pi*S0*(4*eta^2+p^2)/(2*eta);
B=pi*S0/2;
D11=8.732;
D12=2.841;
```

```
D22=8.732;
D66=4.301;
I0=3.89;
a= 0.15;                    %length of board
b=0.0635;                   %width of the board
L_m=0.0013;                 %length of the module
Aw=3.2e-8;                  %lead wire area
Ew=138e9;                   %modulus of lead wire
Em=300e9;                   % modulus of the module
Lw=0.000208;                % length of lead wire
Im=8.336e-17;               %moment inertia of lead wire
z1=[-0.001494 -0.00014];
sigma2=0;
for m=1:2:41
  for n=1:21
    for i=1:2:41
      for j=1:2:41
      sigmn=(n*pi/b)^3*Q11(1,1)+(m*pi/a)^2*(n*pi/b)*(2*Q66(1,1)+Q12(1,1));
      sigij=1358570.847*i^4+42301174.52*j^4+28415140.64*i^2*j*2;
      C = (pi^2/(sqrt(I0)*b^2))*sqrt(D11*m^4*(b/a)^4+
          2*(D12+2*D66)*m^2*n^2*(b/a)^2+D22*n^4);
      D= (pi^2/(sqrt(I0)*b^2))*sqrt(D11*i^4*(b/a)^4+
          2*(D12+2*D66)*i^2*j^2*(b/a)^2+D22*j^4);
      p1=C-pd;
      p2=C+pd;
      p3=p1^2+(eta-etab)^2;
      p4=p2^2+(eta-etab)^2;
      sigma2=sigma2+sigmn*sigij*(1/(m*n*i*j))*
             (256/pi^4)*((-1)^((m+i+j-3)/2))*I*((z1(1,1)^2-z1(1,2)^2)/2);
    end
  end
end
end
rou3_7=sigma2/(5.02*10e12)
```

H.10.9 Correlation coefficient between the failure modes 4 and 5

This can be found using the standard deviation of leaded stress and the standard deviations of failure modes 4 and 5.

H.11 Matlab code for computation of $P(F_i \cap F_j)$

```
clear all
```

```
close all
u = 7.4892; % m1 value
v = 8.089; % m2 value
rou = 5.4527e-10; % correlation coef. value
%uu = inline('(1/sqrt(1-r^2))*exp(-((u)^2-2*r*u*v+v^2)/(2*(1-r^2)))');
format long e
R=((1/(2*pi))*quad(@uu,0,rou) + normcdf(-u)*normcdf(-v))
```

Function

```
function x = uu(r)
u =7.4892;
v=8.089;
x=(1./sqrt(1.-r.^2))*exp(-(u^2-2*r.*u*v+v^2)/(2*(1.-r.^2)));
```

Note: the rest of the correlation coefficient can be found using above codes.

REFERENCES

1. Parry, J., Marooney, C., et. al, "An integrated Approach to Flow, Thermal and Mechanical Modeling of Electronic Devices," *2002 Inter Society Conference on Thermal Phenomena,* pp. 862-868, 2002.

2. Kececioglu, B. D., *Reliability & Life Testing Handbook,* DEStech Publications, Inc., 1148 Elizabeth Ave., #2, Lancaster, PA, Vol. 2, 877 pp., 2002.

3. Akay, H. U., Liu, Y. and Rassaian, M., "Simplification of Finite Element Models for Thermal Fatigue Life Prediction of PBGA Packages", *Journal of Electronic Packaging*, Vol. 125, pp. 347-353, Sep. 2003.

4. Davuluri, P., et al, "Thermomechanical Durability of High I/O BGA Packages," *Transactions of the ASME*, Vol. 124, pp. 266-270, Sep. 2002.

5. Alpern, P., et al, "On the Mode II Popcorn Effect in Thin Packages," *IEEE Transactions on Components and Packaging Technologies,* Vol. 25, No. 1, pp. 56- 65, March, 2002.

6. Alpern, P., et al, "A Simple Model for the Mode I Popcorn Effect for IC Packages with Copper Leadframe," *IEEE Transactions on Components and Packaging Technologies,* Vol. 25, No. 2, pp. 301-308, June, 2002.

7. Gallo, A.A. and Munamarty, R., "Popcorning: A Failure Mechanism in Plastic – Encapsulated Microcircuits," *IEEE Transaction on Reliability*, Vol. 44, No.3 pp. 362-367, 1995.

8. MIL-HDBK-217F, "*Reliability Prediction of Electronic Equipment*," 250 pp., Dec.1991.

9. Zhang, Y. C., *Reliability Quantification of Plates Subjected to Random Vibration and Temperature Loads,* Ph. D. Dissertation, The University of Arizona, 187 pp., 2000.

10. Marks, L. and Caterina, J. A., "*Printed Circuit Assembly Design*," McGraw-Hall, 421 pp., 2000.

11. Dylis, D.D., "PRISM: A New Approach to Reliability Prediction," RAC News Letter, 12 pp. 2001.

12. Bellcore TR-332, "*Reliability Prediction Procedure for Electronic Equipment*", 138 pp. Dec. 1997.

13. John, B. B, "A Survey of Reliability-Prediction Procedures for Microelectronic Devices", *IEEE Transactions on Reliability*, Vol. 41, No. 1, pp 2-12, Mar. 1992.

14. Pecht, M., "Electronic Reliability Engineering in the 21st Century," *2001 Int'l Symposium on Electronic Materials and Packaging,* pp. 1-7, 2001.

15. Parr, J. D., et al, "Enhanced Electronic System Reliability – Challenges for Temperature Prediction," *IEEE Transactions on Components and Packaging Technologies,* Vol. 25, No. 4, pp. 533-538, Dec. 2002.

16. Leonard, C. T., "Mechanical Engineering Issues and Electronics Equipment Reliability: Incurred Costs Without Compensating Benefits," *IEEE Transactions on Components, Hybrids, and Manufacturing Technology*, Vol. 13, No. 4, pp. 895-902, Dec. 1990.

17. Pecht, M., "Are Components Still the Major Problem: A Review of Electronic System and Device Field Failure Returns," *IEEE Transactions on Components, Hybrids, and Manufacturing Technology,* Vol. 15, No. 6, Dec. 1992.

18. Pike, D., et al, "Validation of PRISM Prediction Model with In-service Data," *Proceedings of The 41st Annual Reliability Engineering and Management Institute,* Tucson, No. 7, 14 pp., Nov. 17-20, 2003.

19. Kececioglu, D. B., "*Robust Engineering Design-By-Reliability with Emphasis on Mechanical Components & Structural Reliability,*" DEStech Publications, Inc., 1148 Elizabeth Ave., #2, Lancaster, PA, Vol. 1, 688 pp., 2003.

20. Kim, J., Shin, S., Ryu, D. and Chang, S., "Reliability Evaluation and Failure Analysis for High Voltage Ceramic Capacitor," *2001 Int'l Symposium on Electronic Materials and Packaging,* pp. 286-295, 2001.

21. Suhir, E., "Thermal Stress Modeling in Microelectronics and Photonic Structures, and the Application of the Probabilistic Approach: Review and Extension," *The International Journal of Microcircuits and Electronic Packaging,* Vol. 23, No. 2, Second Quarter, pp. 215-223, 2000.

22. Kececioglu, D.B., "*Reliability Engineering Handbook*", DEStech Publications, Inc., 1148 Elizabeth Ave., #2, Lancaster, PA, Vol. 1, 720 pp., 2002.

23. MIL-STD-721, *Definitions of Terms for Reliability and Maintainability,* 18 pp., 12 Jun. 1981.

24. Hasofer, A. M., and Lind, N.C., "Exact and Invariant Second-Moment Code Format," *Journal of The Engineering Mechanics Division,* EM1, pp. 111-121, Feb. 1974.

25. Grigoriu, M., "Methods for Approximate Reliability Analysis," *Structural Safety,* 1 (1982/1983), pp. 155-165, 1982.

26. Lind, N. C., "Optimal Reliability Analysis By Fast Convolution," *Journal of The Engineering Mechanics Division,* EM3, pp. 447-452, June 1979.

27. Donlinski, K., "First-Order Second-Moment Approximation in Reliability of Structural Systems: Critical Review and Alternative Approach," *Structural Safety,* 1 (1983), pp. 211-231, 1983.

28. Shinozuka, M., "Basic Analysis of Structural Safety," *Journal of Structural Division,* ASCE, Vol. No.3, 109, 1983.

29. Rackwwitz, R., and Fiessler, B., "Structural Reliability under Combined Random Load Sequences," *Computer Structure,* Vol.9, pp. 484-494, 1978.

30. Breitung, K., "Asymptotic Approximations for Multinormal Integrals," *Journal of Engineering Mechanics,* ASCE, Vol. 110, No. 3, pp. 357-366, 1984.

31. Kiureghian, A. D., Lin, H-Z., and Hwang, S-J., "Second-Order Reliability Approximations," *Journal of Engineering Mechanics,* 113, pp. 1208-1225, 1978.

32. Grigoriu, M., "Methods for Approximate Reliability Analysis," *Structural Safety,* 1, pp. 155-165, 1982.

33. Chen, X., and Lind, N. C., "Fast Probability Integration by Three Parameter Normal Tail Approximation," *Structural Safety,* Vol. 1, pp. 269-276, 1983.

34. Wu, Y-T., and Wirsching, P. H., "New Algorithm for Structural Reliability Estimation," *Journal of Engineering Mechanics*, Vol. 113, No. 9, pp. 1319-1336, 1987.

35. Ang, A. H-S., and Tang, W. H., Design, Risk, and Reliability, *"Probability Concepts in Engineering Planning and Design,"* Vol. 2, John Wiley & Sons, 562 pp. 1984.

36. Tang, L. K., and Melchers, R. E., "Improved Approximation for Multinormal Integral," *Structural Safety,* 4, pp. 81-93, 1987.

37. Hohenbichler, M., and Rackwitz, R., "First-Order Concepts in System Reliability," *Structural Safety,* 1, pp. 177-188, 1983.

38. Dolinski, K., "First-Order Second-Moment Approximation in Reliability of Structural Systems: Critical Review and Alternative Approach," *Structural Safety,* 1, pp. 211-231, 1983.

39. Ditlevsen, O., "Narrow Reliability Bounds for Structural Systems," *Journal of Structural Mechanics,* 7(4), pp. 453-472, 1979.

40. Ditlevsen, O., "*Uncertainty Modeling With Applications to Multidimensional Civil Engineering Systems*," McGraw-Hill, 412pp. 1981.

41. Yang, Y., "Reliability of Composite Laminates," *Mechanical Structure & Mechanics,* Vol. 16(4), pp. 523-536, 1989.

42. Johnson, N. L., *"Distributions in Statistics: Continuous Multivariate Distributions,"* John Wiley & Sons, Inc., 333 pp., 1972.

43. Rice, J. R., "*Mathematical Statistics and Data Analysis,*" Second Edition, International Thomson Publishing, 602 pp., 1995.

44. Drezner, Z. and Wesolowsky, G. O., "On the Computation of the Bivariate Normal Integral," *Journal of Statistical Computation and Simulation*, Vol. 35, pp. 101-107, 1990.

45. Owen, D.B., "Tables for Computing Bivariate Normal Probabilities," *The Annals of Mathematical Statistics,* Vol. 27, No. 4, pp. 1075-1090, 1956.

46. Miner, M.A., "Cumulative Damage in Fatigue," *Journal of Applied Mechanics,* A159 – A165, September, 1945.

47. Wahl, N., "Effects of Modeling Assumptions on the Accuracy of Spectrum Fatigue Lifetime Predictions for a Fiberglass Laminate," *AIAA-2002-0023*, pp. 1-9, 2002.

48. Cesare, M. A., and Sues, R. H., "Profes Probabilistic Finite Element System – Bringing Probabilistic Mechanics to the Desktop," *AIAA 99-1607*, pp1-7, 1999.

49. Xin, X., Chicone, C., and Chen, Z., "Analytical Solutions for Failure Evolution With a Nonlinear Local Damage Model," *Journal of Applied Mechanics,* Vol. 68, pp. 835-843, September 2001.

50. Rodin, G. J., "Continuum Damage Mechanics and Creep Life Analysis," *Journal of Applied Mechanics*, Vol. 67, pp. 193-196, March 2000.

51. Schaff, J. R. and Davidson B. D., *Journal of Composite Materials*, Vol. 31, pp. 128-157, 1997.

52. Schaff, J. R. and Davidson B. D., *Journal of Composite Materials*, Vol. 31, pp. 158-181, 1997.

53. Curtis P. T. and Davis A. J., "*Fatigue Life Prediction of Polymer Composite Materials,*" Plenary Lecture at ECCM9, June 2000.

54. Timoshenko, S., Young, D. H., and Weaver, W., Jr., "*Vibration Problems in Engineering,*" Fourth Edition, John Wiley & Son, 521 pp., 1974.

55. Lutes, L. D., and Sarkani, S., *"Statistic Analysis of Structural and Mechanical Vibration,"* Prentice Hall, Upper Saddle River, New Jersey 07458, 509 pp., 1997.

56. Crandall, S. H., and Mark, W. D., *"Random Vibration in Mechanical Systems,"* Academic Press, Inc., Orlando, FL 32778, 166 pp., 1963.

57. Rao, J. S., *Dynamics of Plates,"* Marcel Dekker, Inc., 560 pp., 1999.

58. Timoshenko, S., *"Theory of Plates and Shells,"* McGraw Hill, New York, 492pp., 1940.

59. Reddy, J.N., "*Mechanics of Laminated Composite Plates,"* CRC Press, Inc., 782 pp., 1997.

60. Ashton, J. E., and Whitney, J.M., "*Theory of Laminated Plates,"* Technomic Publication Co., Inc., 750 Summer St., Stamford, Conn. 06901, 153 pp., 1970.

61. Chern, Y-T, *"Forced Vibration Analysis of Plates and Shallow Shells,"* Dissertation, The Ohio State University, 210 pp., 1989.

62. Tummala, R.R., Rymaszewski, E. J. and Klopfenstein, A. G., "*Microelectronics Packaging Handbook,*" Chapman & Hall, 682 pp., 1997.

63. Tummala, R.R., "*Fundamental of Microsystems Packaging*", McGraw-Hill, 967 pp., 2001.

64. Lau, J. H. and Pao Y-H., "*Solder Joint Reliability of BGA, CSP, Flip Chip, and Fine Pitch SMT Assemblies,*" McGraw-Hill, 409 pp., 1997.

65. Dasgupta, A. and Pecht M, "Material Failure Mechanisms and Damage Models," *IEEE Transaction on Reliability*, Vol. 40, No.5, pp. 531-536. 1999.

66. Dasgupta, A. and Hu, J. M., "Failure Mechanism Models for Excessive Elastic Deformation," *IEEE Transaction on Reliability*, Vol.41, No.1, pp. 149-154. 1992.

67. Dasgupta, A. and Hu, J M., 1992b, "Failure Mechanism Models for Plastic Deformation," *IEEE Transaction on Reliability*, Vol. 41, No.2, pp. 168-174, 1992.

68. Dasgupta, A. and Hu, J. M., "Failure Mechanism Models for Brittle Fracture," *IEEE Transaction on Reliability*, Vol. 41, No. 3, pp. 328-335, 1992.

69. Dasgupta, A. and Hu, J. M., 1992d, "Failure Mechanism Models for Ductile Fracture," *IEEE Transaction on Reliability*, Vol. 41, No.4, pp. 489-495, 1992.

70. Dasgupta, A. and Haslach Jr., H. W., "Mechanical Design Failure Models for Buckling," *IEEE Transaction on Reliability*, Vol. 42, No. 1, pp. 9-16, 1993.

71. Dasgupta, A., 1993b, "Failure Mechanism Models for Cyclic Fatigue," *IEEE Transaction on Reliability,* Vol. 42, No. 4, pp. 548-555, 1993.

72. Shah, M. K., "Analysis of Parameters Influencing Stresses in the Solder Joints of Leadless Chip Capacitors," *Journal of Electronic Packaging*, Vol. 112, pp. 147-153, Jun. 1990.

73. Lee, W. W., Nguyen, L. T. and Selvaduray, G. S., "Solder Joint Fatigue Models: Review and Applicability to Chip Scale Packages," *Microelectronics Reliability 40*, pp. 231-244, 2000.

74. Vaynman, S. and McKeown, S. A., "Energy-based Methodology for the Fatigue Life Prediction of Solder Materials," *IEEE Transactions on Components, Hybrids, and Manufacturing Technology,* Vol. 16, No. 3, pp. 317-322, May 1993.

75. Solomon, H. D., "Fatigue of 60/40 Solder, " *IEEE Transactions on Components, Hybrids, and Manufacturing Technology,* Vol. CHMT-9, No.4, pp. 423-432, 1987.

76. Solomon. H. D., "High and Low Temperature Strain-Life Behavior of a Pb Rich Solder," *Journal of Electronic Packaging*, Vol. 112, pp. 123-128, June 1990.

77. Tee, T. Y., Sivakumar, K. and Do-Bento-Vieira, A., "Board Level Solder Joint Reliability Modeling of LFBGA Package," *2000 Int'l Symposium on Electronic Materials & Packaging,* pp. 51-54, 2000.

78. Zhang, X. and Lee, S-W. R., "Thermal Fatigue Life Prediction for Solder Joints with the Consideration of Damage Evolution," *1998 IEEE/CPMT Electronics Packaging Technology Conference,* pp. 279-285, 1998.

79. Palmer, M. A., Redmond, P. E., and Messler, R. W. Jr., "Thermomechanical Fatigue Testing and Analysis of Solder Alloys, " *Transactions of the ASME*, Vol. 122, pp. 48-54, 2000.

80. Wen, S. and Keer, L. M., "A Theory of Fatigue: A Physical Approach with Applications to Lead-Rich Solder," *Journal of Applied Mechanics*, Vol. 69, pp. 1-10, Jan. 2002.

81. Larson, M. C. and Verges, M. A., "Extending the Fatigue Life of Solder Grid Array (SGA) Electronic Packages," *Transactions of the ASME*, Vol. 125, pp. 18-23, 2003.

82. Shi, X. Q., et al, "Reliability Assessment of PBGA Solder Joints Using the New Creep Constitutive Relationship and Modified Energy-Based Life Prediction Model," 2000 Electronics Packaging Technology Conference, pp. 398-405, 2000.

83. Shi, X. Q., et al, "A New Creep Constitutive Model for Eutectic Solder Alloy," *Journal of Electronic Packaging*, Vol. 124, pp. 85-90, June 2002.

84. Lau, J. H., Pan, S. H. and Chang, C., "A New Thermal-Fatigue Life Prediction Model for Wafer Level Chip Scale Package (WLCSP) Solder Joint," *Transactions of the ASME*, Vol. 124, pp. 212-220, 2002.

85. Engelmaier, W., "Generic Reliability Figures of Merit Design Tools for Surface Mount Solder Attachments," *IEEE Transactions on Components, Hybrids, and Manufacturing Technology*, Vol. 16, No. 1, pp. 103-112, Feb. 1993.

86. Pao, Y-H., "A Fracture Mechanics Approach to Thermal Fatigue Life Prediction of Solder Joints," *IEEE Transactions on Components, Hybrids, and Manufacturing Technology,* Vol. 15, No. 4, pp. 559-570, Aug. 1992.

87. Huang, J., et al, "A Dislocation Model of Shear Fatigue Damage and Life Prediction of SMT Solder Joints Under Thermal Cycling," *IEEE Transactions on Components, Hybrids, and Manufacturing Technology,* Vol. 15, No. 4, pp. 553-558, Aug. 1992.

88. Zubelewicz, A., et al, "Micromechanical Method to Predict Fatigue Life of Solder," *Journal of Electronic Packaging*, Vol. 112, pp. 179-182, Jun. 1990.

89. Zhang, X., Lee, S-W. R. and Pao, Y-H., "A Damage Evolution Model for Thermal Fatigue Analysis of Solder Joints," *Transactions of the ASME*, Vol. 122, pp. 200-206, Sep. 2000.

90. Tang, H. and Basaran, C., "A Damage Mechanical-Based Fatigue Life Prediction Model for Solder Joints," *Transactions of the ASME*, Vol. 125, pp. 120-125, Mar. 2003.

91. Stolkarts, V., Keer, L. M. and Fine, M. E., "Constitutive and Cyclic Damage Model of 63Sn-37Pb Solder," *Journal of Electronic Packaging*, Vol. 123, pp. 351-355, Dec. 2001.

92. Clatterbaugh, G. V. and Charles, H. C. Jr., "Technical Memorandum, 1984 IR&D Advanced Packaging Study," The Johns Hopkins University, Applied Physics Laboratory, 39 pp., Jun. 1986.

93. Yeo, A., Lee. C. and Pang, J. H. L., "Flip Chip Solder Joint Fatigue Life Model Investigation," *2002 Electronics Packaging Technology Conference*, pp. 107-114, 2002.

94. Desai, C. S. and Whitenack, R., "Review of Models and the Disturbed State Concept for Thermomechanical Analysis in Electronic Packaging," *Journal of Electronic Packaging,* Vol. 123, pp. 19-33, Mar. 2001.

95. Vianco, P. T. and Burchett, S. N., "Solder Joint Reliability Predictions for Leadless Chip Resistors, Chip Capacitors, and Ferrite Chip Inductors Using the SRS Software," Sandia Report, Sand2001-1665, 28 pp. 2001.

96. Pang, J. H. L. and Chong, D. Y. R., "Flip Chip on Board Solder Joint Reliability Analysis Using 2-D and 3-D FEA Models," *IEEE Transactions on Advanced Packaging,* Vol. 24, No. 4, pp. 499-506, Nov. 2001.

97. Lodge, K. J. and Pedder, D. J., "The Impact of Packaging on the Reliability of Flip-Chip Solder Bonded Devices," *IEEE Transactions on Components, Hybrids, and Manufacturing Technology,* Vol. 13, No. 4, pp. 847-855, Dec. 1990.

98. Waller D. L., Fox, L. R. and Hannemann, R. J., "Analysis of Surface Mount Thermal and Thermal Stress Performance," *IEEE Transactions on Components, Hybrids, and Manufacturing Technology,* Vol. CHMT-6, No.3, pp. 257-266, Sep. 1983.

99. Wong, B. and Helling, D. E., "A Mechanistic Model for Solder Joint Failure Prediction Under Thermal Cycling," *Transactions of the ASME*, Vol. 112, pp. 104-109, Jun. 1990.

100. Engelmaier, W., "The Use Environments of Electronic Assemblies and Their Impact on Surface Mount Solder Attachment Reliability," *IEEE Transactions on Components, Hybrids, and Manufacturing Technology,* Vol. 13, No. 4, pp. 903-908, Dec. 1990.

101. Deshpande, A., M., Subbarayan, G. and Rose, D., "A System for First Order Reliability Estimation of Solder Joints in Area Array Packages," *Transactions of the ASME,* Vol. 122, pp. 6-12, Mar. 2000.

102. Park, T-S. and Lee, S-B., "Mechanical Fatigue Tests of Solder Joint Under Mixed-mode Loading Cases," *2001 Int'l Symposium on Electronic Materials and Packaging,* pp. 438-443, 2001.

103. Lau, J. H. and Lee, S. W. R., "Effects of Build-Up Printed Circuit Board Thickness on the Solder Joint Reliability of a Wafer Level Chip Scale Package (WLCSP)," *IEEE Transactions on Components and Packaging Technologies,* Vol. 25, No. 1, pp. 3-14, Mar. 2002.

104. Noctor, D. M., et al, "Attachment Reliability Evaluation and Failure Analysis of Thin Small Outline Packages (TSOP's) with Alloy 42 Leadframes," *IEEE Transactions on Components, Hybrids, and Manufacturing Technology,* Vol. 16, No. 8, pp. 961-971, Dec. 1993.

105. Darveaux, R., "Effect of Simulation Methodology on Solder Joint Crack Growth Correlation and Fatigue Life Prediction," *Journal of Electronic Packaging,* Vol. 124, pp. 147-154, Sep. 2002.

106. Pang, H. L. J., et al, "Sensitivity Study of Temperature and Strain Rate Dependent Properties on Solder Joint Fatigue Life," *1998 IEEE/CPMT Electronics Packaging Technology Conference,* pp. 184-189, 1998.

107. Frost, H. J. and Howard, R. T., "Creep Fatigue Modeling for Solder Joint Reliability Predictions Including the Microstructural Evolution of the Solder," *IEEE Transactions on Components, Hybrids, and Manufacturing Technology*, Vol. 13, No. 4, pp. 727-735, Dec. 1990.

108. Shin, S. W. and Yu, J., "Creep Deformation of Microstructurally Stable Sn-3.5Ag-xBi Solders," *2001 Int'l Symposium on Electronic Materials and Packaging*, pp. 229-234, 2001.

109. Lau, J. H., "Creep of Solder Interconnects under Combined Loads," *IEEE Transactions on Components, Hybrids, and Manufacturing Technology*, Vol. 16, No. 8, pp. 794-798, Dec. 1993.

110. Jones, W. K., Liu, Y. Q. and Shah M., "Mechanical Properties of Sn-In Solders at Low Temperature," *International Symposium on Advanced Packaging Materials*, pp. 64-67, 1997.

111. Schubert A., et al, "Thermo-Mechanical Properties and Creep Deformation of Lead-Containing and Lead-Free Solders," *2001 International Symposium on Advanced Packaging Materials*, pp. 129-134, 2001.

112. Hernandez, C. L., Vianco, P. T. and Rejent, J. A., "Effect of Interface Microstructure on the Mechanical Properties of Pb-free Hybrid Microcircuit Solder Joints," *IPC/SMTA Electronics Assembly Expo*, S19-2-1 – S19-2-8, 1998.

113. Goh, T. J., "Parametric Finite Element Analysis of Solder Joint Reliability of Flip Chip on Board," *IEEE/CPMT Electronics Packaging Technology Conference*, pp. 57-62, 1998.

114. Liu, C-M. and Chiang, K-N., "Solder Shape Design and Thermal Stress/Strain Analysis of Flip Chip Packaging Using Hybrid Method," *2000 Int'l Symposium on Electronic Materials and Packaging*, pp. 44-50, 2000.

115. Borgesen, P., Li, C. and Conway, H. D., "Mechanical Design Considerations for Area Array Solder Joints," *IEEE Transactions on Components, Hybrids, and Manufacturing Technology*, Vol. 16, No. 3, pp. 272-283, May 1993.

116. Stoyanov, S., et al, "Solder Joint Reliability Optimization," *APACK 2001 Conference on Advances in Packaging*, pp. 178-186, 2001.

117. Syed, A., "Reliability and Au Embitterment of Lead Free Solders for BGA Applications," *2001 International Symposium on Advanced Packaging Materials,* pp. 143-147, 2001.

118. Lee, S-W. R., et al, "Evaluation of Board Level Reliability of Pb-Free PBGA Solder Joints," *8th International Symposium on Advanced Packaging Materials,* pp. 82-89, 2002.

119. Schubert, A., et al, Thermo-Mechanical Reliability of Lead-Free Interconnects, 8th International Symposium on Advanced Packaging Material, pp. 90-96.

120. Solberg, V., "Board Level Reliability Testing of μBGA Packaging with Lead-Free Solder Attachment," *2000 Electronics Packaging Technology Conference,* pp. 10-14, 2000.

121. Xiao, L., et al, "Characterization of Mechanical Properties of Bulk Lead Free Solders," *2000 International Symposium on Advanced Packaging Materials*, pp. 145-151, 2000.

122. Mutoh, Y., et al, "Fatigue Crack Growth Behavior of Lead-Containing and Lead-Free Solders," *Soldering and Surface Mount Technology*, 14/3, 37-45, 2002.

123. Lau, J. H., et al, "HDPUG's Design for Lead-Free Solder Joint Reliability of High-Density Packages," *IPC SMEMA Council APEX*, pp. S42-2-1 – S 42-2-13, 2003.

124. Lau, J. H., et al, "Creep Analysis and Thermal-Fatigue Life Prediction of the Lead-Free Solder Sealing Ring of Photonic Switch," *Journal of Electronic Packaging,* Vol. 124, pp. 403-410, Dec. 2002.

125. Lau, J. H. and Lee, S-W. R., "Reliability of Wafer Level Chip Scale Package (WLCSP) with 96.5Sn-3.5Ag Lead-free Solder Joints on Build-up Microvia Printed Circuit Board," *2000 Int'l Symposium on Electronic Materials & Packaging,* pp. 55-63, 2000.

126. Enger, P.A., "*Structural Analysis of Printed Circuit Board Systems,*" *Springer-Verlag,* 291 pp., 1993.

127. Steinberg, D.S., "*Vibration Analysis for Electronic Equipment,*" Third Edition, John Wiley & Sons, Inc., 416 pp., 2000.

128. Mirman, B. A., "Mathematical Model of a Plated-Through Hole Under a Load Induced by Thermal Mismatch," *"IEEE Transactions on Components, Hybrids, and Manufacturing Technology,"* Vol. 11, No.4, pp. 506-511, Dec. 1988.

129. Munikoti, R.,and Dhar, P., "A New Power Cycling Technique for Accelerated Reliability Evaluation of Plated Through Holes and Interconnects in PCBs," *IEEE Transactions on Components, Hybrids, and Manufacturing Technology,"* Vol. 13, No. 4, pp. 865-872, Dec. 1990.

130. Ahman, M., Teng, S., Hu, M., and Brillhart, M., "Assessing the Reliability of Plated Vias," (no source), pp. 30-37, Nov. 2002.

131. Oien, M. A., "A Simple Model for the Thermo-Mechanical Deformations of Plated Through Holes in Multilayer PWB," *"Proceedings of 14th Annual IEEE Reliability Physics Symposium,"* pp. 121-128, 1976.

132. Beelen-Hendrikx, C. and Verguld, M., "Trends in Electronic Packaging and Assembly for Portable Consumer Products," *2000 Electronics Packaging Technology Conference*, pp. 24-32, 2000.

133. Ho, K. and Teng, A., "Survey on Delamination of IC Packages in Electronic Products," *Int'l Symposium on Electronic Materials & Packaging*, pp. 269-273, 2000.

134. Lin, T. Y., et al, "Failure Analysis of Full Delamination on the Stacked Die Leaded Packages," *Transactions of the ASME*, Vol. 25, pp. 392-399, Sep. 2003.

135. Zakel, E. and Reichl, H., "Investigations of Failure Mechanisms of TAB-Bonded Chips During Thermal Aging," *IEEE Transactions on Components, Hybrids and Manufacturing Technology,* Vol. 13, No. 4, pp. 856-864, 1990.

136. Ling, J., Teoh, H., et al, "Reliability Assessment of High Lead TAB Package," *IEEE Transactions on Components, Hybrids, and Manufacturing Technology*, Vol. 15, No. 6, pp. 1105-1116, 1992.

137. Sarkar, G, et, al, "Effect of Thermal Ageing and Thermal Cycling On the Reliability of Solder Joints of TAB Outer Lead Bonds," *IEEE/CPMT Electronic Technology Conference,* pp. 86-92, 1997.

138. Zhang, J. and Baldwin, D. F., "Thermo-mechanical Reliability of Flip Chip on Organic Board During Power Cycling Tests," *8th International Symposium on Advanced Packaging Materials,* pp. 97-103, 2002.

139. Lee, D. C. Y. and Kim, J., "Measurement of Residual Stresses in Encapsulant of a PQFP," *IEEE/CPMT Electronics Packaging Technology Conference*, pp. 286-290, 1998.

140. Lee, K. O, et al, "Thermo-Mechanical Reliability of the Benzocyclobuten (BCB) film in a WLCSP Process," *Int'l Symposium on Electronic Materials and Packaging,* pp. 84-87, 2001.

141. Hau, W. L. W., et al, "A New Stress Chip Design for Electronic Packaging Applications," *Int'l Symposium on Electronic Materials & Packaging*, pp. 457-463, 2000.

142. Etienne B. and Sandborn, P., "Application-Specific Economic Analysis of Integral Passives in Printed Circuit Boards," *International Symposium on Advanced Packaging Materials*, pp. 399-404, 2001.

143. Goh, T. J., "Thermal and Mechanical Loading Effects on the Reliability of Organic Flip Chip Package," *Journal of Electronic Packaging*, Vol. 123, pp. 83-87, 2001.

144. Pang, H. L. J., Tan, T., L., et al, "Reliability Assessment of a Wirebond Chip-on-board Packaging Subjected to Accelerated Thermal Cycling Loading," *IEEE/CPMT Electronic Packaging Conference*, pp. 93-97, 1997.

145. Im, Y. T., Kim, J. H. and Choi, S. T., "Study on Residual Stress in Viscoelastic Thin Film Using Curvature Measurement Method," *Int'l Symposium on Electronic Materials and Packaging,* pp. 341-346, 2001.

146. Guo, W., Li, Z., et al, "Temperature Gradient Impact on Electromigration Failure in VLSI Metallization," *Fourteenth IEEE SEMI-THERM Symposium*, pp. 122-127, 1998.

147. Engel, P. A., "Failure Models for Mechanical Wear Modes & Mechanisms," *IEEE Transaction on Reliability*, Vol. 42, No. 2, pp. 262-267, 1993.

148. Li, J, Dasgupta, A., "Failure-Mechanism Models for Creep and Creep Rupture," *IEEE Transaction on Reliability*, Vol. 42, No. 3, pp. 339-353, 1993.

149. Li, J, Dasgupta, A., "Failure Mechanism Models for Material Aging due to Interdiffusion," *IEEE Transaction on Reliability*, Vol. 43, No.1, pp.2-10, 1994.

150. Ritter, J. E. and Huseinovic, A., "Adhesion and Reliability of Epoxy/Glass Interfaces," *Journal of Electronic Packaging*, Vol. 23, pp. 401-404, Dec. 2001.

151. Suhir, E., "Stresses in Bi-Metal Thermostats," *"Journal of Applied Mechanics,"* Vol. 53, pp. 657-660, Sept. 1986.

152. Suhir E., "Interfacial Stresses in Bimetal Thermostats," *Journal of Applied Mechanics,* Vol. 56, pp. 595-600, Sept., 1989.

153. Schmidt, R, Alpern, P., Plecher, K. and Tilgner, R., "Investigation of the Adhesion Strength between Molding Compound and Leadframe at Higher Temperature," *IEEE/CPMT Electronics Packaging Technology Conference*, pp. 349-353, 1998.

154. Guo, Y-F, and Zhao, J-H, "A Practical Die Stress Model and Its Applications in Flip-Chip Packages," *"2000 Inter Society Conference on Thermal Phenomena,"* pp. 393-399, 2000.

155. Glaser, J. C., "Thermal Stresses in Compliantly Joined Materials," *"Transaction of the ASME,"* Vol. 112, pp. 24-29, March 1990.

156. Palusinski, O. A., "*Advanced Packaging Design*," Class Notes for ECE 654, The University of Arizona, 10 pp., 2003.

157. Lim, J. H., Lee, W., et al, "Vapor Pressure Analysis of Popcorn Cracking in Plastic IC Packages By Fractures Mechanics", *IEEE/CPMT Electronics Packaging Technology Conference*, pp. 36-42, 1998.

158. Ikeda, T., et al, "Strength Evaluation of Plastic Packages During Solder Reflow Process Using Stress Intensity Factors of V-notch," *Journal of Electronic Packaging,* Vol. 125, pp. 31-38, March 2003.

159. Mercado, L. L. and Chavez, B., "Impact of JEDEC Test Conditions on New-Generation Package Reliability," *IEEE Transactions on Components and Packaging Technologies,* Vol. 25, No. 2, pp. 204-210, June 2002.

160. Bojta, P., "Modeling Moisture Caused Failures in Stress Tests," *24th International Spring Seminar on Electronics Technol*ogy, pp. 129-132, May 2001.

161. Wilde, J, Cheng, Z. N. and Wang, G. Z., "Influences of Packaging Materials on the Solder Joint Reliability of Chip Scale Package Assemblies," *1999 International Symposium on Advanced Packaging Materials,* pp. 144- 149, 1999.

162. Pan, T-Y., and Pao, Y-H., "Deformation in Multiplayer Stacked Assemblies," *Transactions of the ASME,* Vol. 112, pp. 30-34, March 1990.

163. Suhir, E., "An Approximate Analysis of Stresses in Multilayered Elastic Thin Films," *Journal of Applied Mechanics*, Vol. 55, pp. 143-148, March 1988.

164. Rockwitz, R., and Fiessler, B., "Structural Reliability Under Combined Random Load Sequences," *Computer Structure,* Vol.9 pp. 484-494, 1978.

165. Chen, X., and Line, N.C., "Fast Probability Integration by Three-Parameter Normal Tail Approximation," *Structural Safety*, 1, pp. 269-276, 1983.

166. Ozisik, M. N., *Boundary Value Problems of Heat Conduction,* International Textbook Company, Scranton, Pennsylvania, 505 pp., 1968.